

Politecnico di Torino

Politecnico di Torino

Corso di Laurea Magistrale in Ingegneria Energetica e Nucleare

A.a. 2025/2026

Graduation Session Settembre 2026

Techno-Economic Feasibility Analysis of a Renewable Energy Community

Comparative Assessment of Four Scenarios with Energy Flow Modeling and Economic Evaluation

Relatore:

Andrea Lanzini

Candidato:

Gabriele De Benedittis

Tutor aziendale:

Vital Picardi

Abstract

In recent years, increasing attention has been devoted to decentralized energy production. Unlike centralized generation, where electricity is produced by a limited number of large power plants and transmitted over long distance transmission lines, decentralized generation relies on small-scale self-production units distributed across the territory and directly connected to the electrical grid. These models provide significant benefits for the power system by reducing grid congestion and transmission losses, promoting self-consumption, and leveraging smart grids to manage energy flows. Furthermore, they enhance system stability and decrease the need for new infrastructure. Within this framework, Renewable Energy Communities (RECs) represent a crucial instrument for the diffusion and utilization of Renewable Energy Sources (RES), thereby reducing dependence on fossil fuels. A REC offers citizens, public administrations, and small and medium-sized enterprises (SMEs) the opportunity to cooperate in order to produce and virtually share locally generated renewable energy, with the aim of providing economic, social, and environmental benefits to all community members. This thesis presents a techno-economic feasibility study of a Renewable Energy Community located in the municipality of Minervino di Lecce. The analysis is based on real consumption data, which are subsequently converted from monthly to hourly resolution using a procedure provided by the Italian Energy Services Operator (GSE). As a preliminary step, a 1 MW photovoltaic plant is designed, and all the main system components are sized, including inverters, battery energy storage system (BESS), cables, and protection devices. In addition, for the scenario involving the valorization of surplus energy, a small-scale PEM electrolyzer is also sized. Scenario 3 (S3) considers a 100% photovoltaic system integrated with a battery energy storage system operated with a self-consumption maximization strategy; in parallel, a particle swarm optimization (S3-opt) is performed to assess whether an alternative storage capacity would yield a techno-economic improvement over the installed configuration, the results of which confirm the adequacy of the original sizing and lead to its retention throughout the study. Finally, Scenario 4 (S4) extends the previous configuration by introducing, in addition to the storage system, hydrogen production through a small-scale PEM electrolyzer to manage the residual energy surplus. For each scenario, an analysis of energy flows and a techno-economic assessment of system performance are carried out. The simulations are implemented using a code developed in the MATLAB environment.

Table of Contents

List of Tables VI

List of Figures VII

1 Introduction 1
1.1 Thesis structure . . . 2

2 Fundamentals of Photovoltaic Systems 4
2.1 Energy from the Sun . . . 4
2.2 Operating Principle . . . 5
2.3 Main components of a photovoltaic system . . . 7
2.3.1 Photovoltaic Generator . . . 7
2.3.2 Inverter . . . 9
2.3.3 Overcurrent and Overvoltage protection . . . 11
2.3.4 Protection against direct and indirect contact . . . 15
2.3.5 Classification of PV Systems . . . 19
2.4 Modeling and Energy Production of Photovoltaic Systems . . . 21
2.4.1 Equivalent Circuit of the Cell . . . 21
2.4.2 Voltage-Current Characteristic Curve of the Module . . . 22
2.4.3 Variation in Energy Production . . . 22
2.4.4 Standard Test Conditions (STC) . . . 25
2.4.5 Tilt and Orientation . . . 25
2.4.6 Predicted Energy Yield . . . 26
2.4.7 Voltages and Currents in a PV System . . . 26
2.5 Trends in the Growth of Installed Photovoltaic Systems . . . 27

3 Battery Energy Storage System 28
3.1 Introduction . . . 28
3.2 Electrochemical Storage Systems . . . 29
3.2.1 BESS-Lithium-Ion (LI-ION) Storage Systems . . . 29
3.2.2 Performance Parameters of Lithium-Ion Batteries . . . 31

4 Hydrogen and P2H system 33
4.1 Introduction . . . 33
4.2 Renewable Water Splitting and Electrolysis . . . 33
4.2.1 Proton Exchange Membrane Water Electrolysis (PEMWE) . . . 34
4.3 Solar PV-Powered Electrolyser (P2H) . . . 36
4.4 Hydrogen storage . . . 38

5 Renewable energy communities 40
5.1 The European Regulatory Framework . . . 40
5.1.1 The RED II Directive . . . 40
5.1.2 The IEM Directive . . . 41
5.2 The evolution of Italian legislation . . . 42
5.2.1 The Milleproroghe Decree 2020 . . . 42
5.2.2 ARERA Resolution No. 318/2020 . . . 43
5.2.3 Implementing Decree of the Italian Ministry of Economic Development (MISE), 16 September 2020 . . . 44
5.2.4 Legislative Decree 199/2021 and RED II Transposition . . . 44
5.2.5 Integrated Text on Distributed Self-Consumption . . . 45
5.2.6 The CACER Decree (D.M. 414/2023) . . . 46
5.3 Plants Eligible for the DM CACER Incentives . . . 47
5.4 Operating Principles and Economic Mechanisms . . . 47
5.4.1 Shared "Self-Consumed" and "Incentivized" Energy . . . 48
5.4.2 Economic valorization components . . . 48
5.4.3 The ARERA Shared Energy Valuation Fee . . . 48
5.4.4 The Premium Tariff on Shared Energy . . . 49
5.4.5 The Sale of Electricity Injected into the Grid (Dedicated Withdrawal) . . . 49
5.4.6 Synthesis of Energy and Economic Streams . . . 50
5.5 Steps to Create a REC . . . 50

6 Characterization of Case Studies and Load Data Analysis 55
6.1 Introduction . . . 55
6.2 Sample Analysis . . . 56
6.3 Residential End-Users . . . 57
6.4 Industrial End-User . . . 58
6.5 Public Administration . . . 58
6.6 Public Lighting . . . 59
6.7 Aggregate Load Analysis of the Community . . . 60
6.8 Hourly Load Profiling . . . 60

7 Technical Sizing of PV, BESS and H2 Production Systems 64
7.1 Introduction . . . 64
7.2 Characterization of PV plant . . . 64
7.2.1 Installation Site, Orientation Parameters, and Yield Analysis of the Photovoltaic Generation Plant . . . 64
7.2.2 Components of the PV Plant . . . 66
7.2.3 Design Criteria . . . 68
7.2.4 String Layout Optimization . . . 72
7.2.5 Cable Sizing . . . 74
7.3 BESS Sizing . . . 80
7.4 Electrolyzer Sizing . . . 83

8 Operational Scenario Simulation Methodology 85
8.1 Introduction . . . 85
8.2 Methodology of S1 . . . 85
8.3 Methodology of S2 . . . 86
8.3.1 Load Categorisation and Exclusion Criteria . . . 86
8.3.2 Hour Classification: Source and Destination Windows . . . 87
8.3.3 Definition of the Flexibility Coefficient α . . . 87

8.3.4 Sensitivity Analysis, Daily Energy Conservation, and Capacity Constraint 88
8.4 Methodology of S3 . . . 90
8.4.1 Rationale for a Simulation-Based Optimization Approach . . . 92
8.5 Methodology of S4 . . . 96

9 Results and Discussion 98
9.1 Scenario S1 . . . 98
9.2 Scenario 2 . . . 102
9.3 Scenario 3 . . . 108
9.3.1 Optimization: PSO-Based BESS Sizing. . . . 112
9.4 Scenario 4 . . . 119
9.5 Comparative financial analysis of the scenarios . . . 124
9.5.1 Methodology and analysis parameters . . . 124
9.5.2 Scenario S1 . . . 126
9.5.3 Scenario S2 . . . 127
9.5.4 Scenario S3 . . . 129
9.5.5 Scenario S4 . . . 130
9.5.6 Final comparison between scenarios . . . 132

10 Conclusions 134

Bibliography 136

List of Tables

5.1 Fixed, variable, and maximum tariffs based on nominal plant capacity. 49
5.2 Economic valuation mechanisms for energy flows within the REC (Renewable Energy Community). 50

6.1 Structure of the energy consumption table broken down by time-of-use slots. . . 61

7.1 Technical specifications of the JA Solar PV panel[35]. 66
7.2 Technical specifications of the Sigenergy inverter[36]. 67
7.3 Synoptic overview of the electrical and geometric sizing of the PV generator. . . 73
7.4 Summary of electrical protection device characteristics. 79
7.5 Summary of selected cable specifications. 79
7.6 Key technical specifications of the GSL Energy BESS-125K418 unit (values refer to a single cabinet; the installed system comprises two units in parallel). 82
7.7 Technical specifications of the Rubri-PI-0020 PEM electrolyser. 83

8.1 Sensitivity analysis: candidate flexible energy, effective shift after daily capacity constraint, spill, and resulting net increment in shared energy. 89

9.1 Sensitivity analysis on the DR flexibility coefficient α: candidate flexible energy, effective shift after the daily capping constraint, unabsorbed spill, and resulting net increment in shared energy. Note that $\Delta E_{\text{cond}} < E_{\text{shift}}$ for all α values: a small subset of source hours switch state to destination after load removal, reducing shared energy in those hours rather than adding to it one-for-one (115 hours out of 6710 source hours at $\alpha = 10\%$, accounting for the full 2006 kWh gap; see main text). 103
9.2 Trade-off between annualized investor VAN and REC-wide benefit as a function of the weighting parameter α. 115
9.3 Current (2-module) versus discretized knee-point (3-module) BESS configuration. 117
9.4 Composition of CAPEX, OPEX and revenues for scenario S1 126
9.5 Composition of CAPEX, OPEX and revenues for scenario S2 128
9.6 Composition of CAPEX, OPEX and revenues for scenario S3 129
9.7 Composition of CAPEX, OPEX and revenues for scenario S4 131
9.8 Comparative summary of the four scenarios 132

List of Figures

2.1 Extra-atmospheric radiation 5
2.2 Flow of energy between the sun, the atmosphere, and the Earth's surface 5
2.3 Components of solar radiation 6
2.4 Italian solar atlas of annual global horizontal irradiation (GHI) 6
2.5 From cell to PV array 7
2.6 a) Cross section of a traditional silicon module and its constituents. b) Schematic representation of a tandem module with pseudo-squared M2 wafers. Often, the bypass diodes are incorporated in the junction box. 8
2.7 Principle diagram of a single-phase inverter 9
2.8 Operating principle of the PWM technique 10
2.9 I-V curve of the PV generator with maximum power point 10
2.10 System with IT configuration 17
2.11 System with TN configuration 17
2.12 TT system: protection of exposed conductive parts in the user installation by means of a residual current device (RCD) installed at the origin of the installation. 18
2.13 TT system: protection of exposed conductive parts located upstream of the A–B connection point using RCD 18
2.14 TN system: protection of exposed conductive parts without using RCD 19
2.15 Transformerless systems 19
2.16 Equivalent Circuit of the Cell 21
2.17 Voltage-Current Characteristic Curve of the Module 22
2.18 Variation of the characteristic curve I-V of a photovoltaic module as a function of the irradiance on the plane of the module 23
2.19 Variation of the characteristic curve I-V of a photovoltaic module as a function of temperature 23
2.20 Spectrum of solar radiation 24
2.21 Wiring diagram with bypass diodes 24
2.22 Angles that determine the orientation of the PV module 25
2.23 Evolution of the number and power of photovoltaic systems installed in Italy in the period 2010-2024 27

3.1 Load demand profile with energy storage system 29
3.2 Application overview of energy storage system 29
3.3 Charging and discharging method of Li-ion battery. 30
3.4 Utilization of different electrochemical technologies[14] 30

4.1 Various nonrenewable and renewable sources for hydrogen production. 33
4.2 PEM scheme with reactions and some general information. 34

4.3 (a) Schematic of a single cell in proton exchange membrane (PEM) water electrolyzer stack. (b) Photograph of a PEM cell stack. (c) Photographs of details of cell components where 1, bipolar plate; 2, anode current collector; 3, MEA; and 4, cathode current collector.[18] 35
4.4 Schematic of a solar-powered PEM electrolyzer using indirect coupling. 37
4.5 Electrolysis: complete plant 37
4.6 Electrolyzer 37
4.7 Hydrogen storage tanks 39

6.1 Division of the municipal area into two primary substations [32] 56
6.2 Primary cabin selected [32] 56
6.3 Distribution of total annual energy consumption for individual PODs in the residential category 57
6.4 Total monthly consumption per Residential PODs 58
6.5 Total monthly consumption per Industrial POD 58
6.6 Total monthly consumption of PA 59
6.7 Total monthly consumption of PL 59
6.8 Aggregate Load of the Community 60
6.9 Average daily hourly consumption profile with Min-Max envelope 62

7.1 Location of PV plant 64
7.2 Hourly generation profiles categorized by energy season 65
7.3 Monthly generation profiles 65
7.4 PV module dimensions 67
7.5 PV field layout 72
7.6 Calculation of the minimum distance between photovoltaic modules. $\delta_m = -23.45°$ indicates the solar declination at the winter solstice (December 21st), which represents the period when the sun is at its lowest altitude, L is the site latitude, X equal to double the length of the module and β is the Tilt angle. . . 73
7.7 BESS coupling with PV plant and national grid 81

9.1 Scenario S1 — Hourly PV production and aggregated CER load profiles over the reference year (April 2025–March 2026, 8,760 h). 99
9.2 Scenario S1 — PV production and CER consumption profiles over a representative summer week (July 2025), with shared energy highlighted. 99
9.3 Scenario S1 — Annual duration curve of PV hourly production, sorted in descending order. 99
9.4 Scenario S1 — Hourly energy flows over the reference year: (top) PV production split into shared energy and grid-injected surplus; (middle) CER load coverage from PV self-consumption versus grid purchase; (bottom) hourly zonal price P_z and Feed-in Premium tariff (TiP). 100
9.5 Scenario S1 — Comparative analysis of the CER configuration against the no-PV baseline: (top) waterfall decomposition of the annual energy cost, from the baseline cost to the net residual purchase cost, broken down by revenue component; (bottom) monthly benefit by component with cumulative annual value. 101
9.6 Scenario S1 — Monthly breakdown of revenue components (Feed-in Premium, ARERA incentive, bill savings, RID surplus sales) and grid purchase cost. 101

9.7 Annual hourly profiles of PV production and REC consumption for Scenario 2, comparing the original residential-load profile with the Demand-Response-adjusted profile at $\alpha = 10\%$. Since DR redistributes load within each day without altering its daily total, the DR-adjusted consumption curve closely tracks the original one, with visible reductions during source hours and increases during destination hours. 102

9.8 Hourly energy and price flows for Scenario 2 at $\alpha = 10\%$. Top: split of PV production between shared energy ($E_{\text{shared}} = \min(P_{PV}, CER_{DR})$) and surplus sold under the Ritiro Dedicato (RID) scheme. Middle: coverage of DR-adjusted REC consumption by PV (shared energy) versus residual grid purchase. Bottom: hourly zonal price (P_z) and the resulting Premium Tariff (TiP), capped at 100 EUR/MWh. 103

9.9 Monthly shared energy for Scenario 1 (PV only) compared against Scenario 2 under the three tested Demand Response intensities ($\alpha = 5\%, 10\%, 15\%$). The seasonal profile of shared energy is preserved under all α values, with the DR-induced increment consistently present across the year. 104

9.10 Monthly effectively shifted energy versus unabsorbed spill for Scenario 2 at $\alpha = 10\%$, against the available monthly PV surplus. The shift-to-spill ratio deteriorates markedly in the winter months (November–January), when PV surplus availability drops sharply and a large share of candidate flexible energy cannot be absorbed, confirming the structural, PV-resource-limited nature of surplus-driven Demand Response. 104

9.11 Representative summer week (July 2025) for Scenario 2 ($\alpha = 10\%$), showing PV production, original and DR-adjusted REC consumption, original and DR-adjusted residential load (P_{RES}), shared energy and available PV surplus. The DR-shifted residential profile is systematically depressed during morning source hours and boosted during midday destination hours on every day of the week, reflecting the consistently available midday surplus. 105

9.12 Representative winter week (January 2026) for Scenario 2, with the same series as Fig. 9.11. PV surplus is intermittent and concentrated on a small number of days, and the DR-adjusted residential profile shows a correspondingly weaker and less regular deviation from the original load, consistent with the higher winter spill fraction reported in Fig. 9.10. 105

9.13 Comparative analysis of Scenario 2 (PV + DR, $\alpha = 10\%$) against the no-CER baseline. Top: waterfall decomposition of the annual energy cost, from the baseline cost (grey) through retail bill savings, Premium Tariff, ARERA compensation and RID surplus revenue, down to the net residual purchase cost (red); the total REC benefit relative to baseline is indicated by the green arrow. The footnote quantifies the gap between the net purchase cost shown here and the value implied by summing the individual components, arising from the DR-induced recomposition of consumption across retail time bands (fasce orarie). Bottom: monthly benefit by component with the cumulative annual benefit on the secondary axis. 106

9.14 Monthly economic breakdown for Scenario 2 at $\alpha = 10\%$, decomposing gross revenue (Premium Tariff, ARERA compensation, retail bill savings, RID surplus sales) against the residual cost of grid-purchased energy. Revenue components peak in the summer months in line with higher PV output, while the purchase cost remains substantial throughout the year, particularly in the winter months, reflecting the low winter self-sufficiency. 107

9.15 Annual economic KPIs for Scenario 1 (PV only) compared against Scenario 2 under the three tested Demand Response intensities ($\alpha = 5\%, 10\%, 15\%$), decomposed into Premium Tariff (TiP), ARERA compensation, RID surplus revenue and retail bill savings. All components increase monotonically with α, though at a diminishing rate consistent with the growing spill fraction shown in Table 9.1. 107

9.16 Scenario 3, hourly PV production and aggregate REC consumption over the reference year (April 2025–March 2026). By construction, this profile pair is identical to Scenario 1, since battery dispatch operates downstream of both series and does not modify either. 108

9.17 Scenario 3, hourly energy flow breakdown. From top to bottom: allocation of PV production between direct self-consumption, BESS charging and RID surplus; coverage of REC consumption by direct PV supply, BESS discharge and residual grid purchase; BESS charging/discharging power; and hourly zonal price P_z against the Tariffa Premio TiP. 109

9.18 Scenario 3, annual state-of-charge trajectory of the BESS, bounded between $SOC_{min} = 20\%$ and $SOC_{max} = 100\%$. The battery cycles almost daily; shallower, incomplete cycles are visible in late autumn and early winter, reflecting reduced PV availability. 109

9.19 Scenario 3, representative summer week (July 2025): PV production, REC consumption, shared energy, BESS charge/discharge power and state of charge. . . 110

9.20 Scenario 3, representative winter week (January 2026): PV production, REC consumption, shared energy, BESS charge/discharge power and state of charge. Reduced and irregular PV availability results in shallower and less complete battery cycles compared to the summer week. 110

9.21 Scenario 3, comparison against the no-PV, no-storage baseline. Top: waterfall decomposition of the annual energy cost, from the baseline cost (EUR 836816/year) through bill savings, Tariffa Premio, ARERA compensation and RID revenue, down to the residual net cost (EUR 330180/year), for a total benefit of EUR 506636/year (60,5%). Bottom: monthly benefit by component with cumulative annual benefit. 111

9.22 Scenario 3, monthly breakdown of revenue components (Tariffa Premio, ARERA compensation, bill savings, RID surplus) against the residual grid purchase cost. 111

9.23 Scenario 3, dispersion of the PSO optimum across five independent runs with different random seeds, for the single-objective (private VAN) formulation. Both the optimal BESS size E_{opt} and the corresponding VAN are identical across runs (coefficient of variation 0,00%), confirming convergence to the global optimum. . 112

9.24 Scenario 3, 20-year VAN as a function of nominal BESS capacity, obtained by an independent grid sweep of the search space. The PSO optimum coincides with the lower bound of the search range (417,99 kWh), confirming that the VAN decreases monotonically with BESS size and that the current 2-module configuration is already oversized relative to the private investor optimum. . . . 113

9.25 Scenario 3, optimal BESS size as a function of the weighting parameter α in the weighted-sum objective of Eq. 9.1. The optimum collapses onto the upper bound of the search space for $\alpha \leq 0{,}50$ and onto the lower bound for $\alpha \geq 0{,}75$, with the PSO result matching the independent grid-search validation at every sampled α. 114

9.26 Scenario 3, trade-off frontier between annualized private VAN and gross annual REC-wide benefit. Numbered markers correspond to the five sampled values of α (1: $\alpha = 0{,}00$, 2: $\alpha = 0{,}25$, 3: $\alpha = 0{,}50$, 4: $\alpha = 0{,}75$, 5: $\alpha = 1{,}00$); markers sharing the same position indicate coincident optimal solutions. 114

9.27 Scenario 3, weighted objective function (Eq. 9.1) as a function of BESS size, plotted for each sampled value of α. The marker on each curve denotes its grid-search maximum; only for $\alpha = 0{,}50$ does the curve remain visibly non-monotonic, foreshadowing the interior optimum identified by the finer sweep of Figure 9.28. 115
9.28 Scenario 3, refinement of the optimal BESS size over $\alpha \in [0{,}50; 0{,}75]$ (41 equally spaced points). An interior optimum, distinct from both bounds of the search space, is found for $\alpha \in [0{,}6375; 0{,}6687]$, with E_{opt} ranging between 1207,49 and 1223,94 kWh. 115
9.29 Scenario 3, normalized Pareto frontier between annualized VAN and REC-wide benefit, with the chord connecting the two boundary solutions and the knee point ($E_{knee} = 1211{,}4$ kWh) identified as the point of maximum distance from the chord. 116
9.30 Scenario 3, annualized VAN and gross annual REC-wide benefit as a function of BESS size, in real units, over the compromise zone identified by the knee-point analysis. The current 2-module configuration and the discretized 3-module knee-point configuration are marked for reference. 116
9.31 Scenario 3, comparison between the current 2-module configuration and the discretized knee-point 3-module configuration: 20-year private VAN, discounted payback period, and gross annual REC-wide benefit. No payback-period bar is shown for the 3-module configuration, as the discounted cumulative cash flow does not turn non-negative within the 20-year horizon. 117
9.32 Scenario 3, decomposition of the total system value associated with the transition from 2 to 3 BESS modules, into the change in private investor VAN and the present value of the incremental gross REC-wide benefit, capitalized at the same discount rate and horizon via $1/CRF$. 118
9.33 Scenario 4, hourly PV production and aggregate REC consumption over the reference year (April 2025–March 2026). This profile pair is, by construction, identical to Scenario 1 and Scenario 3. 119
9.34 Scenario 4, hourly energy flow breakdown. From top to bottom: allocation of PV production between direct self-consumption, BESS charging, the electrolyzer and RID surplus; coverage of REC consumption by direct PV supply, BESS discharge and residual grid purchase; BESS charging/discharging power; PEM electrolyzer power; and hourly zonal price P_z against the Tariffa Premio TiP. 120
9.35 Scenario 4, PEM electrolyzer power duration curve, ranked from the highest to the lowest operating power over the 1430 annual operating hours. 120
9.36 Scenario 4, representative summer week (July 2025): PV production, REC consumption, shared energy, BESS charge/discharge power, electrolyzer power and state of charge. 121
9.37 Scenario 4, representative winter week (January 2026): PV production, REC consumption, shared energy, BESS charge/discharge power, electrolyzer power and state of charge. 121
9.38 Scenario 4, annual state-of-charge trajectory of the BESS, bounded between $SOC_{min} = 20\%$ and $SOC_{max} = 100\%$. 122
9.39 Scenario 4, comparison against the no-PV, no-storage baseline. Top: waterfall decomposition of the annual energy cost, from the baseline cost (EUR 836816/year) through bill savings, Tariffa Premio, ARERA compensation, RID revenue and hydrogen revenue, down to the residual net cost (EUR 311562/year), for a total benefit of EUR 525254/year (62,8%). Bottom: monthly benefit by component with cumulative annual benefit. 122
9.40 Scenario 4, monthly breakdown of revenue components (Tariffa Premio, ARERA compensation, bill savings, RID surplus, hydrogen revenue) against the residual grid purchase cost. 123

9.41 Scenario 4, monthly hydrogen production (top) and corresponding sale revenue (bottom, at the assumed price of 6,0 EUR/kg). 123
9.42 Discounted cumulated cash flow, scenario S1 127
9.43 Discounted cumulated cash flow, scenario S2 128
9.44 Discounted cumulated cash flow, scenario S3 130
9.45 Discounted cumulated cash flow, scenario S4 132

Chapter 1

Introduction

Over the past few decades, the global energy sector has undergone a profound transformation, driven by two structural pressures that are difficult to disentangle: the mounting scientific evidence on the consequences of climate change and the geopolitical fragility of an energy system still heavily reliant on fossil fuels. The energy crisis of 2021/2022, triggered by the Russian invasion of Ukraine, made it painfully clear how exposure to fossil fuel imports can translate into systemic economic risks far exceeding ordinary price fluctuations. Against this backdrop, the shift toward a decentralized energy model, one built around renewable sources and the active involvement of end users, has ceased to be a matter of political preference and has instead become a strategic imperative. The European Union has responded with a legislative trajectory that has grown progressively more ambitious over time. The Clean Energy for All Europeans Package[1], first presented in 2016 and finalized in 2019, reshaped the regulatory architecture of the sector by setting binding targets on renewables, energy efficiency and electricity market governance. Through Directive 2018/2001/EU[2], the so called RED II, and Directive 2019/944/EU[3], the concept of the energy community was formally introduced into European law for the first time, taking shape in two distinct configurations: the Renewable Energy Community (REC) and the Citizens' Energy Community (CEC). Both frameworks recognize the right of citizens, small and medium-sized enterprises and local authorities to join forces in order to produce, consume, store and share renewable energy. The outbreak of the war in Ukraine accelerated this process considerably: through the REPowerEU plan of 2022, the European Commission raised the binding renewable energy target to 42.5% of gross final energy consumption by 2030, with an aspirational ceiling of 45%. More recently, Directive 2023/2413/EU[4], called also RED III, published in the Official Journal of the European Union on 20 November 2023, further consolidated this framework by introducing specific measures to streamline permitting procedures for renewable installations and by reinforcing the role of energy communities as enabling instruments of the transition. At the national level, the transposition of RED II was carried out through Legislative Decree 199/2021[5], which expanded the operational boundaries of RECs from the secondary substation to the primary substation and raised the maximum eligible plant capacity from 200 kW to 1 MW. The regulatory framework was then completed by Ministerial Decree No. 414 of 7 December 2023[6], issued by the Ministry of Environment and Energy Security and commonly referred to as the CACER Decree, which defines the incentive mechanisms for shared energy and the conditions for accessing the capital grants provided under the National Recovery and Resilience Plan (PNRR). Legislative Decree no. 5 of 9 January 2026[7] (in force from 4 February 2026) implements RED III at the national level, amending previous national legislation and redefining the national objectives for RES 2030[8]. The National Integrated Energy and Climate Plan, updated in 2023 in line with the revised European targets, places energy communities at the center of Italy's decarbonization strategy, acknowledging their contribution to the widespread deployment of small-

and medium-scale renewable installations and to the reduction of energy poverty. Renewable Energy Communities are more than a regulatory instrument: they embody a genuine shift in the way energy is produced, distributed and consumed. The conventional centralized model carries structural inefficiencies that are difficult to overcome. Transmission losses, line congestion during peak hours and a limited ability to respond to localized imbalances between supply and demand are inherent constraints of an architecture designed for an era when generation was concentrated and largely predictable. The growing penetration of non-dispatchable renewable sources, photovoltaics and wind power above all, has introduced a degree of variability that the traditional system struggles to absorb without costly grid reinforcement. Distributed generation, of which RECs represent the most integrated expression at community scale, addresses this challenge at its root: by producing energy close to consumption points, it reduces the volume of power that must flow through high- and medium-voltage networks, eases pressure on transmission infrastructure and improves the overall resilience of the system. When combined with electrochemical storage or with technologies for converting surplus energy, such as hydrogen production through electrolysis, the REC becomes an active entity, capable not only of managing its internal energy flows but also of providing flexibility services to the grid and contributing to system-wide supply-demand balancing. These technical advantages come alongside significant economic and social benefits. For community members, participation in a REC translates into tangible reductions in energy costs, achieved through the valorization of shared energy and the incentive mechanisms established by current legislation. On the employment side, the expansion of RECs stimulates activity in the installation and maintenance of renewable energy plants, with particularly positive effects in areas with limited industrial density. From a social perspective, RECs function as instruments of democratization in energy access: they allow households and organizations that lack suitable surfaces or sufficient capital to install their own systems to nonetheless benefit from the renewable transition, thereby reducing energy inequalities and helping to combat energy poverty. The revenues generated through the incentive tariff can furthermore be reinvested in locally valued public services, setting in motion virtuous cycles of territorial development that carry special significance in small municipalities. It is within this framework that the present thesis is situated. The work proposes a techno-economic feasibility study for the establishment of a Renewable Energy Community in the municipality of Minervino di Lecce, in the province of Lecce. The analysis is structured around four distinct scenarios, designed to assess the impact of different plant configurations and management strategies on energy flows and on the economic sustainability of the investment. The objective is not simply to identify the most profitable configuration, but to understand the extent to which each technological and operational choice reshapes the community's energy profile and its relationship with the incentive mechanisms established by the CACER Decree.

1.1 Thesis structure

The work is organized to guide the reader from the understanding of the technological foundations through to the quantitative evaluation of the scenarios, following a path that moves from the general to the specific and from theory to application. The opening chapters establish the technical and theoretical framework. Three technology areas are covered in sequence: photovoltaic systems, from the physics of the solar cell to the operation of a grid-connected plant, with an overview of inverter topologies, protection devices and MPPT technology; electrochemical storage systems, covering the main components; and finally, hydrogen production through electrolysis, with a closer look at the operating principles of the PEM electrolyzer. This introductory block is not purely descriptive in intent: each technology is presented in direct relation to the role it plays in the scenarios examined later, laying the conceptual groundwork

needed to interpret the case study results. The following chapter addresses the regulatory framework governing Renewable Energy Communities in Italy, tracing the legislative evolution from the transposition of the European RED II and RED III Directives through to the CACER Decree (Ministerial Decree No. 414/2023) and the Consolidated Text on Distributed Self-Consumption (TIAD). The mechanisms for valorizing shared energy are examined in detail, including the structure of the incentive tariff and the ARERA reimbursement component, providing the normative and tariff reference on which the entire subsequent economic analysis rests. The applied section of the work opens with the characterization of the energy demand of the REC. Real consumption data, extracted from the utility bills of the participating users, are processed through a MATLAB code that implements the monthly-to-hourly disaggregation procedure recommended by the GSE, yielding the hourly load profiles over a full year that serve as input for all subsequent simulations. Only once these profiles are established does the design phase begin: the photovoltaic system of 1 MWp is sized and detailed through a single-line diagram covering all main components like modules, inverters, cables and protection devices, followed by the sizing of the electrochemical storage system and, for the scenario involving surplus energy conversion, the PEM electrolyzer. The computational core of the thesis consists of the analysis of four operational scenarios, implemented in MATLAB. For each scenario, energy flows, shares of shared and self-consumed energy and energy performance indicators are evaluated. This analysis is complemented by a comparative techno-economic assessment, which computes discounted cash flows, Net Present Value (NPV) and Payback Time (PBT) for each configuration, with the aim of identifying the most financially efficient solution.

Chapter 2

Fundamentals of Photovoltaic Systems

The energy transition has accelerated significantly in recent years, driven by growing awareness of the need to reduce greenhouse gas emissions and by the urgency of breaking free from dependence on fossil fuels, non-renewable resources destined for depletion and responsible for profound disruptions to global climate equilibrium. Although overall emissions remain high, many analysts believe that with a further push toward renewable energy and clean energy carriers, carbon neutrality by mid-century, while ambitious, is a concretely achievable goal. In this scenario, renewable sources could account for more than 50% of global electricity production before the end of the decade, effectively marking the twilight of the fossil fuel era as the primary source of energy. In this context, the sun represents a resource of extraordinary relevance. At any given moment, the surface of the hemisphere exposed to solar radiation receives more than 50,000 TW of power, an amount of energy roughly ten thousand times greater than humanity's total energy demand. Translating this potential into accessible and manageable electricity lies at the heart of photovoltaic technology development, a technology that stands out for intrinsic qualities that are difficult to match: minimal operating costs, zero emissions during operation, reliability, silent functioning and relatively straightforward installation. Beyond addressing environmental and climate challenges, photovoltaics today represent a concrete economic opportunity and an investment in the well-being of future generations, capable of promoting a more responsible use of the natural resources available to us.

2.1 Energy from the Sun

In the Sun's core, thermonuclear fusion reactions take place ceaselessly at temperatures of millions of degrees, releasing enormous quantities of energy in the form of electromagnetic radiation. Part of this energy reaches the outer atmosphere of the Earth with an average irradiance (solar constant) of approximately 1367 W/m^2 $\pm$ 3%, which varies depending on the Earth-Sun distance (Figure 2.1)[1] and solar activity (sunspots)[9].

Solar irradiance is defined as the intensity of solar electromagnetic radiation incident on a unit area surface [kW/m^2]. This intensity is equal to the integral of the power associated with each frequency value of the solar radiation spectrum. As it passes through the atmosphere, solar radiation is attenuated, since part of it is reflected and absorbed (mainly by water vapour

[1]Because of its elliptical orbit, the Earth is at its closest point to the Sun (perihelion) in December–January and at its furthest point (aphelion) in June–July.

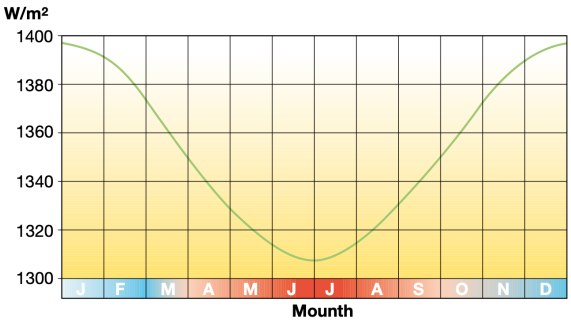


Figure 2.1: Extra-atmospheric radiation

and other atmospheric gases). The radiation that continues is partially scattered by air and by solid particles suspended in the atmosphere (Figure 2.2).

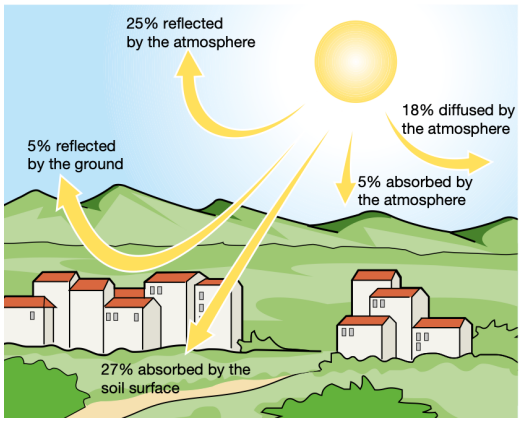


Figure 2.2: Flow of energy between the sun, the atmosphere, and the Earth's surface

Solar radiation is defined as the integral of solar irradiance over a specified time period [kWh/m²]. The radiation reaching a horizontal surface is therefore composed of a direct component, associated with irradiance directly incident on the surface, a diffuse component arriving at the surface from the sky in every direction, and a reflected component from the ground and the surrounding environment of a given surface (Figure 2.3). In winter and under overcast skies, the diffuse component is significantly greater than the direct one. Reflected radiation depends on the ability of a surface to reflect solar radiation and is measured through the albedo coefficient, calculated for each material.

Figure 2.4 shows the Italian solar atlas of annual global horizontal irradiation (GHI) [kWh/m²] [10]. It can be noted that the site of interest for the future design of the PV system is in an excellent location, reaching an annual value of approximately 1700 kWh/m², the energy equivalent of 1 barrel of oil per square metre.

2.2 Operating Principle

A photovoltaic system enables the direct and instantaneous conversion of solar energy into electrical energy without the use of fuel. This technology is based on the photovoltaic effect, a physical phenomenon whereby suitably doped semiconductor materials generate electricity when exposed to solar radiation. The main advantages of photovoltaic systems can be summarized as follows:

- distributed generation at the point of use;
- absence of pollutant emissions during operation;

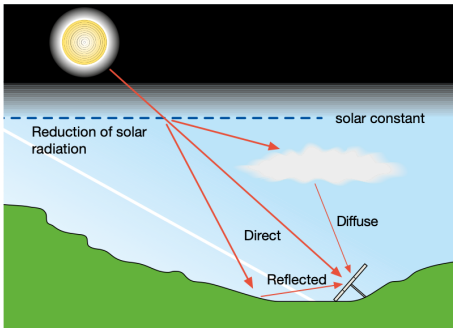


Figure 2.3: Components of solar radiation

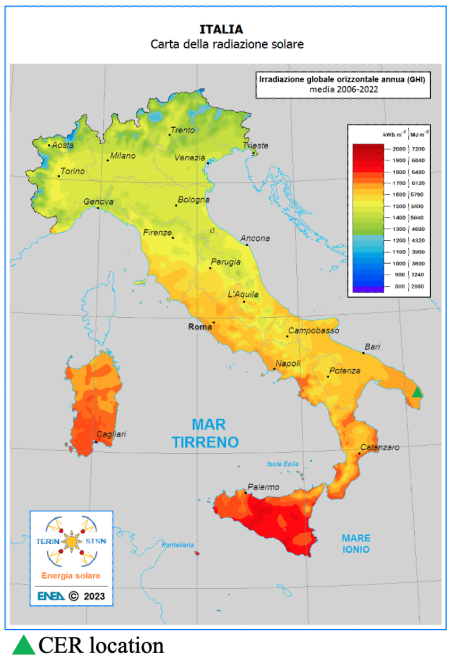


Figure 2.4: Italian solar atlas of annual global horizontal irradiation (GHI)

- reduction in fossil fuel consumption;
- high reliability due to the absence of moving parts, resulting in a typical service life exceeding twenty years;
- low operation and maintenance costs;
- system modularity, allowing power capacity to be increased by adding additional modules according to user requirements.

However, the initial investment cost for the installation of the photovoltaic system remains relatively high, in part because a market that has not yet reached full technical and economic maturity. Furthermore, electricity production is inherently intermittent, as it depends on the variability of the solar resource. The annual electricity production of a photovoltaic system depends on several factors, including: the solar irradiance at the installation site, the tilt and orientation of the modules, the presence of shading and the technical performance of system components, particularly photovoltaic modules and inverters. The main applications of photovoltaic systems include:

- stand-alone systems with energy storage for off-grid users;
- grid-connected systems for low-voltage distribution networks;

- large-scale photovoltaic power plants, typically connected to medium-voltage grids.

A photovoltaic system essentially consists of a generator (photovoltaic modules), a supporting structure for installation on the ground or on buildings, a power conditioning and conversion system, possible energy storage units, electrical panels containing switching and protection devices, and interconnection cables.

2.3 Main components of a photovoltaic system

2.3.1 Photovoltaic Generator

The elementary component of the generator is the photovoltaic cell, in which the conversion of solar radiation into electric current takes place. A photovoltaic module is a set of interconnected photovoltaic cells, protected from the surrounding environment, capable of supplying electrical energy. A photovoltaic panel, on the other hand, is a group of modules mechanically fixed and electrically connected prior to installation on the supporting structure. A set of photovoltaic panels electrically connected in series is called a string. The photovoltaic field (or photovoltaic array) is the set of all the strings of a photovoltaic system and all the components necessary for their operation.

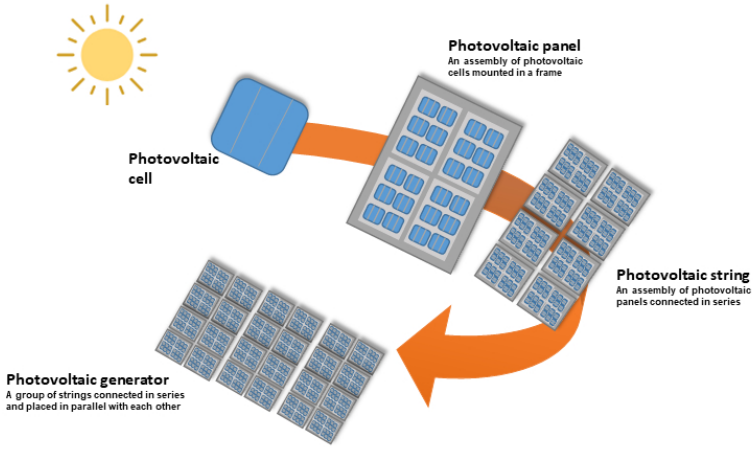


Figure 2.5: From cell to PV array

Within modules, photovoltaic cells are not all identical due to unavoidable manufacturing discrepancies; therefore, two groups of cells connected in parallel may not have the same voltage. Consequently, a circulating current is generated from the group of cells with higher voltage to the one with lower voltage. As a result, part of the power produced by the module is lost within the module itself (mismatch losses). The inequality among cells can also be caused by non-uniform solar irradiance, for example when some cells are shaded, or by their degradation. Such cells behave like a diode that blocks the current produced by the other cells. The diode is subjected to the voltage of the other cells, which may cause junction breakdown with local overheating and damage to the module. Therefore, modules are equipped with bypass diodes that limit this phenomenon by short-circuiting the shaded or damaged portion of the module. Mismatch can also occur between the strings of the photovoltaic field due to differences among modules, uneven irradiance on the strings, shading, and faults in a string. The cells that make up the module are encapsulated using an assembly system that:

- electrically insulates the cells from the external environment;
- protects the cells from atmospheric agents and mechanical stresses;

- resists ultraviolet radiation, low temperatures, temperature fluctuations, and abrasion;
- efficiently dissipates heat, in order to prevent temperature increases from reducing the power output of the module.

These properties must be maintained throughout the expected lifetime of the module. Obviously, at least the barrier on the sunward-side needs to be transparent, and is most commonly a sheet of low-iron tempered glass. The type of interconnection depends on the used solar cell technology: wafer based (c-Si, III-V) or thin-film based (amorphous/microcrystalline silicon, CdTe, copper indium gallium selenide (CIGS), kesterite, perovskite, organic photovoltaics (OPVs), dye-sensitized solar cells (DSSCs), quantum dot). Traditionally, the interconnection between single c-Si solar cells is realized with metal ribbons, generally soldered onto the metal busbars, making part of the cell's outer electrodes. The process to apply the ribbons is called tabbing, whereas stringing is the process of interconnecting cells into strings. Over the years, the c-Si PV industry has developed significant knowledge regarding both, which is nowadays fully automated in production lines. The strings of cells are then aligned and prepared for the encapsulation in the layup phase. The general module components (in order of stacking) are the front module glass, the first layer of encapsulant (traditionally ethylene–vinyl acetate, EVA), the strings of cells, the second layer of encapsulant (again EVA) and the rear barrier, which can be a polymeric back sheet (generally white, but also black or transparent) or a second glass sheet. The function of two encapsulant layers is to integrate all components in a sealed, monolithic package, and to providing structural stability as well as a barrier toward the ambient and environmental factors. Generally, the encapsulation process is carried out by vacuum lamination, melting or cross-linking the encapsulant and sealing the module with temperatures ranging between 100 and 150 °C. The majority of the modules are completed by a frame, usually made of aluminum, to fix the module to the installation structure, often a rack. A junction box, usually sealed at the rear of the module, is used to secure the external leads to the terminals of the modules (often string ends protruding through the back sheet). Perovskite/silicon tandem modules require some extra components when compared with conventional silicon modules, in particular the use of an edge sealant and a larger number of bypass diodes. Crystalline silicon (c-Si) modules have experienced the widest adoption over time and remain the most commonly used technology in installed photovoltaic (PV) systems. Figure 2.6.a illustrates the cross-section of a standard crystalline silicon module, while Figure 2.6.b presents the main components of a tandem module[11].

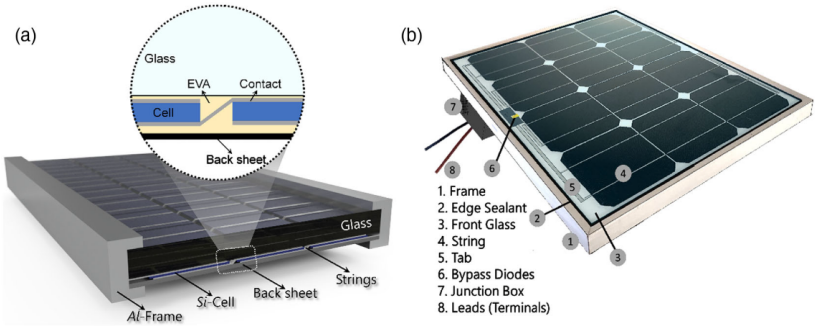


Figure 2.6: a) Cross section of a traditional silicon module and its constituents. b) Schematic representation of a tandem module with pseudo-squared M2 wafers. Often, the bypass diodes are incorporated in the junction box.

Over the past decade, industrial manufacturing of single-junction crystalline silicon (c-Si) photovoltaic modules has undergone significant advancements, particularly in terms of efficiency, design optimization and overall performance. During this period, the power conversion efficiency (PCE) of commercial monocrystalline silicon modules improved impressively from

15% to >21%; at the same time, the typical module area and stability also increased. Higher module PCE comes from improvements in device PCE (enabled by new generations of cell technologies, such passivated emitter, rear cells and passivating-contact cells) and module design, which is mainly aimed at reducing cell-to-module (CTM) losses. The latter is usually accomplished by increasing the device packing density, for instance by using larger wafers (typically at least 6 x6 inches nowadays), half-cut cell configurations, and shingling techniques[2], which minimize inactive areas and resistive losses. Larger modules, nowadays with a nameplate power up to 600 Wp, can also result in lower balance-of-system (BOS) and shipping costs (the typical module size is now often designed toward optimal filling of standard cargo containers). Finally, several companies are already providing more than 25 years of warranty for their new products; some even aim at 50 years of warranty. An additional important technological advancement concerns the development of bifacial photovoltaic cells and modules[11]. Until a few years ago, photovoltaic devices were designed to capture solar radiation exclusively on the front side. However, recent innovations have enabled the absorption of light on both the front and rear surfaces. Bifacial modules can therefore increase the overall energy yield of a photovoltaic system by exploiting the radiation reflected from the underlying surface onto the rear side of the module. This reflected component primarily depends on the ground albedo, with typical energy gains estimated at approximately +5% for installations over grass, +10% over sand, and up to +20% over highly reflective (e.g., white) surfaces[9]. Collectively, these advances in performance, cost, and warranty, all result in ever decreasing LCOE values, which set a continuously increasing ambitious benchmark to be met by emerging PV technologies, aimed at the residential and utility-scale markets.

2.3.2 Inverter

The power conditioning and control system consists of an inverter that converts direct current (DC) into alternating current (AC), while regulating the quality of the output power for grid injection, also by means of an internal L–C filter integrated within the inverter itself. Figure 2.7 shows the basic operating schematic of an inverter. The transistors, used as static switches, are driven by an opening–closing control signal which, in its simplest form, would produce a square-wave output.

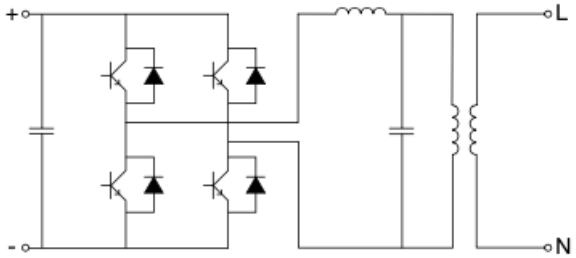


Figure 2.7: Principle diagram of a single-phase inverter

To approximate a sinusoidal waveform as closely as possible, a more advanced technique known as Pulse Width Modulation (PWM) is employed. This method enables control over both the frequency and the RMS value of the output waveform (Figure 2.8).

[2]Shingling technology involves cutting standard solar cells into narrow strips and overlapping them like roof tiles using an electrically conductive adhesive (ECA). This eliminates the need for traditional ribbon busbars and grid gaps, maximizing the active absorber area while mitigating micro-crack formation and resistive losses.

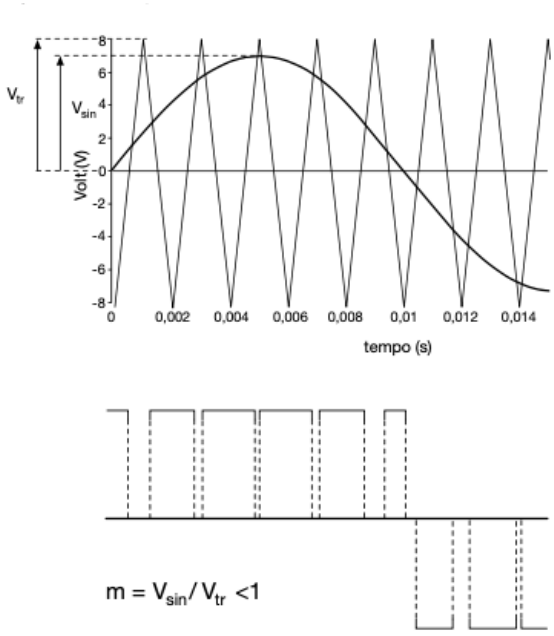


Figure 2.8: Operating principle of the PWM technique

The power delivered by a photovoltaic generator depends on its operating point. To maximize the energy produced by the system, the generator must be matched to the load so that the operating point continuously corresponds to the maximum power point. To this end, a controlled chopper, referred to as a Maximum Power Point Tracker (MPPT), is implemented within the inverter. This device continuously identifies the voltage–current pair at which the generator delivers maximum power. Starting from the I–V curve of the photovoltaic generator shown in the Figure 2.9:

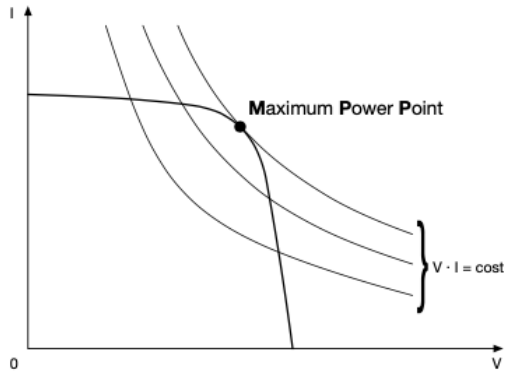


Figure 2.9: I-V curve of the PV generator with maximum power point

The maximum power transfer point corresponds to the point of tangency between the I–V characteristic, for a given value of solar irradiance, and the hyperbola defined by the equation:

$$V \cdot I = \text{const} \tag{2.1}$$

. Commercially available MPPT devices identify the maximum power point on the generator's characteristic curve by introducing small periodic variations in the load, which cause changes in voltage and current values, and by evaluating whether the new $I \cdot V$ product is greater or smaller than the previous one. If an increase is observed, the load conditions continue to be varied in the same direction. Otherwise, the conditions are adjusted in the opposite direction. Due to the required performance characteristics, inverters for stand-alone systems and for grid-connected systems must have different features:

- in stand-alone systems, inverters must be able to supply an AC-side voltage that remains as constant as possible despite variations in generator output and load demand;
- in grid-connected systems, inverters must reproduce the grid voltage as accurately as possible, while simultaneously optimizing and maximizing the energy production of the photovoltaic modules.

2.3.3 Overcurrent and Overvoltage protection

When designing a photovoltaic system, it is necessary to provide, where necessary, protection for the various sections of the system against overcurrents and overvoltages. The following section first provides the conditions for overcurrent protection in the photovoltaic system upstream (DC side) and downstream (AC side) of the inverter; the methods for protecting the system from potential damage caused by direct or indirect lightning strikes are then described.

DC side overcurrent protection

Once the string cables have been sized, it is necessary to evaluate when it is necessary to provide overcurrent protection. The CEI 64-8 part 7:2023 standard describes the requirements for protecting DC cables from overcurrents.

String protection

The standard distinguishes two main cases regarding overcurrent protection of strings:

- CASE A – 1 or 2 strings connected in parallel: in this case, the standard does not require the use of any overcurrent protection device;
- CASE B – parallel connection of more than 2 strings: in this case, overcurrent protection devices must be provided for each of the parallel strings. This is necessary to prevent the maximum reverse current from reaching values that exceed the maximum reverse current that the photovoltaic module itself can withstand ($I_{MOD_MAX_OCPR}$).

In Case A, where the installation of protection devices is not required (and thus a direct parallel connection of (N_s) strings is present), it is necessary to verify that the string cables have an adequate cross-section so that they are self-protected and can withstand any reverse currents generated by the ((N_s - 1)) strings connected in parallel with the string under consideration; therefore, the following condition must be verified:

$$(N_s - 1)\, {I_{\text{SC,max,string}}}^3 \leq {I_z}^4 \tag{2.2}$$

In Case B, where the installation of overcurrent protection devices is required, these must be installed on each string on both the positive and negative poles. It is also necessary to determine the rated current (I_n) of the device. The CEI 64-8 Part 7 specifies how the rated current (I_n) of the device must be selected.

The rated current (I_n) of the device must be:

$$I_n \geq 1{,}1 \cdot I_{sc,\text{max,string}} \tag{2.3}$$

$$I_n \leq I_{\text{MOD_MAX_OCPR}} \tag{2.4}$$

$$I_n \leq I_z \tag{2.5}$$

The overcurrent protection devices required by the standard must be gPV type fuses.

[3]The short circuit current of the string (i.e. the maximum current that the panels can generate if shorted)

[4]DC current carrying capacity of the string cable

Protection of PV sub-arrays

The cables of the PV sub-arrays[5] must also be protected against overcurrents. As for strings, the standard distinguishes two main cases regarding overcurrent protection:

- CASE A – maximum of 2 sub-arrays connected in parallel: in this case, the standard does not require the use of any overcurrent protection device, provided that the following condition is satisfied:
$$I_{\text{SC,max,sub-array}} \leq I_z \tag{2.6}$$
- CASE B – parallel connection of more than 2 sub-arrays: in this case, overcurrent protection devices must be provided for each of the sub-arrays connected in parallel.

In Case B, where the installation of overcurrent protection devices for sub-array cables is required, these devices must be installed on each sub-array in such a way that both the positive and negative poles can be interrupted. It is also necessary to define the rated current (I_n) of the device. CEI 64-8 Part 7 specifies how the rated current (I_n) of the device must be selected. The rated current (I_n) of the device must be:

$$1{,}1 \cdot I_{SC,\text{max,sub-array}} \leq I_n \leq I_z \tag{2.7}$$

In any case, each cable of the (N_a) sub-arrays must be self-protected against reverse currents coming from the ((N_a - 1)) sub-arrays connected in parallel, and therefore the following condition must be satisfied:

$$(N_a - 1)\, I_{SC,\text{max,sub-array}} \leq I_z \tag{2.8}$$

The devices for overcurrent protection on the DC side of the PV sub-arrays may be:

- gPV fuses compliant with CEI EN 60269-6;
- circuit breakers compliant with CEI EN 60947-2 or CEI EN 60898-2.

These devices, in addition to having a rated current (I_n) as defined above, must satisfy the following requirements:

- The operating voltage (U_e) must be greater than the maximum open-circuit voltage ($U_{OC,max}$) of the PV sub-array;
- The rated breaking capacity must be greater than or equal to ($I_{SC,MAX,sub-array}$);
- They must be bidirectional devices.

Protection of PV arrays

The cables of the PV arrays (i.e., the cables connecting the second-level string combiner boxes to the DC input of the inverter) must be self-protected against overcurrents, and therefore the following condition must be satisfied:

$$I_{\text{SC,max,array}} \leq I_z \tag{2.9}$$

In the case where the inverter allows the parallel connection of multiple PV arrays at its input, the array cables must also be protected against overcurrents, and the same considerations made for sub-arrays in Case B of the previous section apply. The devices for overcurrent protection on the DC side of the PV arrays may be:

[5]The cables connecting the first-level string combiner boxes to the second-level string combiner boxes

- gPV fuses compliant with CEI EN 60269-6;
- circuit breakers compliant with CEI EN 60947-2 or CEI EN 60898-2.

These devices, in addition to having a rated current (I_n) as defined above, must satisfy the following requirements:

- The operating voltage (U_e) must be greater than the maximum open-circuit voltage ($U_{OC,max}$) of the PV array;
- The rated breaking capacity must be greater than or equal to ($I_{SC,MAX,array}$);
- They must be bidirectional devices.

AC side overcurrent protection – contribution of the PV inverter to short-circuit current

AC electrical lines located downstream of the PV inverter must be protected against short circuits by means of circuit breakers. These circuit breakers shall be installed on the AC line as close as possible to the inverter output (in order to effectively protect the AC line) and must be capable of interrupting, within a time shorter than that which would bring the cable to its maximum admissible temperature, all fault currents that may occur at any point along the AC electrical line. In generating systems (and therefore also in photovoltaic systems), it must always be considered that a short circuit occurring on the AC lines is not only fed by the utility grid to which the system is connected, but also by the generating source itself (in the present case, the PV inverter). The inverter contributes a relatively small amount of short-circuit current: in general, the maximum current that the inverter can supply is limited by the nature of the photovoltaic source and can typically be estimated as approximately 10% above the inverter's rated current. The inverter short-circuit current contribution is usually specified by the manufacturer in the technical datasheet. In any case, the value of the inverter short-circuit current on the AC side is negligible compared to the fault current provided by the distribution grid. This means that, when sizing the circuit breaker for short-circuit protection, the reference value is effectively the grid's short-circuit current. Protection devices must therefore be selected so as to limit the let-through thermal energy to values tolerable by the AC cable. In the event of a short circuit on the DC side of the inverter, the DC input voltage drops instantaneously and the inverter shuts down and disconnects from the grid. Typically, inverter shutdown times are of the order of a few milliseconds, while disconnection times may be of the order of a few tens of milliseconds. During the interval between shutdown and disconnection, the internal AC capacitors of the inverter, if involved, contribute to the short-circuit current until they are fully discharged. Therefore, in conclusion, in the case of a DC-side short circuit of the inverter, the inverter's contribution to the AC-side short-circuit current is negligible.

Selection of switching and isolating devices

It is advisable to install an isolating device on each string in order to allow inspection or maintenance activities on the string itself without having to shut down other parts of the photovoltaic system (CEI Guide 82-25). In addition, the inverter must be capable of being isolated both on the DC side and on the AC side, in order to allow maintenance operations by excluding both power sources (the grid and the photovoltaic generator) (CEI 64-8/7). On the DC side of the inverter, a load-break switch (switch-disconnector) must be installed. On the AC side, a general isolating device must be provided. The protection device installed at the grid connection point may be used for this purpose; however, if this device is not located in close proximity to the inverter, it is preferable to install an additional isolating device immediately downstream of the inverter.

Surge protection

Photovoltaic systems, which are increasingly widespread, very often require lightning protection due to their location, sensitivity, and economic value. Overvoltages can be caused by direct lightning strikes, indirect lightning effects, and switching surges. CEI 64-8 Part 4, specifies the requirements for protecting electrical installations against transient overvoltages of atmospheric origin as well as those caused by switching operations. Protection against overvoltages is made mandatory by CEI 64-8 in cases where the effects of such overvoltages may lead to consequences affecting:

- human life;
- public services and cultural heritage;
- commercial or industrial activities;
- a large number of people.

In all other cases, it is necessary to determine whether surge protection devices are required by performing a risk assessment, as extensively described in the CEI 81-10 standards, Part 2. Once the risk assessment establishes the need for surge protection, CEI 64-8 Part 7 provides guidance to determine whether surge protection is required on the DC side. The parameter used to determine the need for DC-side surge protection is the length (L) (in meters) of the maximum cable route between the inverter(s) and the connection points of the photovoltaic module strings. This maximum length (L) is compared with the critical length (L_{crit}); the critical length is a tabulated value defined by the same standard as a function of the parameter (N_g), which represents the ground flash density (lightning strikes/km^2/year) in the area of the supply line and connected structures.
If $L \geq L_{\text{crit}}$, the standard requires the installation of surge protection devices on the DC side of the photovoltaic system.
If L $< L_{crit}$, the standard does not require the installation of surge protection devices on the DC side of the photovoltaic system.

The system is designed exclusively to protect:

- the inverter and its interfaces on both the DC and AC sides;
- the DC current generator;
- the equipment for system control and monitoring.

Furthermore, the cabling that must be protected against direct lightning strikes includes:

- the AC power cables from the main distribution board to the inverter;
- the DC cables from the DC generator to the inverter;
- the signal cables connecting the sensors to the control unit.

Equipotential bonding

Where equipotential bonding of the metallic support structures of the photovoltaic modules is required, the equipotential bonding conductor must be connected to any earthing terminal, as specified in CEI 64-8 Part 7. The minimum cross-section of equipotential bonding conductors must comply with the requirements of CEI 64-8 Part 5.

LPS (Lightning Protection System)
The installation of a photovoltaic system on a building, unless it significantly alters the building's geometric characteristics, does not in itself increase the risk of direct lightning strikes. Therefore, the installation of a photovoltaic system does not imply the need to install a Lightning Protection System (LPS), unless one is already present. The need for an LPS must be assessed in accordance with CEI EN 62305-2; if the installation of an LPS is required, it must be designed and installed in accordance with CEI EN 62305-3.

Ground-mounted photovoltaic systems
Let us analyze in slightly more detail the surge protection for a ground-mounted PV system, as it is included in the feasibility study of the Renewable Energy Community (REC) considered in this work. Ground-mounted systems are generally quite extensive and are typically located in rural and isolated areas. They are usually supplied by a three-phase medium-voltage line, which is not shielded and may extend for several kilometers. The line reaches an MV/LV transformer, downstream of which the inverters are installed. It should be noted that a telecommunications line is often also present within the PV system for control and monitoring purposes. First of all, similarly to what is done for buildings, the collection area is evaluated in order to determine whether the structure is exposed to lightning or not. If the structure is not exposed, the DC lines must still be protected. The first step is to provide equipotential bonding between the structure supporting the PV modules and the equipotential bar located near the inverter. This connection should be routed as close as possible to the DC cable in order to minimize the loop area. The CEI EN 62305-4 standard allows the calculation of the induced voltage in such a loop and, consequently, the proper sizing of the SPDs (Surge Protective Device) if the withstand level is exceeded. However, this calculation can be avoided by always installing Class II SPDs near the modules on one side and near the inverter on the other. These Class II SPDs must have a nominal discharge current (I_n) of at least 5 kA, while the required protection level must be determined by considering the withstand capability of the equipment and the installation distances. The above considerations apply to the common case of insulated PV modules. However, if the modules are grounded, Class II SPDs are no longer sufficient and must be replaced with Class I SPDs. In this case, the impulse current (I_{imp}) must be calculated, as specified in the standards, by distributing the lightning current. The required protection level, however, remains unchanged. To protect the AC distribution, Type 1 SPDs are generally installed on the AC side of the inverters. If the structure is exposed, a Lightning Protection System (LPS) must be implemented. An LPS of Class IV or III (LPL III–IV, corresponding to a lightning current of 100 kA, 10/350 μs) is generally sufficient. The LPS can be designed as isolated from the PV system.

2.3.4 Protection against direct and indirect contact

Protection against direct contact

Direct contact is defined as the event resulting from a person coming into contact with an energised conductor within the electrical system. With regard to protection against direct contact, Standard CEI 64-8 Part 7 establishes that all electrical equipment connected to the direct current (DC) side of a photovoltaic system must be considered live even when the alternating current (AC) side is isolated, i.e. when the system is disconnected from the grid. The photovoltaic generator remains energised throughout its exposure to solar radiation, regardless of the state of the AC side. The same standard prescribes that protection against direct contact on the DC side shall be achieved by one of the following measures:

- double or reinforced insulation;

- safety extra-low voltage (SELV and PELV[6]).

For grid-connected photovoltaic systems, given the open-circuit voltage (V_{oc}) levels of the photovoltaic generator, the applicable protective measure against direct contact is double or reinforced insulation. Specifically, CEI 64-8 Part 7 requires the use of Class II equipment or equivalent up to the DC connection point of the photovoltaic converters (inverters). It follows that, in grid-connected photovoltaic systems, photovoltaic modules, wiring and DC combiner boxes must comply with Class II or equivalent requirements.

Protection against indirect contact

An indirect contact is defined as an event caused by a person coming into contact with an exposed conductive part. It is the result of an insulation fault that generates a fault current. CEI 64-8 provides the requirements for achieving protection against indirect contact.

Earthing (grounding)

The concept of earthing in a photovoltaic system may refer both to exposed conductive parts (e.g., the metallic structure of the modules) and to the electrical generation system (i.e., the active parts of the photovoltaic system, such as the cells). A photovoltaic system can be connected to earth only if it is galvanically isolated from the electrical grid (e.g., by means of a transformer). An electrically isolated photovoltaic system may appear, at first glance, to be safer for people touching an active part; however, in reality, the insulation resistance of the active parts to earth is not infinite, and therefore a person can still be traversed by a current that closes through this resistance. This current increases with the system's voltage to earth and with the system size, since the insulation resistance to earth decreases. Moreover, the natural aging of insulating materials, over time and in the presence of humidity, further reduces the insulation resistance. Therefore, in large-scale systems, the current flowing through a person in contact with an active part may cause electric shock, and thus the advantage of isolated systems compared to earthed systems is significant only in small installations.

Systems with transformer

In systems with a transformer, in addition to analyzing whether the photovoltaic system is isolated or earthed, it is necessary, for the purpose of protection against indirect contact, to distinguish between exposed conductive parts located upstream and downstream of the transformer.

Exposed conductive parts upstream of the transformer

System with IT configuration

In this type of system, the active parts are insulated from earth, while the exposed conductive parts are connected to earth (Fig. 2.10).
In photovoltaic systems where the DC side operates with an isolated neutral (IT configuration), protection against earth faults is structured on two distinct levels. In the event of a first earth fault, CEI 64-8 requires that the earthing resistance of the exposed conductive parts be sufficiently low to limit the touch voltage to 120 V with respect to the fault current.

[6]SELV (Safety Extra-Low Voltage) refers to a system with a voltage low enough to prevent electric shock and with no connection to earth. PELV (Protective Extra-Low Voltage) also operates at extra-low voltage levels but may have a connection to earth while still ensuring protection against electric shock.

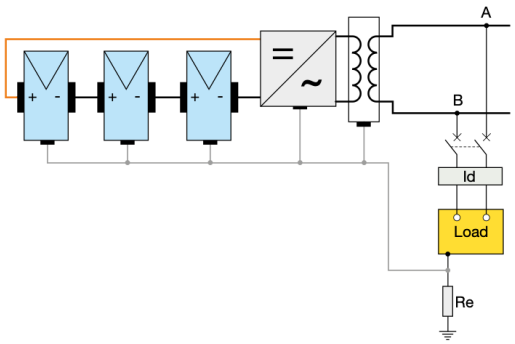


Figure 2.10: System with IT configuration

Since this current is typically very small in systems of limited size, this requirement is generally satisfied without the need for additional design measures. The second critical scenario is that of a double earth fault: if two simultaneous faults occur on conductors of opposite polarity, the photovoltaic generator, behaving as a current source, may impose a dangerous voltage on the interconnected exposed conductive parts. In this case, compliance with the safety condition depends on the product of the short-circuit current of the involved cells and the resistance of the equipotential bonding between the exposed parts. For small-scale systems, this condition is typically satisfied inherently. In large-scale systems, however, an active approach is required: an insulation monitoring device, either integrated into the inverter or installed externally, must detect and signal the first fault before the second occurs, thereby eliminating the hazardous condition at its origin.

System with TN configuration

In this type of system, both the active parts and the exposed conductive parts are connected to the same earthing system (i.e., the earthing system of the user installation). In this way, a TN system is established on the DC side (Fig. 2.11).

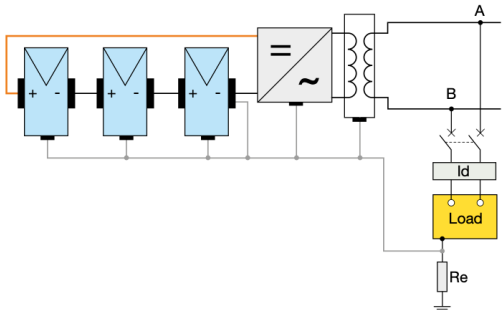


Figure 2.11: System with TN configuration

In the event of an earth fault, a short-circuit current is established, which should be interrupted by overcurrent protection devices. However, this approach presents a specific critical issue in photovoltaic systems: the PV generator, operating as a current source, produces fault currents whose magnitude differs only slightly from the nominal operating current. This behavior makes traditional overcurrent protection devices potentially inadequate to promptly detect and interrupt the fault, resulting in the persistence of a hazardous condition for people. From a safety standpoint, this situation is therefore comparable to a double fault in an IT system, since in both cases the fault current may not reach the tripping thresholds of conventional protection devices.

Exposed conductive parts downstream of the transformer

Utility–user system with TT configuration

The exposed conductive parts belonging to the user installation are protected by a residual current device (RCD) installed at the origin of the installation (Fig. 2.12), and are therefore protected with respect to both the utility grid and the photovoltaic generator.

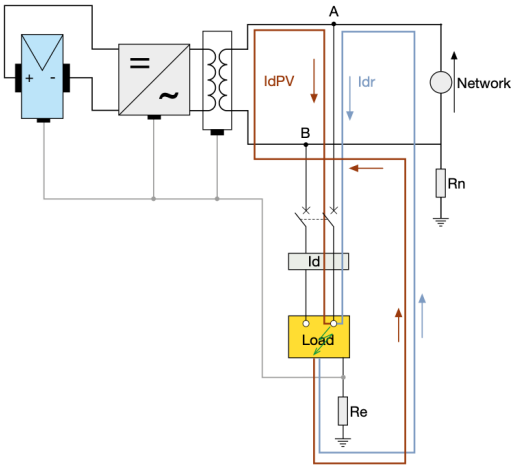


Figure 2.12: TT system: protection of exposed conductive parts in the user installation by means of a residual current device (RCD) installed at the origin of the installation.

For the exposed conductive parts located upstream of the A–B connection point, such as, for example, the transformer enclosure or the inverter enclosure if the transformer is integrated, an additional RCD must be installed as shown in Fig. 2.13. This device detects leakage currents originating from both the grid and the photovoltaic generator. When the RCD trips due to an earth fault current, the inverter enters standby mode due to the loss of grid voltage.

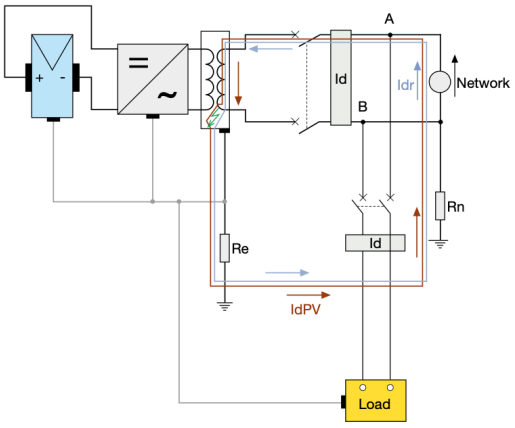


Figure 2.13: TT system: protection of exposed conductive parts located upstream of the A–B connection point using RCD

Utility–user system with TN configuration

If the utility–user system is of the TN type, residual current devices are not required for either supply condition (i.e., whether supplied by the grid or by the photovoltaic generator), provided that the fault current on the AC side is sufficient to ensure the operation of overcurrent protection devices within the time limits prescribed by the standard (Fig. 2.14).

Transformerless systems

In the absence of a galvanic isolation transformer between the photovoltaic system and the grid, the photovoltaic system must have its active parts insulated from earth and effectively becomes an extension of the supply network, which typically has an earthed point (TT or TN system).

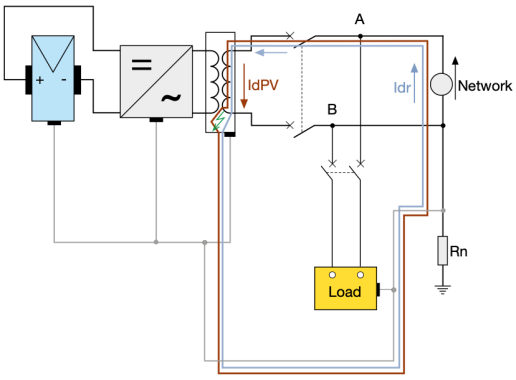


Figure 2.14: TN system: protection of exposed conductive parts without using RCD

On the DC side, an earth fault involving exposed conductive parts causes the operation of the residual current device (RCD) installed downstream of the inverter (Fig. 2.15). Following the tripping of the RCD, the inverter enters standby mode due to the loss of grid voltage; however, the fault remains energized by the photovoltaic generator. For DC-side earth faults and for faults affecting exposed conductive parts upstream of the A–B connection point, the RCD located downstream of the inverter is subjected to a differential current that is not purely alternating. Therefore, this device must be of Type B[7], unless the inverter is designed in such a way that it does not inject DC earth fault currents (CEI 64-8/7).

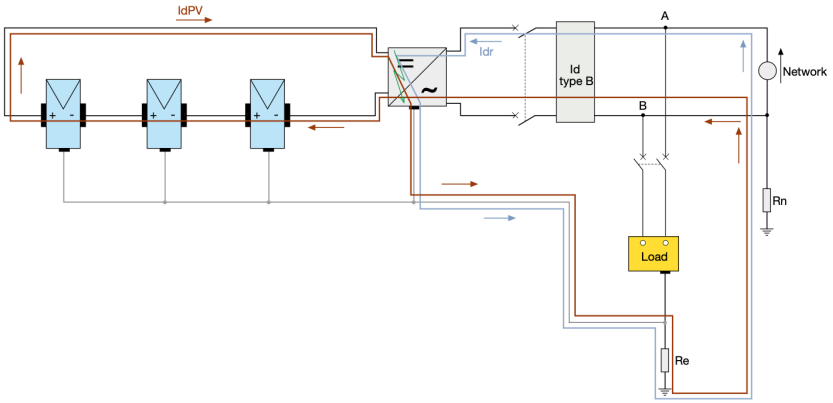


Figure 2.15: Transformerless systems

2.3.5 Classification of PV Systems

Based on their mounting system, photovoltaic systems can be classified as:

Ground-mounted systems

Ground-mounted photovoltaic systems can in turn be divided into 2 macro-categories:

- Fixed systems: systems built on fixed support structures.
- Tracking systems: systems built on structures capable of moving to follow the sun, thereby increasing the solar radiation incident on the photovoltaic modules. Solar trackers can be single-axis, when only the azimuth of the modules is varied during the day based on the position of the sun, or dual-axis, when both the azimuth and the tilt of the modules are varied during the day based on the position of the sun.

[7]A type B residual current device (RCD) is capable of detecting the following types of earth fault currents: alternating current (AC), pulsating unidirectional current, and direct current (DC).

Rooftop systems
In recent years, the installation of PV systems on building rooftops has made enormous strides. Broadly speaking, three macro-types of rooftop PV systems can be defined:

- Integrated PV system (BIPV): PV modules replace, in whole or in part, the function of the architectural elements of buildings, such as coverings and transparent or semi-transparent surfaces on rooftops. PV modules are designed and built not only to perform the function of generating electricity, but also have architectural functions, such as: mechanical rigidity or structural integrity; protection against primary atmospheric impacts: rain, snow, wind, hail; energy efficiency, such as shading, daylighting, thermal insulation; fire protection; noise protection; separation between interior and exterior environments; safety, shelter, or protection. This macro-type can be defined as BIPV (Building Integrated PV).

- Partially integrated PV system: PV modules are fixed to buildings and structures without replacing the construction materials of the structures themselves. The modules occupy the roof surface and are installed so as to be coplanar with the tangential plane of the roof. This macro-type can be defined as BAPV (Building Applied PV).

- Non-integrated PV system: The modules are positioned on the external surfaces of building envelopes, on buildings and structures for any function and purpose. The modules are not coplanar with the tangential plane of the roof. In any case, the rooftop mounting system must be installed applying good engineering practices and respecting the intended use information of its components.

Photovoltaic systems may or may not be connected to the electricity distribution grid. Based on this aspect, photovoltaic systems can be classified as:

Grid-connected photovoltaic systems
These are systems permanently connected to the electricity distribution grid, to which the energy produced is fed after conversion from direct current to alternating current by means of an inverter. The connection can occur at low voltage in accordance with standard CEI 0-21, at medium voltage in accordance with CEI 0-16, or at high voltage in compliance with the Grid Code, with particular reference to Annex A.68. The energy generated is primarily used to power local loads, while any surplus is fed into the grid; during periods of no solar irradiance, the user instead draws the necessary energy from the grid itself. This configuration allows operation without storage systems, using the grid as a balancing element between production and demand. Grid-connected systems also promote distributed generation, reducing transmission losses and helping to decrease peak power demand from the grid during daytime hours of higher consumption.

Island photovoltaic systems (also known as off-grid or stand-alone)
Island photovoltaic systems, also known as off-grid or stand-alone, are not connected to the electricity distribution grid and operate autonomously. The energy produced by the photovoltaic modules is stored in an energy storage system, generally consisting of batteries, which ensures power supply to the loads even during nighttime hours or during periods of low solar radiation. Since the photovoltaic generator provides direct current, if the loads require alternating current, the installation of an inverter is necessary. Such systems are particularly advantageous in isolated or hard-to-reach areas of the electricity grid, where they represent an alternative to traditional generator sets. In these configurations, the photovoltaic array is usually oversized to allow, during hours of solar irradiance, both direct powering of the loads and battery recharging, while maintaining an adequate safety margin to cope with periods of reduced solar energy availability.

Hybrid photovoltaic systems
Hybrid photovoltaic systems can be connected in parallel to the distribution grid but can also operate off-grid and power loads directly.

2.4 Modeling and Energy Production of Photovoltaic Systems

2.4.1 Equivalent Circuit of the Cell

A photovoltaic cell can be modeled as a current source and represented by the equivalent circuit shown in Figure 2.16. The output terminal current I is equal to the current generated by the photovoltaic effect I_g from the ideal current source, minus the diode current I_d and the leakage current I_l. The series resistance R_s represents the internal resistance to the flow of the generated current and depends on the thickness of the P-N junction, the presence of impurities, and contact resistances. The leakage conductance G_l accounts for the current flow to ground during normal operation. In an ideal cell, R_s=0 and G_l=0. Conversely, in a high-quality silicon cell, typical values are $R_s = 0{,}05 \div 0{,}10\,\Omega$ and $G_l = 3 \div 5\,\text{mS}$. The conversion efficiency of the photovoltaic cell is significantly affected even by small variations in R_s, whereas it is much less sensitive to variations in G_l.

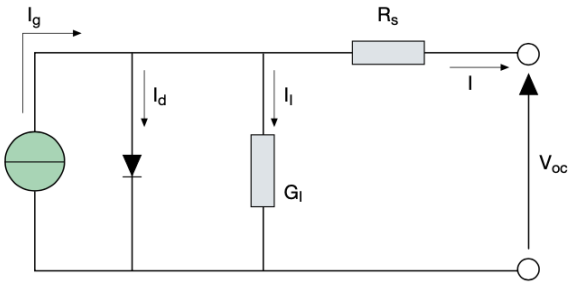


Figure 2.16: Equivalent Circuit of the Cell

The open-circuit voltage V_{oc} occurs when the load does not draw any current ($I = 0$) and is defined by the following relationship:

$$V_{oc} = \frac{I_l}{G_l} \tag{2.10}$$

The diode current is given by the classic expression for forward current:

$$I_d = I_D \left(e^{\frac{QV_{oc}}{AkT}} - 1 \right) \tag{2.11}$$

where:

- I_D is the diode saturation current;
- Q is the electron charge ($1{,}6 \times 10^{-19}\,\text{C}$);
- A is the diode ideality factor, which depends on the recombination factors within the diode (for crystalline silicon, $n \approx 2$);
- k is the Boltzmann constant ($1{,}38 \times 10^{-23}\,\text{J/K}$);
- T is the absolute temperature in Kelvin (K).

The current delivered to the load is therefore given by the expression:

$$I = I_g - I_d - I_l = I_g - I_D \left(e^{\frac{QV_{oc}}{AkT}} - 1 \right) - G_l V_{oc} \tag{2.12}$$

The last term, the leakage current to ground I_l, is negligible in common cells compared to the other two currents. The diode saturation current can therefore be determined experimentally by applying the open-circuit voltage V_{oc} to a cell under dark conditions and measuring the current flowing through the cell.

2.4.2 Voltage-Current Characteristic Curve of the Module

The voltage-current (V-I) characteristic curve of a PV module is shown in Figure 2.17.

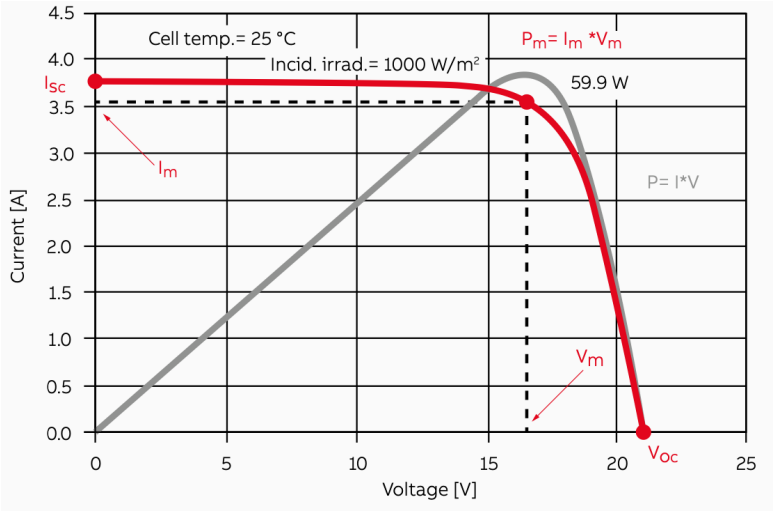


Figure 2.17: Voltage-Current Characteristic Curve of the Module

Under short-circuit conditions, the current generated by the module is at its maximum and corresponds to I_{sc} (short-circuit current). Under open-circuit conditions, the voltage is at its maximum and corresponds to V_{oc} (open-circuit voltage). In both short-circuit and open-circuit conditions, the electrical power generated by the cell/module is zero; in all other conditions, as the voltage increases, the power output also increases: it first reaches the Maximum Power Point (P_m) and then falls rapidly back to zero at open-circuit. A key parameter for comparing the performance of different cells is the Fill Factor (FF), defined as:

$$FF = \frac{P_{max,\text{real}}}{P_{max,\text{ideal}}} = \frac{I_m \cdot V_m}{I_{sc} \cdot V_{oc}} \tag{2.13}$$

2.4.3 Variation in Energy Production

The main factors influencing the electrical energy produced by a photovoltaic (PV) system are:

- Irradiance;
- Module temperature;
- Air Mass (AM);
- Shading.

Irradiance

The characteristic curve of a PV module varies according to the irradiance on the module surface (W/m^2), as shown in Figure 2.18. When irradiance decreases, the generated current decreases proportionally; meanwhile, the open-circuit voltage (V_{oc}) also decreases, but significantly less so.

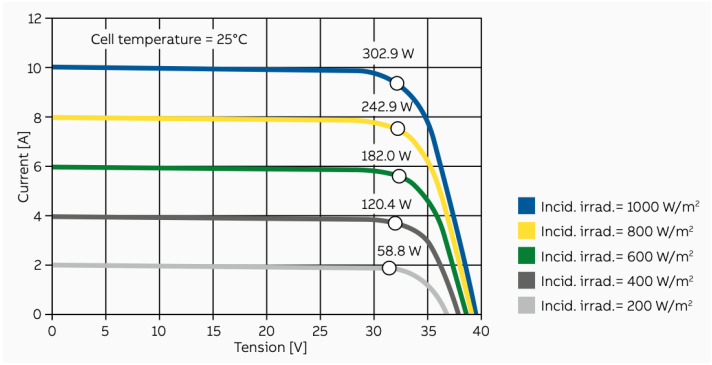


Figure 2.18: Variation of the characteristic curve I-V of a photovoltaic module as a function of the irradiance on the plane of the module

Temperature

The characteristic curve of a PV module varies as a function of temperature (Figure 2.19).

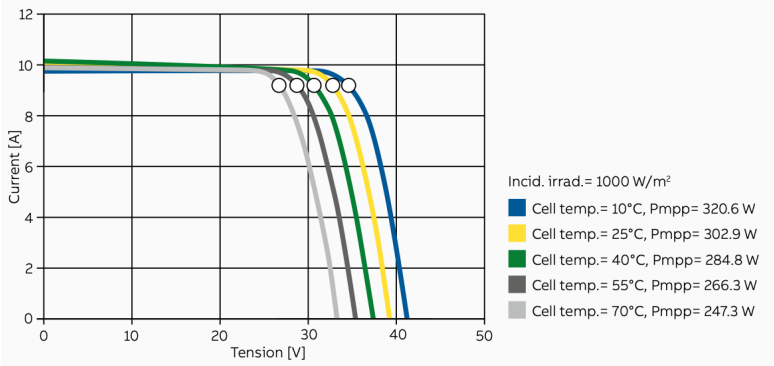


Figure 2.19: Variation of the characteristic curve I-V of a photovoltaic module as a function of temperature

As the temperature of the PV modules increases, the current remains nearly constant, whereas the voltage decreases, leading to a reduction in the module's performance in terms of electrical power output.

Air Mass

Air Mass (AM) also affects PV energy production, as it indicates the variation in the solar radiation power spectral density. The solar spectrum varies depending on the air density. In Figure 2.20, the yellow area represents the solar radiation perpendicular to the Earth's surface absorbed by the atmosphere, while the blue area represents the actual solar radiation reaching the surface. The difference between these curves illustrates the spectral variation caused by the air mass. The Air Mass index (AM) is calculated as follows:

$$AM = \frac{P}{P_0 \sin(h)} \tag{2.14}$$

where P is the atmospheric pressure measured at the specific location and time [Pa], P_0 is the reference atmospheric pressure at sea level (1.013×10^5 Pa), and h is the solar elevation angle (or altitude angle) above the local horizon.

Notable values of AM are:

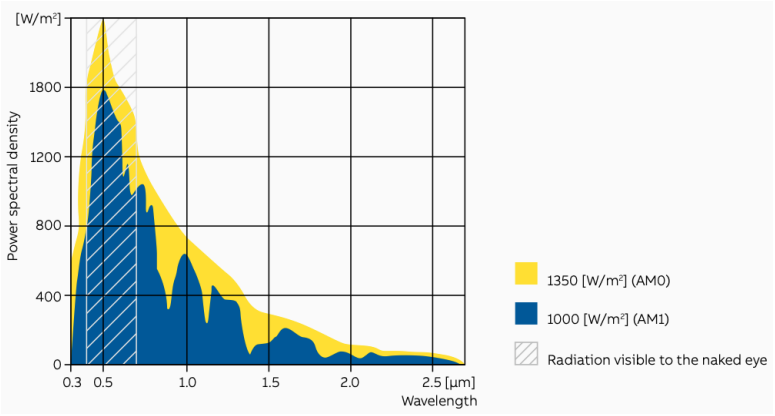


Figure 2.20: Spectrum of solar radiation

- $AM = 0$: outside the atmosphere ($P = 0$);
- $AM = 1$: at sea level with the Sun at the zenith ($P = P_0, h = 90°$);
- $AM = 2$: at sea level with the Sun at an elevation of 30° ($P = P_0, h = 30°$).

Shading

Considering the area occupied by the modules in a PV plant, parts of the photovoltaic generator (one or more cells) may be shaded by various factors, such as trees, debris, chimneys, or clouds. When shaded, a PV cell acts as a passive load rather than a generator. This cell behaves like a diode that blocks the current generated by the other cells in the series string, potentially compromising the entire module's output. Moreover, the shaded cell is forced into reverse bias by the voltage of the remaining cells, which can lead to localized overheating, known as hot spots, and subsequent module failure. To mitigate this, bypass diodes are integrated into the junction boxes. These diodes are connected in anti-parallel with cell strings within the module. This setup allows the current to bypass the shaded string, ensuring continued operation at reduced power. While ideally each cell would have its own bypass diode, for cost-benefit reasons, typically only 2 to 4 diodes are installed per module (see Figure 2.21).

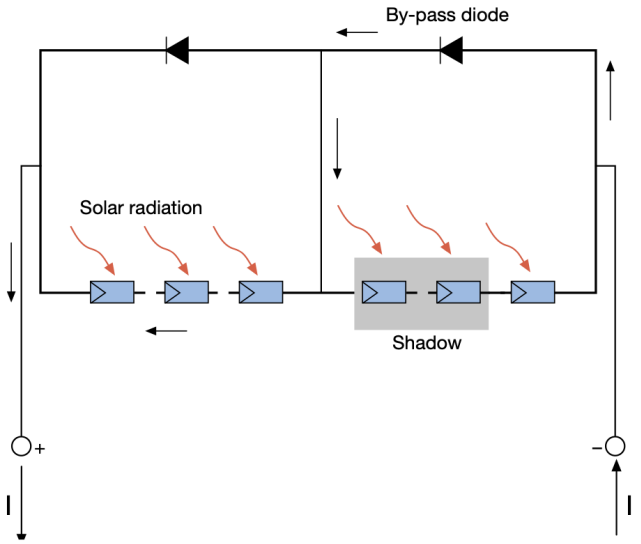


Figure 2.21: Wiring diagram with bypass diodes

2.4.4 Standard Test Conditions (STC)

The electrical performance of a photovoltaic module is typically specified under Standard Test Conditions (STC), corresponding to specific values of irradiance and cell temperature:

- $G_{STC} = 1000$ W/m^2 (Standard Irradiance);
- $T_{STC} = 25$ °C (Standard Cell Temperature).

Additionally, STC specifications require an Air Mass coefficient of $AM = 1{,}5$, which represents a standard solar spectral distribution.

2.4.5 Tilt and Orientation

The maximum efficiency of a PV generator is reached when the angle of incidence is 90°. This depends on the latitude and the solar declination (δ), which varies between +23,45° and −23,45°.

The solar altitude angle α at solar noon is given by:

$$\alpha = 90° - \phi + \delta \tag{2.15}$$

where ϕ represents the latitude and δ is the solar declination angle (+23,45°). The optimal tilt angle β is the complement of α. However, knowing the tilt angle β is not sufficient to determine the optimal orientation. One must also consider the solar path across the celestial vault throughout different periods of the year; therefore, the tilt angle should be averaged over the entire year[8]. This approach maximizes the total annual solar radiation captured (and thus the annual energy yield) compared to the condition of perpendicular irradiance during the solstice only. For fixed installations in the Northern Hemisphere, modules should face True South. The orientation is measured by the azimuth angle γ, which represents the deviation from the optimal South direction (in the Northern Hemisphere) or North (in the Southern Hemisphere). It cab be:

- $\gamma > 0$: Westward orientation;
- $\gamma < 0$: Eastward orientation.

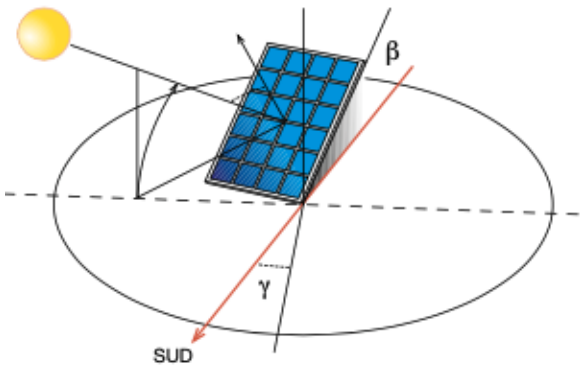


Figure 2.22: Angles that determine the orientation of the PV module

While ground-mounted systems allow for optimal positioning, building-integrated PV (BIPV) is often constrained by the roof's geometry. However, deviations up to 45° from South (South-East or South-West) still yield high energy performance.

[8] In Italy the optimal inclination is approximately 30°.

2.4.6 Predicted Energy Yield

The technical specification IEC TS 61724-3 (Photovoltaic system performance - Part 3: Energy evaluation method) supports the estimation of energy production for a PV system. It provides a mathematical model based on historical meteorological data representative of the installation site.

The predicted energy yield E_p is calculated as:

$$E_p = GHI \cdot \Delta_{GPOA} \cdot \eta_{modules} \cdot A_{modules} \cdot PR \quad [\text{kWh}] \tag{2.16}$$

where:

- GHI is the Global Horizontal Irradiance [kWh/m^2 · year];
- Δ_{GPOA} is the annual transposition gain or loss from the horizontal plane to the plane of the array;
- $\eta_{modules}$ is the initial conversion efficiency of the modules under STC;
- $A_{modules}$ is the total area of the PV array [m^2];
- PR is the Performance Ratio[9]

When the Global Tilt Irradiance (GTI) is directly available, the formula simplifies to:

$$E_p = GTI \cdot \eta_{modules} \cdot A_{modules} \cdot PR \quad [\text{kWh}] \tag{2.17}$$

where GTI represents the Global Irradiance on the tilted plane [kWh/m^2 · year].

2.4.7 Voltages and Currents in a PV System

Photovoltaic modules typically generate currents between 2 A and 15 A, depending on cell technology, and voltages from 30 V to 100 V. To reach the target peak power, modules are connected in series into strings, which are then combined in parallel to form the PV array.

The design trend favors longer strings to minimize wiring complexity and the costs associated with string combiner boxes. The maximum number of modules per string is constrained by:

- The maximum system voltage rating of all DC components (modules, connectors, and cabling);
- The inverter's input operating voltage range (specifically the MPPT window);
- The availability of switchgear and protection devices rated for the specific DC voltage of the system.

[9]The PR measures is a dimensionless metric that represents the ratio of the actual energy output to the theoretical energy output that could be achieved if the system operated continuously under Standard Test Conditions (STC). It serves as a measure of the overall plant quality, accounting for energy losses due to temperature, wiring, inverter inefficiency, soiling, and shading, independently of the incident solar radiation.

2.5 Trends in the Growth of Installed Photovoltaic Systems

As of 31 December 2024, a total of 1,875,870 photovoltaic systems are operational in Italy, with a combined installed capacity of 37002 MW. The chart in Figure 2.23 illustrates the evolution of the number and capacity of photovoltaic systems installed in Italy over the period 2010–2024. As can be observed, the rapid initial growth driven by public incentive schemes was followed, from 2013 onwards, by a more gradual development phase, and then by a new acceleration starting from 2022, sustained by multiple renewable energy incentive mechanisms[12].

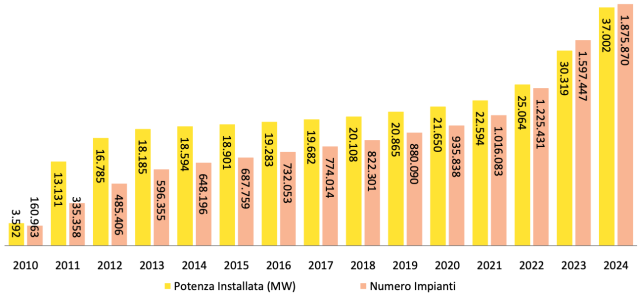


Figure 2.23: Evolution of the number and power of photovoltaic systems installed in Italy in the period 2010-2024

Chapter 3

Battery Energy Storage System

3.1 Introduction

The rapid growth of energy consumption, CO2 emissions, and demand-supply mismatch globally is due to the rising population growth rate and urbanization levels. These issues require development to optimize energy use and minimize fuel consumption. Various alternatives to the use of fossil fuels have been proposed to achieve sustainable energy systems. Renewable energy (RE) technologies with energy storage systems (ESSs) have become widely endorsed solutions among these alternatives. ESS assists renewable energy integration in many ways and manages the decent power balance during a power crisis; thus, the stability of the system has a significant effect on the overall electric system by storing energy during off-peak hours with reduced cost. The micro-grid (MG) concept is proposed by the Consortium for Electric Reliability Technology Solutions (CERTS). CERTS can be defined as a localized entity that consists of distributed energy resources (DERs) and controllable thermal and electrical loads. These loads are connected to the upstream grid for power generation using photovoltaic (PV) panels, wind plants, fuel cells, diesel generators, and microturbines with a storage device. From the utility perspective, MG can be treated as a controlled cell of the power system. From the customer viewpoint, MG can be designed to meet their requirements of reliability, reduced feeder losses and improved efficiency. MG with ESS has become a promising component for future smart grid deployment. However, due to the intermittent nature of renewable energy resources and fluctuating load profiles, the power supply in MG sometimes fails to mitigate the load demands and causes system frequency fluctuation. Therefore, fluctuating renewable energy sources must be smoothed with storage systems to provide high-power quality. Given the increased MG installations, distribution systems pose significant changes in characteristics compared with the present distribution system. Therefore, suitable control strategies must be adopted to manage these differences and improve overall efficiency. Many important considerations exist for the energy storage system in MGs. Efficient management of ESS, power electronic interfaces, charging and discharging, conversion mechanism of power, reliability, and protection from dangers are the major issues for the development of the energy storage system in MG applications. Fig. 3.1 describes the impact of an energy storage system in a power system network.

ESS can be applied for energy arbitrage, peak shaving, load flowing, spinning reserve, voltage support, black start, frequency regulation, power quality, power reliability, renewable energy systems (RESs) shifting, smoothing and firming, transmission and distribution upgrade deferral, congestion relief, and off-grid service, as shown in Fig. 3.2[13].

The aim of this section is to present the current state of Battery Energy Storage Systems (BESS) and to describe their operating principles, as this technology has been selected as the case study for the present work.

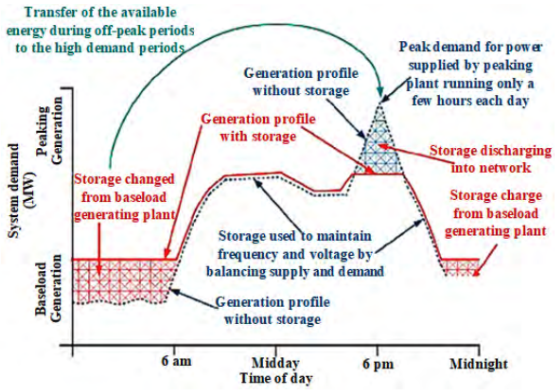


Figure 3.1: Load demand profile with energy storage system

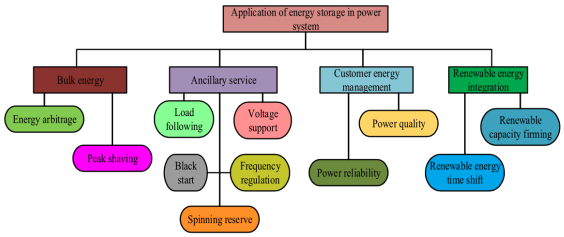


Figure 3.2: Application overview of energy storage system

3.2 Electrochemical Storage Systems

In the electrochemical storage systems (EcSS), chemical energy in the active material is converted into electrical energy. This conversion technique is completed by chemical reaction, and energy is stored as electric current for a specific voltage and time. The level of voltage and current are generated through the series or parallel connections of cells. Conventional rechargeable batteries and flow batteries (FBs) are two techniques that store energy in electrochemical form. However, chemical reaction reduces the life expectancy and energy of battery although minimal maintenance is needed for these batteries. Electrochemical storage devices are available in different sizes, which is the main advantage of this technology. Lead-acid, lithium-ion, sodium-sulfur (NaS), nickel-cadmium (NiCd), nickel- metal hydride (NiMH), and FBs are examples of this storage system. The common EcSS that can be applied in MG is discussed in the following subsection.

3.2.1 BESS-Lithium-Ion (LI-ION) Storage Systems

BESS is widely applicable for various purposes in all sectors (generation, transmission, and distribution) of electrical power systems and thus provides benefits to consumers. Battery capacity is an important determinant in selecting a storage device. The capacity of a battery may be defined as the total quantity of electrical charges that can be delivered in a single discharge by the cell. The state of charge (SoC) can be described as the ratio of remaining capacity to the nominal capacity. The most used variant of battery technologies is Lithium-Ion (LI-ION) Storage Systems. Although lithium-ion batteries were first commercialized in the 1990s, this energy storage technology has become the fastest growing technology in recent years. A Li-ion storage device can store energy at the megawatt scale. The significant advancement of this technology in increasing the levels of energy storage capacity is due to the characteristics of high efficiency (>90%), high energy density, rapid response time (in milliseconds), and attractive self-discharge rate (5% per mount). A schematic of the Li-ion battery along with the charging and discharging method is presented in Fig. 3.3[13].

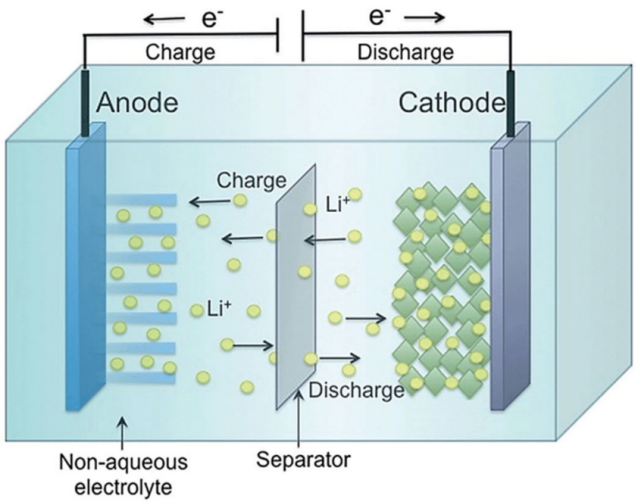


Figure 3.3: Charging and discharging method of Li-ion battery.

The cathode and anode are made from lithium metal oxide (LiCoO2) and graphite carbon cell, respectively. During the charging period, Li-ion passes from cathode to anode. The process is reversed in the case of the discharge period. The electrolyte used here can be formed using an organic solvent with dissolved lithium salt or solid polymer. Complete electrochemical reaction that takes place during the operation of Li-ion battery can be written as follows:
$\mathrm{LiMeO_2 + C \rightleftharpoons Li_{1-x}MeO_2 + Li_xC}$

To prolong the battery life, the current level must maintain the range of maximum dynamic charge current and maximum dynamic discharge current. Moreover, the battery voltage should also maintain the range of maximum charge voltage and maximum discharge voltage. The disadvantages of the Li-ion battery are its cycle depth of discharge (DoD) and high cost. However, the cost of the Li-ion cell is expected to decrease with large-scale production. These batteries are characterized by high gravimetric and volumetric energy density (75–200 Wh/kg and 200–500 Wh/L). It also shows improved efficiency (90%–95%), high power capability, extended lifetime (of approximately 20 years), prolonged cycle operation (8000 full cycles), and a wide temperature range ($-20°C$ to $55°C$)[13]. Thus, this technology has become increasingly popular, indeed, among the various electrochemical technologies, lithium-ion batteries represent the most widely adopted solution, owing to their numerous advantages, which will be discussed in the following sections. Figure 3.4 illustrates the percentage distribution of the different electrochemical technologies.

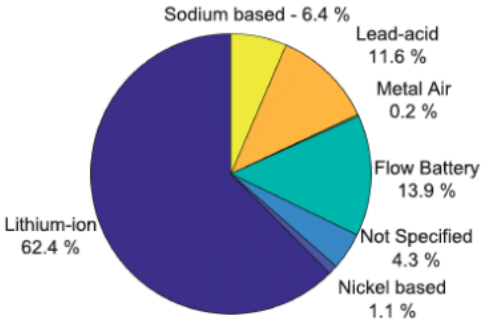


Figure 3.4: Utilization of different electrochemical technologies[14]

For the purposes of the analysis presented in this work, the Li-ion battery is the best-suited storage technology for the operation of the REC.

3.2.2 Performance Parameters of Lithium-Ion Batteries

Storage systems are usually classified and selected based on specific performance parameters. The main parameters for lithium-ion batteries are reported below.

Efficiency

The efficiency of storage systems is a parameter of fundamental importance. Indeed, the European Commission has often reiterated the "efficiency first" concept to emphasize its significance. For storage systems, reference is made to the round-trip efficiency (RTE), which accounts for the entire charging and discharging process, as well as the consumption and losses related to the auxiliary systems supporting the storage unit.

It is defined as: "the percentage ratio between the nominal energy during discharge (from which the energy absorbed by auxiliary services during discharge is subtracted) and the nominal energy during charge (to which the energy absorbed by auxiliary services during charge is added) during a complete charge-discharge cycle (within the acceptable range of state of charge) at nominal discharge and charge power"[15],[16]:

$$\eta_e = \frac{E_{\text{discharge}}}{E_{\text{charge}}} \times 100 \tag{3.1}$$

Adequate efficiency is essential to minimize the renewable energy "lost" during the storage, conversion, and transformation phases. For lithium-ion batteries, this efficiency typically exceeds 90%. Furthermore, it is directly proportional to temperature (due to the reduction in internal resistance) but inversely proportional to the discharge current.

C-rate

The current rate (C-rate) is a parameter that indicates the charging and discharging speed of a battery. It is defined as the ratio between the maximum charge/discharge current (expressed in Amperes) and the battery capacity (expressed in Ampere-hours). This specification is typically provided by the manufacturer[15]. For example, if a battery has a nominal capacity of 10 Ah and is discharged at a C-rate of 1 C, it means the discharge current is 10 A and the battery will take one hour to discharge completely. Conversely, if it is charged at 5 A, the C-rate will be 0.5 C and the charging time will be two hours. The C-rate value significantly impacts performance (charging time, temperature, efficiency) and the battery's lifespan. Therefore, selecting an appropriate value is crucial.

Battery Capacity

The capacity of a battery, measured in Ah, indicates the amount of electric charge that can be drawn from the system during the discharge process. Generally, the capacity value is not constant but varies as a function of temperature and C-rate. The nominal capacity value thus refers to an operating condition sufficiently representative of the battery's functioning at a specific reference temperature[15].

Gravimetric and Volumetric Metrics

The nominal discharge energy, expressed in watt-hours (Wh), represents the maximum energy capacity that the storage system can deliver when discharged at its nominal power rating. To benchmark and evaluate different energy storage technologies independently of their physical size, specific performance parameters are introduced. These include gravimetric specific energy (Wh/kg) and specific power (W/kg), which evaluate performance relative to system mass, as well as volumetric energy density (Wh/L) and power density (W/L), which relate performance to the required physical volume[15].

Service Life and Aging Phenomena

The service life of a battery is defined as the period during which the accumulator operates under normal conditions before its performance degrades below specific operational limits (for example, the limit on battery capacity reduction). Service life is usually expressed in terms of operating cycles (*cycle life*) or years of operation. The nominal energy of batteries tends to decrease over time due to the usage itself and the type of cycles they undergo.

To mitigate the effect of capacity degradation, it is crucial to maintain the system's operation within an optimal State-of-Charge (SOC) range, for instance, by avoiding levels below 15–20%. In this way, wear due to charge and discharge cycles can be partially limited, preventing premature aging phenomena. Cycle-related battery aging leads to an increase in the internal resistance of the modules, reducing power performance, and a yearly decrease in energy capacity, which typically ranges between 1% and 3% of the initial capacity[17]. Furthermore, these phenomena cause a reduction in the RTE value.

For lithium-ion batteries, even with proper routine maintenance and usage within the optimal SOC range, the battery reaches approximately 70% of its initial capacity after about 7000–8000 full charge-discharge cycles, a limit conventionally associated with the end of its service life. Assuming the system performs one full cycle per day, the service life is estimated at approximately 20 years. This lifespan represents a significant advantage of lithium-ion batteries, as it is superior to many other storage solutions. There are four main aging processes that lead to a reduction in capacity and performance[16]:

- **Solid Electrolyte Interphase (SEI):** The thin solid layer that forms on the anode surface during the initial cycles can grow excessively or become damaged; consequently, lithium ions are consumed.
- **Electrolyte Co-intercalation:** Solvent molecules from the electrolyte may intercalate into the electrode material along with lithium ions, causing damage to the crystalline structure and preventing further lithium-ion intercalation.
- **Electrolyte Decomposition:** The electrolyte can decompose at a rate that depends on both temperature and terminal voltage.
- **Structural Changes:** During cycling, structural changes may occur in the electrode material, and the integrity of the electrodes may be compromised due to the continuous expansion and contraction of the active materials.

Self-discharge Rate

Lithium batteries are characterized by low self-discharge rates, allowing them to maintain a charge for several weeks. The self-discharge rate increases with temperature: 0,5% per week at $20°C$, 2% at 40°C, and 4–10% at $60°C$ [16]. The percentage of charge retained relative to storage time approximately follows an exponential function. This means that the self-discharge of a fully charged cell in the first week is greater than that of a partially discharged cell in the following weeks.

Chapter 4

Hydrogen and P2H system

4.1 Introduction

In recent years, global energy shortages and ecological problems caused due to excessive use of fossil fuels have strengthened the position of hydrogen as a future energy carrier. Clean energy production devices such as fuel cells which use hydrogen and oxygen as reactants emphasize the role of hydrogen in future energy infrastructure. A major hurdle in development of such technologies is the production of pure hydrogen gas. Electrolysis of water to break it into hydrogen and oxygen is a promising option for clean fuel production. Depending on the source generated hydrogen can be named green or nongreen hydrogen. Nongreen hydrogen includes white, black, grey, pink, blue, and turquoise. The introduction of hydrogen is gaining importance for a carbon- neutral society, which is possible only from green hydrogen. Thus, RE systems (RES) are important, as they will provide sufficient energy for electrolyzer to split water. The first green hydrogen term was employed by the National Renewable Energy Laboratory (NREL) in 1995 in their green hydrogen report. In 2006, the state of California stated how green hydrogen can be produced from renewable sources such as solar and wind. EU used the first green hydrogen term in 2007. Further hydrogen production has been classified in Figure 4.1 where renewable-based and fossil fuel-based hydrogen productions are listed[18].

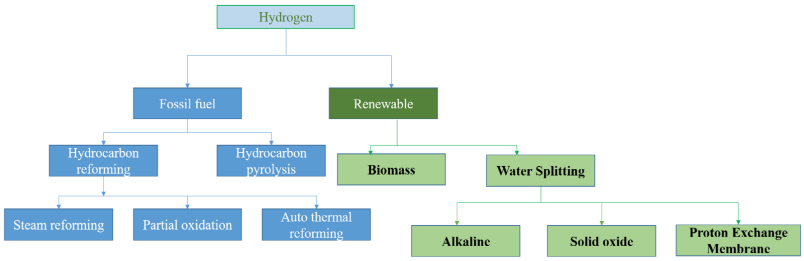


Figure 4.1: Various nonrenewable and renewable sources for hydrogen production.

4.2 Renewable Water Splitting and Electrolysis

One of the most sustainable pathways for hydrogen production is water splitting, primarily achieved through electrolysis. This electrochemical process utilizes electrical energy to dissociate water (H_2O) into hydrogen (H_2) and oxygen (O_2) by driving a direct current (DC) between two electrodes. According to Faraday's Law, the mass of hydrogen produced is directly proportional to the total electric charge passed through the circuit.

The production of "green" hydrogen is achieved by coupling the electrolysis process with renewable energy (RE) sources. To initiate water splitting at standard atmospheric conditions

($P = 1$ atm, $T = 298.15$ K), the minimum energy requirement is governed by the Gibbs free energy change. The fundamental thermochemical reaction is defined as[19]:

$$H_2O \rightarrow H_2 + \frac{1}{2}O_2 \quad \Delta H^\circ = 286 \text{ kJ/mol} \quad \text{(at 25°C, 1 bar)} \tag{4.1}$$

Currently, three main electrolysis technologies are established:

1. Alkaline Water Electrolyzer (AWE);
2. Proton Exchange Membrane Water Electrolyzer (PEMWE);
3. Solid Oxide Water Electrolyzer (SOWE).

In this study, the PEM technology is selected due to its specific technical advantages, which are detailed in the following section. The increasing maturity of electrolyzer technologies has positioned Power-to-Hydrogen (P2H) systems as a strategic gateway toward the hydrogen economy.

4.2.1 Proton Exchange Membrane Water Electrolysis (PEMWE)

A schematic of PEM electrolyzer operation is shown in Fig. 4.2. Water is introduced at the anode, where it undergoes oxidation, producing oxygen gas (O_2), protons (H^+), and electrons (e^-). This is known as the Oxygen Evolution Reaction (OER):

$$H_2O \rightarrow \frac{1}{2}O_2 + 2H^+ + 2e^- \tag{4.2}$$

The protons migrate through the proton-conducting membrane to the cathode, while the electrons flow through an external circuit. At the cathode, protons and electrons recombine to form hydrogen gas (H_2) via the Hydrogen Evolution Reaction (HER):

$$2H^+ + 2e^- \rightarrow H_2 \tag{4.3}$$

The applied electrical energy provides the driving force for this electrochemical reaction.

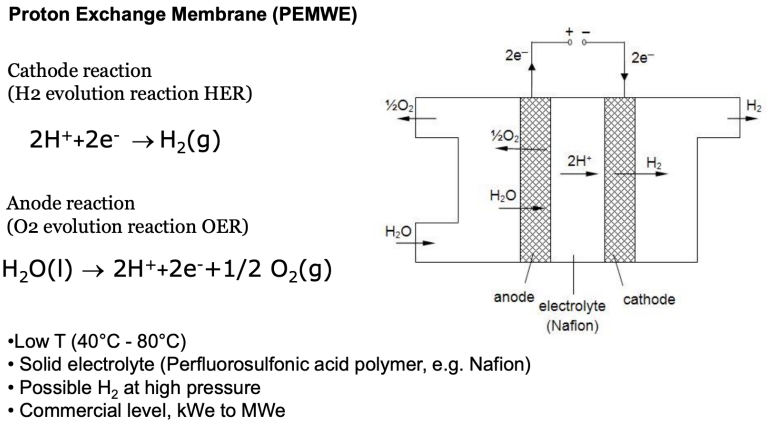


Figure 4.2: PEM scheme with reactions and some general information.

Figure 4.3.a shows a more detailed schematic of the PEMWE's internal structure and working mechanism. The core components of a PEMWE system include the membrane electrode assembly (MEA), gas diffusion layer (GDL), current collector and bipolar plate. The electrolyte used is typically Nafion, a proton-conducting polymer known for its high conductivity and chemical stability, though it is relatively expensive. As shown in 4.3, the PEM membrane divides the

electrolyzer into two half-cells, enabling selective transport of protons while effectively blocking gas crossover, ensuring product purity and safety. The catalysts used in PEMWEs are usually applied directly to the membrane or onto porous transport layers. Common catalyst materials include platinum (Pt) for the cathode and ruthenium or iridium (Ru/Ir) for the anode, selected for their excellent resistance to corrosion in acidic environments. PEMWE technology was first developed in the late 1960s and has since evolved into a leading option for low-temperature water electrolysis, operating typically at temperatures below 100°C. This temperature range is essential for maintaining membrane hydration, which is crucial for efficient proton conduction.

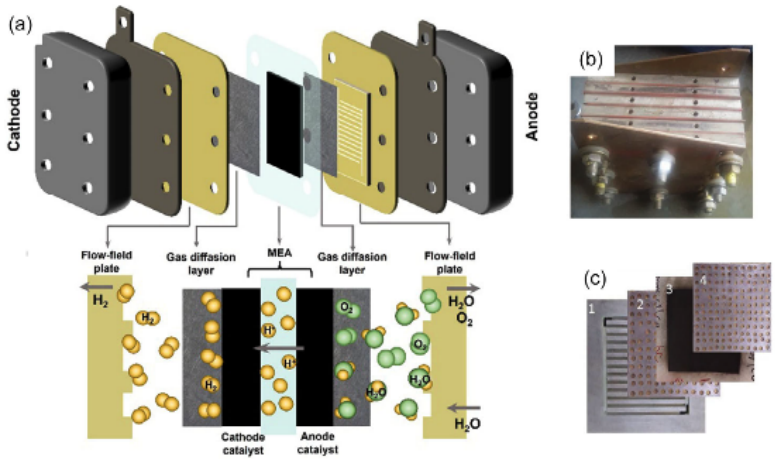


Figure 4.3: (a) Schematic of a single cell in proton exchange membrane (PEM) water electrolyzer stack. (b) Photograph of a PEM cell stack. (c) Photographs of details of cell components where 1, bipolar plate; 2, anode current collector; 3, MEA; and 4, cathode current collector.[18]

PEM technology offers several notable advantages for hydrogen production. It enables high efficiency with respect to other types of electrolyzer, the generation of high-purity hydrogen, supports high current densities (typically around 2 A/cm^2), and features a fast dynamic response, making it highly compatible with intermittent RE sources. PEM systems also operate at low temperatures (< 100°C) and produce oxygen as a valuable byproduct. The membrane in PEM electrolyzers is typically made of Nafion, a perfluorosulfonic acid polymer, which provides high proton conductivity (0,1 $\pm$ 0,02 S/cm), supports high-pressure operation, and has a low thickness range of 20–300 μm.

This solid electrolyte, combined with a catalyst-coated membrane, allows PEM systems to achieve high working voltages and current densities while maintaining a compact design. A unique feature of PEM technology is its reversibility, enabling the same system to function as both an electrolyzer and a fuel cell. More recent studies highlight the scalability potential of PEMWE, with current densities reaching 4 A/cm^2, 10 A/cm^2, 20 A/cm^2, and even 25 A/cm^2[18]. Achieving high current densities at high efficiency reduces the active cell area and material requirements, thus supporting cost-effective scale-up for large-scale hydrogen production. However, for broader deployment, reducing the reliance on expensive materials such as platinum, iridium, and Nafion remains a critical challenge.

The thermodynamic efficiency of an electrolyzer can be written as follows [20]:

$$\eta_{EC} = \frac{\dot{n}_{H_2} \cdot \Delta\bar{h}(T)}{V_{cell} \cdot I} = \frac{\frac{I}{2F} \cdot \Delta\bar{h}(T)}{V_{cell} \cdot I} = \frac{\Delta\bar{h}(T)/2F}{V_{cell}} = \frac{V_{tn}}{V_{cell}} \tag{4.4}$$

Where:

- $\dot{n}_{H_2}$ is the molar flow rate of hydrogen [mol/s];

- $\Delta\bar{h}(T)$ is the molar enthalpy of the reaction [J/mol];
- V_{cell} is the cell operating voltage [V];
- I is the current [A];
- F is the Faraday constant ($\approx$ 96485 C/mol);
- V_{tn} is the thermoneutral voltage [V].

4.3 Solar PV-Powered Electrolyser (P2H)

PV systems have strong potential for powering electrolyzers, as both operate on DC power. Proper sizing of the PV system and electrolyzer is critical. Due to the intermittent nature of solar power, a smaller-capacity electrolyzer is often more efficient. It ensures steady operation even with fluctuating input, while any surplus energy can be stored in a battery if included in the system.

Integrating PV systems with hydrogen production can be achieved through various coupling methods:

- **Direct coupling:** In a directly coupled system, the PV array is connected straight to the electrolyzer without any intermediate power electronics. This streamlined setup can lower both system costs and energy losses typically associated with power converters. However, it also demands precise matching between the PV array's output characteristics and the electrolyzer's operational requirements to ensure efficient performance. Since the electrolyzer's efficiency is closely tied to current density, fluctuations in solar energy can pose a challenge. When solar output drops, the resulting low current may fall below optimal levels for hydrogen production. In such conditions, hydrogen and oxygen can begin to diffuse back through the electrolyte, reducing the system's overall efficiency.

- **Indirect coupling:** This approach uses electrical converters such as DC–DC converters equipped with maximum power point tracking (MPPT) between the PV system and the electrolyzer, as shown in Figure 4.4. These converters enable the PV system to consistently operate at its maximum power point, even under changing weather conditions, thereby optimizing energy transfer and boosting hydrogen production. Although this setup comes with higher costs and some energy losses due to conversion, it provides greater operational flexibility and better resilience against power losses in PV modules.

- **Integration with storage systems:** This setup integrates energy storage systems such as batteries into the PV-hydrogen production system. Energy storage plays a crucial role in buffering the variability of solar output, helping to stabilize the current delivered to the electrolyzer. This improves the system's overall stability, reliability, and efficiency within the context of this study.

In this study, an indirect coupling configuration paired with a Battery Energy Storage System (BESS) has been selected.
A complete PV-electrolyzer setup involves more than just the cell stack. Essential components include a water supply system, power supply or voltage regulator, water circulation pump, heat exchanger, control and instrumentation systems, gas separators for hydrogen (and optionally oxygen), as well as comprehensive safety features (Fig. 4.5).

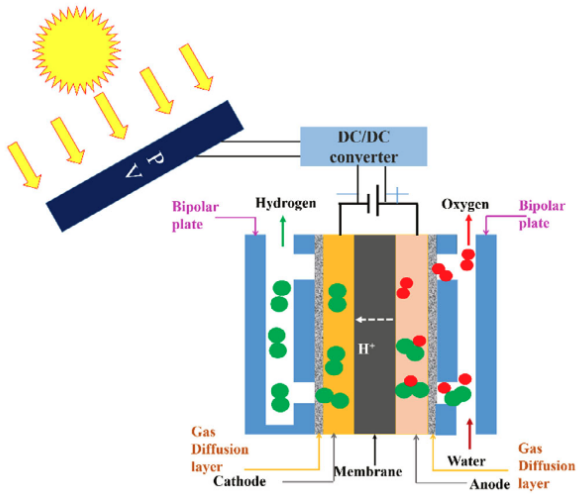


Figure 4.4: Schematic of a solar-powered PEM electrolyzer using indirect coupling.

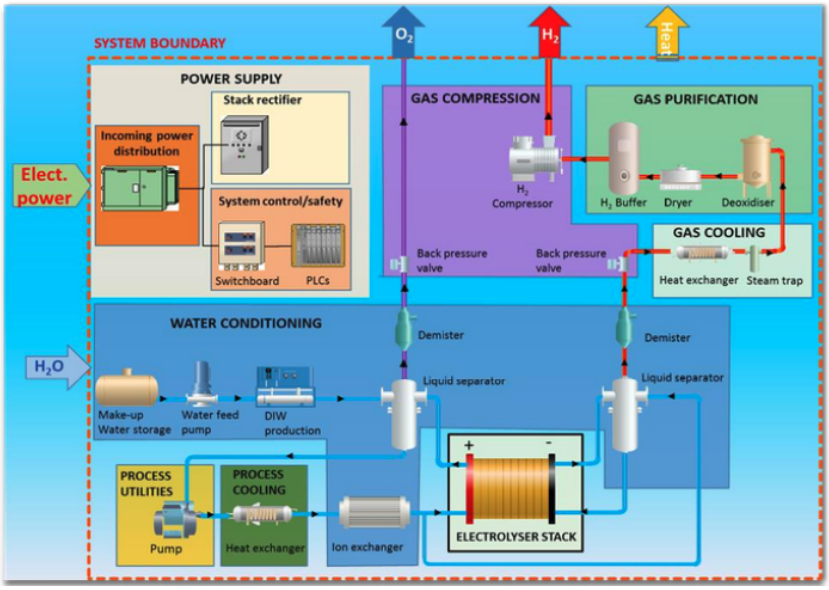


Figure 4.5: Electrolysis: complete plant

The P2X strategy has been applied to a Renewable Energy Community (REC) in order to analyze its viability to maximize the energy Self-Consumption (SC), mitigate Greenhouse Gas (GHG) emissions and reduce community annual costs. Hydrogen, produced in a P2X unit, can convert electricity surplus from renewables into hydrogen via an electrolyzer (Fig. 4.6) and store it.



Figure 4.6: Electrolyzer

In recent years, P2X technology has received significant attention from the energy sector due to its flexible nature suitable for power systems. As an electrical load, Power-to-Hydrogen (P2H) production needs to accommodate the fluctuating solar energy or provide auxiliary services, e.g., peak shaving and frequency regulation, for the power system. Converting electricity into hydrogen by means of water electrolysis represents a viable solution for balancing local power grids. The potential role of PtG systems for storing the RES excess and mitigating renewable fluctuations in distributed energy systems has been widely analyzed in literature; similarly, the role of hydrogen for balancing power grids by means of fuel cells has been investigated. Nevertheless, hydrogen is not the best option for balancing Variable Renewable Energy Sources (VRES) on electricity networks due to the low round-trip efficiency of the Power-to-Gas-to-Power process. More interesting is the hydrogen application for purposes not directly correlated to electricity re-generation. It can be used for producing alternative fuels, such as Synthetic Natural Gas (SNG), methanol, ammonia and dimethyl ether (DME).

However, the production of electro-fuels requires large-scale reactors, representing a barrier for implementation in small-scale energy communities. Hydrogen can instead be a vector for the transport sector decarbonization. While hydrogen refueling stations and vehicles are not yet widespread, a viable solution for small-scale applications is the blending of hydrogen with Natural Gas (NG). For low volume fractions, there are no significant changes in the main parameters of both gas infrastructure and gas-driven end-use devices. This solution exploits the current widespread gas infrastructure, avoiding the need for dedicated new networks.

4.4 Hydrogen storage

Hydrogen storage is a critical technology for the advancement of hydrogen-based systems in stationary power applications. Under normal conditions (273,15 K and 1 bar), 1 kg of hydrogen occupies a volume of approximately 11 m^3. To overcome this low volumetric energy density, hydrogen must be densified using several physical or chemical pathways:

1. Mechanical compression;
2. Cryogenic liquefaction;
3. Interaction with a solid matrix (adsorption, absorption);
4. Reversible chemical reactions.

To determine the most suitable solution for the proposed Power-to-Hydrogen (P2H) architecture, the following storage methodologies are evaluated[21]:

- **Compressed Gas Storage:** This technology is characterized by a high Technical Readiness Level (TRL). It employs high-pressure vessels, typically operating up to 700 bar (with prototypes reaching 1000 bar). Despite its maturity, it is constrained by the intrinsic properties of the hydrogen molecule (high specific heat (c_p) and low density, even if compressed to hundreds of bars - at 700 bar the density reaches only 57,47 kg/m^3).
- **Liquid Hydrogen Storage (LH_2):** Achieved through condensation below the normal boiling point ($-253°C$), liquid storage provides a density of approximately 71 kg/m^3. However, the liquefaction process involves a significant energy penalty, accounting for 20–30% of the hydrogen's Lower Heating Value (LHV).
- **Solid-State Storage:** This method utilizes the absorption/desorption process within specific materials, such as metal hydrides. It allows for operation within a wide temperature window (ambient to 500°C) and at lower pressures. The release kinetics are thermally

driven, providing high intrinsic safety since hydrogen is not released without active heating. Despite high volumetric densities (≈ 150 kg/m^3), the significant gravimetric weight and cycle-life degradation remain primary R&D challenges.

- **Liquid Organic Hydrogen Carriers (LOHC):** LOHCs (e.g., benzene, toluene) are substances that undergo reversible hydrogenation (exothermic) and dehydrogenation (endothermic) cycles. This approach facilitates hydrogen transport using existing liquid fuel infrastructure.

In this analysis, the physical-based compressed gas technology using high-pressure tanks was selected (Fig. 4.7). This solution is currently the most economically viable and technically suitable for the analyzed energy community scenarios, as alternative methods like cryogenic or solid-state storage involve higher capital expenditures and operational complexity.



Figure 4.7: Hydrogen storage tanks

Chapter 5

Renewable energy communities

5.1 The European Regulatory Framework

The Clean Energy for All Europeans Package (hereinafter CEP), developed on the basis of a European Commission proposal of November 2016 and adopted in its final version in June 2019, comprises a set of legislative measures covering the sectors of energy efficiency, renewable energy and the electricity market. The package, consisting of four regulations and four directives, places the consumer at the centre of the European Union's energy policy, assigning them an active role in pursuing the ambitious decarbonisation objectives established under the Paris Agreement, adopted at the twenty-first Conference of the Parties (COP 21) in 2015 [22].

Among the objectives of the CEP is the establishment of an enabling framework for the active participation of consumers in the energy transition, through instruments designed to promote the collective involvement of final customers in accelerating the shift from fossil fuels to renewable energy sources. In this context, two directives are of particular relevance with regard to the central role assigned to end users in the transition process:

1. Directive 2018/2001/EU of the European Parliament and of the Council of 11 December 2018 on the promotion of the use of energy from renewable sources, known as the Renewable Energy Directive (hereinafter RED II);

2. Directive 2019/944/EU of the European Parliament and of the Council of 5 June 2019 on common rules for the internal market for electricity, known as the Internal Electricity Market Directive (hereinafter IEM).

5.1.1 The RED II Directive

The RED II Directive was introduced with the aim of promoting the development of energy from renewable sources across the territory of the European Union, fostering the active participation of citizens and, more broadly, of final customers in the energy transition process. To this end, the directive introduces a set of enabling instruments based on models of participation of increasing complexity, defining and regulating individual self-consumption, collective self-consumption and Renewable Energy Communities (hereinafter REC) [2].

The RED II first defines the renewable energy self-consumer as a final customer who, operating at their own premises within defined boundaries or, where permitted by the Member State, at other sites, produces renewable electricity for their own consumption and may store or sell self-produced renewable electricity, provided that, for entities other than households, such activities do not constitute their primary commercial or professional activity. The directive further defines renewable energy self-consumers acting collectively as a group of at least two renewable energy self-consumers acting collectively and located in the same building or block

of flats. These new categories were introduced to broaden the participation of households in energy production and consumption processes[1].

The RED II further introduces renewable energy communities, defining them as a legal entity that:

- is based on open and voluntary participation, is autonomous and is effectively controlled by shareholders or members located in the proximity of the renewable energy production installations that are owned and developed by the legal entity in question;

- has shareholders or members that are natural persons, small and medium-sized enterprises (SMEs) or local authorities, including municipal administrations;

- has as its primary purpose the provision of environmental, economic or social benefits at community level to its shareholders or members, or to the local areas in which it operates, rather than the generation of financial profits.

5.1.2 The IEM Directive

The IEM Directive aims primarily to adapt the European Union electricity market to the ongoing technological and structural changes. The configurations it introduces therefore relate exclusively to the production and exchange of electrical energy, whether generated from renewable or conventional sources, and are established as new actors in the electricity market, authorised to undertake activities such as energy distribution and supply. Similarly to the RED II Directive, the IEM Directive introduces a set of categories of increasing complexity to encourage the participation of final customers, and other actors, in the electricity market [3].

The first two categories are those of the active customer and the collectively acting active customer, defined as a final customer or a group of final customers acting jointly who consume or store electricity produced at their own premises located within a defined area or, where permitted by the Member State, at other premises, or who sell self-produced electricity or participate in flexibility or energy efficiency schemes, provided that such activities do not constitute their primary commercial or professional activity. The directive further introduces citizen energy communities (hereinafter CEC), defined as a legal entity that:

- is based on voluntary and open participation and is effectively controlled by members or shareholders that are natural persons, local authorities, including municipal administrations, or small enterprises;

- has as its primary purpose the provision of environmental, economic or social benefits at community level to its members or shareholders, or to the local areas in which it operates, rather than the generation of financial profits;

- may participate in the generation, including from renewable sources, distribution, supply, consumption, aggregation and storage of energy, in energy efficiency services, or in electric vehicle charging services, or provide other energy services to its members or shareholders.

[1]Energy produced by an installation on the roof of a residential building may be made available to individual residents and not solely to the building's common services.

5.2 The evolution of Italian legislation

5.2.1 The Milleproroghe Decree 2020

In early 2020, Italy initiated a process of partial and anticipatory transposition of the RED II Directive, with the aim of testing the effects, implications and potential criticalities associated with the introduction of collective self-consumption schemes and renewable energy communities. This pilot phase of transposition began with the Milleproroghe Decree, Legislative Decree No. 162/19, which entered into force in February 2020 [23]. In particular, Article 42-bis introduced for the first time into Italian legislation the definitions of renewable energy self-consumers acting collectively and renewable energy community, drawing directly from the definitions provided by the RED II Directive without substantial modifications.

The categories of users eligible for membership of these configurations are as follows:

- in the case of collective self-consumers, final customers may participate, subject to the condition that, for entities other than households, the activities related to self-consumption do not constitute their primary commercial or professional activity;
- in the case of renewable energy communities, natural persons, small and medium-sized enterprises (SMEs), territorial bodies or local authorities, including municipal administrations, may participate, provided that membership of the REC does not constitute their primary professional activity.

The decree introduces a number of specific constraints and characteristics applicable to collective self-consumption schemes and energy communities that are not present in the RED II Directive. The installations forming part of these two configurations may produce electrical energy exclusively from renewable energy generation technologies, subject to the following conditions:

- the rated power of each installation must not exceed 200 kW;
- the renewable energy installations held by the self-consumption schemes or RECs must have entered into operation after the entry into force of the conversion law of Legislative Decree No. 162/19, i.e. from 1 March 2020.

The concept of proximity, which defines the geographical perimeter of the two configurations, is established as follows:

- for collective self-consumption schemes, proximity refers to the requirement that installations and consumers be located within the same building or residential block;
- for RECs, proximity concerns the requirement that installations and users be connected to low-voltage electricity networks fed, at the date of establishment of the association, by the same secondary substation (MV/LV).

The activities permitted to both configurations include the production, sale, storage and sharing of self-produced energy. Energy sharing takes place using the existing distribution network; the decree therefore does not provide for the construction of new network infrastructure, nor for the transfer of any portion of the existing public network for private use by the self-consumption scheme or the community. The concept of shared energy is defined according to a virtual approach: it corresponds to the minimum value, in each hourly period, between the energy produced and fed into the grid by the renewable energy installations forming part of the configuration and the energy withdrawn from the grid by all associated final customers.

With respect to the share of energy that is produced and shared within the community, the decree provides for:

- exemption from the tariff components that are not technically applicable to shared energy, insofar as it is instantaneously self-consumed within the same portion of the low-voltage network;

- the introduction of an incentive tariff designed to reward instantaneous self-consumption and the use of energy storage systems.

The determination of the value of the tariff components not applicable to shared energy, and therefore subject to restitution by the Energy Services Manager (hereinafter GSE), is entrusted to the Regulatory Authority for Energy, Networks and Environment (hereinafter ARERA). The relevant provisions are set out in ARERA Resolution 318/2020, published in August 2020. The definition of the incentive schemes is instead the responsibility of the Ministry of Economic Development (hereinafter MISE), and was established by the Ministerial Decree of 16 September 2020. These instruments marked the continuation of the pilot phase, preparatory to the full transposition of the RED II Directive, initiated in Italy with the Milleproroghe Decree.

5.2.2 ARERA Resolution No. 318/2020

The regulatory framework for distributed energy sharing is governed by the ARERA Resolution 318/2020/R/eel. This resolution defines the economic regulation and procedures for electrical energy shared either by a group of renewable energy self-consumers acting collectively within a single building (or condominium) or within a Renewable Energy Community (REC) [24].

In synthesis, the resolution identifies the tariff components that are technically not applicable to the share of energy internally shared within these two configurations. Since this energy does not fully utilize the high-voltage transmission and distribution grids, these components are subject to a refund managed by the GSE (*Gestore dei Servizi Energetici*).

The specific value of the tariff components identified by ARERA differs according to the system configuration:

1. **Renewable energy self-consumers acting collectively:** the economic framework includes:

   - A refund, applied to the shared energy quota, of specific variable unit components related to transmission ($TRASE$) and distribution ($BTAU$);
   - An additional economic benefit reflecting the reduction in network losses, as the energy is consumed within the same physical site where it is generated.

2. **Renewables Energy Communities (RECs):** the economic framework includes exclusively:

   - A refund, applied to the shared energy quota, of the variable unit tariff components linked to transmission ($TRASE$) and distribution ($BTAU$).

The economic relief resulting from the reimbursement of these tariff components amounts approximately to:

- 10 €/MWh of shared energy for collective self-consumption schemes;

- 8 €/MWh of shared energy for Renewable Energy Communities (RECs).

5.2.3 Implementing Decree of the Italian Ministry of Economic Development (MISE), 16 September 2020

The framework for direct financial incentives is established by the MISE (*Ministero dello Sviluppo Economico*) Decree of September 16, 2020. This decree defines the specific incentive tariff applied to the share of energy internally shared within both collective self-consumption structures and Renewable Energy Communities (RECs) [25].

The electricity generated by renewable energy sources (RES) plants within these configurations qualifies for a feed-in premium tariff over a 20-year operational lifetime, provided that the energy is shared among the participants. The incentive tariff is structured as follows:

- 100 €/MWh if the production plant is part of a collective self-consumption configuration from renewable sources;
- 110 €/MWh if the production plant is integrated within a Renewable Energy Community (REC).

5.2.4 Legislative Decree 199/2021 and RED II Transposition

The initial phase of 2021 was characterized by the deployment of the first pilot Renewable Energy Communities (RECs) and collective self-consumption schemes. These early configurations operated under strict regulatory constraints, specifically a maximum capacity limit of 200 kW per plant and a geographical boundary restricted to the secondary substation level, meaning that all members and production assets had to be connected under the same medium-to-low voltage (MV/LV) transformer. This pilot phase was critical to identifying systemic bottleneck points ahead of the definitive transposition of European Directives RED II (2018/2001/EU) and IEM (2019/944/EU).

The formal and definitive transposition of the RED II Directive was achieved through *Decreto Legislativo 8 novembre 2021, n. 199*, which introduced radical changes compared to the transient regulatory framework [5].

A primary regulatory modification concerns the mathematical and physical definition of "shared energy". Shared energy is defined as the minimum, within each hourly period t, between the electricity generated and injected into the grid by renewable plants and the electricity withdrawn by the group of associated final consumers:

$$E_{shared}(t) = \min\left(\sum E_{inj}(t), \sum E_{with}(t)\right) \tag{5.1}$$

While the legal definition of shared energy expands geographically to the whole market zone and explicitly includes energy storage systems under the community's control, the allocation of direct economic incentives is restricted to a specific subset of this volume. According to Article 5 and Article 8 of the decree, for installations with a capacity up to 1 MW within a REC or a collective self-consumption scheme, a dedicated premium tariff is granted to reward instantaneously self-consumed energy. The framework limits this premium incentive to energy that is:

- Generated exclusively from renewable energy sources (RES);
- Produced by plants with a capacity not exceeding 1 MW (an upgrade from the previous 200 kW limit);
- Injected by plants that entered into commercial operation after the decree's effective date;

- Shared among production assets and consumption units connected under the geographical perimeter of the same **Primary Substation (HV/MV)** (*Cabina Primaria*), substantially expanding the pilot boundary which was limited to the secondary substation (MV/LV).

Specifically, the major innovations introduced by the transposition decree regarding the architecture of RECs involve the following topics:

- **Eligible Members:** Membership has been broadened to include physical persons, Small and Medium Enterprises (SMEs), local authorities, municipalities, research and training institutes, religious institutions, third-sector organizations, and environmental protection bodies. For private enterprises, participation in the REC must not constitute their primary commercial or industrial activity.

- **Existing Assets Integration:** The inclusion of pre-existing renewable plants is permitted, provided their capacity does not exceed 30% of the total power capacity operating within the community.

- **Scope of Activities:** The operational scope of the community has been expanded. RECs are authorized to manage alternative renewable energy vectors, promote smart-home (*domotics*) and energy efficiency interventions, provide electric vehicle (EV) charging services, operate as retail electricity suppliers, and offer ancillary or flexibility services to the power grid. Every activity must align with the primary purpose of delivering environmental, economic, or social community benefits rather than financial profits.

The decree entered into force on December 15, 2021, setting a precise timeline for secondary enabling acts:

- Within 90 days, ARERA was mandated to issue the technical regulations regarding tariff component unbundling for shared energy;

- Within 180 days, the MISE was tasked with updating the incentive mechanisms via a specific ministerial decree, ensuring transitional pathways to protect investments made during the pilot phase.

5.2.5 Integrated Text on Distributed Self-Consumption

ARERA, with Resolution 120/2022 of March 22, 2022, launched a procedure for the implementation of the provisions indicated by Legislative Decree 199/21, regarding self-consumption. The resolution planned to define a new integrated text, aimed at the enhancement of "extended" self-consumption, starting from the transitional regulation adopted with Resolution 318/2020, to take into account the new prescriptions. Within the scope of the procedure launched with resolution 120/2022, with the consultation document 390/2022, published in August 2022, ARERA specified which configurations achieve forms of "distributed" self-consumption (including Renewable Energy Communities - RECs) and indicated to innovate the current regulation for the economic valuation and incentivization of the aforementioned schemes, in order to take into account the new definitions and the new perimeters, prepared by the decree with which the RED II Directive is fully transposed. Ultimately, the regulatory process for the implementation of the provisions of Legislative Decree 199/21 led, with ARERA resolution 727/2022 of December 27, 2022, to the approval of the "Integrated Text on Distributed Self-Consumption" (TIAD hereinafter) [26].

The TIAD governs the procedures and economic regulation relating to the electricity subject to distributed self-consumption. The document recalls the definitions provided by decree

199/21 for the various configurations identified as distributed self-consumption schemes, including RECs, distinguishing between electricity shared within the same market zone, electricity self-consumed in the area under the same primary substation, and incentivized as per regulatory provisions.

Since the valuation of distributed self-consumption is now referred to the HV/MV transformation substation (no longer to the MV/LV substation, which defined the perimeter of the configurations in the "pilot" phase), the criteria are outlined on the basis of which grid operators identify, in a conventional manner, the areas under each primary substation starting from the actual configuration of the electricity grids. Furthermore, it is envisaged that the areas will be accessible online, initially on the websites of the individual distributors and, subsequently, on the GSE website, thus simplifying the procedures for the establishment and management of the configurations, preventing referents from having to interface with distributors, as occurs during the transitional period. The methods by which the GSE quantifies the electricity subject to economic valuation and incentivization are also defined. A significant change compared to Resolution 318/2020 concerns the update of the valuation of self-consumed electricity for energy communities, due to the expansion of the reference area. In fact, the valuation of distributed self-consumption is equal to the variable part of the transmission tariff (TRASE), excluding the variable part of the distribution tariff (BTAU), as the electricity distribution grid is extensively used. Meanwhile, the incentive tariff is subject to definition by the Ministry of the Environment and Energy Security (MASE, hereinafter), pursuant to decree 199/2021.

The TIAD follows and replaces resolution 318/2020 starting from the later date between March 1, 2023, and the date of entry into force of the MASE decree, by which economic incentives are defined. Finally, it is envisaged that, from the date on which the TIAD becomes applicable, already existing configurations for collective self-consumption and RECs will merge into the provisions defined by the document.

5.2.6 The CACER Decree (D.M. 414/2023)

The current operational and economic framework for energy sharing configurations in Italy is governed by the Decree of the Minister of the Environment and Energy Security (MASE) of December 7, 2023, n. 414, widely referred to as the *Decreto CACER* (entered into force on January 24, 2024) [27]. This decree establishes the new procedures for granting incentives aimed at promoting renewable energy source (RES) power plants integrated within Renewable Energy Communities (RECs), collective self-consumption groups, and remote self-consumers.

The framework is structured around two main incentive mechanisms, both managed and regulated by the GSE (*Gestore dei Servizi Energetici*):

- **Incentive Premium Tariff (Feed-in Premium):** An operational support incentive (*contributo in conto esercizio*) granted for a 20-year period, applied directly to the eligible shared energy volume. The eligible configurations include RECs, collective self-consumers in buildings, and remote self-consumers. This tariff can be applied for up to 30 days following the achievement of a national capacity ceiling of 5 GW of incentivized power, and under no circumstances later than December 31, 2027.

- **Capital Grant (Contributo a Fondo Perduto):** As a complementary measure to the premium tariff, a dedicated capital subsidy was implemented to accelerate the deployment of RECs, specifically within small municipalities. Funded by the National Recovery and Resilience Plan (PNRR) under Mission M2C2, Investment 1.2, this program allocated 2.2 billion EUR for non-repayable grants. The subsidy covered up to 40% of the eligible capital expenditures (CAPEX), subject to specific cost caps per unit of capacity, for new RES installations up to 1 MW. This measure was restricted to configurations located in municipalities with fewer than 50,000 inhabitants. While this PNRR capital grant

acted as a crucial driver for launching early REC projects nationwide, the application window for this specific funding program officially closed on November 30, 2025. Since this capital subsidy is no longer accessible for new project developments, it will be omitted from the economic and financial analysis performed in this study. The economic viability of the investment will therefore be evaluated under standard market conditions, relying exclusively on the cash flows generated by the premium incentive tariff, physical self-consumption savings, and the commercialization of surplus electricity injected into the grid. This approach ensures a conservative simulation of the investment's feasibility in the total absence of non-repayable public grants.

Consequently, this thesis work is strictly based on this latter regulatory configuration, which represents the current reference framework for the synthesis, sizing, and economic optimization of RECs in Italy.

5.3 Plants Eligible for the DM CACER Incentives

Not all renewable energy production plants can be included in a REC and access the incentive mechanisms. The GSE Operating Rules [28] define precise requirements related to the type of source, the date of construction, and the temporal relationship with the constitution of the community itself. To access the incentives provided by the CACER Decree, renewable energy plants must comply with the following requirements:

- Powered by renewable sources with a maximum capacity of 1 MW;
- Newly constructed or new sections of existing plants;
- Multiple plants permitted within each configuration, even with different producers;
- Entered into operation after December 16, 2021, and, solely for RECs, after the formal constitution of the Community;
- Realized exclusively with newly manufactured components in the case of photovoltaic systems, or refurbished components for other technologies;
- In compliance with the requirements set by the DNSH (Do No Significant Harm) principle;
- Biogas or biomass plants: compliance with the criteria described by the CACER Decree;
- Not intended for hydrogen production with emissions > 3 ton CO_2eq./ton H_2;
- Not operating under Net Metering (SSP) or benefiting from other electricity production incentives;
- Excluding the share of capacity built to satisfy the mandatory integration of renewables in newly constructed buildings;
- Plants already in operation as of 15/12/2021 can be included in a configuration, up to a limit of 30%, but can only benefit from the shared energy tariff (valuation fee).

5.4 Operating Principles and Economic Mechanisms

The sustainability of a REC is based on a "virtual" energy sharing model and on precise incentive mechanisms managed by the Energy Services Manager (GSE).

5.4.1 Shared "Self-Consumed" and "Incentivized" Energy

The pivotal concept of the REC model is that of "shared energy". This is a virtual quantity, calculated by the GSE on an hourly basis, which does not imply a direct physical transfer of electrons from the producer to the consumer. The national distribution grid acts as a vehicle for transmission and balancing. For each hour h of the year, the shared energy $E_{\text{shared},h}$ is defined as the minimum between the total energy injected into the grid by the REC plants and the total energy withdrawn from the grid by all consumer members within the same virtual perimeter (the primary substation).

$$E_{\text{shared},h} = \min\left(\sum_{p} E_{\text{injected},p,h}\ ,\ \sum_{c} E_{\text{withdrawn},c,h}\right) \tag{5.2}$$

Where:

- $E_{\text{injected},p,h}$ is the energy [kWh] injected into the grid in hour h by the plant of producer p.
- $E_{\text{withdrawn},c,h}$ is the energy [kWh] withdrawn from the grid in hour h by consumer member c.

The total annual shared energy, on which the main incentive mechanisms are based, is the sum of these hourly values. This energy flow represents the degree of simultaneity between production and consumption within the community and is the primary object of economic valuation and optimization strategies through energy storage systems, as analyzed in this thesis.

5.4.2 Economic valorization components

The energy produced and shared within the REC generates value through three main economic streams, which are calculated and paid by the GSE. For configurations admitted to the distributed self-consumption service, economic contributions are recognized for each production plant contributing to the shared energy, for a duration of 20 years. The contributions due to the admitted configurations can be of three types:

- **Valuation of self-consumed electricity:** through the refund of the tariff components provided for by ARERA Resolution 727/2022/R/eel;
- **Incentivization (premium tariff):** of the shared electricity pursuant to the CER Decree;
- **Fee for the withdrawal of electricity injected into the grid (RID):** by the GSE, where requested.

It is essential to analyze these components separately, since their interaction determines the optimal management strategy of the plants, particularly regarding energy storage systems.

5.4.3 The ARERA Shared Energy Valuation Fee

In addition to the premium tariff, a second contribution is recognized on shared energy, known as the shared energy valuation fee for distributed self-consumption. This amount, defined by ARERA, aims to return to the REC the value of certain tariff components relating to grid costs (such as avoidable transmission losses) that are not incurred thanks to local generation and the simultaneity between production and consumption [26]. Unlike the premium tariff, this fee is not an incentive in the strict sense, but rather a proper technical and economic compensation. Its unit value is updated annually by the Authority.

5.4.4 The Premium Tariff on Shared Energy

The premium tariff represents the main direct incentive granted to the REC. It is an economic contribution, recognized for a period of 20 years, applied to each kWh of shared energy, with the aim of promoting simultaneity between production and consumption. Its value is not fixed, but is calculated on an hourly basis according to a formula defined by the CACER Decree [29]. This formula depends on two main factors: the capacity of the production plant and the hourly zonal electricity price (P_z). The regulation provides for three different capacity brackets, each corresponding to a fixed part of the tariff and a different maximum cap. The general formula for the Provisional Incentive Tariff (TIP_h) is therefore:

$$TIP_h = \text{Fixed Part} + \max\left(0\,,\, 180 - P_{z,h}\right) \tag{5.3}$$

As can be seen, the tariff consists of a fixed part (60, 70, or 80 €/MWh depending on the capacity size) and a variable part that decreases as the market price increases. When the zonal price P_z exceeds 180 €/MWh, the variable part drops to zero and the premium tariff coincides solely with the fixed part. Additionally, for photovoltaic plants only, a correction factor is provided to take into account the different solar irradiation levels nationwide. This correction provides an additional amount for plants located in the regions of Central and Northern Italy. For the Southern regions and the Islands, where higher irradiation is assumed, no correction is applied. The aforementioned details are summarized and illustrated in Table 5.1.

Table 5.1: Fixed, variable, and maximum tariffs based on nominal plant capacity.

Nominal capacity kW	**Fixed tariff** (based on plant)	**Variable tariff** (based on Zonal Price)	**Maximum total tariff PV plants**		
			South	*Center*	*North*
$P \leq 200$	80 €/MWh*	$\max\left(0\,,\, 180 - P_{z,h}\right)$ €/MWh	120 €	124 €	130 €
$200 < P \leq 600$	70 €/MWh*	$\max\left(0\,,\, 180 - P_{z,h}\right)$ €/MWh	110 €	114 €	120 €
$P > 600$	60 €/MWh*	$\max\left(0\,,\, 180 - P_{z,h}\right)$ €/MWh	100 €	104 €	110 €

* Plus geographical component for photovoltaic (PV) plants: +4 €/MWh in Central regions; +10 €/MWh in Northern regions.

5.4.5 The Sale of Electricity Injected into the Grid (Dedicated Withdrawal)

The energy produced and injected into the national electricity grid is remunerated through market mechanisms managed by the Energy Services Manager (GSE). Currently, the main options are Dedicated Withdrawal (RID) and Net Metering (SSP), although the latter is undergoing a progressive phase-out for new plants. Dedicated Withdrawal represents a simplified method of selling energy: the producer transfers the share of energy injected into the grid to the GSE, receiving an economic fee in return.

The remuneration is based on the Hourly Zonal Price (P_z), which reflects the wholesale price formed on the Day-Ahead Market (MGP) in the specific zone where the plant is located [30]. This revenue stream introduces an element of uncertainty, as it is linked to electricity market fluctuations. Furthermore, an inverse correlation is established with the premium tariff on shared energy: since the latter decreases as P_z increases, a complex economic optimization problem arises. In such a scenario, the management of energy storage systems becomes crucial to strategically balance revenues from the RID and sharing incentives.

5.4.6 Synthesis of Energy and Economic Streams

To summarize the concepts presented, it is useful to schematize the main energy streams that characterize the balance of a REC and the economic mechanisms associated with them. For each hour h, the following fundamental energy streams are defined:

1. **Shared Energy ($E_{\mathbf{shared},h}$):** the share of energy produced and virtually consumed by all members of the REC. It forms the basis for calculating the incentives.

2. **Energy Injected into the grid ($E_{\mathbf{injected},h}$):** the share of energy produced by the REC plants or from the discharge of batteries or BESS that is injected into the national electricity grid and subsequently sold.

3. **Withdrawn Energy ($E_{\mathbf{withdrawn},h}$):** the share of energy that the REC members purchase from the grid.

Table 2.4 links these energy streams with their respective revenue streams for the REC, as defined by current regulations.

Table 5.2: Economic valuation mechanisms for energy flows within the REC (Renewable Energy Community).

Energy Flow	**Valuation Mechanism**	**Economic Value [€/MWh]**
Shared Energy within the REC	Premium Tariff (CACER)	Variable formula: TIP_h with caps and adjustments
Shared Energy within the REC	ARERA Valorization Fee	Value defined by ARERA
Energy Injected into the Grid	Dedicated Withdrawal (RID)	Hourly Zonal Price (Pz_h)
Withdrawn Energy	Purchase from Supplier	*(Cost for members, not revenue for the REC)*

As can be seen from the table, the economic objective of a REC is twofold:

- To maximize shared energy, in order to access the Premium Tariff and the ARERA valuation fee;
- To manage the energy injected into the grid, selling it at the most advantageous market price possible.

5.5 Steps to Create a REC

The establishment of a Renewable Energy Community (REC) represents an articulate process involving regulatory, technical, and organizational aspects. It is not limited solely to the construction of renewable energy production plants, but requires the definition of a structure capable of ensuring efficient management of the community and a correct allocation of economic and energy benefits among participants. In this context, both compliance with the requirements set by current regulations and the presence of the technical conditions necessary for the operation of the configuration are fundamental. This section therefore analyzes the main operational phases for the establishment of a REC, focusing on the legal and technical aspects that allow its activation and development [31].

Phase 1: Context Analysis (Initial scoping)

An initial group of promoting entities is identified, along with the areas already available for the construction of renewable production plants, and the broad consumption/production profile of the initiative's promoters and plants. In particular:

- Any public or private entity, including individual citizens, can promote the establishment of a REC.
- A REC must include at least two final customers, acting as shareholders or members of the community and one production plant.
- The usable surfaces for the construction of the plants within the reference perimeter (primary substation) are identified.
- Other potentially interested members are identified among whom to promote the initiative.

Phase 2: Promotion (Community engagement)

Participatory processes are launched aimed at gathering potential memberships. In this phase, promoters may organize public events/debates targeted at illustrating the specific characteristics of the project to be implemented. More in detail:

- Promotion moments for the initiative are organized, also differentiated by target audience (e.g., citizens, businesses, etc.), to increase the number of potential members, highlighting environmental, social, and economic benefits.
- It is important to highlight that membership does not require any change of supplier, nor administrative burdens, and that members can withdraw at any time and exit the configuration, without prejudice to any fees agreed upon in case of early withdrawal for co-participation in the investments incurred, which must in any case be fair and proportionate.

Municipalities can also promote a REC: a policy document must be prepared outlining the objectives to be pursued and defining the commitment of the Entity, for example by providing economic resources for planning/design, acting as an aggregating entity, raising awareness in the territory, collecting citizen memberships, and managing the REC from an administrative and maintenance perspective. A public notice will then be issued to promote the opportunity to become members of a REC. Municipalities can be members of a REC both as producers, installing plants on municipal surfaces, and as consumers, withdrawing electricity from the grid for a user point included in the configuration as the holder of the relevant bill; alternatively, they can make their own spaces (a building roof or an area) available for the benefit of a REC without being members.

Phase 3: Vision and Model (Strategic definition)

The strategic vision of the Community and the model of the future REC are defined, and a project idea agreed upon among potential members is formulated, identifying the environmental, economic and social goals to be pursued. More precisely:

- The roles and responsibilities of the promoters and further types of members (e.g., producers, consumers, sponsors, financiers) are established.
- The conditions under which the initiative is actualized are identified (e.g., minimum shared energy from the plants to be included in the configuration, minimum economic resources necessary for the launch).

- The concrete activities that the REC can carry out, the potential financial inflows and outflows, and the reference legal model for the establishment are evaluated.

Phase 4: Collection of Memberships (Grid perimeter validation)

After promoting the REC, memberships are collected, verifying the condition of "proximity", namely belonging to the same primary substation.[2]

Phase 5: Feasibility Study and Design (Technical and economic validation)

After gathering memberships for the REC and defining the potential surfaces usable for plant construction, the process moves to the actual feasibility study, which is structured on three main levels: technical, legal-managerial, and economic-financial.

On the **technical level**, available surfaces for the plants, access requirements for incentives, and hourly consumption and production profiles are analyzed in order to estimate shareable and incentivizable energy. This requires a quantitative characterization of three fundamental quantities: the aggregate demand (the sum of the hourly withdrawals of all members), the expected hourly generation of the RES plants and, where applicable, the capacity of the energy storage systems, which allow for the temporal decoupling of production and consumption, increasing the share of shared energy. In this phase, the most suitable operational model is also defined, which depends strictly on the role assumed by the involved entities: the *consumer* participates solely with their consumption POD and benefits from the distribution of incentives; the *prosumer* owns both a production plant and a withdrawal point, enjoying both bill savings from physical self-consumption and incentives on the share injected into the grid and shared with the community; finally, the *pure producer* makes a dedicated plant available, whose energy is entirely injected into the grid. The plants do not necessarily have to be owned by the REC: they can belong to third parties, provided that the community has availability and control over them, regulated by a specific contract.

On the **legal and managerial level**, the most appropriate legal form is defined (association, cooperative, etc.), the governance model is structured and the methods for distributing economic benefits among members are identified, taking into account the expected social and environmental impacts.

On the **economic-financial level**, a plan is developed to verify the sustainability of the investment, and potential financing strategies are explored for the plants that the REC intends to build, including public tenders, equity, bank loans, ESCo contracts or crowdfunding instruments.

Phase 6: Constitution of the REC (Legal formalization)

The fundamental documents for the establishment of the entity (bylaws, articles of association) and the contracts necessary to place the production plants at the disposal of the REC and to regulate relations between the entity and its members are drafted.

The REC must be constituted, choosing the most appropriate form for the specific case, as an autonomous legal entity that, acting in its own name, can exercise rights and be subject to obligations. Current regulations stipulate that the REC must not have a non-profit purpose, meaning it is a non-profit entity.

[2]On the GSE website, it is possible to consult the Interactive Map of primary substations to view the relevant conventional area and the reference code (consisting of 11 alphanumeric characters, for example "AC001E00934").

It is therefore necessary for the members of the REC to define and approve the Articles of Association and the Bylaws of the REC, which describe the general principles, purposes, goals and operational rules of the energy community.

The Shareholders' Assembly is the venue for participation in the life of the REC; its task is to define a Regulation on the allocation of amounts deriving from energy sharing, which can be directed, for example, toward energy poverty mitigation interventions, social initiatives, environmental redevelopment or social support in the local area where the REC operates.

Phase 7: Plant Implementation (Construction and grid connection)

The plants (or plant) for renewable energy production are constructed through engineering design, obtaining any necessary authorizations, installation and connection to the electricity distribution grid. Multiple renewable energy plants with different producers, different surfaces and relative authorization procedures can be present within the REC and they do not necessarily have to coincide with one of the final customers, provided they are powered by the same primary substation. The expenses that had to be considered are:

- For the design and construction of the plant(s);
- The coverage of administrative costs.

The regulation adopted by each REC establishes the rules for the eventual reimbursement of expenses to the members who incur them, using the amounts deriving from the Energy Sharing of the REC.

Phase 8: Access to GSE Contributions (Commercial operation activation)

At this stage, the request for access to incentives can be submitted to the GSE through the customer portal. The Referent, i.e., the legal representative of the REC in relations with the GSE, submits the request electronically for the shared electricity valuation and incentive service to the GSE. The GSE carries out a technical-administrative review of the information and documentation sent and communicates the outcome of the investigation to the Referent. If the outcome is positive, the GSE will sign the Contract, which regulates the distributed self-consumption service. The REC enters commercial operation.

Phase 9: Management (Operational lifecycle)

Once established, the REC enters its operational phase, which lasts for the entire incentive period (20 years). This phase includes:

- **Operational management:** monitoring plant production, routine and extraordinary maintenance;
- **Energy management:** balancing demand and supply, optimizing the use of energy storage systems and monitoring hourly energy flows;
- **Administrative and financial management:** managing relations with the GSE for receiving incentives, managing members (new admissions or withdrawals) and allocating economic benefits among members according to the criteria established in the bylaws.

This last aspect is among the most delicate of the entire governance: the regulation does not impose a single model, leaving the community free to define its own split methods autonomously.

However, the CACER Decree introduces a precise constraint to protect the social impact of the benefits: the proceeds of the premium tariff referring to the share of shared energy up to 55%, reduced to 45% for RECs that have also benefited from the PNRR capital grant, can be freely distributed among all members. Any share exceeding these thresholds must instead be allocated exclusively to consumers other than companies (natural persons, local authorities, religious bodies, etc.) or used for social purposes with positive impacts on the territories where the plants operate.

Chapter 6

Characterization of Case Studies and Load Data Analysis

6.1 Introduction

This section constitutes the analytical foundation of the entire feasibility study. After describing the operational principles of the PV plant, the battery storage system, and the electrolyzer, and after outlining the regulatory framework and operational principles of RECs, the work now shifts to the analysis of specific case studies, all based on the constitution of a REC located in Minervino di Lecce:

- **Scenario 1 (S1 hereinafter):** REC constituted with a PV plant and no storage system
- **Scenario 2 (S2 hereinafter):** REC constituted with a PV plant and no storage system, but with the implementation of a Demand Response (DR) strategy
- **Scenario 3 (S3 hereinafter):** REC constituted with a PV plant and a Battery Energy Storage System (BESS); within this scenario, a particle swarm optimization (S3-opt) is additionally carried out on the storage capacity to verify the adequacy of the installed sizing
- **Scenario 4 (S4 hereinafter):** REC constituted with a PV plant, a Battery Energy Storage System (BESS), and H_2 production

The objective of this chapter is to describe in detail the sample of real end-users composing the energy community, conducting a quantitative characterization of their energy consumption profiles. Through data analysis, hourly consumption patterns will be identified for each user category, highlighting the daily and seasonal dynamics that define the energy demand of the territory. This load characterization constitutes an indispensable preliminary step for the subsequent modeling, simulation, and economic evaluation of the plant configurations presented in the following chapters. Once the hourly load profiling has been completed, the design of the 1 MWp PV plant is carried out; this is subsequently coupled with a BESS and, further, with an electrolyzer whose technical parameters are rigorously defined. The hourly generation profile of the plant is then analyzed. This is followed by the modeling of the energy flows characterizing the REC, implemented through MATLAB code for each scenario, yielding data on the shared, and therefore eligible for incentives, energy. This chapter thus establishes the methodological foundations upon which the entire comparative analysis of results is based, which constitutes the subject of the following chapter.

6.2 Sample Analysis

The location chosen for the establishment of the REC is Minervino di Lecce,, a municipality located in the province of Lecce, which also includes the hamlets of Specchia Gallone and Cocumola, which area is divided by two primary substations (Fig. 6.1) making slightly more complicated the definition of the loads, especially those pertaining to the Public Administration (PA hereinafter) and Public Lighting (PL hereinafter). The primary substation chosen as the aggregation perimeter of the energy community is the AC001E00101 visible in Figure 6.2. Below is described the methodology for the definition of the hourly profiles of residential users, industries, PA and PL.

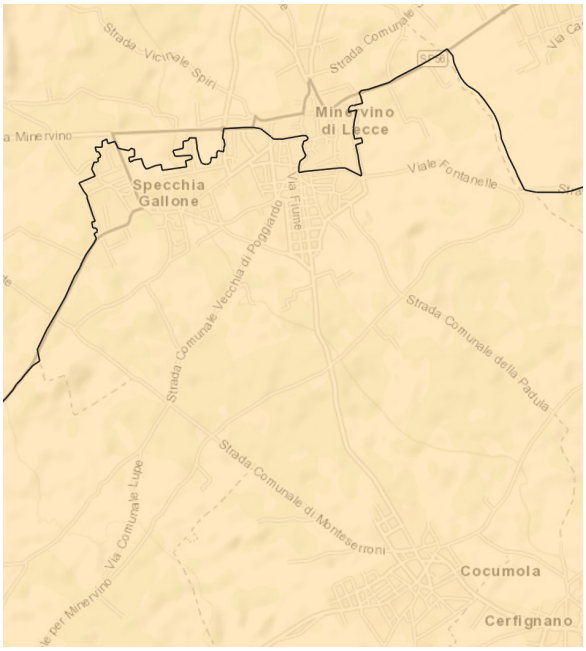


Figure 6.1: Division of the municipal area into two primary substations [32]



Figure 6.2: Primary cabin selected [32]

6.3 Residential End-Users

To ensure an analysis grounded in real and representative data, a sample of 6 metering points (PODs) located within the territory was selected. The data collected consist of the meter readings of each POD, extracted from electricity bills covering the period from 01/04/2025 to 31/03/2026. The sample was deliberately constructed to be heterogeneous, in order to reproduce the complexity of a genuine local community. Unlike industrial loads or public lighting, whose profiles are often predictable, residential consumption is influenced by a multitude of socio-demographic factors: household size, age distribution, working habits, and lifestyle. Accordingly, data were collected from households comprising between 2 and 5 members, with contracted power ratings of 3 kW and 4.5 kW. To project the results of the analysis onto a realistic scale, the 2021 ISTAT census data on the number of households present in the municipality were used as a reference. The municipality consists of 1,525 households. Considering that the municipality is served by two primary substations, as previously described, and that the prevailing building typology in the area is characterised by single-family dwellings, it is assumed that 80% of households fall within the catchment area of the primary substation under study. Of these, a REC membership rate of 70% is subsequently assumed.

$$N_{\text{members}} = 1525 \times 0{,}8 \times 0{,}7 = 854 \tag{6.1}$$

This yields a REC scenario comprising 854 equivalent households. The sample of 6 residential end-users was therefore scaled up to represent this broader aggregate. The underlying assumption of this extrapolation is that the initial sample, although numerically limited, is qualitatively representative of the diversity of the local population, encompassing households with differing characteristics and energy needs. The resulting scaling factor is approximately 142,33. As shown in Figure 6.3, the annual energy consumption of the individual residential PODs varies significantly, ranging from a minimum of approximately 2000 kWh to a maximum of approximately 4500 kWh. This variability reflects the coexistence of households with markedly different consumption patterns and behaviours, from small to larger and more energy-intensive family units. Figure 6.4 illustrates the monthly consumption profiles for the reference year for each of the 6 PODs in the sample.

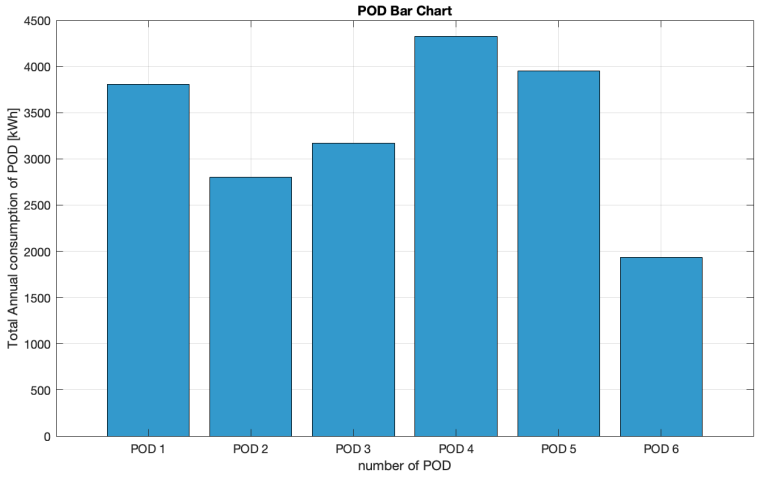


Figure 6.3: Distribution of total annual energy consumption for individual PODs in the residential category

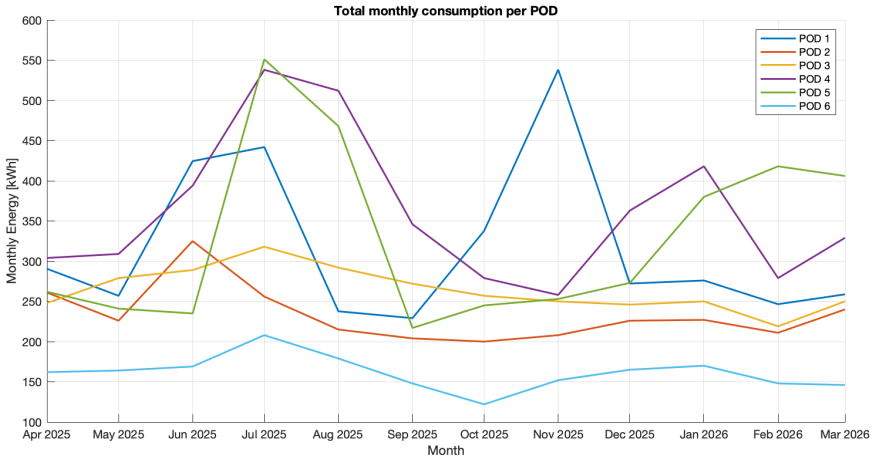


Figure 6.4: Total monthly consumption per Residential PODs

6.4 Industrial End-User

Regarding the industrial load profile to be included in the Renewable Energy Community, it was decided to include a single industrial user, given that it represents the only industrial facility within the catchment area of the reference primary substation, with a contracted power demand of 30 kW. The data collection procedure is analogous to that described for the residential end-users: meter readings were extracted from electricity bills covering the period from 01/04/2025 to 31/03/2026. Figure 6.5 illustrates the monthly consumption profile for the reference year of the industrial POD.

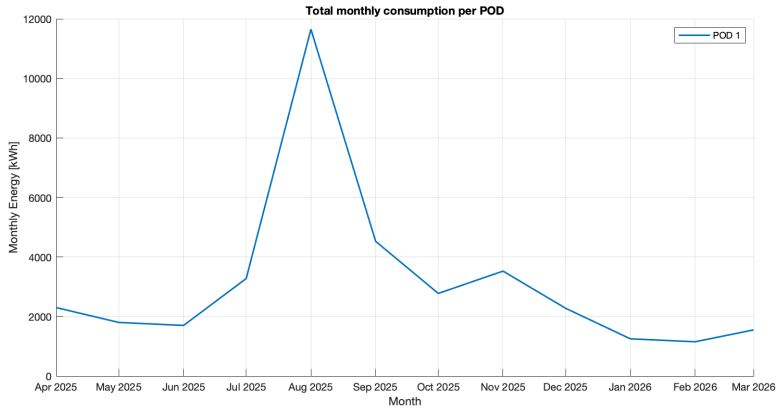


Figure 6.5: Total monthly consumption per Industrial POD

6.5 Public Administration

In order to obtain an estimate of the electricity consumption of municipal facilities, which represent potential loads to be included in the REC configuration, the municipal administration involved in the study was asked to provide the monthly consumption values reported in the electricity supply bills for the various buildings under their jurisdiction, covering the period from 01/04/2025 to 31/03/2026. The data were provided as Excel files, relating to 17 PODs, with no information regarding the physical location of each building. This makes it difficult to determine which end-users fall within the boundaries of the selected primary substation and which do not. Accordingly, a consumption figure equal to 80% of the total was assumed, on

the basis that the majority of public buildings are located within the catchment area of the selected primary substation. Figure 6.6 illustrates the aggregated monthly consumption of all municipal building PODs for the reference year.

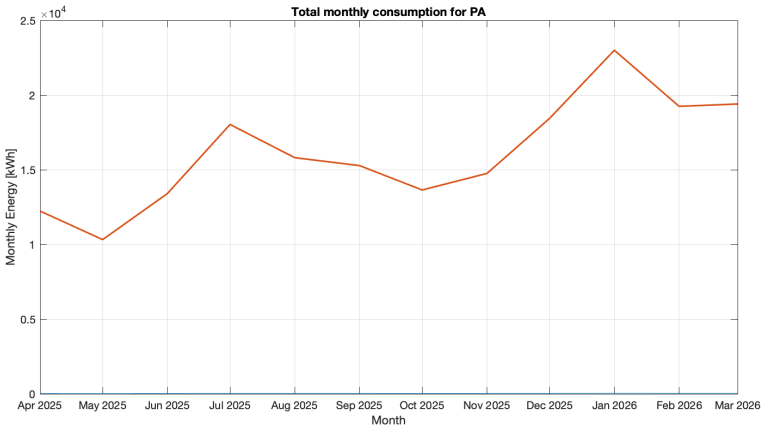


Figure 6.6: Total monthly consumption of PA

6.6 Public Lighting

In order to obtain an estimate of the electricity consumption attributable to public lighting, the municipal administration involved in the study was asked to provide the monthly consumption values reported in the electricity supply bills for the various PODs under their jurisdiction, covering the period from 01/04/2025 to 31/03/2026. The data were provided as Excel files, relating to 26 PODs, with no information regarding the physical location of each point of supply. This makes it difficult to determine which end-users fall within the boundaries of the selected primary substation and which do not. Accordingly, a consumption figure equal to 80% of the total was assumed, on the basis that the majority of public lighting infrastructure is located within the catchment area of the selected primary substation. Figure 6.7 illustrates the aggregated monthly consumption of all public lighting PODs for the reference year.

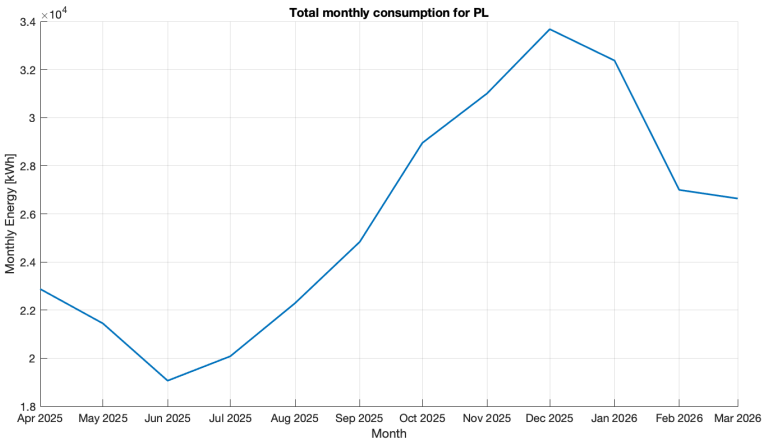


Figure 6.7: Total monthly consumption of PL

6.7 Aggregate Load Analysis of the Community

The summation of the individual consumption profiles defines the aggregate load of the REC, that is, the total energy demand that the generation plant and the storage system will be required to manage. Figure 6.8 shows the breakdown of the total annual consumption, amounting to approximately 3387 MWh.

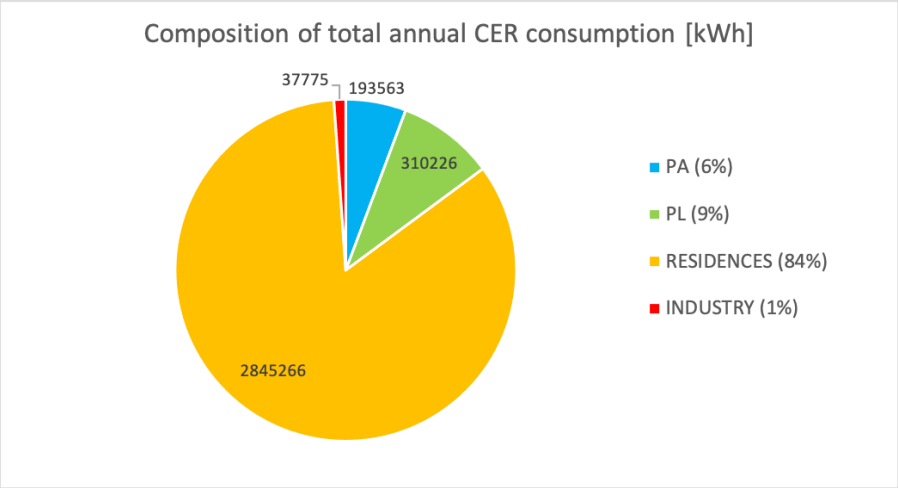


Figure 6.8: Aggregate Load of the Community

6.8 Hourly Load Profiling

Although second-generation (2G) smart meters are technically capable of recording and making available energy withdrawals at a quarter-hourly resolution, this level of granularity could not be obtained for any of the end-users included in the present configuration, regardless of category. Both first-generation (1G) and second-generation (2G) meters are present, in comparable proportion, across all four end-user categories considered (Public Administration, Public Lighting, residential, and industrial). For POD equipped with 1G meters, quarter-hourly data is unavailable as a matter of measurement capability, since these meters are inherently limited to monthly, time-of-use-aggregated readings. For POD equipped with 2G meters, quarter-hourly readings would in principle be accessible, but their retrieval requires the POD holder to actively request and activate a delegation towards the distributor's client portal; due to limited availability and time constraints on the part of the individual POD holders, this step could not be completed for any of the end-users involved in this study. As a result, the only data that could be consistently obtained across the entire configuration were monthly consumption values, disaggregated by time-of-use band, as reported on the electricity bill. For this reason, the analysis presented in this section is based on this common data source, uniformly across all four end-user categories. The electricity bill is the document periodically made available to the final customer by the energy supplier; it reports information on the customer's consumption, the amounts invoiced, payment terms, and other details relevant to the management of the supply contract. The reliability of the source data is therefore guaranteed by their origin: they constitute official fiscal measurements obtained from the electronic meters of the distribution network operator. These meters comply with the Measuring Instruments Directive (MID, 2014/32/EU), which certifies their accuracy and reliability for billing purposes. The consumption values reported in the bill for the relevant period, provided the end-user is equipped with a remotely read electronic meter, are broken down by time-of-use band. Electronic meters installed for electricity consumption measurement are indeed capable of recording customer

withdrawals distinguishing the time band in which they occur. The time bands, as defined by the Italian Regulatory Authority for Energy, Networks and Environment (ARERA), are time periods to which different energy prices correspond, and are structured as follows:

- **Band F1:** Monday to Friday, from 08:00 to 19:00, excluding national public holidays;
- **Band F2:** Monday to Friday from 07:00 to 08:00 and from 19:00 to 23:00; Saturday from 07:00 to 23:00, excluding national public holidays;
- **Band F3:** Monday to Saturday from 00:00 to 07:00 and from 23:00 to 00:00; Sundays and public holidays, all hours of the day.

An illustrative example of the data structure collected for the monthly electricity consumption of end-users, broken down by time band and expressed in kilowatt-hours [kWh], is provided in Table 6.1.

Table 6.1: Structure of the energy consumption table broken down by time-of-use slots.

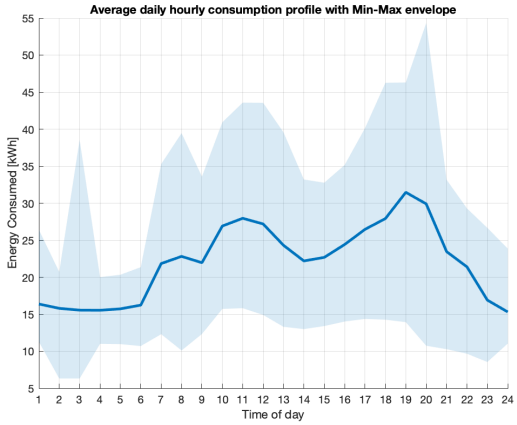
Year	**Month**	**Reading TOU1 [kWh]**	**Reading TOU2 [kWh]**	**Reading TOU3 [kWh]**	**TOU1 [kWh]**	**TOU2 [kWh]**	**TOU3 [kWh]**
2025	3	9956,744	9540,598	11830,284	–	–	–
2025	4	10055,186	9621,694	11941,356	98,442	81,096	111,072
2025	5	10128,287	9709,738	12037,150	73,101	88,044	95,794
2025	6	10265,985	9812,176	12221,461	137,698	102,438	184,311
...	...	...	...	...	...	...	...

Having identified the end-users to be considered as loads within the REC, for which the monthly electricity consumption values disaggregated by time band are known for the reference year, the annual hourly load profiles must be derived. Estimating the hourly consumption of the municipal end-users included in the configuration is a more complex task, subject to greater uncertainty, in the absence of real measured data on the hourly energy withdrawals from the grid by the electrical loads. Despite the availability in the scientific literature of various methodologies for generating or estimating hourly load profiles from monthly electricity consumption data reported in bills, as proposed in [33], the approach outlined by the Gestore dei Servizi Energetici (GSE) was adopted in this work. The GSE has indeed established a procedure for profiling electricity withdrawals on an hourly basis, to be applied in cases where real hourly consumption measurements are unavailable [34]. The approach consists of adopting standard hourly load profiles that depend on the type of end-user and have been made available for a reference year by the GSE. Specifically, four different withdrawal curves are provided for low-voltage (LV) end-users, according to their category:

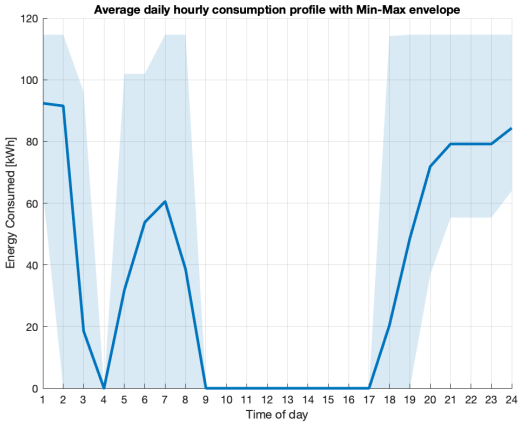
1. hourly withdrawal profile for domestic end-users;
2. hourly withdrawal profile for public lighting end-users;
3. hourly withdrawal profile for public electric vehicle charging infrastructure end-users;

4. hourly withdrawal profile for non-domestic end-users.

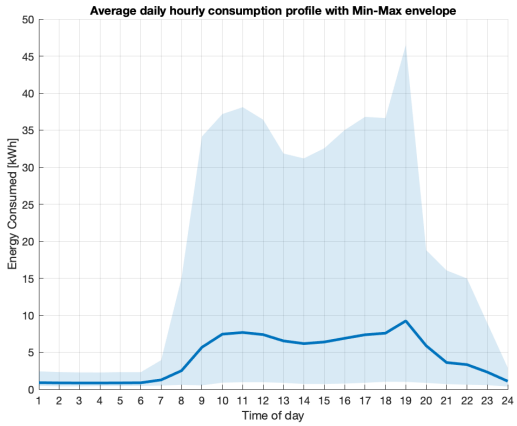
For each end-user considered in the study, a standard load profile is first assigned based on its category. This profile is then scaled so that the total monthly consumption in each time band, where a time-differentiated tariff applies, matches the value reported in the bill. The extraction of the profiles required to proceed with the feasibility analysis was carried out by means of a dedicated module implemented in MATLAB. Figure 6.9 shows the mean daily hourly profiles with min–max envelopes for the four categories of end-users belonging to the REC.



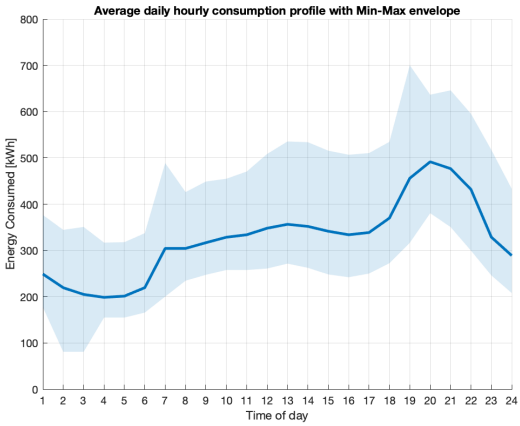
(a) Average daily hourly consumption profile with Min-Max envelope for PA



(b) Average daily hourly consumption profile with Min-Max envelope for PL



(c) Average daily hourly consumption profile with Min-Max envelope for Industrial End-User



(d) Average daily hourly consumption profile with Min-Max envelope for Residential End-User

Figure 6.9: Average daily hourly consumption profile with Min-Max envelope

The key observations from these figures are briefly summarized below:

- **Public Administration:** The consumption profile is predominantly diurnal, with a peak during the central morning hours (between 09:00 and 13:00), corresponding to the opening hours of offices and schools. A marked reduction, a pronounced valley, in withdrawals is observed during the central hours of the day, particularly evident at weekends and during months with higher solar irradiance (spring and summer). This dynamic is indicative of pre-existing photovoltaic installations on public buildings: physical self-consumption reduces grid withdrawals, generating a net drop precisely when the baseline consumption of public administration facilities is at its minimum.

- **Public Lighting:** This category exhibits an exclusively nocturnal profile. Consumption is zero during daylight hours and activates consistently from dusk to dawn. This load is highly predictable and perfectly anti-correlated with photovoltaic generation, representing an ideal opportunity for the sharing of stored energy.
- **Industrial End-User:** The profile is characterised by a sustained and approximately constant consumption plateau during working hours (approximately from 08:00 to 20:00). It is worth noting that this end-user exhibits a substantially higher workload during summer, representing an ideal opportunity for the sharing of energy instantaneously generated by the PV plant.
- **Residential End-Users:** The profile follows the typical double-peak pattern, with consumption beginning to rise in the morning (around 07:00–09:00) and a pronounced evening peak (between 18:00 and 23:00), corresponding to households returning home and the use of domestic appliances.

Chapter 7

Technical Sizing of PV, BESS and H2 Production Systems

7.1 Introduction

Having characterized in detail the consumption profile of the potential Renewable Energy Community, this chapter focuses on the definition of the generation system, the electrochemical storage system, and the hydrogen production unit. The technological components of the photovoltaic plant, the BESS, and the electrolyzer are sized and their technical characteristics are described. The objective is to rigorously define the technical parameters of the core assets of the REC under study.

7.2 Characterization of PV plant

7.2.1 Installation Site, Orientation Parameters, and Yield Analysis of the Photovoltaic Generation Plant

To meet the energy demand of the REC, a grid-connected production plan was assumed, that is, a plant not associated with any existing physical end-user but connected directly to the medium-voltage network through its own grid connection point (POD). It is assumed that the promoter and owner of the plant is the REC itself, whose establishment is promoted by the Municipal Administration of the territory under study. A flat, municipally owned plot of land free from significant shading was identified for the installation of the plant (Figure 7.1).



Figure 7.1: Location of PV plant

This strategic choice maximizes the energy yield of the plant and simplifies the authorization and construction phases. The orientation parameters, defined by means of the PVGIS simulation tool, were optimized to maximize annual energy output and are reported below:

- **Geographical Coordinates:** the coordinates of the installation site are characterized by a latitude of 40,079° and a longitude of 18,417° (expressed in decimal degrees).

- **Array type:** fixed ground-mounted structure.
- **Tilt angle:** 35° with respect to the horizontal plane.
- **Azimuth:** 0°, corresponding to a due-south orientation.

This configuration ensures excellent solar exposure throughout the year, with an estimated annual global irradiation on the collector plane of 1947,76 kWh/m^2. On the basis of this configuration, the PVGIS software generated the hourly generation profile for an entire year. This vector of 8760 values constitutes the fundamental input for all subsequent simulations. To fully characterize the behavior of the plant, its generation patterns are analyzed on both a seasonal and a monthly basis.

The analysis of the hourly generation data obtained from PVGIS reveals a non-trivial behavior regarding the seasonal distribution of the system's energy yield. As illustrated in Figure 7.2, the mean hourly peak power during the spring season (MAM) reaches 695,1 kW, slightly exceeding the summer peak (JJA) of 692,8 kW. Furthermore, the total monthly energy profile in 7.3 demonstrates that May achieves a performance level ($1{,}62 \times 10^5$ kWh) virtually identical to June ($1{,}60 \times 10^5$ kWh) and closely trailing July ($1{,}73 \times 10^5$ kWh).

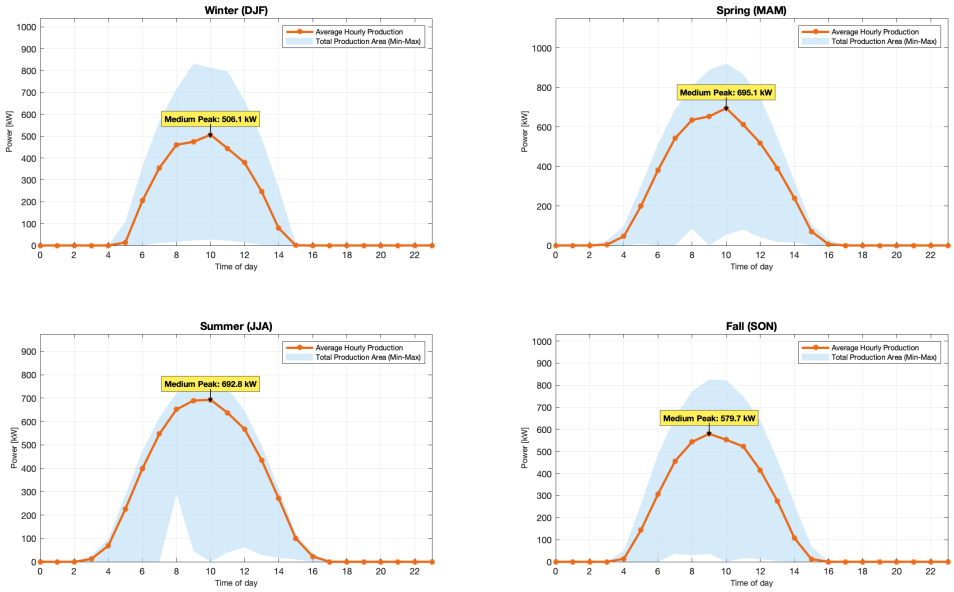


Figure 7.2: Hourly generation profiles categorized by energy season

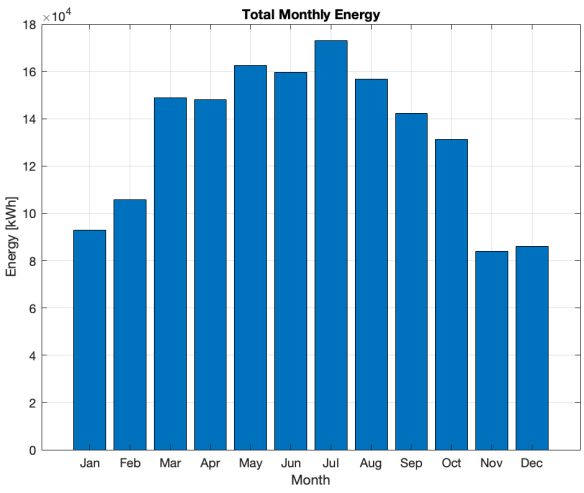


Figure 7.3: Monthly generation profiles

This trend, which may initially appear counterintuitive given the higher theoretical solar irradiance of the summer solstice, is a well-documented physical phenomenon driven by the thermal derating of photovoltaic modules. The electrical efficiency of silicon-based PV cells is strictly dependent on their operating temperature T_c. While solar irradiance maximizes during June and July, the concurrently high ambient temperatures and reduced wind cooling elevate the cell temperature well above the Standard Test Conditions ($STC = 25°C$), often exceeding 60°C. The maximum power output P_{mp} decreases linearly according to the temperature coefficient γ (typically ranging between $-0{,}35\%/°C$ and $-0{,}40\%/°C$), as formulated below:

$$P_{mp}(T_c) = P_{mp,STC} \cdot [1 + \gamma \cdot (T_c - 25°C)] \tag{7.1}$$

In contrast, the spring months, particularly May, benefit from high horizontal irradiance coupled with mild ambient temperatures and stronger ventilation. This combination prevents the severe thermal degradation of the semiconductor, allowing the panels to operate closer to their nominal efficiency. Additionally, the fixed tilt angle of the array (optimized for annual performance or mid-season sub-optimal angles) ensures a more perpendicular angle of incidence during spring than during the peak summer weeks, where the solar altitude angle reaches its zenith. This geometric advantage, combined with the favorable thermal state, fully justifies the prominent production envelope and the outstanding absolute peaks observed in the spring dataset.

7.2.2 Components of the PV Plant

The plant design was finalized to achieve a nominal DC power of approximately $1\,\mathrm{MW_{dc}}$, in compliance with the power limit imposed on plants admitted to REC configurations. High-efficiency bifacial n-type photovoltaic modules were selected as the generation technology, in order to maximize energy output per unit of occupied area; their technical specifications are summarized in the corresponding Table 7.1 and dimensions shown in the Figure 7.4.

PV Panel Characteristics			
Manufacturer	JA SOLAR		
Model	JAM72D40-600/LB		
Peak Power	P	**600**	W
Open-Circuit Voltage	V_{oc}	**52,4**	V
Maximum Power Voltage	V_{mp}	**43,76**	V
Short-Circuit Current	I_{sc}	**14,48**	A
Maximum Power Current	I_{mp}	**13,71**	A

Table 7.1: Technical specifications of the JA Solar PV panel[35].

The conversion from direct current (DC) to alternating current (AC) is entrusted to three-phase string inverters, specifically the Sigen Hybrid Inverter 110M1-HYB, whose technical specifications are likewise summarized in the corresponding Table 7.2.

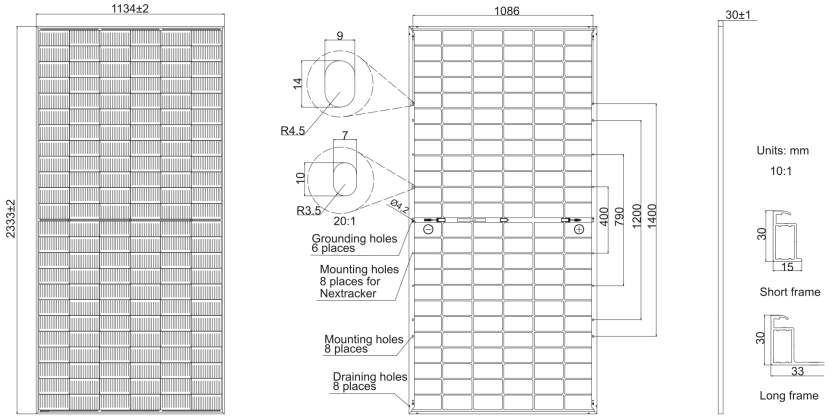


Figure 7.4: PV module dimensions

Inverter Characteristics			
Manufacturer	SIGENERGY		
Model	110M1-HYB		
Max DC Input Power	$P_{\text{in dc, max}}$	**220**	kW
AC Output Power	P_{ac}	**110**	kW
MPPT Voltage Range	$V_{\text{inv, mppt min}} - V_{\text{inv, mppt max}}$	**160–1000**	V
Number of MPPTs		**8**	
Number of Strings per MPPT		**2**	
Max Input Voltage	$V_{\text{in inv, max}}$	**1100**	V

Table 7.2: Technical specifications of the Sigenergy inverter[36].

The decentralized power conversion architecture is typically adopted in PV plants where the photovoltaic generator is subject to varying irradiance conditions, for example, modules with different tilt angles, different azimuth orientations, or partial shading on portions of the array. By employing multiple small-capacity inverters equipped with multi-MPPT functionality, PV strings operating under different irradiance conditions can be distributed across separate MPPT inputs, thereby maximizing the energy yield of all strings within the generator. A further advantage of string inverters relates to conversion efficiency: string inverters generally achieve higher conversion efficiency than centralized inverters. Many modern string inverters incorporate DC fuses and DC disconnect switches as standard, eliminating the need for DC combiner boxes in the installation. The use of string inverters implies that the AC outputs of individual inverters are connected in parallel through AC junction panels, which typically include thermal-magnetic circuit breakers to protect the AC lines between the junction panel and each inverter. The decentralized architecture also offers a significant operational and maintenance advantage: in the event of an inverter failure, only a fraction of the PV generator is taken out of service and energy production is not entirely compromised. Furthermore, in the event of a string inverter fault, replacement is straightforward and rapid.

Although the design choices adopted for this plant result in all modules being subject to identical irradiance conditions, string inverters were nonetheless selected in view of the multiple advantages described above. The combination of these components yields a DC-to-AC ratio R,

defined as:

$$R = \frac{P_{\text{DC, PV GEN}}}{P_{\text{AC, Max Inv}}} \tag{7.2}$$

equal to $R = 1{,}3$, where $P_{\text{DC, PV GEN}}$ is the DC power of the PV array and $P_{\text{AC, Max Inv}}$ is the maximum AC power of the inverter stage. When $R > 1$ (DC oversizing), two distinct effects arise compared to the case $R < 1$:

- during the central hours of the day, the inverter output power is limited by the inverter itself (clipping);
- energy generation is increased during the hours in which the power produced by the PV generator falls below the inverter rated limit.

It can therefore be stated that operating with $R > 1$ reduces the incidence of inverter costs within PV plants, since, for a given value of $P_{\text{AC, Max Inv}}$, two relevant consequences follow compared to the case $R < 1$:

- minimization of capital costs in terms of €/kW_{AC};
- maximization of the energy yield of the PV plant.

7.2.3 Design Criteria

Assuming the use of monocrystalline silicon modules with a unit peak power of 600 W_p, a total of 1,665 modules would be required, calculated as:

$$N_{\text{modules}} = \frac{999000\,\text{W}}{600\,\text{W}} = 1665 \tag{7.3}$$

Taking into account the string voltage, which determines the DC input voltage of the inverter, and the total current of the parallel-connected strings, which primarily governs cable sizing, the modules are arranged across 7 inverters. Each of the first 6 inverters is connected to 8 pairs of strings, each string comprising 15 modules in series, with each pair connected to a dedicated MPPT input. The seventh inverter is connected to 7 pairs of strings of 15 modules in series plus one additional single string of 15 modules in series. The total module count is therefore:

$$N_{\text{modules}} = 15 \times 2 \times 8 \times 6 + 15 \times 2 \times 7 + 15 = 1665 \tag{7.4}$$

yielding a total installed peak power of 999 kW_p.

The actual sizing procedure was carried out by applying standard electrical design rules [9], implemented in a Microsoft Excel spreadsheet. The module and inverter parameters are entered as inputs, and the appropriate configuration is subsequently selected by computing the relevant voltage and current quantities and verifying compliance with the limits listed and described below:

1. Determination of Module $V_{\text{OC, MAX}}$ and $V_{\text{OC, MIN}}$

The open-circuit voltage V_{OC} of a photovoltaic module depends on the ambient conditions at the installation site. The maximum and minimum open-circuit voltages are calculated in accordance with Annex B of CEI 64-8/7, Chapter 712, as follows:

$$V_{\text{OC, MAX}} = V_{\text{OC, STC}} \cdot \left[1 + \frac{\beta}{100} \cdot (T_{\text{min}} - 25)\right] \tag{7.5}$$

$$V_{\text{OC, MIN}} = V_{\text{OC, STC}} \cdot \left[1 + \frac{\beta}{100} \cdot (T_{\text{max}} - 25)\right] \tag{7.6}$$

where:

- $T_{\min}$ and $T_{\max}$ are respectively the minimum and maximum design temperatures at the installation site of the PV plant [°C];
- $V_{\text{OC, STC}}$ is the open-circuit voltage of the PV module under Standard Test Conditions (STC) [V];
- β is the temperature coefficient of the module open-circuit voltage, expressed in $\left[\%\,\text{K}^{-1}\right]$.

2. Determination of Module $V_{\text{MPP, MAX}}$ and $V_{\text{MPP, MIN}}$

The maximum power point voltage V_{MPP} of a photovoltaic module depends on the ambient conditions at the installation site. The maximum and minimum values are calculated as follows:

$$V_{\text{MPP, MAX}} = V_{\text{MPP, STC}} \cdot \left[1 + \frac{\beta}{100} \cdot (T_{\min} - 25)\right] \tag{7.7}$$

$$V_{\text{MPP, MIN}} = V_{\text{MPP, STC}} \cdot \left[1 + \frac{\beta}{100} \cdot (T_{\max} - 25)\right] \tag{7.8}$$

where:

- $T_{\min}$ and $T_{\max}$ are respectively the minimum and maximum design temperatures at the installation site of the PV plant [°C];
- $V_{\text{MPP, STC}}$ is the maximum power point voltage of the PV module under Standard Test Conditions (STC) [V];
- β is the temperature coefficient of the module voltage, expressed in $\left[\%\,\text{K}^{-1}\right]$.

3. Determination of Module $I_{\text{SC, MAX}}$

The short-circuit current I_{SC} of a PV module varies as a function of the cell operating temperature. Since I_{SC} is proportional to cell temperature, it reaches its maximum value at the maximum cell temperature. On this basis, the maximum short-circuit current $I_{\text{SC, MAX}}$ of the PV module is calculated as follows:

$$I_{\text{SC, MAX}} = I_{\text{SC, STC}} \cdot [1 - \alpha \cdot (25 - T_{\text{cell}})] \tag{7.9}$$

where:

- $I_{\text{SC, STC}}$ is the short-circuit current of the PV module under Standard Test Conditions (STC) [A];
- α is the temperature coefficient of the short-circuit current, expressed in $\left[\%\,\text{K}^{-1}\right]$;
- T_{cell} is the maximum design cell temperature at the installation site [°C].

It should be noted that $I_{\text{SC, STC}}$ is the short-circuit current of the PV module measured under Standard Test Conditions (STC). In accordance with CEI 64-8/7 Chapter 712 and IEC 60364-7-712, a mandatory overcurrent safety factor of 1,25 must be applied to $I_{\text{SC, STC}}$ when sizing protective devices and verifying current limits. This factor accounts for the possibility that, under certain atmospheric conditions such as cloud-edge enhancement or high-altitude clear-sky irradiance, the in-plane irradiance may temporarily exceed the STC reference value of $1000\,\text{W/m}^2$, leading to short-circuit currents higher than the rated $I_{\text{SC, STC}}$. The corrected current to be used in the verification of Equation 7.9 therefore becomes:

$$I_{\text{SC, MAX, design}} = 1{,}25 \times I_{\text{SC, MAX}} \tag{7.10}$$

This conservative approach ensures that all current-carrying conductors, protective devices, and inverter input stages remain within their rated limits even under transient irradiance conditions exceeding the STC reference.

4. Determination of String $I_{\mathbf{SC,\ MAX}}$

The total current in a string of series-connected PV modules equals the current generated by a single module. Accordingly, the maximum short-circuit current of the string $I_{\text{SC, MAX, String}}$ is equal to the maximum short-circuit current of the individual PV module $I_{\text{SC, MAX, Module}}$:

$$I_{\text{SC, MAX, String}} = I_{\text{SC, MAX,design}} \tag{7.11}$$

5. Determination and Verification of the Number of Modules per String

The number of PV modules connected in series within each string must satisfy both an upper and a lower bound, imposed respectively by the inverter's maximum input voltage and by its MPPT voltage window. The maximum number of modules per string $N_{\text{MAX, Modules}}$ is determined by the condition that the string open-circuit voltage must never exceed the maximum DC input voltage of the inverter, in order to prevent damage caused by overvoltage:

$$N_{\text{MAX, Modules}} \leq \frac{V_{\text{MAX, Inv}}}{V_{\text{OC, MAX, Module}}} \tag{7.12}$$

where $V_{\text{MAX, Inv}}$ is the maximum DC input voltage accepted by the inverter and $V_{\text{OC, MAX, Module}}$ is the maximum open-circuit voltage of a single PV module as defined in Equation 7.5. Conversely, the minimum number of modules per string $N_{\text{MIN, Modules}}$ is governed by the requirement that the string voltage at the maximum power point must always remain above the inverter start-up voltage and within the lower bound of the MPPT voltage range. Should the string voltage fall below these thresholds, the inverter would fail to start and would be unable to track the MPP:

$$N_{\text{MIN, Modules}} \geq \frac{V_{\text{MPPT, MIN, Inv}}}{V_{\text{MPP, MIN, Module}}} \tag{7.13}$$

where $V_{\text{MPPT, MIN, Inv}}$ is the lower bound of the inverter MPPT voltage range and $V_{\text{MPP, MIN, Module}}$ is the minimum maximum power point voltage of a single module as defined in Equation 7.8. Once both bounds have been established, the chosen number of series modules per string $N_{\text{Modules, String}}$ must be verified to satisfy the following inequality:

$$N_{\text{MIN, Modules}} < N_{\text{Modules, String}} < N_{\text{MAX, Modules}} \tag{7.14}$$

where $N_{\text{MAX, Modules}}$ is the maximum and $N_{\text{MIN, Modules}}$ is the minimum number of modules connectable in each string. Compliance with this inequality ensures that the inverter operates safely and within its rated MPPT range under all design temperature conditions.

6. Determination of the Maximum Number of Strings per Inverter

Assuming that the inverter has been correctly sized with respect to the rated power of the PV generator, the maximum number of strings per inverter is determined automatically as a function of the maximum DC current accepted by the inverter. For string inverters equipped with independent MPPT inputs, the maximum number of strings that may be connected in parallel to a single MPPT channel is defined by the condition that the sum of the currents of all strings connected to the same MPPT must not exceed the maximum current accepted by the inverter for that individual MPPT input:

$$N_{\text{MAX, Strings, MPPT}} \leq \frac{I_{\text{MAX, DC, MPPT, Inv}}}{I_{\text{SC, MAX, String}}} \tag{7.15}$$

where $I_{\text{MAX, DC, MPPT, Inv}}$ is the maximum DC current accepted by the inverter on a single MPPT input and $I_{\text{SC, MAX, String}}$ is the maximum short-circuit current of a single string as defined in Equation 7.11.

7. Inverter Power Selection

Once the number of modules per string $N_{\text{Modules, String}}$ has been determined, the power of each individual string can be calculated from the rated power of a single PV module:

$$P_{\text{String}} = P_{\text{Module}} \times N_{\text{Modules, String}} \tag{7.16}$$

where P_{Module} is the rated peak power of a single PV module [W_p] and $N_{\text{Modules, String}}$ is the number of modules connected in series per string. The maximum DC input power of the inverter must then be greater than or equal to the total power delivered by all parallel-connected strings assigned to that inverter:

$$N_{\text{Strings}} \times P_{\text{String}} \leq P_{\text{DC, MAX, Inv}} \tag{7.17}$$

where N_{Strings} is the number of strings connected in parallel to the inverter and $P_{\text{DC, MAX, Inv}}$ is the maximum DC input power rating of the inverter.

8. Verification of String Voltage Against the Inverter MPPT Window

Once the number of series-connected modules per string has been determined, the resulting string voltage values must be verified against the MPPT operating window specified in the inverter datasheet. Specifically, the following two conditions must be satisfied simultaneously:

$$V_{\text{MPP, MIN, Module}} \times N_{\text{Modules, String}} \geq V_{\text{MPPT, MIN, Inv}} \tag{7.18}$$

$$V_{\text{OC, MAX, Module}} \times N_{\text{Modules, String}} \leq V_{\text{MAX, Inv}} \tag{7.19}$$

The first condition ensures that the string voltage at the maximum power point under the most unfavourable thermal conditions (maximum design temperature) remains above the lower bound of the inverter MPPT range, guaranteeing that the inverter can track the MPP at all times. The second condition ensures that the string open-circuit voltage under the coldest design conditions (minimum design temperature) does not exceed the absolute maximum DC input voltage of the inverter, thereby preventing damage due to overvoltage. Compliance with both inequalities confirms that the inverter operates safely and efficiently within its rated MPPT window across the full range of design temperatures.

9. Verification of Maximum Short-Circuit Current

The maximum short-circuit current delivered to each MPPT input of the inverter must be verified against the corresponding rated limit reported in the inverter datasheet. The total current injected into a single MPPT channel is the sum of the short-circuit currents of all strings connected in parallel to that channel. The following condition must therefore be satisfied:

$$I_{\text{SC, MAX, String}} \times N_{\text{Strings, MPPT}} \leq I_{\text{sc, DC, MPPT}} \tag{7.20}$$

where $N_{\text{Strings, MPPT}}$ is the number of strings connected in parallel to the MPPT input under consideration. This verification ensures that the DC wiring, the inverter input stage, and any associated protective devices are not subjected to currents exceeding their rated values under worst-case irradiance and temperature conditions. Failure to satisfy this condition would

require either a reduction in the number of parallel strings per MPPT or the selection of an inverter with a higher input current rating.

7.2.4 String Layout Optimization

The definition of the geometric layout of the modules on the available surface represents a primary constraint for the subsequent electrical configuration of the strings. This approach is essential to guarantee a homogeneous cabling topology, minimize Joule-effect losses within the direct current (DC) conductors, and optimize overall string management. The analysis of electrical boundaries, dictated by the input voltage operating windows of the inverters, established that each string can be composed of a minimum of 5 to a maximum of 19 modules connected in series. From a mechanical and structural standpoint, the mounting systems accommodate the installation of two superimposed rows of modules per structural rack. To reconcile the geometric field constraints with electrical symmetry, the optimal solution identified and previously verified, entails the configuration of strings consisting of 15 modules each. The comprehensive layout of the photovoltaic generator is structured as follows and as illustrated in Figure 7.5:

- 13 double-row structures of 120 modules in total, geometrically symmetric, subdivided into an upper row of 60 modules and a lower row of 60 modules;
- 1 double-row structure containing 105 modules in total, geometrically asymmetric, subdivided into an upper row of 52 modules and a lower row of 53 modules.

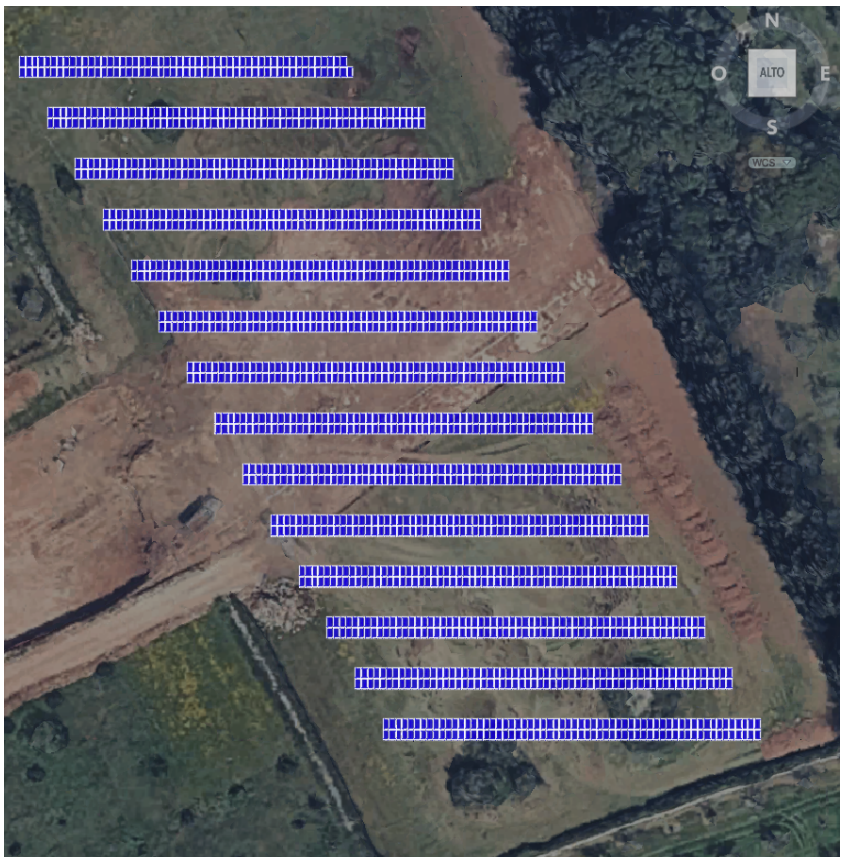
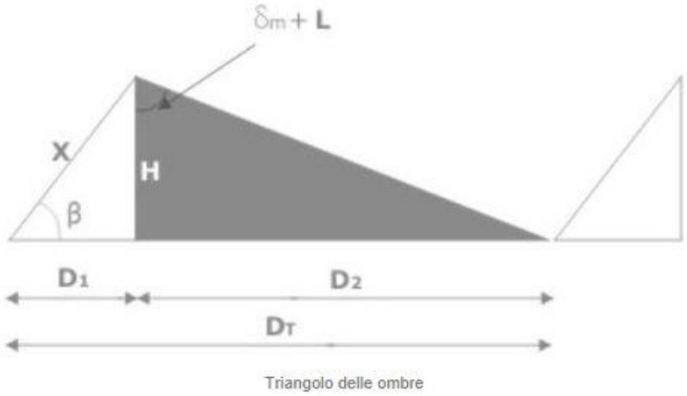


Figure 7.5: PV field layout

The pitch distance between parallel rows of the anchoring structures has been analytically determined to mitigate mutual shading phenomena (self-shading) during the central hours of the critical day (winter solstice), thereby preserving the local minimum solar altitude angle, as described in Figure 7.6. The result highlights a minimum structural pitch distance of 5,355 m.



Triangolo delle ombre

$$D_1 = X \bullet \cos\beta$$
$$H = X \bullet sen\,\beta$$
$$D_2 = H \bullet \tan(\delta_m + L)$$
$$D_T = D_1 + D_2$$

Figure 7.6: Calculation of the minimum distance between photovoltaic modules. $\delta_m = -23.45°$ indicates the solar declination at the winter solstice (December 21st), which represents the period when the sun is at its lowest altitude, L is the site latitude, X equal to double the length of the module and β is the Tilt angle.

The architecture features two distinct inverter capacities configured as follows:

- **6 units of** 110 **kW Inverters**: equipped with 8 independent MPPT inputs, each managing 2 parallel-connected strings of 15 modules (16 total strings per inverter);
- **1 unit of** 110 **kW Inverter**: equipped with 8 total MPPT inputs, of which 7 are configured with 2 parallel-connected strings, and 1 dedicated MPPT is assigned to a single string of 15 modules (15 total strings per inverter).

Consequently, the overall PV generator comprises 111 strings, resulting in a total count of 1665 photovoltaic modules. Based on the nominal rating of the single module, the total peak DC power of the PV array is 999 kWp, establishing an optimized DC-to-AC sizing ratio for the conversion system.

Table 7.3: Synoptic overview of the electrical and geometric sizing of the PV generator.

System Parameter	**Value**	**Unit of Measurement**
Modules per single string	15	[–]
Total number of strings	111	[–]
Total number of installed modules	1665	[–]
String inverters – 110 kW (8 MPPT × 2 str.)	6	[n.]
String inverter – 110 kW (7 MPPT × 2 str. + 1 MPPT × 1 str.)	1	[n.]
Total Generator Power	**999**	**[kWp]**

7.2.5 Cable Sizing

We proceed with the sizing of the electrical system cables and the choice of protection devices by adhering to the theory described in chapter 2.3. The guidelines for the cable sizing methodology are set out in CEI 64-8/5, Chapter 52. The DC current-carrying capacity I_z of the string cables is affected by the installation conditions. The rated current-carrying capacity I_z of the selected cable must satisfy the following criterion under the actual installation conditions:

$$I_z \geq I_0 \cdot k_1 \cdot k_2 \cdot k_3 \cdot k_4 \geq I_{\text{SC, MAX, String}} \tag{7.21}$$

where:

- I_z is the effective current-carrying capacity of the cable under actual installation conditions [A];
- I_0 is the reference current-carrying capacity of the cable as tabulated under standard installation conditions [A];
- k_1 is the correction factor accounting for ground temperature if different from 20 °C;
- k_2 is the correction factor accounting for the proximity effect between adjacent cables;
- k_3 is the correction factor accounting for burial depth if different from 0,8 m;
- k_4 is the correction factor accounting for the thermal resistivity of the surrounding medium.

For cables installed in air, the correction factors must be determined in accordance with CEI-UNEL 35024/1 *"Elastomeric or thermoplastic insulated electrical cables for rated voltages not exceeding 1000 V AC and 1500 V DC — Current-carrying capacities under steady-state conditions for cables installed in air"*. For buried cables, the applicable standard is CEI-UNEL 35026 *"Elastomeric or thermoplastic insulated electrical cables for rated voltages of 1000 V AC and 1500 V DC — Current-carrying capacities under steady-state conditions for buried cables"*.

Cable Selection for Strings and DC-Side Protections

The string cable must comply with the European coding for solar cables; therefore, cables must be of the H1Z2Z2-K type.

To meet the requirements of the CEI 64-8 standard, Part 7, which mandates the use of Class II insulation equipment or equivalent on the DC side of photovoltaic systems up to the DC inverter connection terminals, the cables used must be:

- provided with insulation having a rated voltage not less than the nominal voltage of the system, installed in trunking or ducting with insulation characteristics complying with the CEI EN 50085 series, or in conduits with insulation characteristics complying with the CEI EN 61386 series;
- or cables suitable to withstand electrical, thermal, mechanical, and environmental stresses with a protection that provides the same reliability as double insulation.

Considering that:

- the maximum open-circuit voltage ($V_{\text{OC,MAX}}$) of the selected PV module (nominal power of 600 W under STC conditions) is 52,4 V under STC;
- the strings consist of 15 modules; the maximum open-circuit voltage of the string ($V_{\text{OC,MAX,string}}$) at the minimum temperature is 857,5 V.

The selected H1Z2Z2-K cables, with a rated DC voltage U_0/U of 1,8/1,2 kV, guarantee double insulation characteristics for the system consisting of strings with a $V_{\text{OC,MAX,string}}$ equal to 857,5 V.

The DC current-carrying capacity I_z of the string cables must be greater than or equal to the maximum short-circuit current of the string, in order to ensure overload protection for the string cables:

$$I_z \geq I_{\text{SC,MAX,string}} \tag{7.22}$$

The DC current-carrying capacity I_z of the string cables is also influenced by the cable installation conditions. For sizing purposes, the tables provided in the cables' technical datasheet can be used. In terms of the DC current-carrying capacity I_z, it has been considered that the string cables, both the positive and negative poles, are installed in in an underground pipe. Therefore, for sizing purposes, reference is made to the penultimate column of the table in the datasheet [37], and additional correction factor K_2 in the formula 7.21 equal to 0,8 need to be considered to taking into account the proximity between the ducts [38].

In terms of DC current-carrying capacity I_z, 4 mm^2 cables are already more than sufficient to withstand the $I_{\text{SC,MAX,string}}$.

Upon completion of the current-carrying capacity verification, the voltage drop verification must be performed. Under maximum operating power of the string at STC, the voltage drop must be $< 3\%$. For calculation purposes, a maximum voltage drop of 2% will be assumed; since the $V_{\text{OC,MAX,string}}$ is equal to 857,5 V, the maximum allowable voltage drop must be equal to 17,2 V. The string circuit up to the string combiner box will have a maximum length l of 100 m (round trip). Assuming the use of H1Z2Z2-K cables for the string connection (with a resistivity of 0,0213 $\Omega \cdot \text{mm}^2/\text{m}$ at 70°C), the cable cross-section is given by the following formula:

$$S = \frac{2 \cdot \rho \cdot l \cdot I_{\text{SC,MAX,string}}}{\Delta V} \tag{7.23}$$

Therefore, the cable cross-section must be greater than 4,6 mm^2 to guarantee a maximum voltage drop of 2%.

The cable that satisfies all the conditions described so far is the H1Z2Z2-K cable, with a rated DC voltage U_0/U of 1,8/1,2 kV and a cross-section of 1×6 mm^2. Once the cable cross-section has been defined, the specific let-through energy verification must be carried out. Since for photovoltaic modules, and consequently also for the strings, the short-circuit current value I_{sc} is only slightly higher than the operating current value I_{mpp}, the verification must be performed according to the overcurrent protections adopted to protect the string cables. Although there are no strings connected in parallel, fuses are selected as overcurrent protection for increased safety. The fuses installed in the fuse holders must be gPV fuses with a rated current I_n satisfying the following condition:

$$1{,}1 \cdot I_{\text{sc}} \leq I_n < I_{\text{MOD_MAX_OCPR}} \tag{7.24}$$

Where $I_{\text{MOD_MAX_OCPR}}$ is the maximum reverse current that the PV module itself can withstand, which is identified from the module datasheet. In the case under analysis, $I_{\text{MOD_MAX_OCPR}} =$ 30 A. From the calculation, the fuses to be used for both the positive and negative poles of each individual string are 25 A gPV fuses.

In light of this, the following condition must therefore be satisfied:

$$I_z \geq I_n \geq I_{\text{SC,MAX,string}} \tag{7.25}$$

The H1Z2Z2-K cable, with a rated DC voltage U_0/U of 1,8/1,2 kV and a cross-section of

1×6 mm^2, is suitable with respect to the specific let-through energy verification ($I^2 \cdot t = K^2 \cdot S^2$)[1]. In addition to overcurrent protection, the Surge Protective Device (SPD) must also be sized. SPDs protect the inverter from transient overvoltages caused by indirect lightning strikes or switching operations on the grid. When the overvoltage exceeds the maximum continuous operating voltage (U_c) of the surge arrester, it lowers its impedance towards earth, limiting the voltage at the load terminals to the voltage protection level U_p. For the selection of the DC-side SPD, reference is made to the following technical rules:

- Type 2 DC is the standard solution for photovoltaic systems.
- The voltage U_c must be $\geq V_{\text{oc}}$ of the string (at minimum temperature).
- Verify the protection level U_p with respect to the impulse withstand voltage of the inverter: $U_p <$ Inverter impulse withstand voltage.

Cable Selection and AC-Side Protections

Given the photovoltaic generator and the selected inverter, the photovoltaic array is isolated from earth without galvanic isolation between the DC side and the AC side. In accordance with the IEC 62548-1 standard, the insulation resistance of the photovoltaic array to earth must be measured at least once every 24 hours; for this reason, it must be verified that the inverter is equipped with its own internal insulation measurement device. This functionality is integrated within the inverter: the all-current-sensitive residual current monitoring unit monitors both AC and DC fault currents and redundantly disconnects the product from the public grid in the event of fault current surges > 30 mA.

Since the system is equipped with 7 inverters, these must be paralleled in an AC combiner box. The line from the inverter combiner box to each individual inverter must be sized according to the maximum output current of the inverter, available in its datasheet, and must be capable of withstanding the short-circuit currents involved.

For sizing purposes, the use of FG16OR16-type cables is preferred, and the tables provided in the cables' technical datasheet can be used [39]. In terms of AC current-carrying capacity I_z, it has been considered that the multi-core cables are installed in underground pipe at a depth of 0,8 m with a soil temperature of 20°C, with zero distance between ducts. Therefore, for sizing purposes, reference is made to the last column of the table in the datasheet, and additional correction factor K_2 in the formula 7.21 equal to 0,85 need to be considered to taking into account the proximity between the pipe [38].

Depending on the type of distribution network (TN/TT/IT), the requirements of CEI 64-8/4 for protection against indirect contacts and of IEC 60947-2 for the selection of protective equipment must be adopted, as described in Section 2.3.4.

The AC line from each inverter to the inverter combiner box must be protected. In accordance with the provisions of the CEI 64-8 standard, the protection device (Circuit Breaker -

[1]For the purpose of protecting the connection cable (string-to-subcombiner box connection), the protection device must be chosen such that the following relationship is satisfied for every short-circuit value (CEI 64-8) up to a maximum of $(x-1) \cdot 1{,}25 \cdot I_{\text{sc}}$:

$$(I^2t) \leq K^2S^2 \tag{7.26}$$

Where:

- (I^2t) is the Joule integral for the short-circuit duration (in A^{2}s);
- K is a characteristic constant of the cable, depending on the type of conductor and insulation material;
- S is the cable cross-section (in mm^2).

CB, in italian DDG) must be coordinated with respect to the operating current I_B (which, in the case of PV systems, corresponds to the maximum output current of the inverter) and the current-carrying capacity of the AC cable line I_z up to the inverter combiner box; therefore, the following condition must be verified:

$$I_B < I_n < I_z \tag{7.27}$$

Where:

- I_B is the maximum AC current deliverable by the inverters;
- I_n is the rated current of the planned miniature or moulded case circuit breaker;
- I_z is the continuous current-carrying capacity of the wiring system.

The circuit breaker must have a Type B or Type C tripping characteristic curve. The circuit breaker must have an operating voltage compatible with the nominal output voltage of the inverter, which is 400 V. Since the maximum AC current deliverable by the inverter is equal to 165,4 A, considering the standard sizes of Moulded Case Circuit Breakers (MCCBs), a 200 A circuit breaker could be used, to be selected based on other parameters that might influence the choice (breaking capacity, operating temperatures, cable dimensions, etc.). The busbars of the combiner box where the inverter lines are paralleled must also be protected. The protection device must be coordinated with respect to the operating current I_B, which, in this case, corresponds to the sum of the currents deliverable by the 7 inverters, and the current-carrying capacity I_z of the busbars from the individual circuit breakers of each inverter up to the main parallel circuit breaker; therefore, the following condition must be verified:

$$I_B < I_n < I_z \tag{7.28}$$

Where:

- I_B is the maximum AC current deliverable by the 7 inverters;
- I_n is the rated current of the circuit breaker planned for the inverter parallel connection;
- I_z is the continuous current-carrying capacity of the panel busbars.

The circuit breaker must feature a Type B or Type C tripping characteristic curve and may be connected to the interface protection system and, therefore, must be motorized and equipped with an undervoltage release coil and a remote-reclosing coil.

The inverter combiner box must also contain:

- The Interface Protection System (SPI) with the connection line for the voltage measurement inputs (this line must be equipped with fuse-switch disconnectors) located upstream of the parallel circuit breaker, which will act as the Interface Device (DDI);
- A power supply line for the Uninterruptible Power Supply (UPS) that powers the Interface Protection System (SPI), hence, both the relay acting as the interface protection and the undervoltage coil circuit installed for tripping the Interface Device, located upstream of the parallel circuit breaker acting as the Interface Device;
- A production meter with the relative Current Transformers (CTs) installed on the busbars and the connection line for the voltage measurement inputs (this line must be equipped with fuse-switch disconnectors);
- Type 1 Surge Protective Devices (SPDs), as the distance between the inverters and the point where the power supply line enters the building is greater than 10 m.

For the sizing of the cables coming from the combiner box and directed to the transformer, the use of FG16R16-type cables is preferred for this section of the electrical system, and the tables provided in the cables' technical datasheet can be used [40]. In terms of AC current-carrying capacity I_z, it has been considered that each phase is realized by three single-core cables laid in mutual contact within the same underground conduit, with the three conduits (one per phase) installed at a depth of 0,8 m, with a soil temperature of 20°C, and spaced from one another by 0,25 m. Therefore, for sizing purposes, reference is made to the last column of the table in the datasheet, multiplying the current-carrying capacity by an additional correction factor K_2 in the formula 7.21 of 0,8 need to be considered to taking into account the proximity between the pipe [38].

Another element to be considered in the electrical design is the Backup Protection Device (DDR - Dispositivo di Rincalzo). The backup protection is a secondary system to the Interface Device (DDI), which is mandatory for systems with a rated power > 20 kW. Its operation is described as follows:

- If the DDI fails to open within 0,5 seconds from the tripping command issued by the Interface Protection System (SPI), the backup protection intervenes;
- The backup protection directly commands the Main Circuit Breaker (DG - Dispositivo Generale) via a shunt trip coil;
- The feedback on the status of the DDI is read by the SPI.

Finally, since 2022, the use of the Plant Central Controller (CCI - Controllore Centrale di Impianto) has been introduced with the V1 and V2 variants of the CEI 0-16 standard. The Plant Central Controller (CCI) is a monitoring and control system that, installed at the delivery point, allows Distribution System Operators (DSOs) to monitor and regulate the generation plant, enabling its participation in grid balancing. Among the fundamental requirements introduced by the regulation are the functionalities PF1 (Monitoring), PF2 (Regulation and Control), and PF3 (Participation in Flexibility Markets and Plant Optimization), sending real-time data to the DSO, which is indispensable for ensuring the safety and stability of the national electrical system. The Plant Central Controller (CCI) is mandatory for photovoltaic/wind power plants connected to the Medium Voltage (MV) grid with a capacity ≥ 100 kW, according to the ARERA resolution 385/2025/R/EEL.

A comprehensive summary of the electrical characteristics of both the selected cables and protection devices is presented in Table 7.4 and in Table 7.5.

Table 7.4: Summary of electrical protection device characteristics.

Device	**Voltage [V]**	**Rated Current I_n [A] / Comm.**
DG (Main Circuit Breaker)	–	1400
DDR (Backup Protection)	–	1400
DDI (Interface Device)	–	1400
CB (Inverter Circuit Breaker / DDG)	–	200
SPD-DC	1000	–
SPD-AC	400	–
gPV-string (String Fuses)	–	25
fuse-SPI (Interface Protection Fuses)	–	6

Table 7.5: Summary of selected cable specifications.

Application	**Cable Type and Cross-section**
String cable	H1Z2Z2-K 1×6 mm^2
AC cable: Inverter to Inverter Combiner Box	FG16OR16 3×240 mm$^2 + 150$ mm^2
AC cable: Inverter Combiner Box to Transformer	FG16R16 3×630 mm^2/fase

7.3 BESS Sizing

Defining the characteristics of an energy storage system within a Renewable Energy Community requires an analysis that balances technical and economic considerations. The two key quantities to be determined are the storage capacity, expressed in kilowatt-hours and the nominal charge and discharge power, expressed in kilowatts. From an energy standpoint, the system must be capable of retaining a significant portion of the excess energy generated during peak photovoltaic production hours, thereby limiting grid injection during time slots that are least favourable from an economic perspective. From a power standpoint, the sizing must ensure responsiveness in both directions: a charge rate sufficient to absorb sudden surges in PV output and a discharge capability adequate to support community consumption during periods of low solar availability. Striking the right balance is essential: an undersized system would fail to perform effectively as an energy buffer, whereas an oversized one would impose a disproportionate burden on capital expenditure relative to the achievable benefits, potentially rendering the project economically unviable.

For this study, given the 1 MWp photovoltaic plant capacity and following a thorough analysis of the hourly load and generation profiles, the selected storage solution consists of two units connected in parallel of the *Liquid-cooled Hybrid Cabinet BESS-125K418*, manufactured by GSL Energy, yielding a total nominal capacity of $2 \times 418 = 836$ kWh and an aggregate nominal power of $2 \times 125 = 250$ kW [41]. The system employs lithium iron phosphate ($LiFePO_4$) cells, whose technical advantages for stationary storage applications are discussed in Chapter 3.

The energy sizing criterion is derived from the surplus and deficit analysis. The average daily energy surplus amounts to 1388,4 kWh, while the average daily energy deficit is 6307,8 kWh. The latter being approximately 4,5 times larger than the former. This disparity clarifies the functional role of the BESS within the system: it is not intended to cover the community's energy requirements, but rather to act as a temporal buffer capable of shifting a portion of the daytime surplus towards the evening hours, thereby extending the window of shareable and incentivisable energy. The storage capacity was therefore sized to capture approximately half of the average daily surplus, reserving the remaining fraction for electrolyzer feeding in Scenario 4. However, the nominal capacity of 836 kWh does not correspond to the energy quantity effectively manageable within a single cycle. Adopting an operational depth of discharge (DoD) of 80%, consistent with standard practice for $LiFePO_4$ cells subjected to deep daily cycling, the usable capacity is:

$$E_{\text{usable}} = E_{\text{nom}} \times \text{DoD} = 836 \times 0{,}80 = 669 \text{ kWh} \tag{7.29}$$

Accounting further for the AC-to-AC round-trip efficiency of the system, estimated from the European efficiency of the integrated hybrid inverter ($\eta_{\text{inv}} \approx 98{,}1\%$) and the coulombic efficiency of the $LiFePO_4$ cells ($\eta_{\text{bat}} \approx 97\%$):

$$\eta_{\text{RT}} = \eta_{\text{inv}}^2 \times \eta_{\text{bat}} \approx 0{,}981^2 \times 0{,}97 \approx 93{,}4\% \tag{7.30}$$

The squared exponent applied to η_{inv} reflects the bidirectional nature of the conversion process: the integrated hybrid inverter operates once during the AC-to-DC charging stage and once during the DC-to-AC discharging stage, introducing a conversion loss at each pass. The energy effectively deliverable after accounting for conversion losses is therefore:

$$E_{\text{del}} = E_{\text{usable}} \times \eta_{\text{RT}} = 669 \times 0{,}934 \approx 625 \text{ kWh} \tag{7.31}$$

This value corresponds to 45% of the average daily surplus, providing quantitative justification for the adopted sizing criterion: the selection of 836 kWh nominal capacity is consistent with the objective of capturing approximately half of the available surplus once operational

constraints are properly accounted for. Regarding cycle life, the manufacturer datasheet specifies a minimum of 6500 cycles under standard test conditions (0,5C charge and discharge rate, 70% end-of-life capacity retention). Since the system operates at a lower C-rate of 250 kW/836 kWh ≈ 0,30C, the electrochemical stress imposed on the cells is lower than under the rated test conditions, which is expected to translate into a cycle life exceeding the guaranteed figure. Assuming one full equivalent cycle per day on average, the estimated service life exceeds 17 years (6500/365 ≈ 17,8 years), a result fully compatible with the 20-year investment horizon typical of CER feasibility analyses and consistent with the 10-year commercial warranty provided by the manufacturer. From an architectural standpoint, the storage system is integrated into the plant under an *AC coupling* scheme. In this configuration, the 1 MWp photovoltaic array remains connected to its dedicated string inverters, as described in the preceding chapter, which inject the generated energy onto the shared AC bus of the plant. The BESS operates on the same AC bus and the control logic measures the net surplus available at the point of connection on an hourly basis and commands the storage system to charge up to its 250 kW power limit. AC coupling is the most appropriate architectural solution at the scale of the present installation, as it preserves the existing electrical configuration of the PV field and allows the BESS charge to be managed as a controllable load on the AC node, without imposing compatibility constraints on the MPPT trackers of the string inverters. It should be noted that, during peak summer irradiance hours, the PV surplus power may significantly exceed the 250 kW threshold: under such conditions, the BESS absorbs at full rated power while the non-storable excess is either injected into the grid or, in Scenario 4, routed to the electrolyzer. This structural limitation is inherent to the chosen system size and is correctly represented in the MATLAB model through a power constraint enforced at each hourly simulation interval.

Figure 7.7 provides an overview of the coupling with PV system and grid of the selected device.

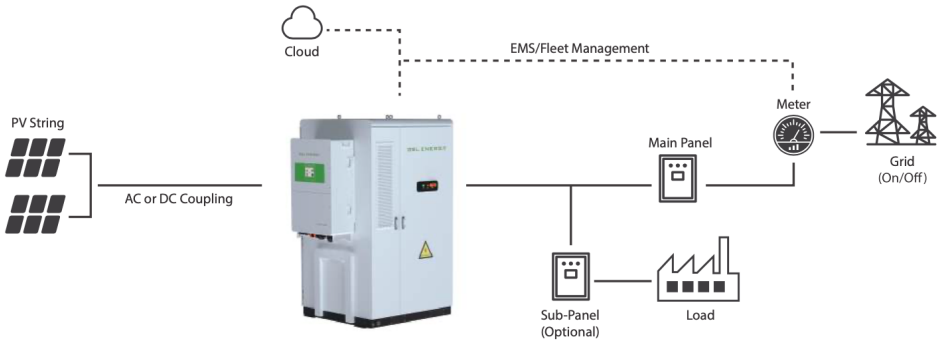


Figure 7.7: BESS coupling with PV plant and national grid

The principal technical parameters of the selected storage unit, as declared by the manufacturer, are summarized in Table 7.6 [41].

Table 7.6: Key technical specifications of the GSL Energy BESS-125K418 unit (values refer to a single cabinet; the installed system comprises two units in parallel).

Parameter	**Value (single unit)**	**Value (2 units)**
Battery		
Chemistry	$LiFePO_4$	—
Nominal energy capacity	418 kWh	836 kWh
Battery operating voltage	561–748 V	—
Rated voltage	665,6 V	—
Battery capacity	314 Ah (2P208S)	—
Max charge/discharge current	200 A × 2	—
Cycle life	≥6500 cycles @ 0,5C/0,5C, 70% EOL	
Operating temperature	Charge: 0–55 °C; Discharge: −20–55 °C	
Inverter (SUN-125K-SG02HP3-EU-GM10)		
Nominal AC power	125 kW	250 kW
Max AC apparent power	135 kVA	270 kVA
Rated AC current	189,4 A	—
Max efficiency	98,70%	—
European efficiency	98,10%	—
AC voltage	220/380 V, 230/400 V (3L+N+PE)	
AC frequency	50 Hz (45–55 Hz)	
THD_i	<3% at nominal power	
System		
Enclosure protection	IP55	—
Thermal management	Liquid cooling	
Fire protection	Aerosol suppression + smoke detection	
Dimensions (W×D×H)	1,240×1,320×2,380 mm (battery cabinet only)	
Weight (battery cabinet)	≈3,500 kg	—
Warranty	10 years	
Certifications	UN38.3, IEC62619, CE, CEI 0-21, VDE-AR-N 4105, IEC 62109	

7.4 Electrolyzer Sizing

The sizing of the PEM electrolyzer follows directly from the energy balance established in the preceding sections. Once the BESS has been allocated a nominal capacity of 836 kWh, the average daily energy surplus available for hydrogen production is obtained as the difference between the total average daily surplus and the nominal storage capacity of the battery system:

$$E_{\text{el}} = E_{\text{surplus,avg}} - E_{\text{BESS,nom}} = 1388{,}4 - 836 \approx 552 \text{ kWh/day} \tag{7.32}$$

The surplus generation profile, derived from the hourly analysis, exhibits a characteristic daily window of positive net generation spanning between 5 and 8 hours depending on the season and meteorological conditions, with shorter windows in winter and longer ones during summer months. The implied electrolyzer power range is therefore:

$$P_{\text{el}} \in \left[\frac{E_{\text{el}}}{t_{\max}}, \frac{E_{\text{el}}}{t_{\min}}\right] = \left[\frac{552}{8}, \frac{552}{5}\right] \approx [69,\ 110] \text{ kW} \tag{7.33}$$

A rated power of 100 kW falls within this interval and represents a balanced selection: it is large enough to utilize a significant fraction of the available surplus during shorter generation windows, while avoiding over-sizing relative to days with limited excess production. On this basis, the selected unit is the *Rubri-PI-0020* PEM hydrogen electrolyzer system, rated at 100 kW with a hydrogen output capacity of 20 Nm^3/h. The key technical parameters of the selected unit are summarized in Table 7.7 [42].

Table 7.7: Technical specifications of the Rubri-PI-0020 PEM electrolyser.

Parameter	**Value**
Model	Rubri-PI-0020
Technology	Proton Exchange Membrane (PEM)
Rated electrical power	100 kW
Hydrogen output capacity	20 Nm^3/h
Output pressure	$\leq$ 3 MPa (adjustable)
Hydrogen purity	$\geq$ 99.999%
Specific energy consumption	$\leq$ 4,6 kWh/Nm^3
Water consumption	20 L/h
Power modulation range	20%–120% of rated power

The choice of PEM technology is motivated in detail in Chapter 4. From an operational standpoint, the characteristic most relevant to the present application is the wide power modulation range of 20%–120% of rated power (20–120 kW in absolute terms). The lower bound of 20 kW defines the minimum dispatch threshold enforced as a hard constraint on the electrolyzer in the Scenario 4 MATLAB model: during hours in which the residual surplus after BESS charging falls below this value, the electrolyzer cannot be dispatched and the corresponding energy is injected into the grid via the RID mechanism. The upper bound of 120% provides an additional operational margin during hours of particularly abundant surplus.

It is acknowledged that both the BESS and the electrolyzer have been sized on the basis of average daily energy flows rather than through a rigorous dynamic optimization over the full annual profile. A more precise co-sizing procedure would be required for an engineering-grade design; for the purposes of this feasibility study, however, the approximation is considered acceptable, as it does not affect the qualitative validity of the comparative scenario analysis conducted in the following chapters.

Chapter 8

Operational Scenario Simulation Methodology

8.1 Introduction

This chapter presents the methodology adopted to model the four operational scenarios investigated in this study, ranging from the baseline photovoltaic configuration to the fully integrated system including demand response, battery storage, and green hydrogen production. Each scenario builds incrementally on the previous one, introducing an additional technological layer to the energy community architecture while preserving a common set of boundary conditions, namely the hourly load profile of the aggregated CER members, the photovoltaic generation profile derived from PVGIS and the regulatory framework governing shared energy and incentive allocation under the rule impose by GSE. The chapter is organized into four sections, each dedicated to one scenario and structured to describe, in sequence, the energy balance logic implemented and the assumptions underlying its numerical implementation in MATLAB. Taken together, these four sections provide the methodological foundation for the comparative techno-economic analysis presented in the following chapter, where the results obtained from each configuration are discussed and critically compared.

8.2 Methodology of S1

Scenario 1 reproduces the baseline configuration of the Renewable Energy Community: the 1 MWp ground-mounted PV plant feeding the aggregate hourly load of the CER, with no storage or demand-flexibility mechanism interposed between generation and consumption. The simulation runs on an hourly basis over the full reference year (April 2025–March 2026, 8760 hours) and moves through four stages: economic parameter setup, data import, hourly energy-balance computation and annual KPI aggregation, followed by a comparative assessment against a no-PV baseline and an estimate of avoided CO_2 emissions. Economic parameters are set exogenously, ahead of the simulation loop. Retail electricity prices are differentiated across the three standard Italian tariff bands (F1 peak, F2 intermediate, F3 off-peak). The GSE premium tariff (*Tariffa Premio*, TiP) on shared energy is computed hour by hour following the D.Lgs. 199/2021 formula using the base and cap values applicable to plants above 600 kW. The ARERA valorization coefficient on shared energy is applied as a flat per-MWh rate, consistent with the current CACER framework. Hourly input data like aggregate CER load, PV production, tariff band and zonal price are read from the reference Excel file. The hourly energy balance follows a direct self-consumption logic with no intermediate storage: shared energy is the hour-by-hour minimum of PV production and CER load, production in excess of load is treated as surplus fed into the grid, and load in excess of production is met by grid purchase. At each run the model

checks that shared energy plus surplus reconstructs total PV production, and that shared energy plus grid purchase reconstructs total CER load, flagging any deviation beyond numerical tolerance. Economic flows follow directly from the energy balance. Revenues comprise the TiP incentive and the ARERA coefficient, both applied to shared energy; the retail bill saving, corresponding to the retail price avoided on the self-consumed share of load; and the *Ritiro Dedicato* (RID) revenue from surplus sold at the hourly zonal price. The only cost term is the retail cost of grid purchase covering the residual load. These flows are aggregated into annual KPIs together with two standard CER performance indices: the self-consumption index (share of PV production actually shared) and the self-sufficiency index (share of CER load covered by shared energy). The model also tracks whether the self-consumption index exceeds 55%, the threshold set by the *Decreto CACER* on the destination of incentive proceeds. The check is purely informational. A second block reframes the same results from the members' perspective, comparing the CER configuration against a theoretical baseline in which the entire CER load is purchased at retail price with no PV plant installed.

Finally, avoided CO_2 emissions are estimated by applying the national grid emission factor (EF_{el} = 0,216 $kgCO_2/kWh$, ISPRA 2025, updated to 2023 reference data) to two quantities: total PV production, giving an upper-bound estimate under the assumption that all generated energy displaces grid supply, and shared energy alone, giving a more conservative lower-bound estimate limited to energy actually displacing grid purchase within the CER.

8.3 Methodology of S2

8.3.1 Load Categorisation and Exclusion Criteria

As described in the load profiling section, the CER of Minervino di Lecce comprises four distinct consumption categories: residential users, public lighting (PL), public administration (PA) and small industrial users. From the perspective of demand-side flexibility, only the residential component is considered eligible for DR participation in S2. This choice is motivated by category-specific constraints that effectively render the remaining components non-flexible within the operational framework of the CER:

- **Public lighting** operates on an astronomically determined schedule governed by sunrise and sunset times, supplemented by fixed municipal dimming programmes. Its activation is dictated by external, non-controllable boundary conditions, and no voluntary time-shifting is admissible without institutional intervention beyond the CER's governance scope.
- **Public administration** buildings present, in principle, some degree of flexibility through HVAC scheduling and internal lighting control. However, in the absence of building automation infrastructure and given the institutional constraints on occupancy patterns and service continuity, coordinated DR participation is not considered implementable through the voluntary behavioural mechanism assumed in S2. This category is therefore conservatively excluded as a modelling assumption, consistent with a worst-case estimation of the community's flexible potential.
- **Small industrial and artisanal users** represent a marginal fraction of total consumption (1%). Although certain process loads may in theory exhibit limited flexibility, the absence of process automation, combined with the negligible weight of this category on total CER demand, makes its inclusion unjustifiable on methodological grounds. This component is accordingly excluded.

The effective pool of flexible demand is therefore restricted to the residential category, whose hourly profile $P_{RES}(t)$ constitutes the sole input to the DR shifting algorithm.

8.3.2 Hour Classification: Source and Destination Windows

The DR model rests on a dynamic, data-driven classification of each hour of the year into one of two categories, determined by the instantaneous relationship between PV generation and total CER demand:

- **Source hours**: hours in which PV generation < total CER demand. In these hours, PV generation does not cover total CER demand, so shared energy is limited by generation, not by consumption. Removing a fraction of the residential load in these hours does not reduce shared energy, since generation remains the binding constraint.
- **Destination hours**: hours in which PV generation > total CER demand. In these hours, shared energy is limited by consumption. Adding load in these hours directly increases shared energy by the same amount, up to the available surplus.

Out of the 8760 annual hours, 6710 (76,6%) are classified as source hours and 2050 (23,4%) as destination hours.

8.3.3 Definition of the Flexibility Coefficient α

The fraction of residential electrical consumption eligible for time-shifting within source hours is quantified through a dimensionless flexibility coefficient α, such that the flexible energy extracted from source hours on each day d is:

$$E_{\text{flex}}(d) = \alpha \cdot \sum_{t \in H_{\text{src}}(d)} P_{\text{RES}}(t) \tag{8.1}$$

where $H_{\text{src}}(d)$ denotes the subset of source hours belonging to day d. It is important to note that α is applied exclusively to the residential load in source hours, not to the total annual residential consumption. The annual candidate flexible energy is therefore:

$$E_{\text{flex,ann}} = \alpha \cdot \sum_{t \in H_{\text{src}}} P_{\text{RES}}(t) = \alpha \cdot 2173{,}404 \text{ MWh} \tag{8.2}$$

where the sum extends over all 6710 source hours of the year, corresponding to 2173,404 MWh of residential consumption, 76,4% of total annual residential energy. The remaining 23,6% falls in destination hours and is already coincident with PV surplus, hence not subject to shifting.

The numerical value of α is grounded in the empirical literature on demand-side flexibility in the Italian residential sector. The primary quantitative reference is the study by Mancini et al. [43], which characterizes the flexibility potential of a cluster of 751 Italian dwellings through direct sub-metering measurements conducted over two years (2018–2019). The study identifies the shiftable load categories as washing machines, dishwashers, and tumble dryers, and defines a yearly Flexibility Index FI_y as the ratio of effectively shiftable energy to total electrical consumption, obtaining $FI_y = 10{,}3\%$ for the Italian residential sector, with a strategy effectiveness of 34% under a price-responsive scheduling strategy. This effectiveness figure implies that a real deployment of the DR mechanism would activate only approximately one third of the theoretical flexible potential; the values of α adopted in this study therefore represent ceiling estimates of achievable load shifting rather than expected operational outcomes.

Critically, the sample characterized by Mancini et al. exhibits a heating system composition of 98,5% natural gas boilers, with electrically driven heating representing less than 2% of the sample. This structural feature closely matches the thermal infrastructure of Minervino di Lecce, where space heating relies predominantly on gas-fired systems, as is typical of the southern Apulian building stock. Consequently, the electrical consumption profile on which FI_y is computed is essentially free from thermal electric loads, and the transfer of this index

to the present CER context is methodologically consistent without requiring corrections for heating electrification.

A broader quantitative reference is provided by O'Connell et al. [44], who reviewed multiple demand response demonstration projects across European and North American contexts and reported flexibility values ranging from 7–9% of baseline consumption on average, reaching 10–25% of peak load under Critical Peak Pricing conditions. These figures are drawn from an aggregated review of heterogeneous pilot projects, including mixed-use and commercial building contexts with higher automation levels than those assumed here, rather than from a single homogeneous experimental campaign. Their transfer to the present residential context is therefore indicative rather than directly prescriptive, and they are used solely as an independent upper-bound reference consistent with the range adopted in this study.

Finally, Ercoli et al. [45] demonstrate, in the specific context of Italian renewable energy communities, that centralized DR coordination of building thermal loads can shift between 12% and 56% of aggregate electrical demand depending on community composition, PV system size and seasonal conditions. While these figures pertain to thermostatic loads rather than appliance-based shifting, they confirm that demand-side flexibility magnitudes of the order considered here are physically achievable and economically relevant in Italian energy community configurations.

8.3.4 Sensitivity Analysis, Daily Energy Conservation, and Capacity Constraint

Given the inherent uncertainty associated with any behavioral assumption applied to a real community operating under voluntary participation, a sensitivity analysis is performed over three values of α:

- $\alpha_{\text{low}} = 5\%$: conservative lower bound, corresponding to spontaneous participation without any smart home infrastructure or coordinating signal beyond the CER statute. Only the most easily deferrable loads, such as washing machine cycles or occasional dishwasher runs, are assumed to be shifted by a fraction of members.

- $\alpha_{\text{mid}} = 10\%$: central estimate, directly calibrated on the Flexibility Index of Mancini et al. [43] for the Italian residential sector. This scenario assumes moderate voluntary participation by CER members, incentivized through the internal statute provision that redistributes a larger share of the GSE incentive to members who contribute to improving shared energy.

- $\alpha_{\text{high}} = 15\%$: optimistic upper bound, approaching the lower end of the range reported by O'Connell et al. [44] for automated demand response in European pilots. This scenario requires a higher degree of member engagement and is considered an upper performance reference rather than a baseline expectation.

Two physical constraints govern the shifting algorithm and must be respected simultaneously for each day d.

Energy conservation: the total residential consumption must be identical before and after the shift. Load is not reduced, it is only relocated in time:

$$\sum_{t=1}^{24} P_{\text{RES,DR}}(d,t) = \sum_{t=1}^{24} P_{\text{RES}}(d,t) \tag{8.3}$$

This constraint operates on total daily energy without preserving the tariff-band composition of consumption. The DR mechanism inevitably redistributes load across time-of-use bands,

since source hours and destination hours belong to different tariff periods. This recomposition of the *fascia* structure introduces a systematic asymmetry in the economic analysis: the retail savings computed on shared energy at hourly tariff prices do not algebraically equal the reduction in grid purchase costs.

Daily surplus capacity constraint: on any given day d, the shifted energy cannot exceed the available PV surplus in destination hours. If $E_{\text{flex}}(d) > S_{\text{tot}}(d)$, only the absorbable fraction is shifted and the remainder, denoted spill, stays in its original time slot:

$$E_{\text{shift}}(d) = \min\Big(E_{\text{flex}}(d),\, S_{\text{tot}}(d)\Big), \qquad S_{\text{tot}}(d) = \sum_{t \in H_{\text{dst}}(d)} S(t) \tag{8.4}$$

The energy shifted to destination hours is distributed proportionally to the instantaneous surplus $S(t)$, ensuring that load is preferentially added in hours of maximum PV availability:

$$\Delta P_{\text{RES,dst}}(t) = E_{\text{shift}}(d) \cdot \frac{S(t)}{S_{\text{tot}}(d)}, \qquad t \in H_{\text{dst}}(d) \tag{8.5}$$

The load removal from source hours is applied proportionally to the instantaneous residential demand $P_{\text{RES}}(t)$, scaled by a factor $\xi(d) = E_{\text{shift}}(d)/E_{\text{flex}}(d) \leq 1$ to account for days on which the daily capacity constraint is binding:

$$\Delta P_{\text{RES,src}}(t) = \alpha \cdot \xi(d) \cdot P_{\text{RES}}(t), \qquad t \in H_{\text{src}}(d) \tag{8.6}$$

It is noted that the proportional removal rule does not incorporate a lower bound on the residual hourly consumption. In a limited number of source hours where the margin between total CER demand and PV generation is small, the load reduction may bring the modified consumption profile below the PV generation level, causing a marginal reduction of shared energy in those hours that partially offsets the gain achieved in destination hours. For the central scenario ($\alpha = 10\%$), this effect involves 115 hours out of 6710 source hours (1,7%) and results in a net shared energy loss of 2006 kWh, which explains the discrepancy between $E_{\text{shift,ann}} = 179624$ kWh and $\Delta E_{\text{cond}} = 177618$ kWh reported in Table 8.1. A comparable effect, of smaller and larger magnitude respectively, is observed in the low- and high-α scenarios, consistent with the fact that a more aggressive proportional removal increases the frequency with which the residual consumption profile approaches the PV generation floor. This is considered a second-order limitation of the proportional rule-based approach and has a negligible impact on the economic results.

The effective flexible energy volumes, after application of the daily capacity constraint, are reported in Table 8.1. The spill column quantifies the structural limitation of DR without storage: energy that cannot be absorbed because the daily PV surplus is insufficient, a condition that occurs predominantly in the winter months (November–January) when solar irradiance is lowest and the gap between residential demand and PV generation is largest.

Table 8.1: Sensitivity analysis: candidate flexible energy, effective shift after daily capacity constraint, spill, and resulting net increment in shared energy.

Scenario	α	$E_{\text{flex,ann}}$ [MWh]	$E_{\text{shift,ann}}$ [MWh]	E_{spill} [MWh]	Spill [%]	ΔE_{cond} [MWh]
Low	5%	108,7	93,5	15,1	13,9%	+92,9
Mid	10%	217,3	179,6	37,7	17,4%	+177,6
High	15%	326,0	256,7	69,3	21,3%	+252,5

The spill fraction increases with α, reflecting diminishing returns: as more load is made available for shifting, the daily surplus capacity becomes the binding constraint more frequently. The spill is concentrated in the winter season, where the structural mismatch between low PV generation and high residential demand leaves insufficient daily surplus to absorb the candidate flexible energy. This is an inherent limitation of the rule-based DR approach in the absence of a storage buffer, and directly motivates the introduction of the Battery Energy Storage System in Scenario 3, which can decouple the temporal constraint between surplus availability and load shifting.

8.4 Methodology of S3

Scenario S3 extends the baseline photovoltaic configuration analyzed in S1 with the addition of a battery energy storage system (BESS), evaluating the impact of intra-day energy time-shifting on self-consumption, shared energy and the overall economic performance of the renewable energy community. The storage system consists of two GSL-BESS-125K418 units, based on lithium iron phosphate (LiFePO4) chemistry, for a combined nominal capacity of 835,98 kWh. The BESS is AC-coupled to the same inverter bus as the photovoltaic plant, resulting in a single point of connection (POD) between the PV+BESS system and the public grid. This configuration choice, common for ground-mounted CER installations, is a determining factor in the definition of shared energy adopted in the model, discussed below.

An operational depth of discharge of 80% is imposed, bounding the state of charge (SOC) between 20% and 100%, which yields a usable energy window of 668,78 kWh. The maximum charge and discharge power is set at 250 kW AC (125 kW per unit), and the declared round-trip efficiency of 93,4% is decomposed into symmetric charge and discharge efficiencies,

$$\eta_c = \eta_d = \sqrt{\eta_{RT}} \approx 0{,}966, \tag{8.7}$$

consistent with standard practice for AC-coupled systems where a single integrated inverter mediates both conversion directions. The initial SOC is conventionally set at 50%.

The hourly input data of CER aggregate consumption, PV production, tariff band and zonal price are imported from the same reference dataset used across all four scenarios (8760 hourly records covering April 2025–March 2026), following the identical parsing and tariff-band classification logic described for Scenario 1.

The core of the model is an hourly dispatch algorithm implementing a self-consumption-first strategy, under which the battery is charged only from photovoltaic surplus and discharged only to cover residual community demand, without ever exchanging energy directly with the grid. For each hour, two mutually exclusive operating conditions are evaluated.

When production exceeds consumption, $P_{PV}(t) \geq C_{CER}(t)$, direct self-consumption is set equal to the community load,

$$E_{sc}(t) = C_{CER}(t), \tag{8.8}$$

and the resulting surplus is used to charge the battery up to the minimum of the available surplus, the rated charge power and the residual capacity to full SOC. Any surplus exceeding these limits is exported to the grid as RID surplus.

When consumption exceeds production, $P_{PV}(t) < C_{CER}(t)$, direct self-consumption is set equal to the instantaneous PV output,

$$E_{sc}(t) = P_{PV}(t), \tag{8.9}$$

and the resulting deficit is covered by battery discharge up to the minimum of the deficit itself, the rated discharge power and the energy actually available above the minimum SOC threshold. Any residual, uncovered deficit is purchased from the grid.

The state of charge is updated at each timestep according to

$$SOC(t+1) = SOC(t) + \frac{P_{charge}(t)\,\eta_c}{E_{nom}} \qquad \text{(charging)} \tag{8.10}$$

$$SOC(t+1) = SOC(t) - \frac{P_{disch}(t)}{\eta_d\,E_{nom}} \qquad \text{(discharging)} \tag{8.11}$$

with the result clamped within the admissible SOC bounds at every step. The nominal capacity E_{nom} is used as the reference base for the SOC update, consistent with the standard definition of state of charge as a fraction of the battery's total nameplate capacity, independently of the depth-of-discharge limits imposed on its usable range. The usable energy window E_{utile}, by contrast, is reserved for the calculation of equivalent full cycles (see below), since it is the energy actually cycled within the admissible SOC band that is representative of the battery's operational duty and relevant to degradation considerations, rather than the full nameplate capacity, part of which is permanently excluded from operation by the 80% DoD constraint.

Shared incentivised energy is defined as

$$E_{shared}(t) = E_{sc}(t) + P_{disch}(t), \tag{8.12}$$

i.e. the sum of direct instantaneous self-consumption and battery discharge delivered to the community load. This formulation reflects the physical configuration of the plant: since the BESS sits behind the single PV POD, energy diverted into the battery during charging never crosses the grid interface and therefore cannot, by construction, contribute to the GSE-metered injection in the hour in which it is stored. The benefit of storage materializes one step later, when discharge effectively re-injects previously curtailed surplus into hours of residual community deficit, increasing the matched (shared) energy relative to the no-storage case. The model therefore assumes an aggregated-configuration perspective, consistent with a single-producer, single-POD plant, rather than a POD-by-POD allocation among individual community members. This simplification is standard in techno-economic feasibility studies at this stage of design, since granular POD-level allocation depends on membership contracts rather than on plant engineering.

The economic flows are computed hourly using the same remuneration structure adopted in S1: the parametric GSE Tariffa Premio (TiP), capped at the normative ceiling, the ARERA valorisation corrective on shared energy, retail bill savings applied to the shared energy at the tariff-band-specific price, revenue from RID surplus sale at the hourly zonal price and the cost of residual grid purchases, with shared energy now including the battery discharge contribution as defined above.

Annual key performance indicators are aggregated from the hourly series, including the Self-Consumption Index (ratio of directly self-consumed and stored PV energy to total PV production) and the Self-Sufficiency Index (ratio of directly and battery-covered community demand to total community consumption), together with the equivalent number of full charge-discharge cycles per year, computed as the ratio between annual charged AC energy and the usable energy window.

Avoided CO_2 emissions are estimated by applying the national grid emission factor (0,216 $kgCO_2/kWh$, ISPRA 2025 report, 2023 reference data) to both total PV production (upper bound) and shared energy (lower bound), following the same convention adopted in S1. Finally, the scenario is compared against a no-CER baseline in which the entire community demand is purchased from the grid at retail tariff-band prices, allowing the net annual benefit, decomposed

into bill savings and additional CER revenues (TiP, ARERA corrective, RID), to be expressed both in absolute terms and as a percentage reduction relative to the baseline energy cost.

8.4.1 Rationale for a Simulation-Based Optimization Approach

The BESS sizing adopted in the baseline Scenario 3 model (two GSL-BESS-125K418 units, 835,98 kWh nominal capacity) is a manufacturer-driven configuration rather than an economically optimized one. To assess whether this size is defensible from an investment standpoint, and to characterize how the trade-off between private profitability and community-wide benefit evolves with storage capacity, the nominal BESS energy E_{nom} is treated as a decision variable and optimized over its feasible range, while every other design parameter, namely the power-to-energy ratio (C-rate), the depth of discharge, the round-trip efficiency and the initial state of charge, is held fixed at the values used in the baseline dispatch model. The objective function cannot be expressed in closed form as a function of E_{nom}: for each candidate capacity, the hourly dispatch simulation described in the previous paragraph must be re-run over the full 8760-hour reference year, since the state-of-charge trajectory, the power caps and the resulting shared, self-consumed and surplus energy series all depend nonlinearly on E_{nom} through the min$(\cdot)$ and max$(\cdot)$ clipping operators embedded in the dispatch logic. This makes the objective function a black-box, non-differentiable function of a single continuous variable, for which gradient-based optimization is not directly applicable. Particle Swarm Optimization (PSO) was selected as the optimization method for this reason, and because, being formulated here for a single design variable, it also allows a straightforward and independent validation via exhaustive grid search.

Particle Swarm Optimization: Theoretical Background. PSO is a population-based stochastic optimization method, originally proposed by Kennedy and Eberhart [46], that emulates a swarm of candidate solutions (particles) moving through the search space in search of the optimum. Each particle i is characterized, at iteration k, by a position x_i^k (a candidate value of E_{nom}) and a velocity v_i^k, updated at every iteration according to

$$v_i^{k+1} = w\, v_i^k + c_1 r_1 \left(p_i - x_i^k\right) + c_2 r_2 \left(g - x_i^k\right) \tag{8.13}$$

$$x_i^{k+1} = x_i^k + v_i^{k+1} \tag{8.14}$$

where p_i is the best position found so far by particle i (its own memory), g is the best position found so far by the swarm (the collective memory), w is an inertia weight, c_1 and c_2 are acceleration coefficients, and r_1, r_2 are random numbers drawn uniformly in $[0; 1]$ at every iteration. The velocity update therefore combines three effects: the particle tends to keep moving in its current direction (inertia), it is pulled back toward the best point it has personally found (individual memory), and it is pulled toward the best point found by the whole swarm (collective memory). This combination of individual and collective behavior, together with the randomness in r_1 and r_2, allows the swarm to explore the search space broadly while still converging toward good solutions, which is why PSO is well suited to an objective function that is non-smooth and cannot be optimized with gradient-based methods. The swarm size and iteration budget used here (forty particles, one hundred maximum iterations) follow standard practice for a single decision variable, and their adequacy is confirmed a posteriori by the stability check described below, rather than assumed a priori.

Single-Objective Formulation: BESS Sizing for Investor VAN. The single-objective problem searches for the nominal BESS capacity that maximizes the investor's discounted Net Present Value (VAN) over the twenty-year horizon,

$$E^*_{\text{nom}} = \arg \max_{E_{\text{nom}} \in [E_{\text{mod}}; E_{\text{ub}}]} \text{VAN}(E_{\text{nom}}) \tag{8.15}$$

where $E_{\text{mod}} = 417{,}99$ kWh is the nominal capacity of a single commercial module and $E_{\text{ub}} = 1388{,}42$ kWh is the upper bound of the search interval, taken as the average daily PV surplus over the reference year. Since *particleswarm* performs minimization by default, the objective function passed to the solver is $-\text{VAN}(E_{\text{nom}})$. For each candidate E_{nom}, the power caps are rescaled proportionally to preserve the C-rate of the reference product ($P_{\max} = C_{\text{rate}} \cdot E_{\text{nom}}$, with $C_{\text{rate}} = 250/835{,}98 = 0{,}2990$), the full hourly dispatch is re-simulated, and the resulting shared energy and surplus series feed into the same after-tax discounted cash flow model used for the fixed-size configuration: linear depreciation of the incremental BESS CAPEX over fifteen years, corporate tax at 24% applied to the after-depreciation cash flow, and discounting at 4% over the twenty-year horizon. Only the fraction of TiP and ARERA revenue actually retained by the investor, rather than redistributed to REC members, contributes to the taxable cash flow, consistent with the CACER incentive-sharing scheme adopted for the baseline scenario.

Convergence and Robustness Verification. Because PSO is a stochastic algorithm, a single execution does not, by itself, guarantee that the reported optimum is the global one rather than a local optimum the swarm happened to converge to. To address this, the optimization is repeated over five independent runs, each initialized with a different but reproducible random seed, and the resulting optimal capacities and VAN values are compared across runs. Convergence is considered stable if the coefficient of variation of the optimal capacity across runs,

$$CV = \frac{\sigma_{E^*}}{\mu_{E^*}} \times 100 \tag{8.16}$$

where $\mu_{E^*} = \frac{1}{5}\sum_{i=1}^{5} E^*_i$ and σ_{E^*} denote, respectively, the sample mean and the sample standard deviation of the optimal capacity E^*_i obtained across the five independent PSO runs, remains below a 5% threshold; values above this threshold would indicate that the swarm size or the iteration budget is insufficient, and would call for re-tuning before the result could be reported as definitive. As a second, independent verification, the objective function is also evaluated over a uniform grid of sixty points spanning the entire feasible interval $[E_{\text{mod}}; E_{\text{ub}}]$, without any stochastic component: this validation sweep confirms that the PSO optimum coincides with the global maximum of the sampled curve, independently of the algorithm's internal randomness.

Multi-Objective Formulation: Weighted-Sum Trade-off between Investor VAN and REC Benefit. Optimizing exclusively for investor VAN characterizes only one of the two economic perspectives relevant to a REC, namely the private return of the party financing the storage asset. The community as a whole benefits from a larger BESS beyond what accrues to the investor, through the incentive share redistributed to members, avoided surplus injection at unfavorable RID prices, and increased bill savings from higher self-sufficiency. To capture this second perspective, a gross annual REC-wide benefit metric is defined, before taxation and independent of the incentive-sharing split,

$$B(E_{\text{nom}}) = R_{\text{TiP}} + R_{\text{ARERA}} + R_{\text{RID}} + R_{\text{risparmio}} - \text{OPEX} - \frac{\text{CAPEX}(E_{\text{nom}})}{n_{\text{dep}}} \tag{8.17}$$

where the last term is the equivalent annual capital cost of the incremental BESS investment under straight-line depreciation, included so that the metric remains comparable, on an annual basis, across different storage sizes. Since $\text{VAN}(E_{\text{nom}})$ is a present value over twenty years while

$B(E_{\text{nom}})$ is an annual flow, the two are made commensurable by annualizing the VAN through the Capital Recovery Factor,

$$CRF = \frac{i(1+i)^n}{(1+i)^n - 1} \tag{8.18}$$

with $i = 0{,}04$ and $n = 20$ years, so that $\text{VAN}_{\text{ann}}(E_{\text{nom}}) = \text{VAN}(E_{\text{nom}}) \cdot CRF$ represents the constant annual annuity, discounted at the same rate, equivalent to the twenty-year VAN. The two objectives are then combined into a single objective through the weighted-sum method,

$$J(E_{\text{nom}}; \alpha) = \alpha \cdot \text{VAN}_{\text{ann}}(E_{\text{nom}}) + (1-\alpha) \cdot B(E_{\text{nom}}) \tag{8.19}$$

for a set of weights $\alpha \in \{0; 0{,}25; 0{,}50; 0{,}75; 1\}$, where $\alpha = 1$ recovers the pure investor-VAN problem of the previous paragraph and $\alpha = 0$ reduces to maximizing the gross REC-wide benefit alone. For each value of α, both a grid-based estimate, obtained by reusing the same sixty-point sweep of VAN_{ann} and B computed once and recombined algebraically for every α, and a continuous PSO refinement are computed, and the two are cross-checked against each other as a further robustness safeguard.

Pareto Optimality and the Weighted-Sum Method. In a problem with two objectives to maximize, a feasible solution E_1 is said to dominate another feasible solution E_2 if it is at least as good in both objectives and strictly better in at least one,

$$\text{VAN}_{\text{ann}}(E_1) \geq \text{VAN}_{\text{ann}}(E_2) \text{ and } B(E_1) \geq B(E_2), \text{ with at least one strict inequality} \tag{8.20}$$

A solution is Pareto optimal if no other feasible solution dominates it, and the set of all such solutions, mapped into the objective space $\left(\text{VAN}_{\text{ann}}, B\right)$, forms the Pareto frontier [47]: the set of non-dominated trade-offs between private return and system-wide benefit, beyond which no further simultaneous improvement of both objectives is possible. A relevant feature of the present problem is that, since $\text{VAN}_{\text{ann}}(E_{\text{nom}})$ is verified to be monotonically decreasing and $B(E_{\text{nom}})$ monotonically increasing over the entire feasible interval, every feasible capacity is non-dominated: no E_{nom} can improve one objective without worsening the other anywhere in the domain, so the entire search interval coincides with the Pareto frontier, and the problem reduces entirely to the choice of where on this frontier to operate. The weighted-sum method is the most direct way to explore this frontier, since for any choice of non-negative weights the maximizer of $J(E_{\text{nom}}; \alpha)$ is guaranteed to be Pareto optimal. The method is however sensitive to the relative numerical scale of the two objectives being combined: since VAN_{ann} and B enter the weighted sum as $\alpha \cdot \text{VAN}_{\text{ann}} + (1-\alpha) \cdot B$, and the two quantities differ by roughly one order of magnitude in this problem, one term numerically dominates the sum for almost every value of α, so the maximizer collapses onto the single-objective optimum of the dominant term, that is, onto one of the two bounds of the search interval, everywhere except in a narrow band of α close to the value that offsets this scale imbalance.

Refinement of the Transition Region. To determine whether the trade-off between the two objectives admits a genuine interior compromise, or is instead dominated everywhere by the two bounding solutions, the weight α is refined over a finer grid within the interval where the coarse sweep shows the optimal capacity shifting between the bounds of the search space. For each refined value of α, the corresponding maximizer of $J(E_{\text{nom}}; \alpha)$ is located on the pre-computed grid of VAN_{ann} and B. This refinement is used to confirm whether an interior optimum exists, and, if so, to bound the narrow range of α in which it becomes numerically visible, consistent with the scale imbalance discussed above. Because the grid-based estimate

reuses, for computational efficiency, the same coarse capacity grid on which $\mathrm{VAN}_{\mathrm{ann}}$ and B were originally sampled, the optimal capacity read off this refinement can only take one of the values on that grid, producing a step-wise (staircase) pattern in $E_{\mathrm{opt}}(\alpha)$ whose step width reflects the spacing of that grid rather than any instability in the underlying trade-off; this motivates the independent, higher-resolution verification described in the following paragraph.

Knee-Point Selection on the Normalized Pareto Frontier. As an alternative, weight-free criterion for selecting a compromise BESS size, the discretized Pareto frontier is analyzed directly for its knee point, defined as the point where a further improvement in one objective would require the largest sacrifice in the other. Both objectives are first rescaled through min-max normalization over the sampled range of the frontier,

$$f_1(E_{\mathrm{nom}}) = \frac{\mathrm{VAN}_{\mathrm{ann}}(E_{\mathrm{nom}}) - \mathrm{VAN}_{\mathrm{ann}}^{\mathrm{min}}}{\mathrm{VAN}_{\mathrm{ann}}^{\mathrm{max}} - \mathrm{VAN}_{\mathrm{ann}}^{\mathrm{min}}}, \qquad f_2(E_{\mathrm{nom}}) = \frac{B(E_{\mathrm{nom}}) - B^{\mathrm{min}}}{B^{\mathrm{max}} - B^{\mathrm{min}}} \tag{8.21}$$

so that both extremes of the frontier map to the corners $(1;0)$ and $(0;1)$ of the unit square. Under the assumption, verified empirically on the sampled frontier, that the trade-off between the two normalized objectives is monotonic between these two extremes, the chord connecting them is the line $f_1 + f_2 = 1$, and the perpendicular distance of any frontier point from this chord is proportional to $f_1 + f_2 - 1$. The knee point is then identified as the capacity maximizing this quantity,

$$E_{\mathrm{knee}} = \arg\max_{E_{\mathrm{nom}}} \Big[f_1(E_{\mathrm{nom}}) + f_2(E_{\mathrm{nom}}) - 1 \Big] \tag{8.22}$$

which corresponds to the frontier point farthest, in the normalized objective space, from the segment joining the two single-objective optima. To rule out the possibility that this result is an artifact of the coarse sixty-point sweep, the hourly dispatch simulation is re-run on a locally refined grid concentrated around the region where the knee point and the interior compromise window identified through the weighted-sum refinement are both located, and the two independent criteria are cross-checked for agreement.

Discretization onto Commercial Module Sizes and System-Value Decomposition. Since the continuous optimum E_{knee} is not, in general, an integer multiple of the commercial module capacity $E_{\mathrm{mod}} = 417{,}99$ kWh, it is discretized by rounding to the nearest feasible number of modules, $n_{\mathrm{mod}} = \mathrm{round}(E_{\mathrm{knee}}/E_{\mathrm{mod}})$, and the corresponding discretized capacity $n_{\mathrm{mod}} \cdot E_{\mathrm{mod}}$ is compared against the current two-module baseline configuration by re-evaluating VAN, discounted payback period and gross annual REC benefit at both sizes. To characterize the economic implication of upgrading from the baseline to the discretized knee-point configuration, the incremental value is decomposed into two components on different accounting bases: the change in private, after-tax investor VAN, $\Delta\mathrm{VAN}$, and the present value of the incremental gross REC-wide benefit, obtained by capitalizing the annual benefit increment ΔB at the same discount rate and horizon through the inverse Capital Recovery Factor, $PV(\Delta B) = \Delta B / CRF$. The sum of the two, $\Delta\mathrm{VAN} + PV(\Delta B)$, is reported as an indicative total system value associated with the capacity upgrade; since the first term is net of taxation borne by the investor while the second is a gross, REC-wide quantity not net of the taxation the investor pays on the incentive share it retains, this total is presented as a system-level indicator of value redistribution across the REC membership rather than as a cash flow accruing to any single economic subject.

8.5 Methodology of S4

Scenario S4 extends Scenario S3 with the addition of a proton-exchange membrane (PEM) electrolyzer, evaluating the technical and economic feasibility of directing residual photovoltaic surplus, after battery charging, toward on-site hydrogen production. The electrolyzer is modelled on the Rubri-PI-0020 unit, with a nominal power of 100 kW, a modulation range between 20% and 120% of nominal power (20–120 kW), and a constant specific energy consumption (SEC) of 4,6 kWh/Nm^3 H_2, taken from the manufacturer's nameplate value. This constant-efficiency assumption is conservative, since actual specific consumption typically degrades at partial load, and it is adopted in the absence of a manufacturer-supplied part-load efficiency curve. Hydrogen mass flow is derived from the standard hydrogen density at normal conditions, $\rho_{H_2} = 0{,}08988$ kg/Nm^3:

$$m_{H_2}(t) = \frac{P_{el}(t)}{SEC} \cdot \rho_{H_2}, \qquad SEC = 4{,}6 \text{ kWh/Nm}^3, \tag{8.23}$$

corresponding to an effective specific consumption of approximately 51,18 kWh/kg$_{H_2}$. The battery energy storage subsystem is unchanged from Scenario 3, retaining identical capacity, power, efficiency and SOC-update parameters and is not restated here.

The hourly dispatch algorithm extends the S3 self-consumption-first logic with the electrolyzer as a third-priority load on the surplus side. Within an hour of photovoltaic surplus ($P_{PV}(t) \geq C_{CER}(t)$), direct self-consumption is first satisfied, the battery is then charged up to its available capacity and rated power (absolute priority, as in S3), and only the residual surplus after battery charging is offered to the electrolyzer: if this residual surplus is at or above the minimum technical threshold of 20 kW, the electrolyzer operates at the minimum between the available surplus and its maximum power of 120 kW. Below this threshold the unit remains off, with no partial standby mode modelled. Any surplus remaining after both storage and electrolysis is exported to the grid as RID surplus. Within an hour of deficit, the electrolyzer is kept off by construction, and the dispatch follows the same battery-discharge-then-grid-purchase logic as S3.

The electrolyzer is modelled as a separate withdrawal point (POD) within the aggregated CER configuration, distinct from the single production POD shared by the PV plant and the battery. This topological assumption determines the definition of shared incentivized energy adopted in the model,

$$E_{shared}(t) = E_{sc}(t) + P_{disch}(t) + P_{el}(t), \tag{8.24}$$

which differs from the treatment of battery charging in S3: whereas the battery sits behind the same meter as the PV plant and therefore cannot, by construction, generate shared energy while charging, the electrolyzer is treated as an independent consuming member of the community, whose withdrawal is matched against the aggregate net injection of the configuration.

Under the GSE definition of shared energy as the hourly minimum between aggregate injection and aggregate withdrawal, and given that the dispatch logic imposes

$$P_{el}(t) \leq P_{PV}(t) - C_{CER}(t) - P_{charge}(t) \tag{8.25}$$

at every hour by construction, aggregate withdrawal $\Big(C_{CER}(t) + P_{el}(t)\Big)$ never exceeds aggregate net injection $\Big(P_{PV}(t) - P_{charge}(t)\Big)$. The resulting shared energy therefore reduces exactly to

$$C_{CER}(t) + P_{el}(t) = E_{sc}(t) + P_{el}(t) \tag{8.26}$$

in surplus hours (with the battery discharge term adding in deficit hours), consistent with the expression implemented in the code. This assumption reflects a plausible administrative configuration for an electrolyzer participating in a CER as a distinct member entity, though it should be noted that regulatory practice on this specific configuration is not yet fully consolidated in the Italian framework.

The restriction of electrolyzer operation to surplus hours only, rather than allowing grid-supplied operation at any hour, is retained both as an economic choice, avoiding retail-priced electricity purchases that would erode the margin on hydrogen sales, which the model does not otherwise account for, and, more substantively, as a modelling proxy for the temporal correlation criteria of the EU Delegated Regulation on renewable hydrogen (Renewable Energy Directive II), which requires renewable electricity used for electrolysis to be temporally correlated with its generation (monthly correlation permitted until 2029, hourly correlation required from 2030 onward).

The economic model retains the remuneration structure of S3: TiP, ARERA valorization corrective and RID surplus revenue, all computed on the shared energy series as redefined above. It excludes electrolyzer consumption from retail bill savings, since

$$R_{savings} = P_{retail} \cdot \Big(E_{sc}(t) + P_{disch}(t)\Big) \tag{8.27}$$

accounts only for energy that displaces a purchase the community would otherwise have made. The electrolyzer represents an additional load with its own dedicated revenue stream rather than a substitute for retail consumption. Hydrogen revenue is computed as

$$R_{H_2} = P_{H_2} \cdot m_{H_2}(t), \tag{8.28}$$

using an indicative central price of 6 EUR/kg, consistent with the current EU green hydrogen price range (4–8 EUR/kg).

Annual key performance indicators extend those of S3 with hydrogen-specific metrics: annual hydrogen output (Nm^3 and kg), electrolyzer operating hours and capacity factor and effective specific consumption. The Self-Consumption Index is redefined to include the energy directed to electrolysis alongside direct self-consumption and battery charging, reflecting the share of PV production retained on-site in any form. The Self-Sufficiency Index, by contrast, retains the S3 definition based solely on direct self-consumption and battery discharge, since electrolyzer consumption is an additional load rather than a means of covering community demand.

Environmental performance is assessed through two independent avoided-emissions components:

- an **electricity-side** component, following the same ISPRA 2025 grid emission factor (0,216 $kgCO_2$/kWh, 2023 reference data) applied to both total PV production and shared energy as in previous scenarios;
- a **hydrogen-side** component, obtained by comparing the renewable hydrogen output against the CertifHy fossil fuel comparator for grey hydrogen (10,92 $kgCO_2$/kg H_2, steam methane reforming without carbon capture), yielding the emissions avoided by displacing conventional hydrogen production.

Finally, the comparison against the no-CER baseline follows the same structure as previous scenarios, decomposing the total annual benefit into retail bill savings and additional CER revenues, now including hydrogen sales alongside TiP, ARERA and RID, expressed both in absolute terms and as a percentage of baseline energy cost.

Chapter 9

Results and Discussion

This chapter presents and discusses the energy, economic, and environmental results obtained from the simulation of the four REC scenarios, illustrating the hourly, monthly, and seasonal graphical output generated by the MATLAB model. For each scenario, the analysis covers the resulting energy balance and self-consumption/self-sufficiency indices, the economic performance relative to the no-PV baseline, the regulatory implications of the shared-to-injected energy ratio under the CACER Decree, the avoided CO_2 emissions based on the ISPRA national grid emission factor and the economic evaluation of the investment. Particular attention is given to the incremental contribution of each additional technology layer, in order to isolate the specific value it adds to overall REC performance. A comparative synthesis of the main indicators across all four scenarios closes the chapter.

9.1 Scenario S1

The reference-year simulation (April 2025–March 2026) yields an annual PV production of 1591,3 MWh against an aggregate REC consumption of 3386,8 MWh. Of the energy generated, 1084,5 MWh (68,2%) is shared instantaneously with the community load, while the remaining 506,8 MWh is exported to the grid and remunerated through the withdrawal tariff (RID); the residual 2302,3 MWh of community consumption is met by grid purchases. These figures satisfy both energy balances by construction (PV production = shared energy + surplus, and REC consumption = shared energy + grid purchase), confirming internal consistency of the hourly dispatch model.

The resulting performance indices are a Self-Consumption Index (SCI) of 68,2% and a Self-Sufficiency Index (SSI) of 32,0%. The relatively high SCI, despite the plant covering less than half of total demand, reflects the load structure of the community: with the residential class accounting for approximately 84% of aggregate consumption, the load profile remains substantial even during off-peak solar hours, so that a comparatively undersized PV plant (1 MWp against 3,4 GWh/yr of demand) still finds sufficient concurrent demand to absorb most of its output. This is visible in the annual hourly profile of Figure 9.1, where the community consumption trace (blue) rarely falls below the PV production envelope (yellow) even in the shoulder seasons, and is confirmed at finer resolution by the representative summer week of Figure 9.2, in which the PV output is almost entirely enclosed within the load curve, leaving only a limited midday surplus.

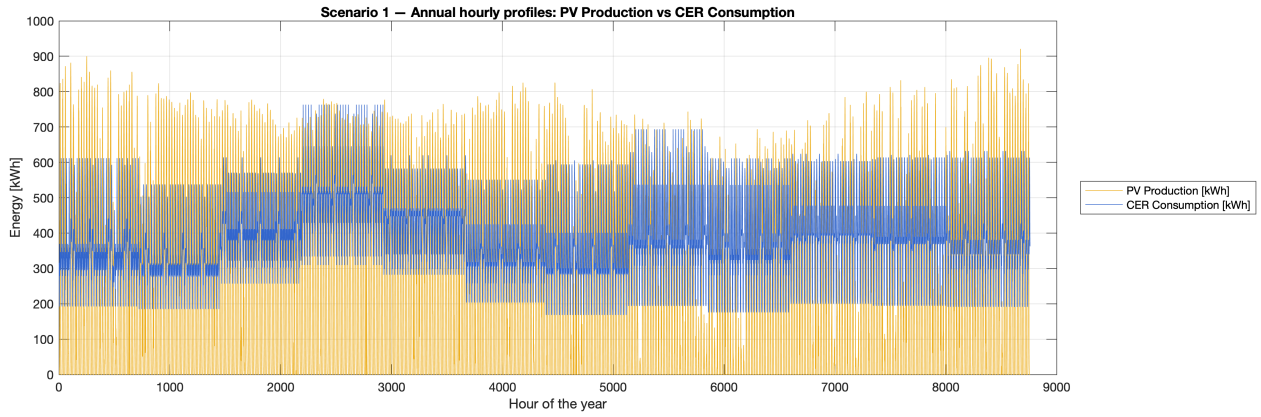


Figure 9.1: Scenario S1 — Hourly PV production and aggregated CER load profiles over the reference year (April 2025–March 2026, 8,760 h).

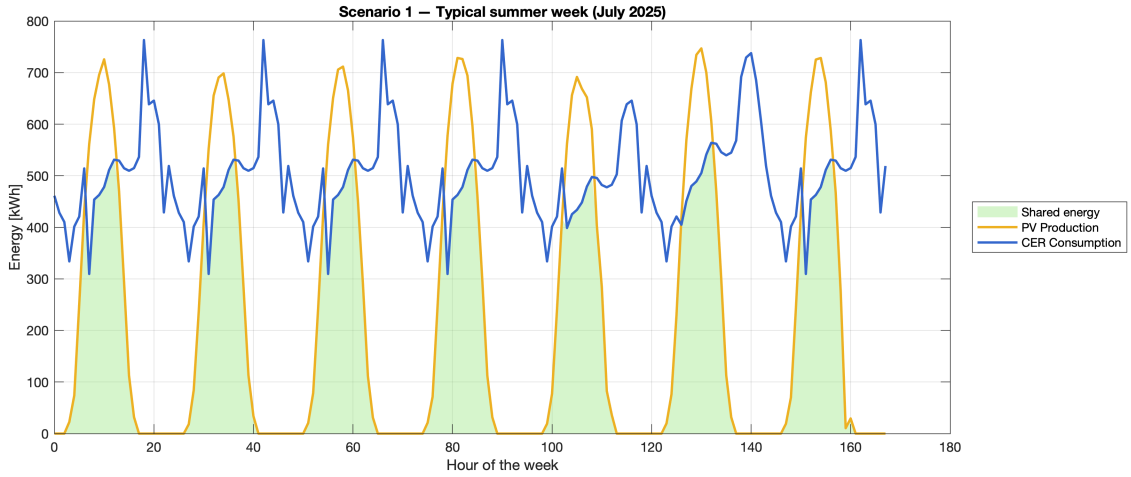


Figure 9.2: Scenario S1 — PV production and CER consumption profiles over a representative summer week (July 2025), with shared energy highlighted.

Production profile and PV allocation. The PV load duration curve (Figure 9.3) shows a peak instantaneous output of approximately 920 kWh (consistent with a plant of 1 MWp operating at a peak performance ratio close to 0,92) and zero output for roughly 52–53% of the year, in line with the expected solar fraction at this latitude (Minervino di Lecce, Puglia).

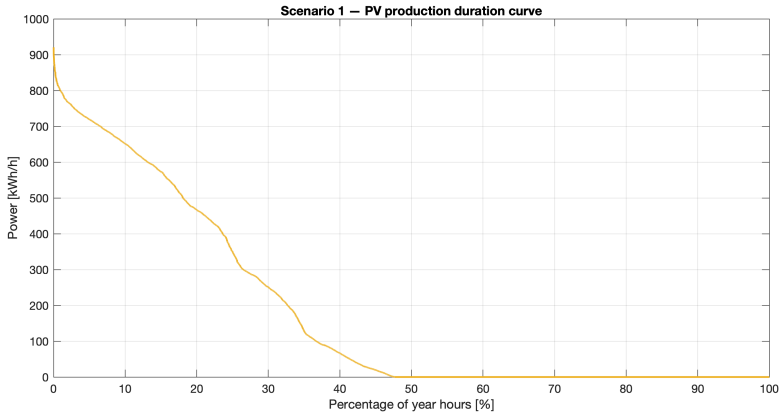


Figure 9.3: Scenario S1 — Annual duration curve of PV hourly production, sorted in descending order.

The two-panel breakdown of Figure 9.4 further disaggregates the PV output into shared and exported quotas over the full year and superimposes the hourly zonal price (Pz) with the premium tariff (TiP), showing that the TiP, capped at 100 €/MWh, tracks below the zonal

price for a large majority of hours, which is consistent with its role as a top-up rather than a market-replacing mechanism.

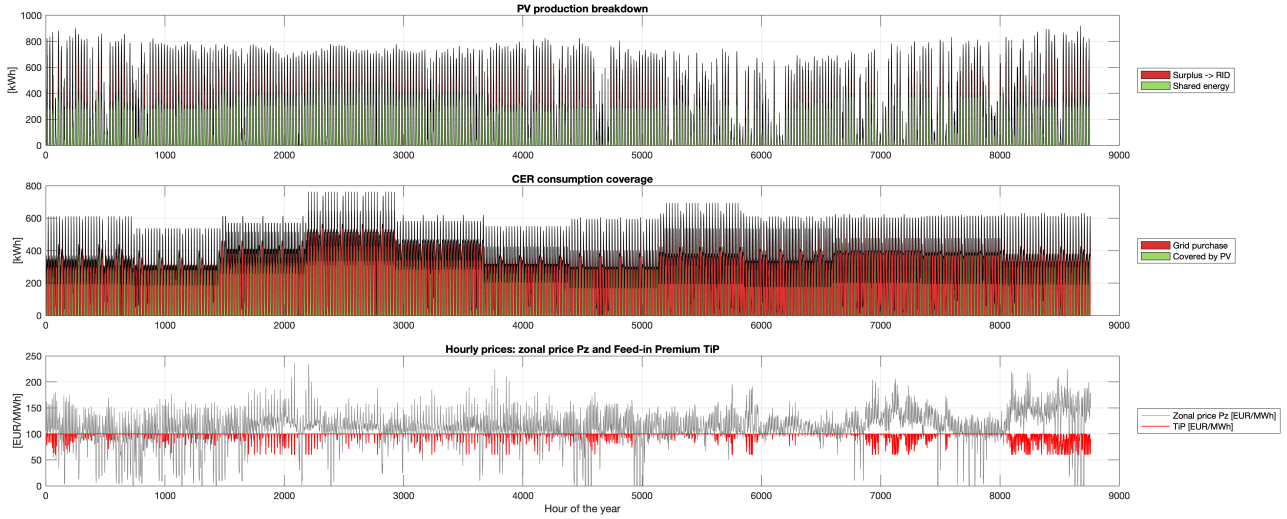


Figure 9.4: Scenario S1 — Hourly energy flows over the reference year: (top) PV production split into shared energy and grid-injected surplus; (middle) CER load coverage from PV self-consumption versus grid purchase; (bottom) hourly zonal price P_z and Feed-in Premium tariff (TiP).

Economic performance. From an economic standpoint, the model returns gross incentive revenues of 453030 €/yr, decomposed into a direct bill saving of 281531 €/yr, a premium tariff (TiP) revenue of 107044 €/yr, an ARERA compensation of 10303 €/yr, and a surplus sale (RID) revenue of 54153 €/yr. Benchmarked against the no-PV baseline cost of 836816 €/yr, this corresponds to an aggregate reduction of the community's energy expenditure of 54,1%, and constitutes the correct comparative metric to characterise the value generated by the REC relative to the counterfactual scenario, as illustrated by the waterfall decomposition in Figure 9.5 (top panel). It is worth noting that the final bar of that waterfall, labelled "Net purchase cost" (383786 €/yr), does not represent the actual cost paid for grid-purchased energy, which amounts to 555285 €/yr, as reported separately in the monthly breakdown of Figure 9.6, but rather a net portfolio cost obtained by offsetting the residual grid purchase against the monetary incentives collected (TiP + ARERA + RID = 171499 €/yr). The two quantities answer different questions, 555285 €/yr is the cash actually disbursed for electricity procurement, while 383786 €/yr is that same disbursement net of incentive cash inflows, and are both retained here as complementary indicators, with the figure caption/legend updated accordingly to avoid conflating the two. The monthly decomposition (Figures 9.6 and 9.5, bottom panel) shows the expected seasonal pattern, with the bill-saving component peaking in July (in phase with PV output) and the RID and TiP components partially compensating the reduced self-consumption share in the winter months (November–January), when grid purchases dominate the energy mix.

Regulatory threshold. A regulatory constraint arises from the ratio between shared and injected energy (68,2%), which exceeds the 55% threshold set by the CACER Decree for the free distributability of premium-tariff proceeds among REC members (a threshold reduced to 45% for RECs that have also received PNRR capital grants – not applicable here, since S1 assumes no public capital contribution). Consequently, the share of TiP revenue associated with the fraction of shared energy exceeding 55% of the injected energy cannot be freely allocated among all members, but must be reserved for non-corporate consumers or for initiatives with a social/territorial impact, as prescribed by the Decree. This constraint does not alter the aggregate economic results reported above, but it is relevant to the REC's internal revenue-distribution scheme and should be accounted for in any member-level (rather than system-level) economic analysis.

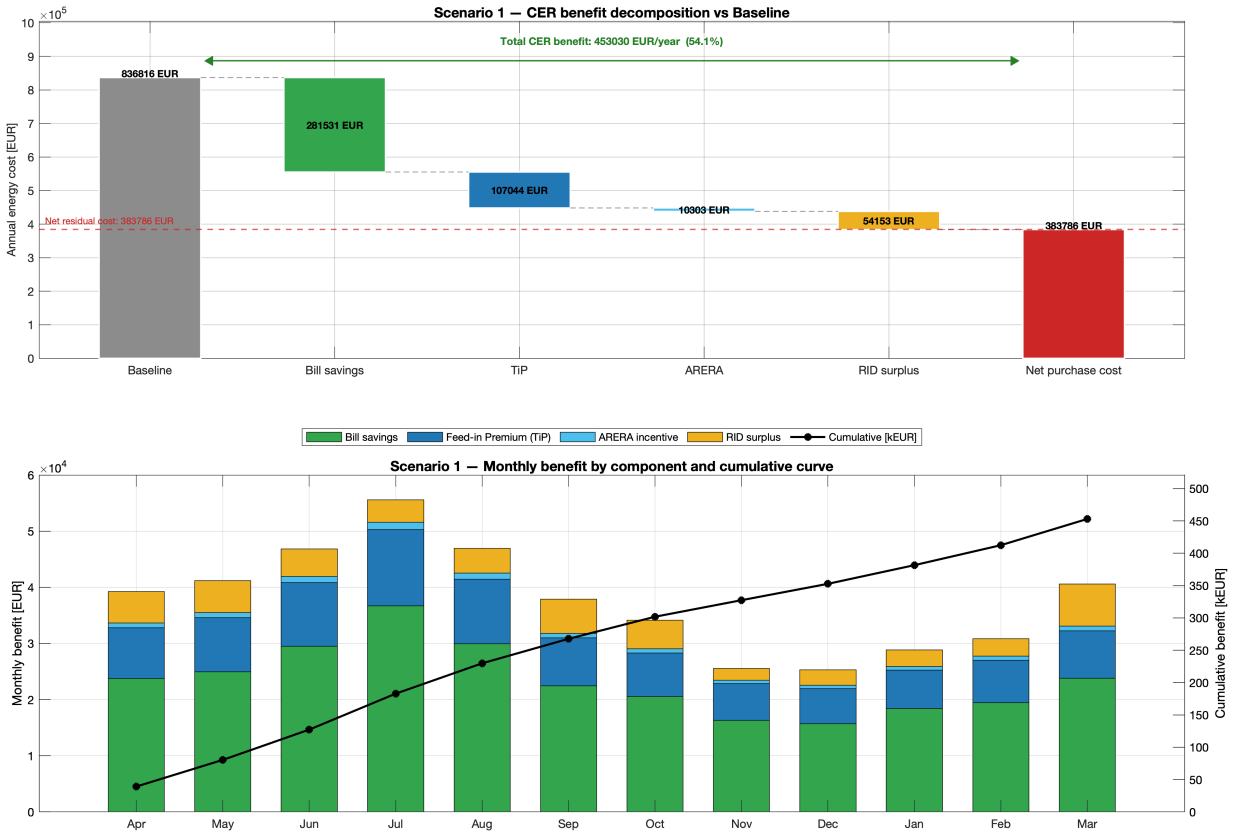


Figure 9.5: Scenario S1 — Comparative analysis of the CER configuration against the no-PV baseline: (top) waterfall decomposition of the annual energy cost, from the baseline cost to the net residual purchase cost, broken down by revenue component; (bottom) monthly benefit by component with cumulative annual value.

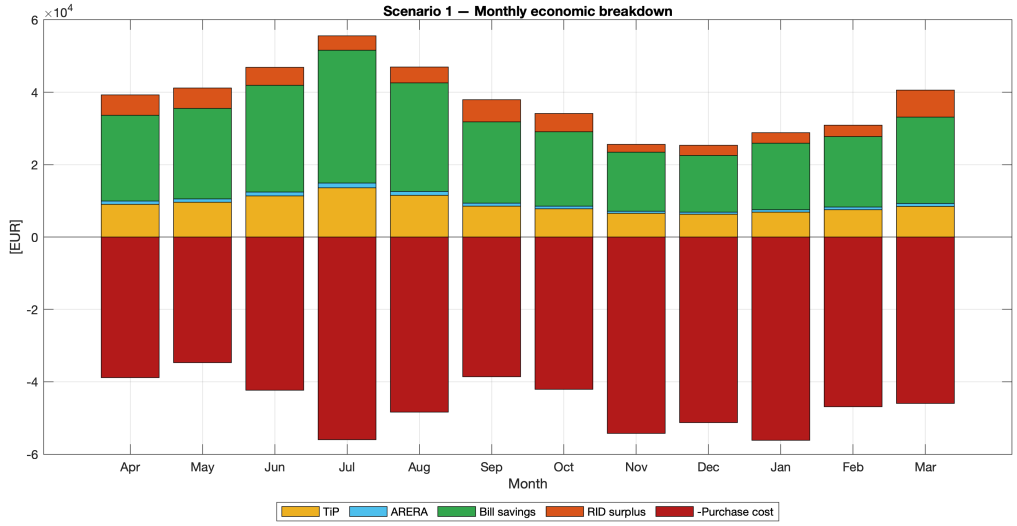


Figure 9.6: Scenario S1 — Monthly breakdown of revenue components (Feed-in Premium, ARERA incentive, bill savings, RID surplus sales) and grid purchase cost.

Environmental impact. Finally, the environmental assessment, based on the 2023 ISPRA grid emission factor (0,216 $kgCO_2/kWh$), yields an avoided emission of 343,7 tCO_2/yr on an upper-bound basis (computed on total PV production, i.e. assuming the exported surplus also displaces grid generation) and 234,2 tCO_2/yr on a lower-bound basis (computed only on the instantaneously shared energy, i.e. the fraction directly consumed within the community). The two bounds bracket the actual avoided-emission value, which depends on assumptions about the marginal generation mix displaced by the exported surplus and is not resolved further within the scope of this scenario.

9.2 Scenario 2

Scenario 2 extends the PV-only baseline of Scenario 1 by introducing a rule-based Demand Response (DR) mechanism acting exclusively on the residential load component (84,0% of total REC consumption, 2845,3 MWh/year). The mechanism identifies, for each day of the year, source hours in which PV production falls short of REC consumption ($P_{PV}(t) < C_{CER}(t)$, 76,6% of annual hours) and destination hours in which a PV surplus is available ($P_{PV}(t) > C_{CER}(t)$, 23,4% of annual hours, corresponding to 506,8 MWh of available annual surplus). A share α of the residential load in source hours is proportionally removed and redistributed into destination hours in proportion to the available surplus, subject to a daily energy-conservation constraint and a daily capping rule that limits the shift to the surplus actually available on that day.

Figure 9.7 shows the annual hourly profiles of PV production and REC consumption, with and without DR at the central sensitivity value $\alpha = 10\%$. Because DR only redistributes load within each day without altering its daily total, the DR-adjusted consumption profile (dashed) closely tracks the original one, with visible reductions during source hours and increases during destination hours; the overall seasonal envelope of consumption is therefore unchanged.

Figure 9.8 decomposes these hourly dynamics into three complementary views. The top panel splits PV production into the shared-energy component and the surplus sold under the Ritiro Dedicato (RID) scheme, showing that surplus events are concentrated but not negligible throughout the year, consistent with the 506,8 MWh of available annual surplus identified in the hour classification. The middle panel shows the coverage of DR-adjusted REC consumption, with residual grid purchase remaining the dominant term for most of the year given the low winter self-sufficiency. The bottom panel compares the hourly zonal price (P_z) against the resulting Premium Tariff (TiP): since $TiP(t) = \min(TiP_{\text{base}} + \max(0, PUN_{\text{ref}} - P_z(t)), TiP_{\text{cap}})$, the incentive is compressed toward its 100 EUR/MWh cap whenever $P_z(t)$ falls below the 180 EUR/MWh reference, and is correspondingly eroded during price spikes: since $TiP_{\text{base}} + (PUN_{\text{ref}} - P_z) < TiP_{\text{cap}}$ whenever $P_z > PUN_{\text{ref}} - (TiP_{\text{cap}} - TiP_{\text{base}}) = 140$ EUR/MWh, the TiP curve tracks below its cap precisely during the sharp Pz peaks visible in the figure.

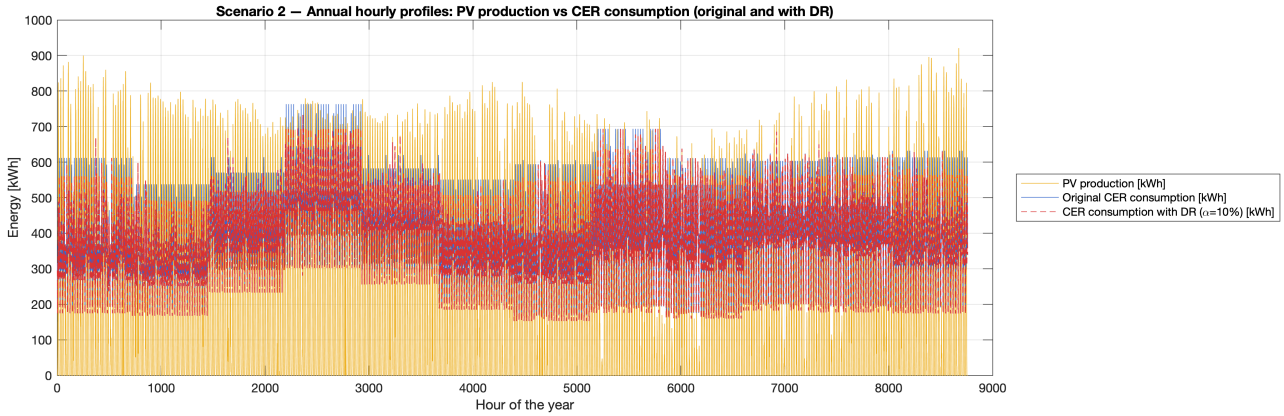


Figure 9.7: Annual hourly profiles of PV production and REC consumption for Scenario 2, comparing the original residential-load profile with the Demand-Response-adjusted profile at $\alpha = 10\%$. Since DR redistributes load within each day without altering its daily total, the DR-adjusted consumption curve closely tracks the original one, with visible reductions during source hours and increases during destination hours.

Sensitivity on α. Three values of the DR intensity parameter were tested ($\alpha = 5\%, 10\%, 15\%$), corresponding to increasing shares of residential source-hour consumption made available for shifting. The results are summarized in Table 9.1: shared energy increases monotonically with α, from 1177,4 MWh/year ($\alpha = 5\%$, +8,6% over the no-DR baseline of 1084,5 MWh/year) to 1337,0 MWh/year ($\alpha = 15\%$, +23,3%).

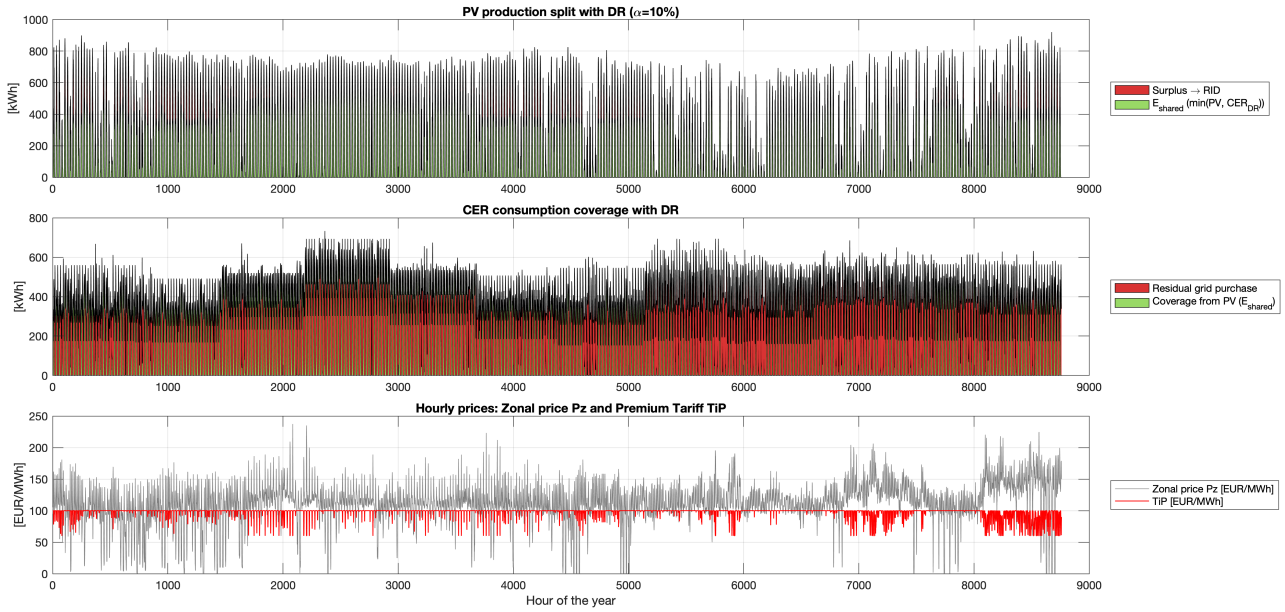


Figure 9.8: Hourly energy and price flows for Scenario 2 at $\alpha = 10\%$. Top: split of PV production between shared energy ($E_{\text{shared}} = \min(P_{PV}, CER_{DR})$) and surplus sold under the Ritiro Dedicato (RID) scheme. Middle: coverage of DR-adjusted REC consumption by PV (shared energy) versus residual grid purchase. Bottom: hourly zonal price (P_z) and the resulting Premium Tariff (TiP), capped at 100 EUR/MWh.

This increase is accompanied by a growing share of candidate flexible energy that cannot be absorbed by the available surplus (spill), rising from 13,9% of candidate energy at $\alpha = 5\%$ to 21,3% at $\alpha = 15\%$, indicating diminishing marginal returns as the DR intensity increases and the surplus-hour capacity saturates.

Table 9.1: Sensitivity analysis on the DR flexibility coefficient α: candidate flexible energy, effective shift after the daily capping constraint, unabsorbed spill, and resulting net increment in shared energy. Note that $\Delta E_{\text{cond}} < E_{\text{shift}}$ for all α values: a small subset of source hours switch state to destination after load removal, reducing shared energy in those hours rather than adding to it one-for-one (115 hours out of 6710 source hours at $\alpha = 10\%$, accounting for the full 2006 kWh gap; see main text).

α	$E_{\text{flex,ann}}$ [kWh]	$E_{\text{shift,ann}}$ [kWh]	E_{spill} [kWh]	Spill [%]	ΔE_{cond} [kWh]
5%	108670	93548	15122	13,9%	+92902
10%	217340	179624	37716	17,4%	+177618
15%	326011	256703	69307	21,3%	+252520

Figure 9.9 shows this trend is consistent across all months, with the seasonal profile of shared energy preserved under all three α values.
The central scenario ($\alpha = 10\%$) is analyzed in detail hereafter. Of the 217,3 MWh/year of residential load flagged as candidate for shifting in source hours, 179,6 MWh/year were effectively redistributed into destination hours, while 37,7 MWh/year (17,4% of candidate energy) could not be absorbed by the available surplus and remained subject to daily capping, active on 73 of 365 days. The resulting increment in shared energy, however, is slightly smaller than the energy shifted (177,6 MWh/year rather than 179,6 MWh/year). This second-order effect arises because the proportional removal of residential load in source hours is scaled uniformly across the day and does not verify, hour by hour, whether the reduced consumption remains above PV production. In 115 of the 6710 source hours (1,7%), the removal is large enough that $C_{CER,DR}(t)$ drops below $P_{PV}(t)$: the hour switches state from source to destination, but its binding constraint changes from PV availability to the (now lower) residual load, so shared energy in those hours falls from 41,5 MWh to 3,5 MWh, a net loss of 2,0 MWh that exactly accounts for the gap.

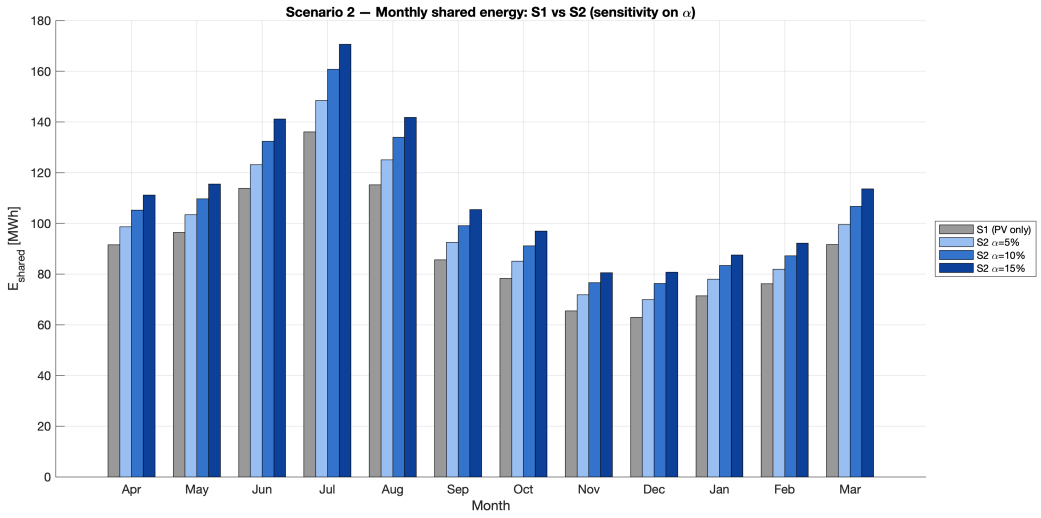


Figure 9.9: Monthly shared energy for Scenario 1 (PV only) compared against Scenario 2 under the three tested Demand Response intensities ($\alpha = 5\%, 10\%, 15\%$). The seasonal profile of shared energy is preserved under all α values, with the DR-induced increment consistently present across the year.

This is a structural limitation of the rule-based proportional redistribution rather than a numerical artifact, and it has a negligible impact on the aggregate results (1,1% of the shifted energy at $\alpha = 10\%$).

Figure 9.10 shows a marked seasonal asymmetry in the shift/spill dynamic: during the summer months, when PV surplus is abundant, nearly all candidate flexible energy is successfully shifted with negligible spill (e.g., July: 24,7 MWh shifted against a monthly surplus of 36,9 MWh); during the winter months, when surplus availability drops sharply, a substantially larger share of candidate energy is spilled (e.g., November: 11,2 MWh shifted against 9,2 MWh spilled, i.e., approximately 45% of candidate energy unabsorbed). This confirms that the effectiveness of surplus-driven DR is intrinsically constrained by PV resource availability, and is therefore most valuable as a complement to, rather than a substitute for, storage-based flexibility (addressed in Scenario 3).

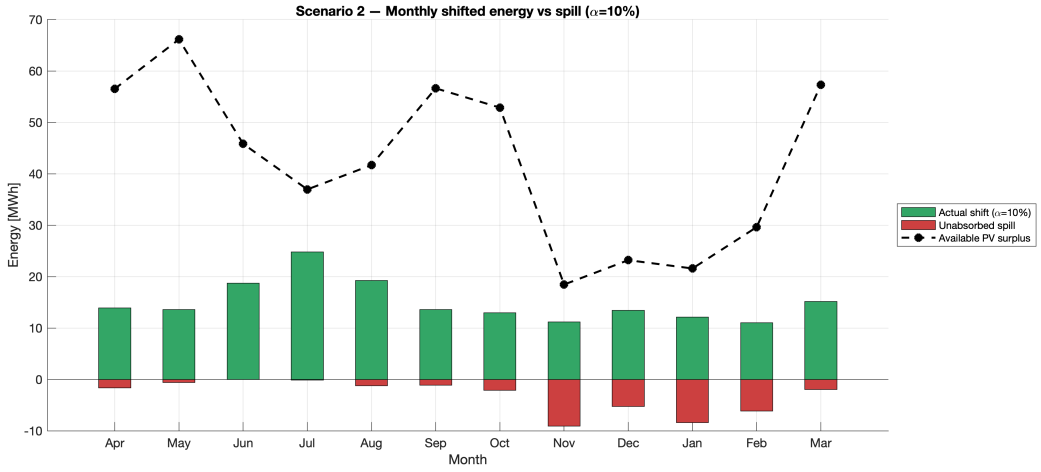


Figure 9.10: Monthly effectively shifted energy versus unabsorbed spill for Scenario 2 at $\alpha = 10\%$, against the available monthly PV surplus. The shift-to-spill ratio deteriorates markedly in the winter months (November–January), when PV surplus availability drops sharply and a large share of candidate flexible energy cannot be absorbed, confirming the structural, PV-resource-limited nature of surplus-driven Demand Response.

Typical weekly profiles. Given this seasonal asymmetry, both a representative summer week (July 2025, Fig. 9.11) and a representative winter week (January 2026, Fig. 9.12) are presented, unlike Scenario 1 where a single week was sufficient to characterize the PV-load balance. In the summer week, the DR-shifted residential profile (P_{RES} with DR) is systematically

depressed during the morning source hours and boosted during the midday destination hours on every day of the week, tracking a regular and repeatable pattern driven by the consistently available midday surplus (visible as the shaded surplus area beneath each daily PV peak). In the winter week, PV surplus is intermittent and concentrated on a small number of days (e.g., Thursday, where a brief but sharp PV peak creates a narrow shifting opportunity), and the DR-adjusted profile shows a correspondingly weaker and less regular deviation from the original residential load, consistent with the higher winter spill fraction quantified above.

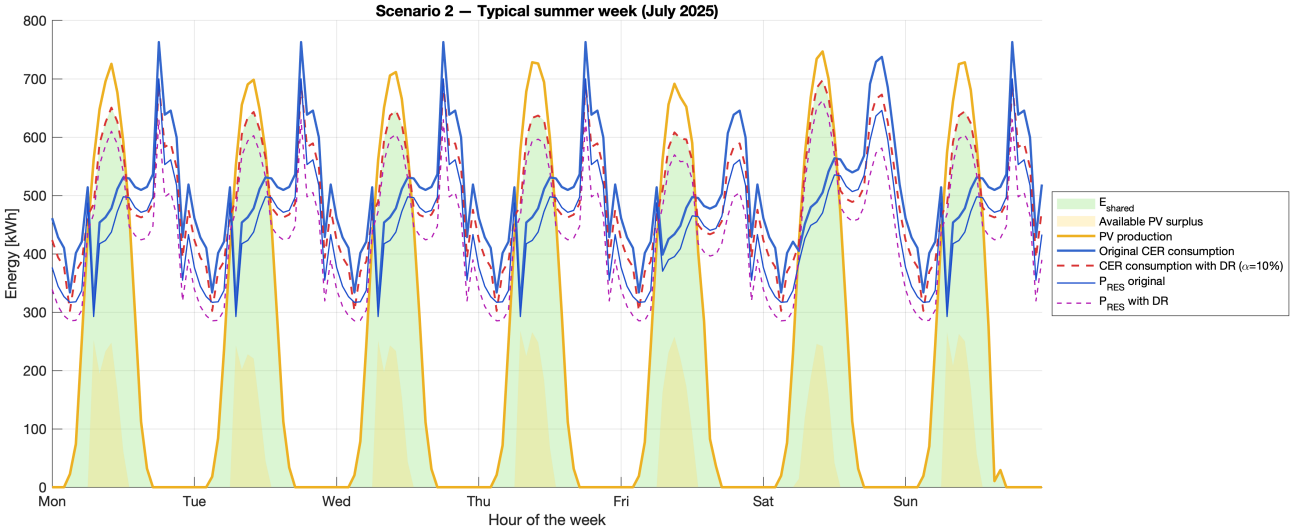


Figure 9.11: Representative summer week (July 2025) for Scenario 2 ($\alpha = 10\%$), showing PV production, original and DR-adjusted REC consumption, original and DR-adjusted residential load (P_{RES}), shared energy and available PV surplus. The DR-shifted residential profile is systematically depressed during morning source hours and boosted during midday destination hours on every day of the week, reflecting the consistently available midday surplus.

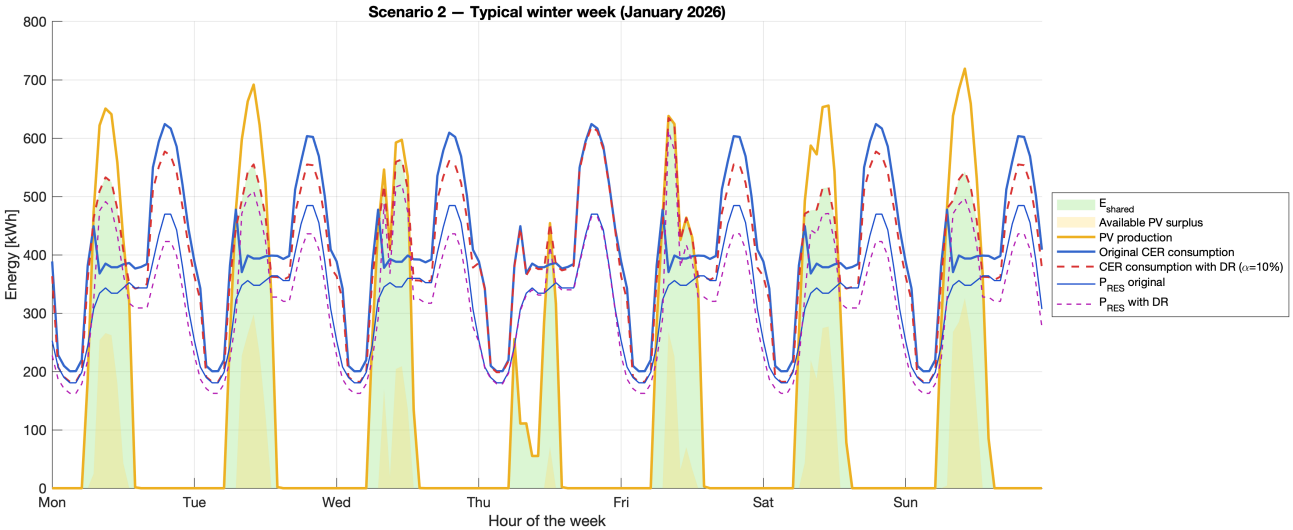


Figure 9.12: Representative winter week (January 2026) for Scenario 2, with the same series as Fig. 9.11. PV surplus is intermittent and concentrated on a small number of days, and the DR-adjusted residential profile shows a correspondingly weaker and less regular deviation from the original load, consistent with the higher winter spill fraction reported in Fig. 9.10.

Regulatory threshold. At $\alpha = 10\%$, the ratio of shared to injected energy (Self-Consumption Index, IAC) reaches 79,3%, further above the 55% CACER threshold than in Scenario 1 (68,2%); the Self-Sufficiency Index (IAS), i.e., the share of total REC consumption covered by shared PV energy, is 37,3%. Since DR redistributes load into surplus hours without increasing PV production, the IAC increase relative to Scenario 1 is a direct and expected consequence of the mechanism. As in Scenario 1, since the REC does not benefit from PNRR capital grants,

the 55% threshold applies and a share of TiP proceeds exceeding this ratio must be reserved for non-corporate consumers or social purposes, consistent with the redistribution mechanism established under the CACER Decree.

Economic performance. At $\alpha = 10\%$, the REC generates 124444 €/year in Premium Tariff (TiP) revenue, 11990 €/year in ARERA compensation, and 34661 €/year from surplus sales at the zonal price (RID), alongside 330238 €/year in retail bill savings on shared energy, for a total gross revenue of 501333 €/year. Against a residual grid purchase cost of 512217 €/year, this yields a net bill saving of 324599 €/year relative to the no-CER baseline (836816 €/year) and additional CER revenue of 171095 €/year, for a total benefit of 495694 €/year, corresponding to a 59,2% reduction relative to the baseline energy cost (Fig. 9.13). The 5639 €/year gap between gross revenue and the net baseline benefit arises because DR redistributes consumption across retail time bands (fasce orarie), which affects the bill-savings calculation independently of the shared-energy volume; this is noted explicitly in the figure caption and does not indicate a balance error.



Figure 9.13: Comparative analysis of Scenario 2 (PV + DR, $\alpha = 10\%$) against the no-CER baseline. Top: waterfall decomposition of the annual energy cost, from the baseline cost (grey) through retail bill savings, Premium Tariff, ARERA compensation and RID surplus revenue, down to the net residual purchase cost (red); the total REC benefit relative to baseline is indicated by the green arrow. The footnote quantifies the gap between the net purchase cost shown here and the value implied by summing the individual components, arising from the DR-induced recomposition of consumption across retail time bands (fasce orarie). Bottom: monthly benefit by component with the cumulative annual benefit on the secondary axis.

Figure 9.14 shows the monthly economic breakdown, with the benefit components (TiP, ARERA, bill savings, RID) peaking in the summer months in line with higher PV output, against a residual purchase cost that remains substantial throughout the year (particularly November–February) due to the low winter self-sufficiency. Figure 9.15 confirms that all economic KPIs increase monotonically with α, mirroring the shared-energy trend, though the diminishing returns identified above suggest that intensifying DR beyond $\alpha = 15\%$ would yield limited additional benefit relative to the growing spill fraction.

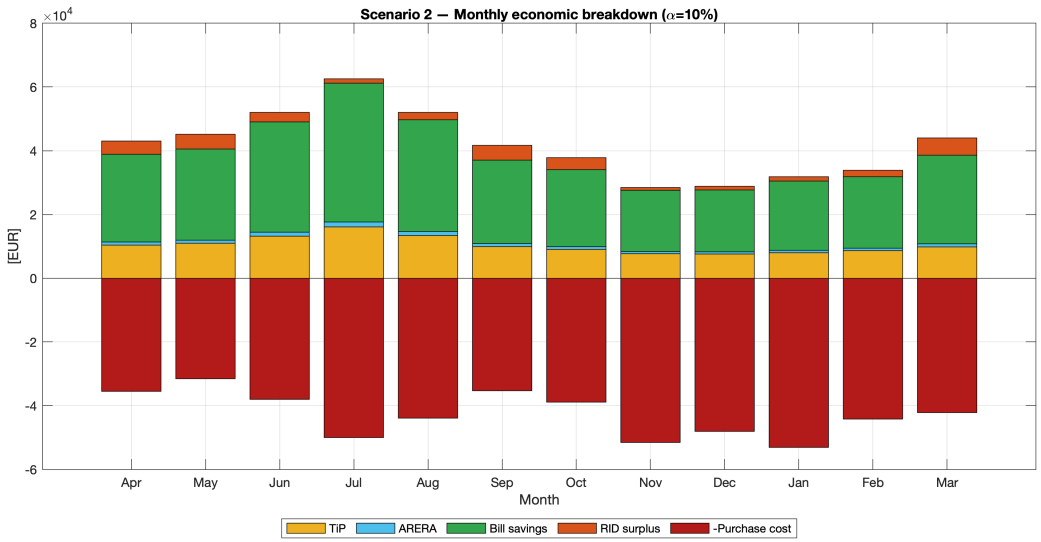


Figure 9.14: Monthly economic breakdown for Scenario 2 at $\alpha = 10\%$, decomposing gross revenue (Premium Tariff, ARERA compensation, retail bill savings, RID surplus sales) against the residual cost of grid-purchased energy. Revenue components peak in the summer months in line with higher PV output, while the purchase cost remains substantial throughout the year, particularly in the winter months, reflecting the low winter self-sufficiency.

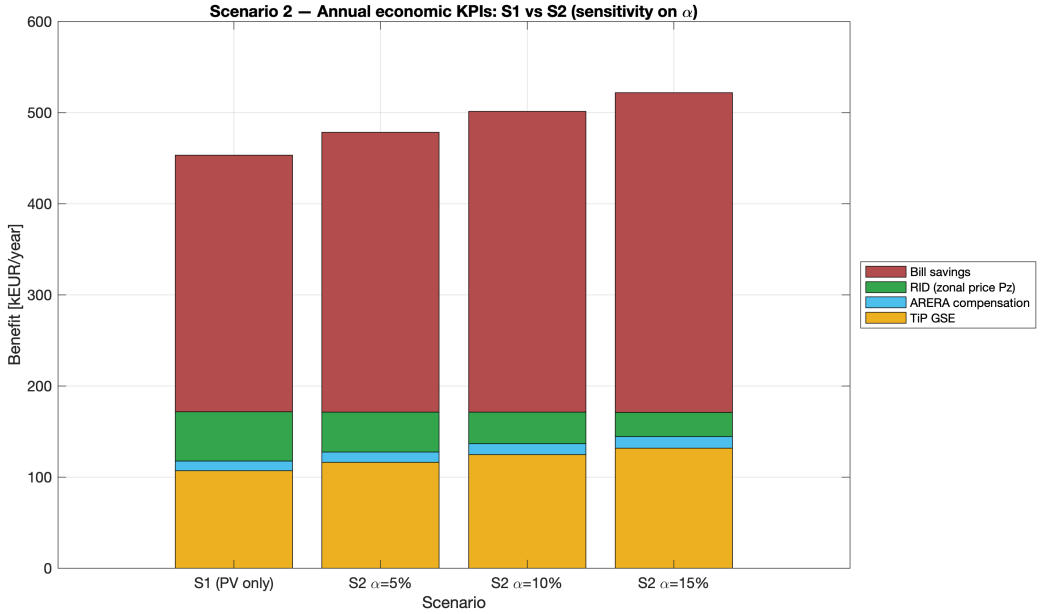


Figure 9.15: Annual economic KPIs for Scenario 1 (PV only) compared against Scenario 2 under the three tested Demand Response intensities ($\alpha = 5\%, 10\%, 15\%$), decomposed into Premium Tariff (TiP), ARERA compensation, RID surplus revenue and retail bill savings. All components increase monotonically with α, though at a diminishing rate consistent with the growing spill fraction shown in Table 9.1.

Environmental impact. Applying the ISPRA 2025 national grid emission factor (0,216 $kgCO_2/kWh$, 2023 reference year), avoided emissions range between a lower bound of 272,6 tCO_2/year (computed on shared energy only) and an upper bound of 343,7 tCO_2/year (computed on total PV production), unchanged from Scenario 1 since DR does not affect PV generation.

9.3 Scenario 3

Scenario 3 extends the baseline configuration of Scenario 1 by coupling the 1 MWp ground-mounted PV plant with a 2 × 125 kW / 835,98 kWh AC-coupled lithium iron phosphate ($LiFePO_4$) battery energy storage system (GSL-BESS-125K418, self-consumption-first dispatch). The underlying hourly PV production (1591,3 MWh/year) and REC consumption (3386,8 MWh/year) profiles are, by construction, identical to Scenario 1: the BESS operates entirely downstream of both series and does not alter either, unlike the demand-response mechanism of Scenario 2, which reshapes the consumption profile itself. Figure 9.16 therefore reproduces the same PV-versus-consumption pattern already presented in Scenario 1.

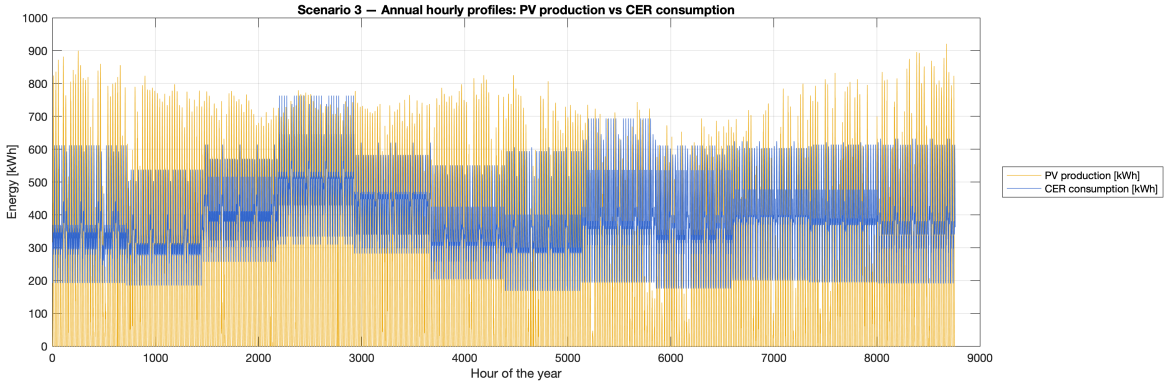


Figure 9.16: Scenario 3, hourly PV production and aggregate REC consumption over the reference year (April 2025–March 2026). By construction, this profile pair is identical to Scenario 1, since battery dispatch operates downstream of both series and does not modify either.

Figure 9.17 shows the resulting hourly allocation of PV production and REC consumption coverage over the year. Over the reference year the battery absorbs 217,1 MWh of charging energy and returns 203,0 MWh to the load, for round-trip losses of 14,3 MWh, consistent with the assumed 93,4% round-trip efficiency net of the change in stored energy between the first and last hour of the year, corresponding to 324,6 equivalent full cycles relative to the 668,78 kWh usable energy window (80% depth of discharge on the 835,98 kWh nominal capacity).

The annual state-of-charge trajectory (Figure 9.18) shows the battery cycling almost daily between its 20% and 100% bounds, with several shallower cycles concentrated in late autumn and early winter (approximately hours 4600–5000, 5800–6200 and 6800–7000), reflecting periods of reduced PV availability.

Typical weekly profiles. The representative summer and winter weeks (Figures 9.19 and 9.20) confirm this pattern at hourly resolution: in July the battery reaches full charge daily and discharges deeply and predictably during the evening peak, whereas in January the charge/discharge cycles are shallower and occasionally incomplete, consistent with lower and more irregular PV availability.

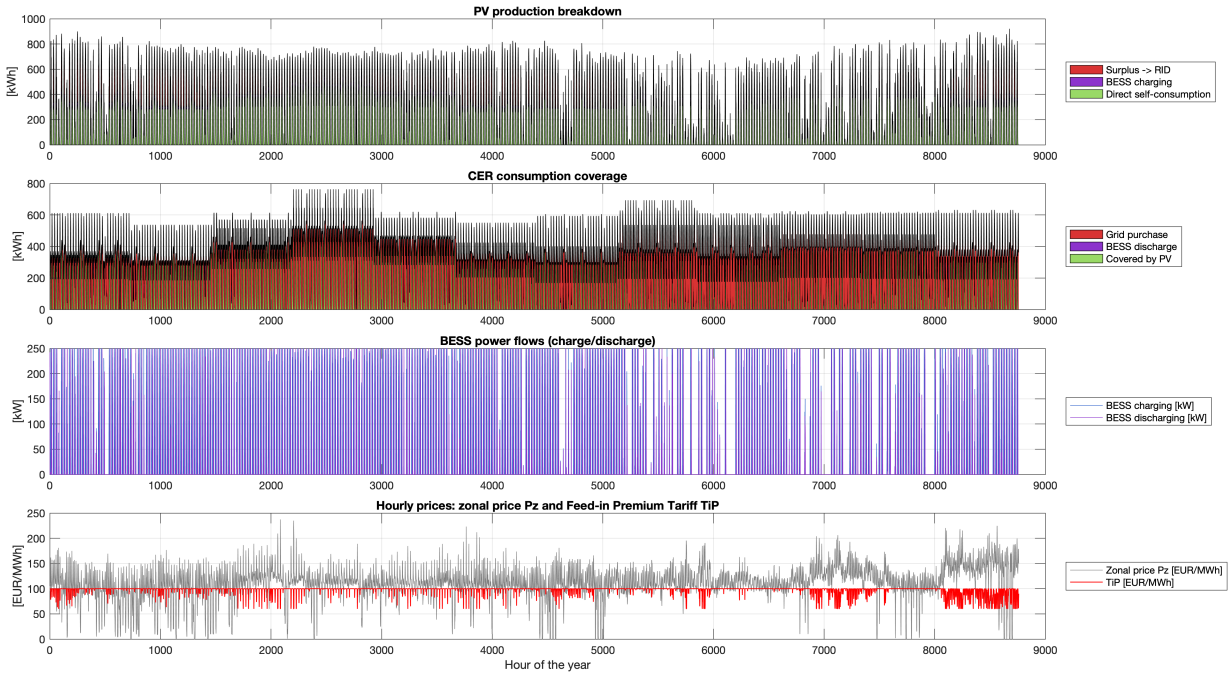


Figure 9.17: Scenario 3, hourly energy flow breakdown. From top to bottom: allocation of PV production between direct self-consumption, BESS charging and RID surplus; coverage of REC consumption by direct PV supply, BESS discharge and residual grid purchase; BESS charging/discharging power; and hourly zonal price P_z against the Tariffa Premio TiP.

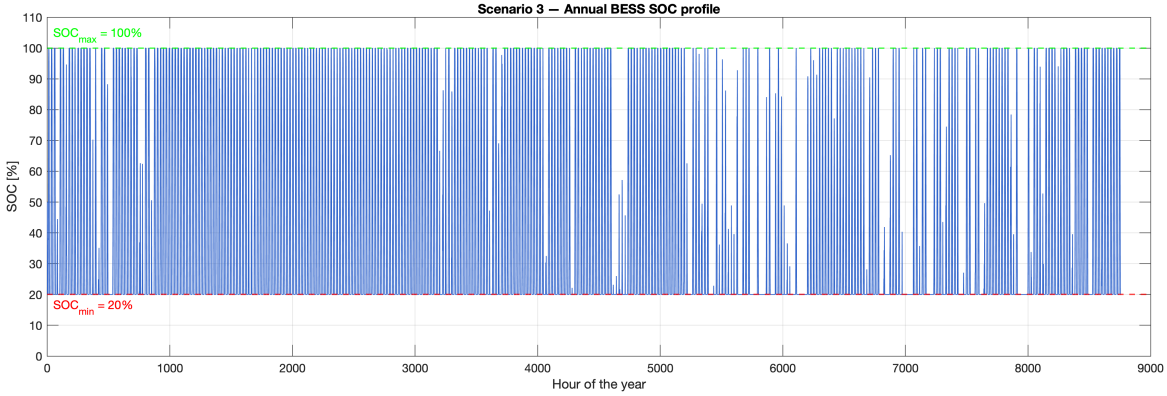


Figure 9.18: Scenario 3, annual state-of-charge trajectory of the BESS, bounded between $SOC_{min} = 20\%$ and $SOC_{max} = 100\%$. The battery cycles almost daily; shallower, incomplete cycles are visible in late autumn and early winter, reflecting reduced PV availability.

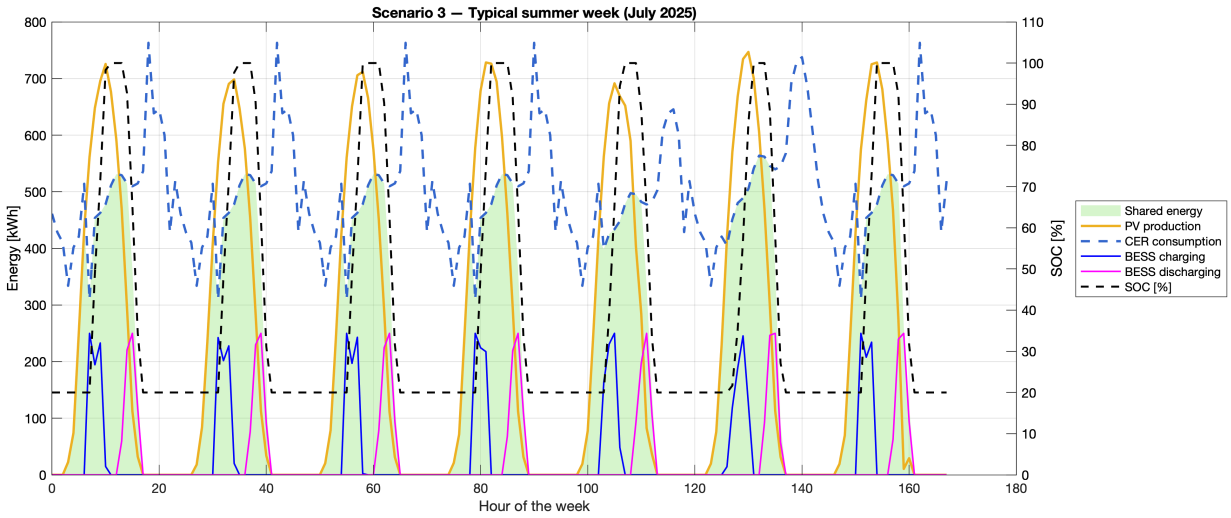


Figure 9.19: Scenario 3, representative summer week (July 2025): PV production, REC consumption, shared energy, BESS charge/discharge power and state of charge.

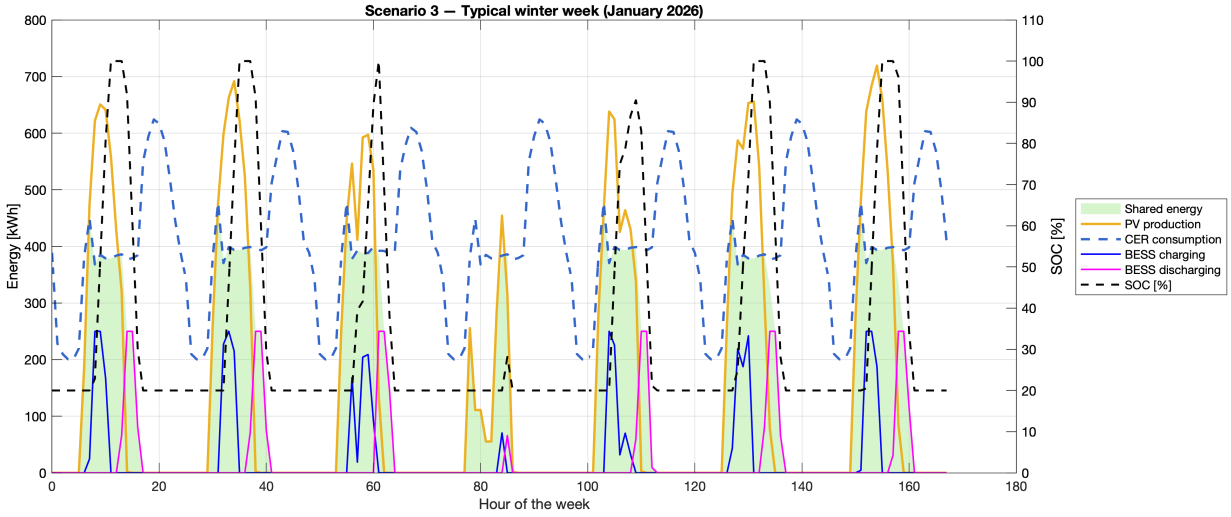


Figure 9.20: Scenario 3, representative winter week (January 2026): PV production, REC consumption, shared energy, BESS charge/discharge power and state of charge. Reduced and irregular PV availability results in shallower and less complete battery cycles compared to the summer week.

The battery raises the Self-Consumption Index (IAC) to 81,8% and the Self-Sufficiency Index (IAS) to 38,0%, against a shared-to-injected energy ratio of 80,9%. As this ratio exceeds the 55% threshold set by the CACER Decree for RECs not benefiting from PNRR capital grants, a share of the Tariffa Premio proceeds is subject to redistribution toward non-corporate members or social purposes, as already discussed for Scenario 1.

Economic Performance. On the economic side (Figure 9.21), the REC generates EUR 127241/year in Tariffa Premio revenue, EUR 12231/year in ARERA compensation, EUR 27798/year from RID sales of the residual surplus, and EUR 339365/year in avoided retail purchases (bill savings) on the self-consumed and stored share of the load, against a residual grid-purchase cost of EUR 497451/year. Relative to a no-PV, no-storage baseline in which the entire REC load is purchased at retail tariffs (EUR 836816/year), this amounts to a total annual benefit of EUR 506636/year, equal to a 60,5% reduction relative to the baseline energy cost.

The monthly decomposition (Figure 9.22) shows bill savings as the dominant component throughout the year, peaking in July, with the Tariffa Premio contribution comparatively larger in the winter months when the zonal price P_z is more frequently below the PUN_{ref} reference used in the incentive formula.

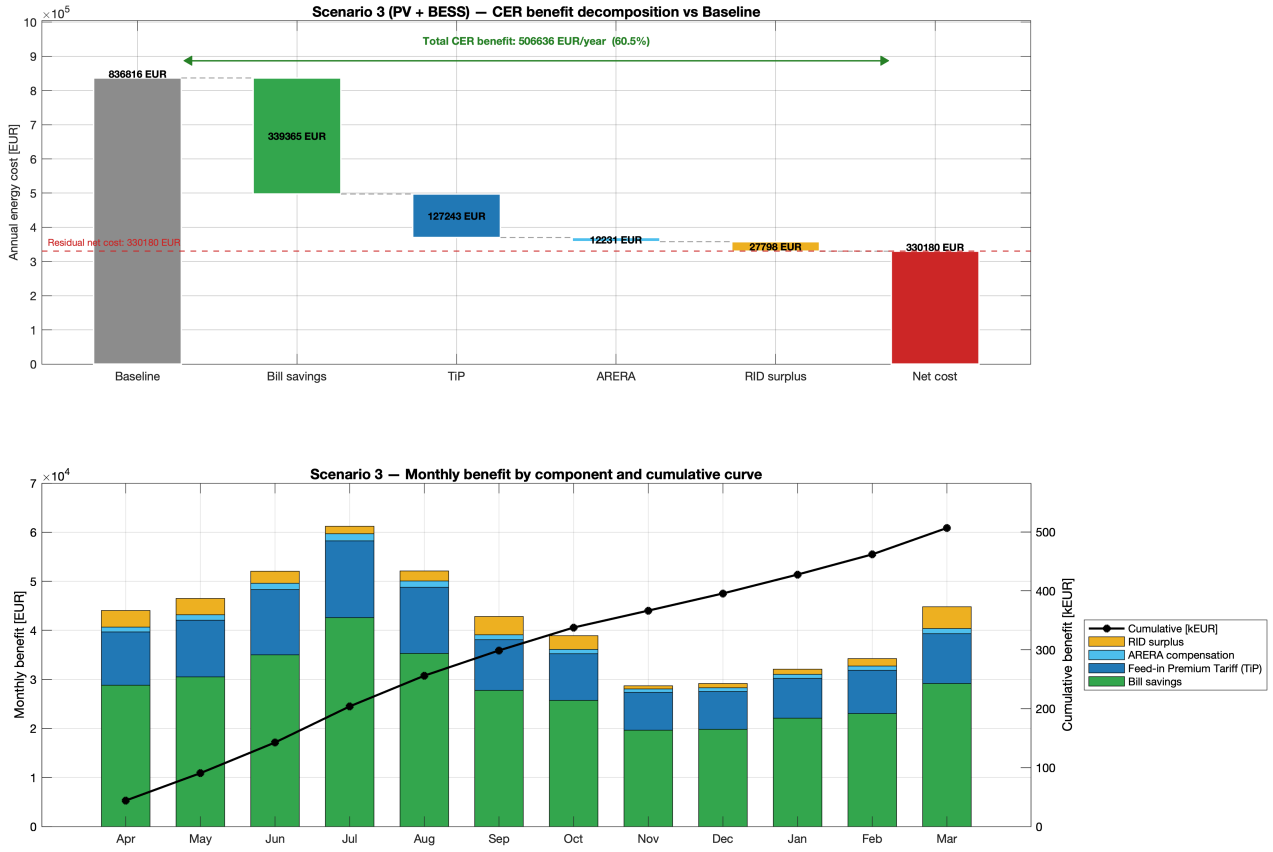


Figure 9.21: Scenario 3, comparison against the no-PV, no-storage baseline. Top: waterfall decomposition of the annual energy cost, from the baseline cost (EUR 836816/year) through bill savings, Tariffa Premio, ARERA compensation and RID revenue, down to the residual net cost (EUR 330180/year), for a total benefit of EUR 506636/year (60,5%). Bottom: monthly benefit by component with cumulative annual benefit.

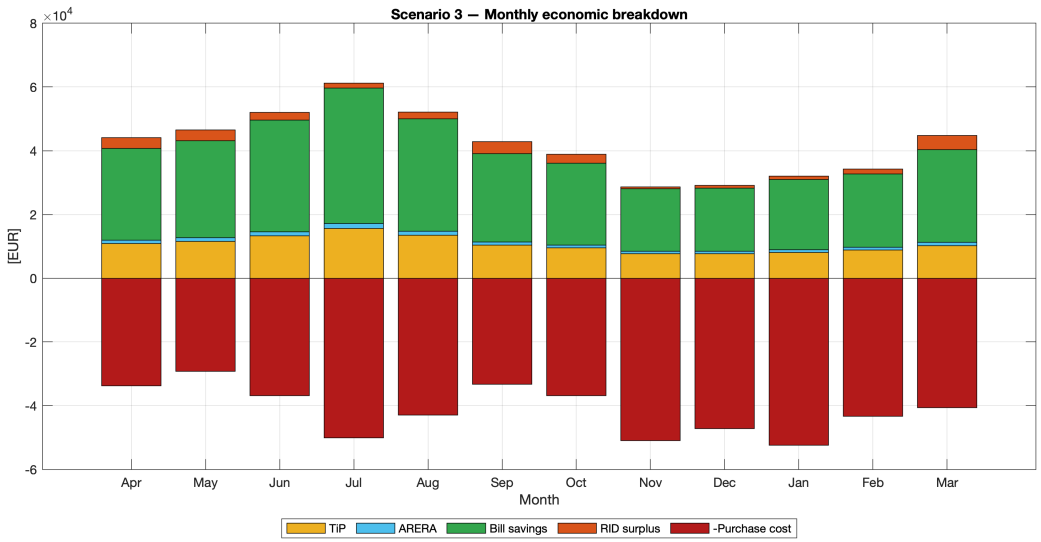


Figure 9.22: Scenario 3, monthly breakdown of revenue components (Tariffa Premio, ARERA compensation, bill savings, RID surplus) against the residual grid purchase cost.

Environmental Impact. Using the ISPRA 2025 grid emission factor for reference year 2023 (0,216 $kgCO_2/kWh$), avoided emissions range between 278,1 tCO_2/year (lower bound, computed on the shared energy only) and 343,7 tCO_2/year (upper bound, computed on total PV production).

9.3.1 Optimization: PSO-Based BESS Sizing.

Building on the fixed 2-module configuration analysed above, a Particle Swarm Optimization (PSO) procedure was used to investigate whether resizing the nominal BESS capacity E_{nom} could better serve either the private investor's or the REC's interests, keeping the commercial C-rate (0,299 kW/kWh), depth of discharge, round-trip efficiency and all other CAPEX/OPEX items fixed. The search space spans one module (417,99 kWh) to an upper bound of 1388,42 kWh, set by the average daily PV surplus.

Single-Objective Optimization: Private VAN. Maximising the 20-year discounted private VAN (Tariffa Premio and ARERA captured at the investor's 25% share, 100% of RID revenue, net of OPEX, 15-year straight-line depreciation and 24% IRES) converged, across five independent runs with different random seeds, to the same solution with zero dispersion (coefficient of variation 0,00%): the lower bound of the search space, E_{nom} = 417,99 kWh, one module, with VAN = EUR 175335 (Figure 9.23).

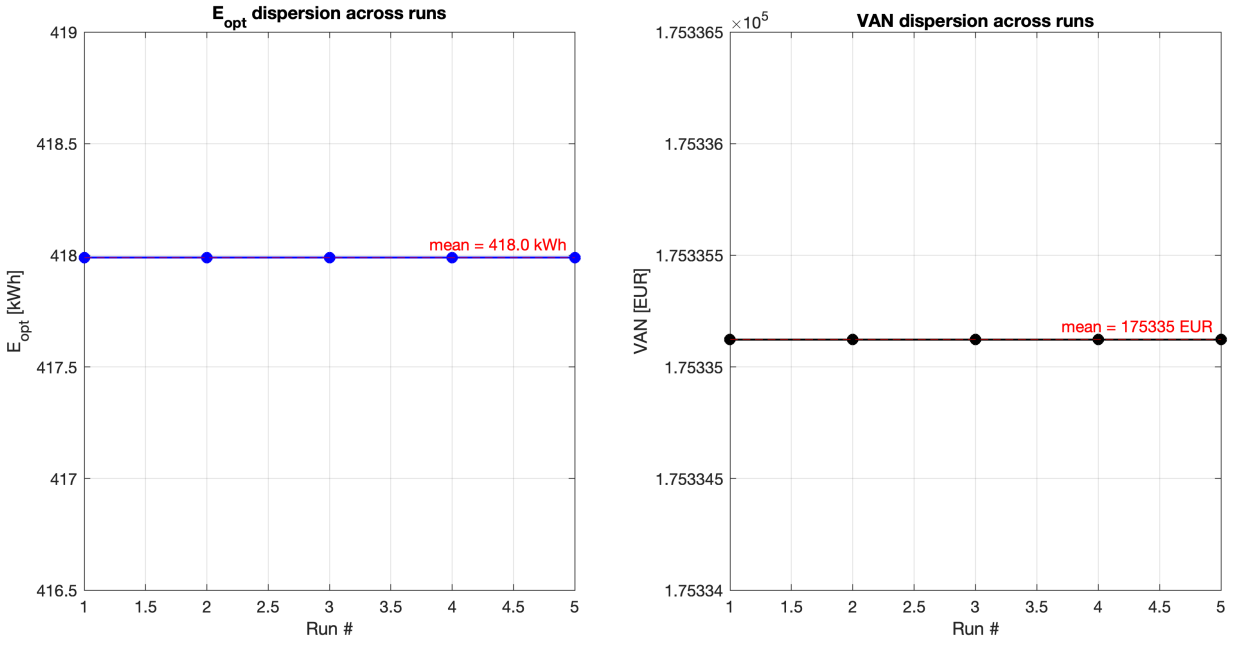


Figure 9.23: Scenario 3, dispersion of the PSO optimum across five independent runs with different random seeds, for the single-objective (private VAN) formulation. Both the optimal BESS size E_{opt} and the corresponding VAN are identical across runs (coefficient of variation 0,00%), confirming convergence to the global optimum.

A validation grid sweep over the full search range (Figure 9.24) confirms this is a genuine global optimum rather than a local one, with VAN decreasing monotonically as E_{nom} increases: even the current 2-module configuration (VAN = EUR 27127) is already oversized relative to the pure investor optimum, by a VAN gap of EUR 148208 (546,3%). This reflects the fact that only 25% of incentive revenue accrues to the investor while 100% of the additional capital cost does, so private profitability decreases monotonically with battery size across the explored range.

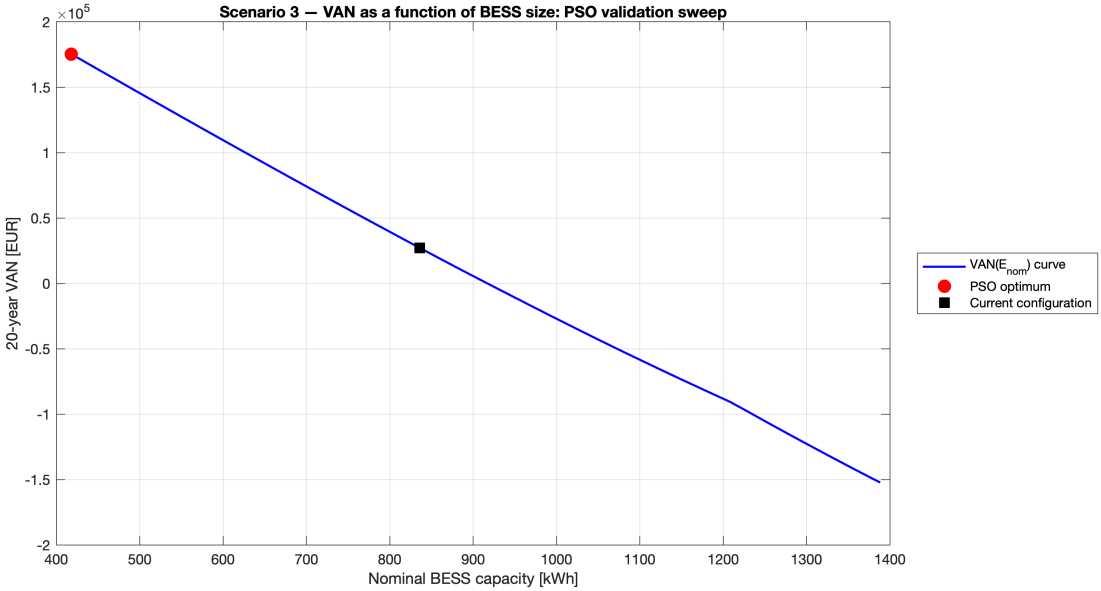


Figure 9.24: Scenario 3, 20-year VAN as a function of nominal BESS capacity, obtained by an independent grid sweep of the search space. The PSO optimum coincides with the lower bound of the search range (417,99 kWh), confirming that the VAN decreases monotonically with BESS size and that the current 2-module configuration is already oversized relative to the private investor optimum.

Multi-Objective Optimization: VAN vs. System Benefit. To capture the trade-off between private profitability and REC-wide value, a weighted-sum formulation was solved,

$$\max_{E_{nom}} \ \alpha \cdot \mathrm{VAN}_{ann}(E_{nom}) + (1-\alpha) \cdot B_{ann}(E_{nom}), \qquad \alpha \in [0{,}1], \tag{9.1}$$

where VAN_{ann} is the 20-year VAN annualized via the Capital Recovery Factor ($CRF = i(1+i)^n/[(1+i)^n - 1] = 0{,}07358$ for $i = 4\%$, $n = 20$ years) and B_{ann} is the gross annual REC-wide benefit (100% of Tariffa Premio, ARERA, RID and bill savings, net of OPEX and the annualized BESS capital cost). A coarse sweep over $\alpha \in \{0; 0{,}25; 0{,}50; 0{,}75; 1\}$ (Table 9.2, Figures 9.25 and 9.26) again collapses onto the two bounds of the search space: $\alpha \leq 0{,}50$ selects the upper bound (1388,42 kWh, VAN = −EUR 152315, B_{ann} = EUR 480502/year), while $\alpha \geq 0{,}75$ selects the lower bound (417,99 kWh, VAN = EUR 175335, discounted payback period 13,24 years, B_{ann} = EUR 432588/year). This bang-bang pattern reflects a scale mismatch between the two objectives, since VAN_{ann} is of order 10^4 EUR/year while B_{ann} is of order 10^5 EUR/year: for the weights sampled here, one term numerically dominates the sum almost everywhere, and only a narrow band of α, resolved by the refinement below, offsets this imbalance.

Since $\mathrm{VAN}_{ann}(E_{nom})$ and $B_{ann}(E_{nom})$ move monotonically in opposite directions over the entire search range, every explored capacity is Pareto-efficient: no feasible resizing improves one objective without worsening the other, so the weighted-sum sweep explores the frontier itself rather than a larger set that would first need to be filtered for dominance. The weighted objective itself, plotted against BESS size for each sampled α (Figure 9.27), is monotonic over the search range for every value except $\alpha = 0{,}50$, whose visibly non-monotonic shape anticipates the interior optimum isolated by the finer sweep below.

A refinement of the sweep within the transition interval $\alpha \in [0{,}50; 0{,}75]$, using 41 equally spaced points, locates a narrow interior band, $\alpha \in [0{,}6375; 0{,}6687]$, with E_{opt} ranging between 1207,49 and 1223,94 kWh (Figure 9.28). The step-wise appearance of E_{opt} within this band reflects the resolution of the sixty-point capacity grid reused for the refinement, rather than any instability in the underlying trade-off, as confirmed by the finer-resolution simulation used to locate the knee point below.

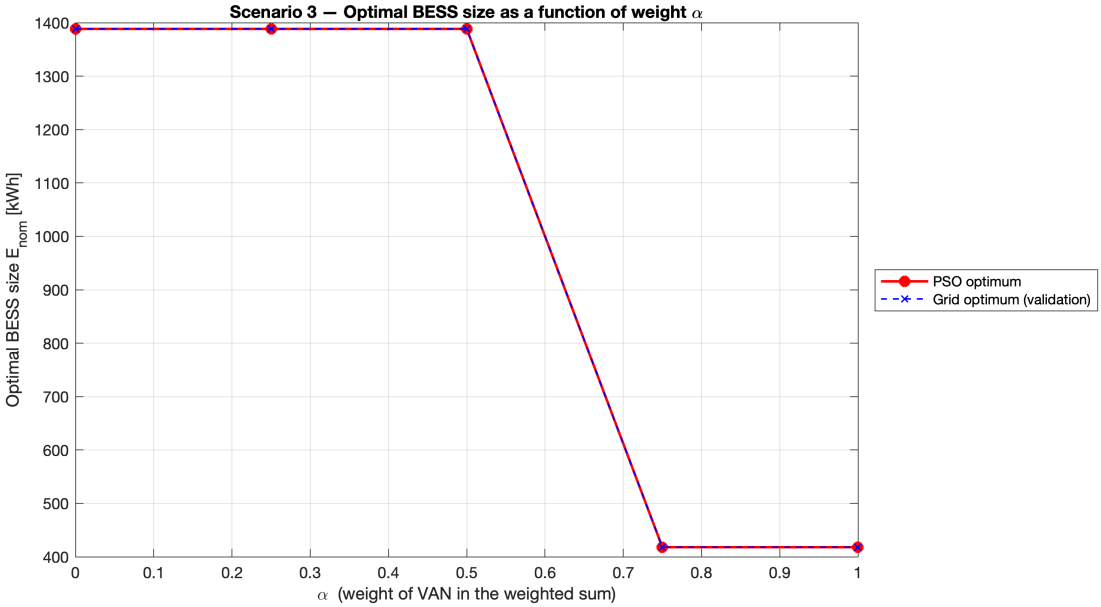


Figure 9.25: Scenario 3, optimal BESS size as a function of the weighting parameter α in the weighted-sum objective of Eq. 9.1. The optimum collapses onto the upper bound of the search space for $\alpha \leq 0{,}50$ and onto the lower bound for $\alpha \geq 0{,}75$, with the PSO result matching the independent grid-search validation at every sampled α.

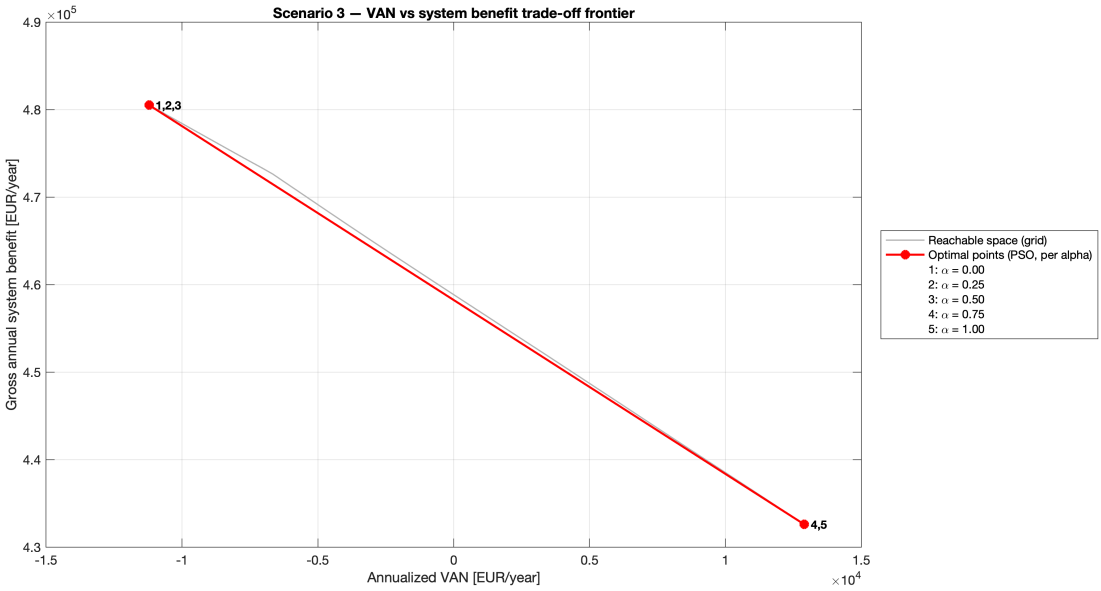


Figure 9.26: Scenario 3, trade-off frontier between annualized private VAN and gross annual REC-wide benefit. Numbered markers correspond to the five sampled values of α (1: $\alpha = 0{,}00$, 2: $\alpha = 0{,}25$, 3: $\alpha = 0{,}50$, 4: $\alpha = 0{,}75$, 5: $\alpha = 1{,}00$); markers sharing the same position indicate coincident optimal solutions.

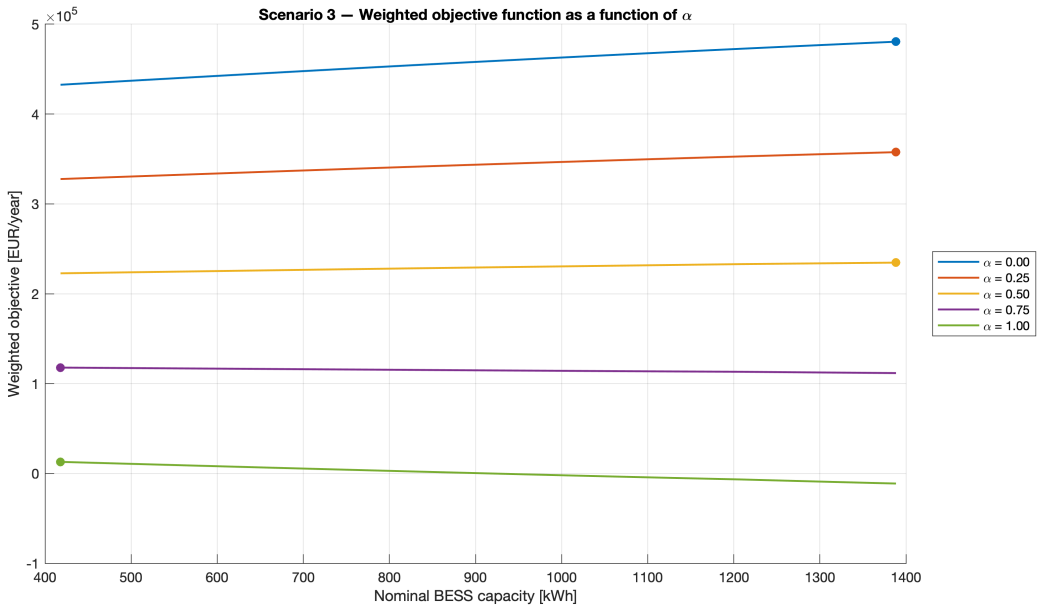


Figure 9.27: Scenario 3, weighted objective function (Eq. 9.1) as a function of BESS size, plotted for each sampled value of α. The marker on each curve denotes its grid-search maximum; only for $\alpha = 0{,}50$ does the curve remain visibly non-monotonic, foreshadowing the interior optimum identified by the finer sweep of Figure 9.28.

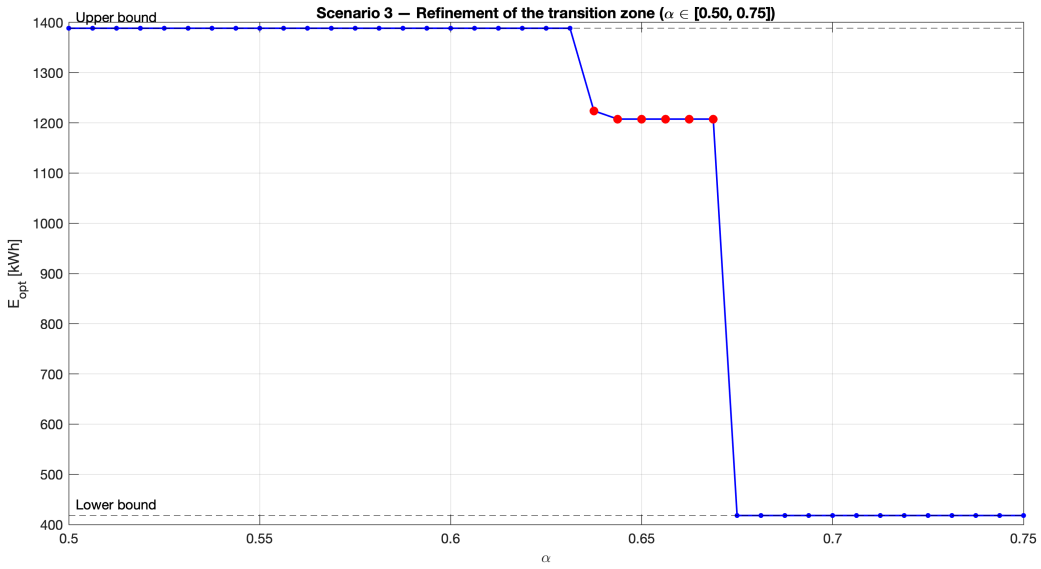


Figure 9.28: Scenario 3, refinement of the optimal BESS size over $\alpha \in [0{,}50; 0{,}75]$ (41 equally spaced points). An interior optimum, distinct from both bounds of the search space, is found for $\alpha \in [0{,}6375; 0{,}6687]$, with E_{opt} ranging between 1207,49 and 1223,94 kWh.

Table 9.2: Trade-off between annualized investor VAN and REC-wide benefit as a function of the weighting parameter α.

α	E_{opt} [kWh]	VAN (20y) [EUR]	PBT [years]	B_{ann} [EUR/year]
0,00	1388,42	−152315	–	480502
0,25	1388,42	−152315	–	480502
0,50	1388,42	−152315	–	480502
0,75	417,99	175335	13,24	432588
1,00	417,99	175335	13,24	432588

Knee-Point Selection and Discretization. Since the weighted-sum criterion still requires an arbitrary choice of α, a complementary, α-independent selection criterion was applied: the knee point of the normalized Pareto frontier, identified as the point of maximum distance from the chord connecting the two boundary solutions (Figure 9.29). This yields $E_{knee} =$ 1211,41 kWh, within 3,92 kWh of the interior window found above, and the two independent criteria therefore converge on the same compromise size, supporting the robustness of the result (Figure 9.30). At this size, the 20-year VAN is −EUR 91565 (annualized −EUR 6738/year), the discounted payback period does not fall within the 20-year horizon, and the gross annual REC-wide benefit is EUR 472786/year.

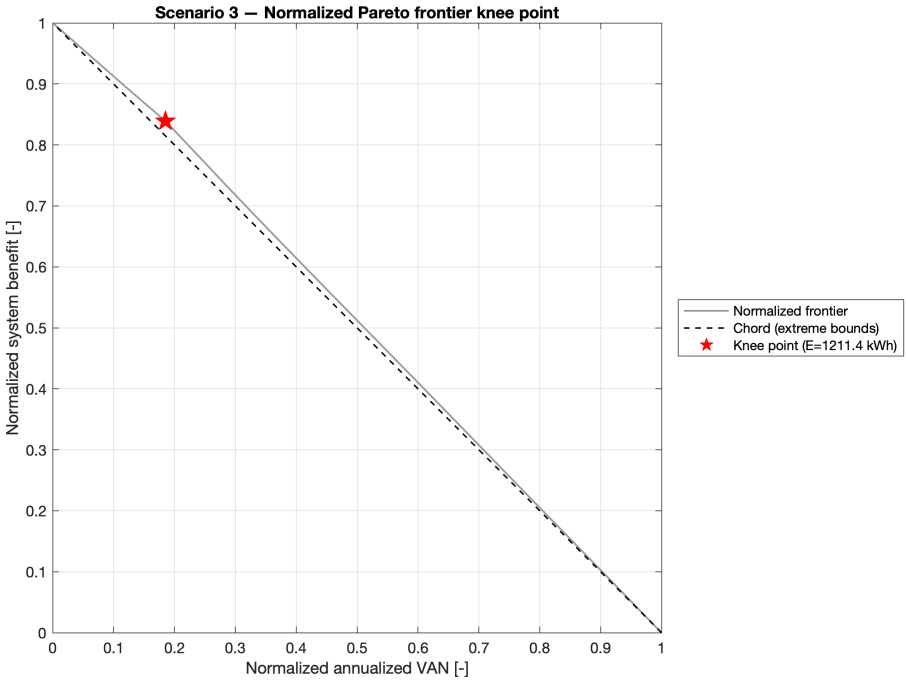


Figure 9.29: Scenario 3, normalized Pareto frontier between annualized VAN and REC-wide benefit, with the chord connecting the two boundary solutions and the knee point ($E_{knee} = 1211{,}4$ kWh) identified as the point of maximum distance from the chord.

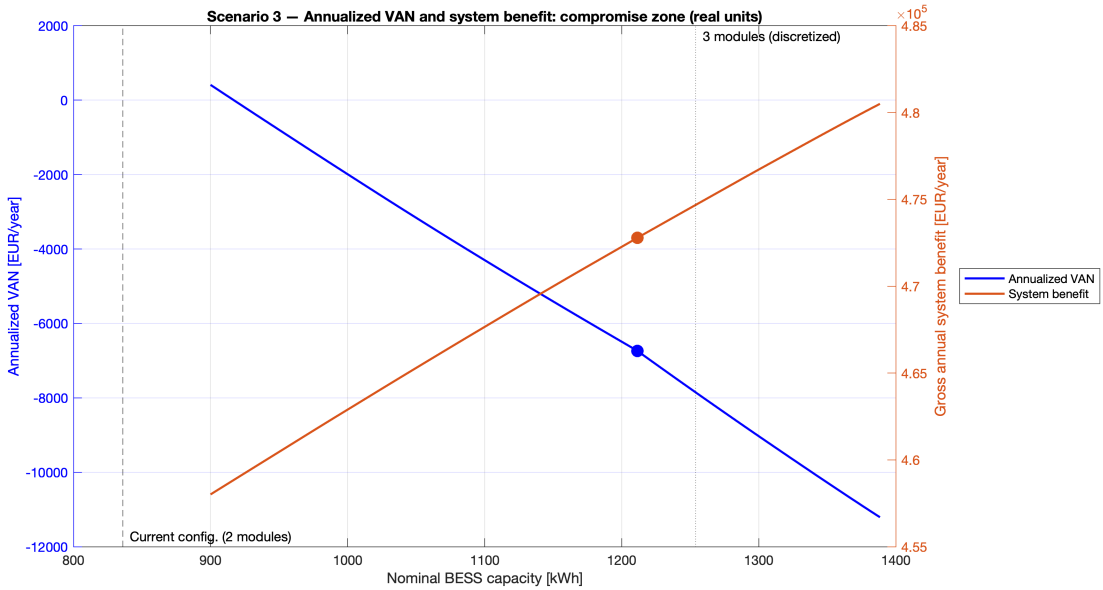


Figure 9.30: Scenario 3, annualized VAN and gross annual REC-wide benefit as a function of BESS size, in real units, over the compromise zone identified by the knee-point analysis. The current 2-module configuration and the discretized 3-module knee-point configuration are marked for reference.

Discretizing E_{knee} to the nearest integer number of commercial modules (417,99 kWh each) yields 3 modules, E_{nom} = 1253,97 kWh, a deviation of 42,56 kWh (10,2% of one module step) from the continuous knee value. Table 9.3 (Figure 9.31) compares this discretized configuration against the current 2-module installation: moving from 2 to 3 modules increases CAPEX by EUR 55000, turns the private VAN negative (from +EUR 27127, discounted payback 18,55 years, to −EUR 106717, with the discounted payback period no longer falling within the 20-year horizon), while increasing the gross REC-wide benefit by EUR 19880/year (+4,4%, from EUR 454802/year to EUR 474682/year).

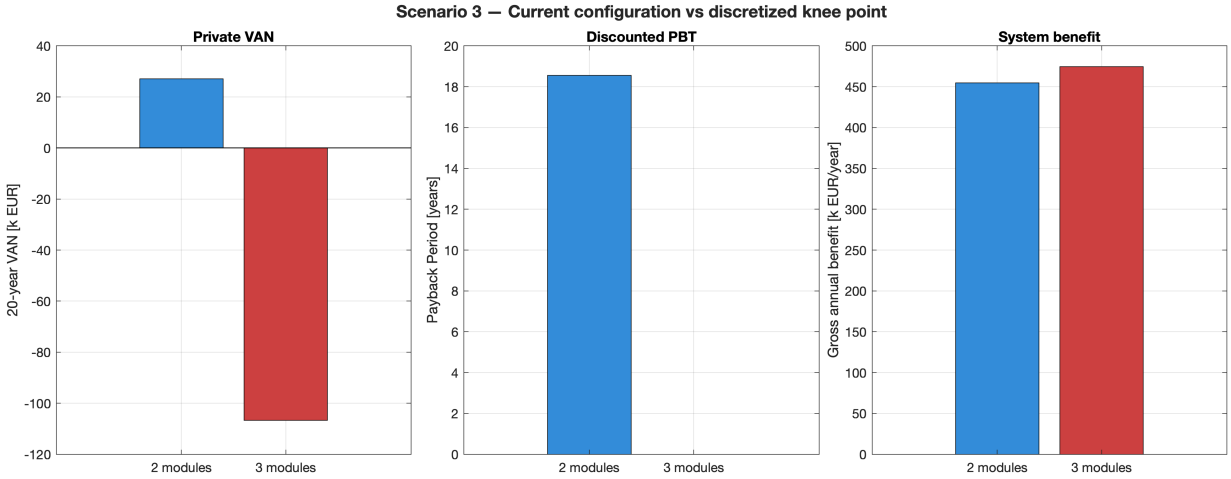


Figure 9.31: Scenario 3, comparison between the current 2-module configuration and the discretized knee-point 3-module configuration: 20-year private VAN, discounted payback period, and gross annual REC-wide benefit. No payback-period bar is shown for the 3-module configuration, as the discounted cumulative cash flow does not turn non-negative within the 20-year horizon.

Table 9.3: Current (2-module) versus discretized knee-point (3-module) BESS configuration.

Configuration	E_{nom} [kWh]	VAN (20y) [EUR]	PBT [years]	B_{ann} [EUR/year]
Current (2 modules)	835,98	27127	18,55	454802
Discretized knee (3 modules)	1253,97	−106717	–	474682

System Value Decomposition. To reconcile the negative private VAN of the 3-module configuration with its higher system-wide benefit, the transition from 2 to 3 modules is decomposed into a private and a community value component (Figure 9.32). The additional capital expenditure (EUR 55000) and the private VAN loss (EUR 133844) are more than offset by capitalizing the incremental gross REC-wide benefit (EUR 19880/year) at the same discount rate and horizon via $1/CRF \approx 13{,}59$: a present value of EUR 270170. Summing the private VAN change and this present value gives a positive total system value of EUR 136326, indicating that the 3-module upgrade redistributes value from the investor toward the REC membership rather than destroying it in aggregate. This decomposition mixes two different accounting bases, an after-tax private cash-flow basis for the VAN term and a gross, REC-wide basis for the community-benefit term not net of the taxation borne by the investor on the incentive share it retains, and is presented here as a system-level indicator rather than as a cash flow accruing to any single economic subject.

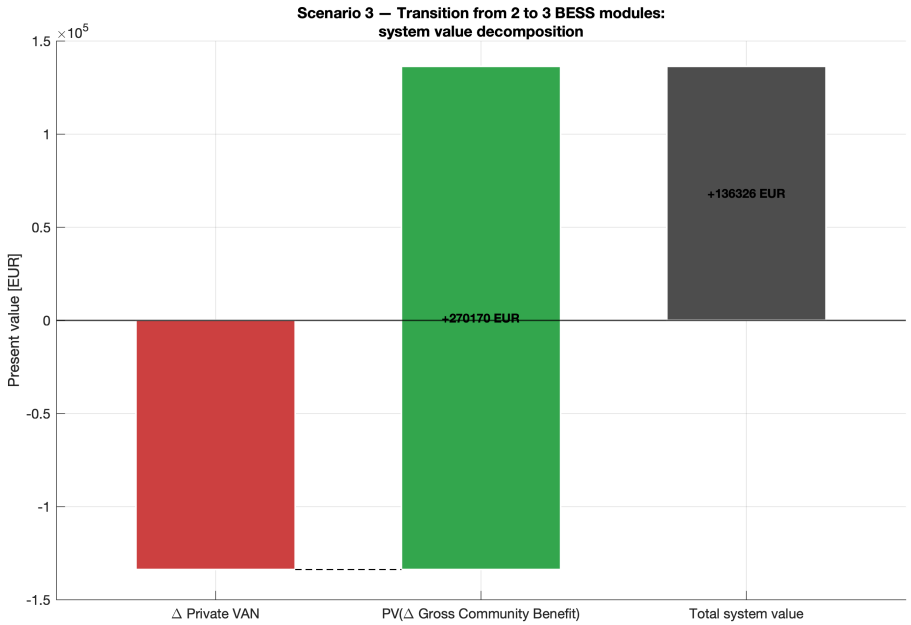


Figure 9.32: Scenario 3, decomposition of the total system value associated with the transition from 2 to 3 BESS modules, into the change in private investor VAN and the present value of the incremental gross REC-wide benefit, capitalized at the same discount rate and horizon via $1/CRF$.

Implications for the Cross-Scenario Comparison. Neither the continuous knee-point size nor its 3-module discretization is carried forward as the reference Scenario 3 configuration for the economic comparison presented in the following chapter. At both sizes the 20-year private VAN remains negative, EUR −91565 at the continuous knee and EUR −106717 once discretized to 3 modules, and in neither case does the discounted payback period fall within the 20-year analysis horizon: the additional capital committed to the third module is not recovered by the investor over the period considered, even though the gross REC-wide benefit continues to rise. The knee-point analysis is therefore retained as a diagnostic tool, useful for quantifying how far private profitability and community value diverge as BESS size increases beyond the investor optimum, rather than as a sizing criterion adopted in practice. The current 2-module configuration, with a positive 20-year VAN of EUR 27127 and a discounted payback period of 18,55 years, remains the reference case used for Scenario 3 throughout the rest of this work.

9.4 Scenario 4

Scenario 4 adds a 100 kW PEM electrolyzer (Rubri-PI-0020) downstream of the BESS analyzed in Scenario 3, converting residual PV surplus into green hydrogen after battery charging.

The underlying hourly PV production (1591,3 MWh/year) and REC consumption (3386,8 MWh/year) profiles are, once again, identical to Scenario 1 and Scenario 3. Figure 9.33 therefore reproduces the same pattern already presented for the two previous scenarios.

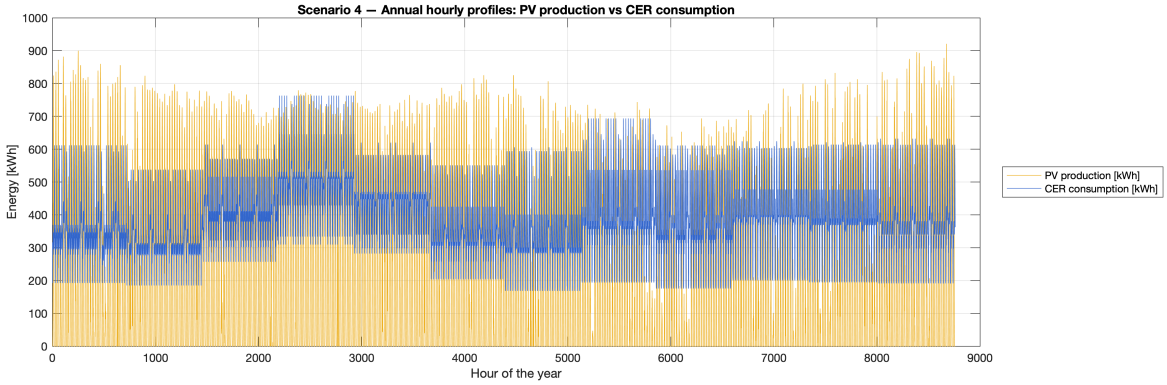


Figure 9.33: Scenario 4, hourly PV production and aggregate REC consumption over the reference year (April 2025–March 2026). This profile pair is, by construction, identical to Scenario 1 and Scenario 3.

Battery operation is unaffected by the addition of the electrolyzer: charging (217,1 MWh), discharging (203,0 MWh), losses (14,3 MWh) and equivalent cycles (324,6) match Scenario 3 exactly, since the BESS retains absolute dispatch priority over the electrolyzer on the PV surplus. The electrolyzer instead absorbs 147,1 MWh of the residual surplus, corresponding exactly to the reduction in RID-exported surplus relative to Scenario 3 (from 289,7 to 142,6 MWh), producing 2874,5 kg of hydrogen (31981,0 Nm^3) over 1430 hours of operation, a 16,3% capacity factor.

Figure 9.34 shows the resulting hourly allocation of PV production and REC consumption coverage over the year. The top two panels confirm the dispatch hierarchy at annual resolution: PV surplus is absorbed first by the BESS and only the residual reaches the electrolyzer, visible as a comparatively thin red band beneath the direct self-consumption and BESS charging layers, while REC consumption is covered predominantly by direct PV supply and BESS discharge, with grid purchase filling the residual gap year-round. The BESS power flow panel shows charging and discharging both saturating at the 250 kW AC limit on most days, consistent with the 324,6 equivalent annual cycles already discussed. The electrolyzer power panel shows a markedly more irregular pattern than the BESS: dense clusters of operation at or near the 120 kW ceiling in spring, summer and early autumn, against long stretches of complete inactivity in the winter months once daily surplus falls below the 20 kW start-up threshold, mirroring the seasonal PV availability already seen in the annual profile. The bottom panel confirms that the Feed-in Premium Tariff TiP tracks the inverse of the zonal price P_z as designed, remaining close to its 100 EUR/MWh cap whenever P_z drops well below the 180 EUR/MWh reference and narrowing toward zero as P_z approaches or exceeds it.

The electrolyzer power duration curve (Figure 9.35) shows it running near its 120 kW maximum for roughly the first 950 hours of operation, then ramping down smoothly toward the 20 kW minimum threshold as available post-BESS surplus diminishes, consistent with the seasonal PV pattern already discussed for the earlier scenarios.

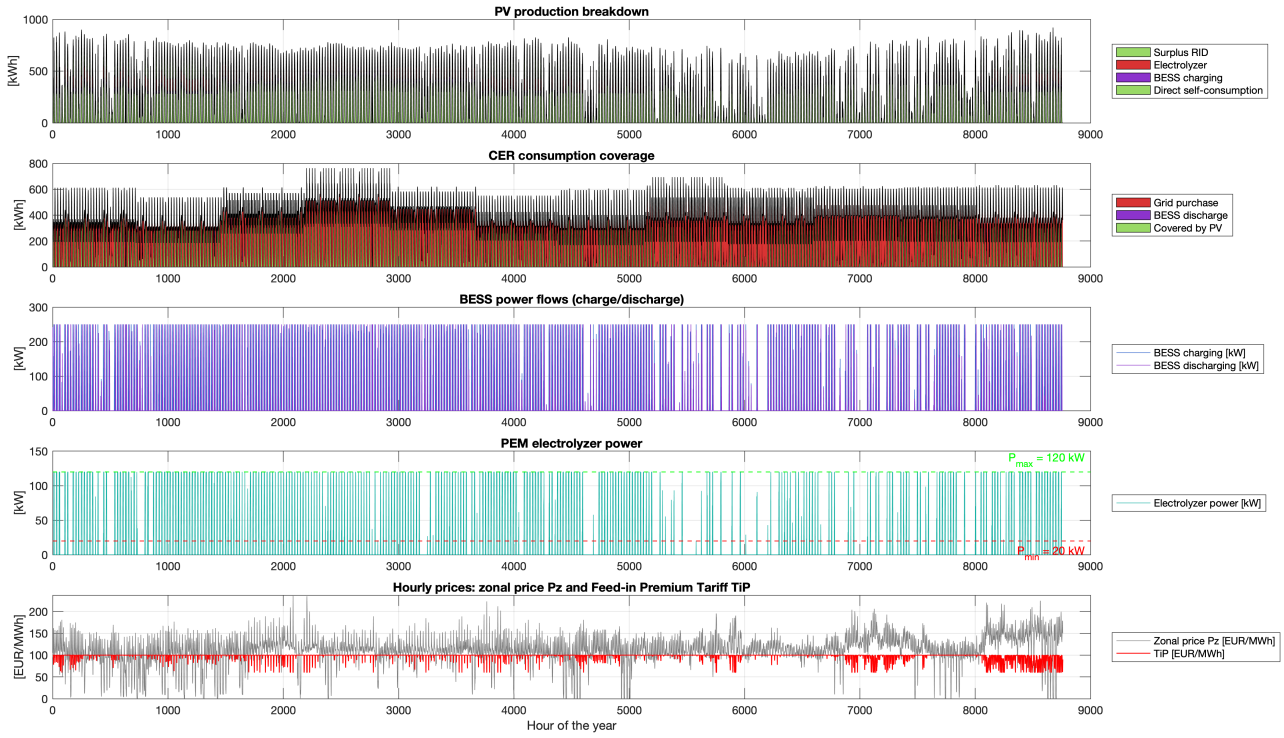


Figure 9.34: Scenario 4, hourly energy flow breakdown. From top to bottom: allocation of PV production between direct self-consumption, BESS charging, the electrolyzer and RID surplus; coverage of REC consumption by direct PV supply, BESS discharge and residual grid purchase; BESS charging/discharging power; PEM electrolyzer power; and hourly zonal price P_z against the Tariffa Premio TiP.

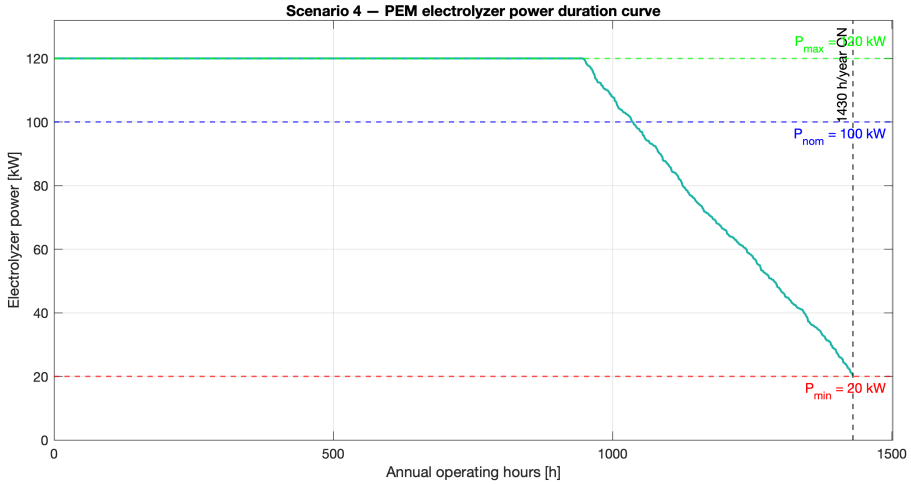


Figure 9.35: Scenario 4, PEM electrolyzer power duration curve, ranked from the highest to the lowest operating power over the 1430 annual operating hours.

Typical weekly profiles. The representative summer and winter weeks (Figures 9.36 and 9.37) show the electrolyzer engaging shortly after the BESS reaches full charge each day, running at or near its 120 kW ceiling around the PV peak and switching off once the post-BESS surplus drops below the 20 kW threshold, more frequently and for shorter windows in January than in July.

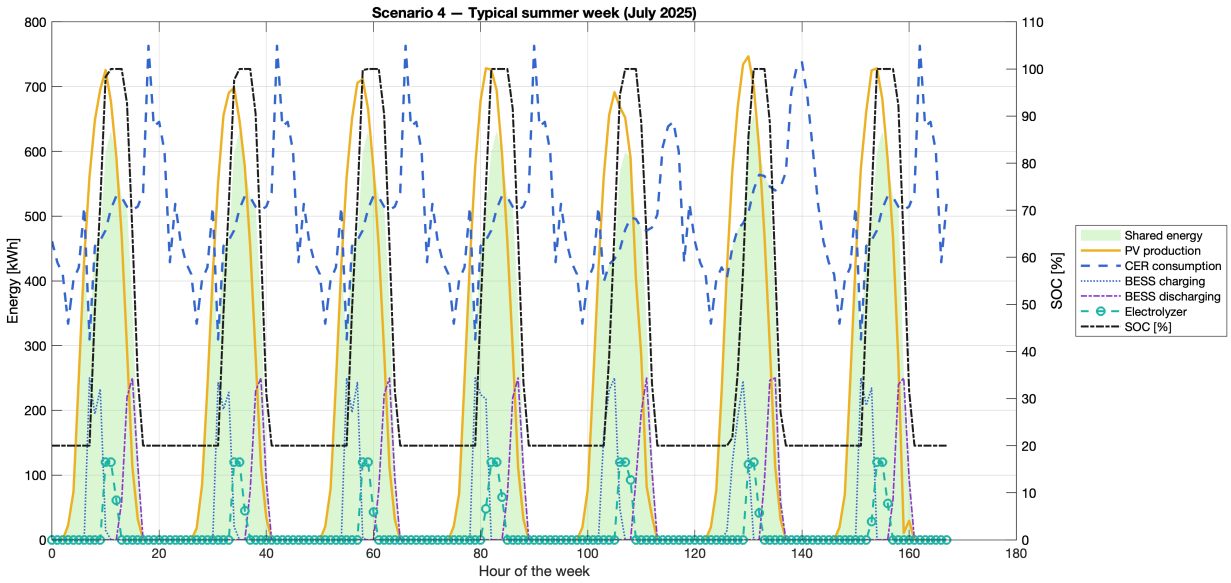


Figure 9.36: Scenario 4, representative summer week (July 2025): PV production, REC consumption, shared energy, BESS charge/discharge power, electrolyzer power and state of charge.

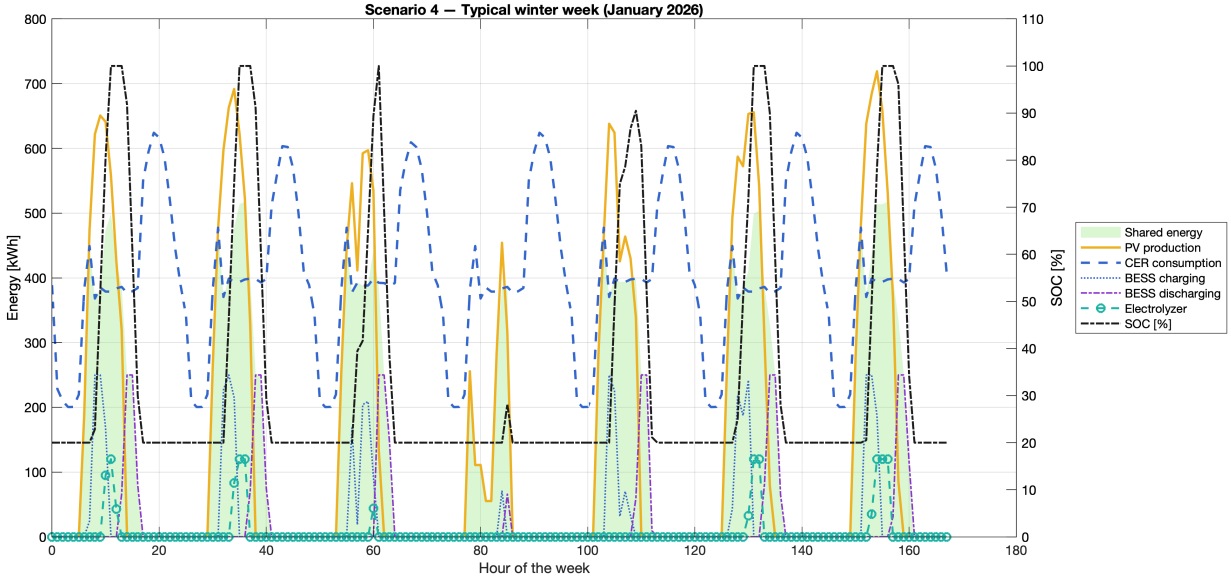


Figure 9.37: Scenario 4, representative winter week (January 2026): PV production, REC consumption, shared energy, BESS charge/discharge power, electrolyzer power and state of charge.

By diverting surplus that would otherwise be exported at the zonal price, the electrolyzer raises the Self-Consumption Index (IAC) to 91,0%, up from 81,8% in Scenario 3, while the Self-Sufficiency Index (IAS) remains unchanged at 38,0%, since the electrolyzer is an additional load rather than a source covering REC demand. The shared-to-injected energy ratio also rises, to 90,2%, further above the 55% CACER Decree threshold already discussed for the previous scenarios. The annual state-of-charge trajectory (Figure 9.38) confirms that battery cycling is unchanged from Scenario 3, since the electrolyzer only draws on the surplus remaining after the BESS has already been charged to its target level.

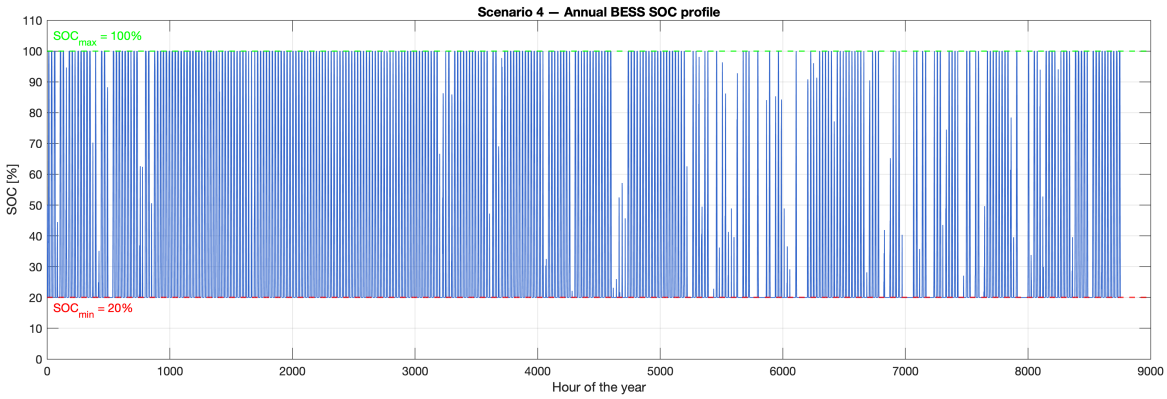


Figure 9.38: Scenario 4, annual state-of-charge trajectory of the BESS, bounded between $SOC_{min} = 20\%$ and $SOC_{max} = 100\%$.

Economic Performance On the economic side (Figure 9.39), the REC generates EUR 141708/year in Tariffa Premio revenue, EUR 13629/year in ARERA compensation, EUR 13306/year from RID sales of the residual surplus, and EUR 17247/year in hydrogen sales, at the assumed price of 6,0 EUR/kg, against a residual grid-purchase cost of EUR 497451/year. Bill savings remain EUR 339365/year, unchanged from Scenario 3, since they depend only on the self-consumed and stored share of the load, which the electrolyzer does not alter. Both TiP and ARERA revenue rise relative to Scenario 3 (from EUR 127243 and EUR 12231, respectively), reflecting the larger shared-energy base, while RID revenue falls (from EUR 27798), as part of the surplus previously exported is now converted to hydrogen.

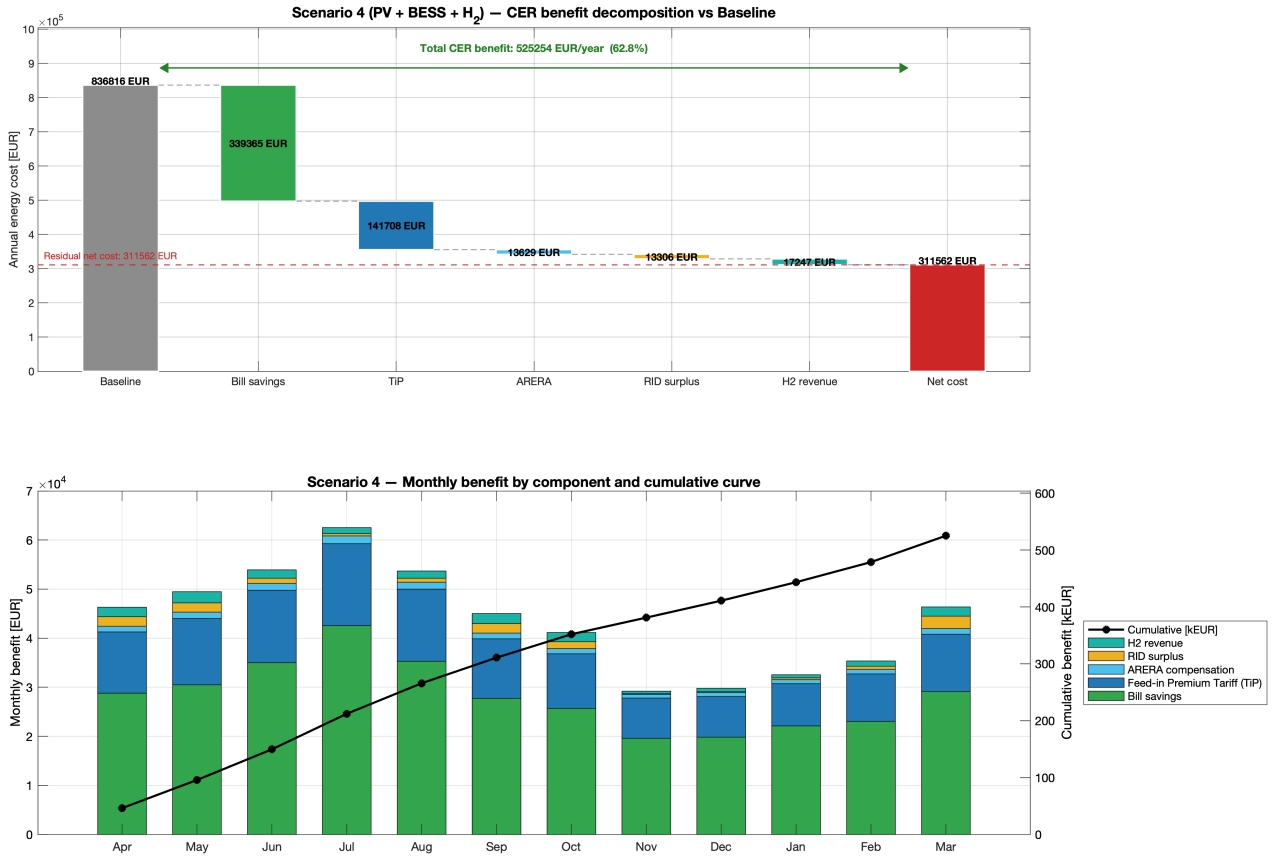


Figure 9.39: Scenario 4, comparison against the no-PV, no-storage baseline. Top: waterfall decomposition of the annual energy cost, from the baseline cost (EUR 836816/year) through bill savings, Tariffa Premio, ARERA compensation, RID revenue and hydrogen revenue, down to the residual net cost (EUR 311562/year), for a total benefit of EUR 525254/year (62,8%). Bottom: monthly benefit by component with cumulative annual benefit.

Relative to the no-PV, no-storage baseline (EUR 836816/year), this amounts to a total annual benefit of EUR 525254/year, a 62,8% reduction in energy cost, up from the 60,5%

obtained in Scenario 3. The monthly decomposition (Figure 9.40) again shows bill savings as the dominant component, peaking in July, while hydrogen revenue peaks in May and September, when PV surplus is ample but ambient demand for direct self-consumption is comparatively lower.

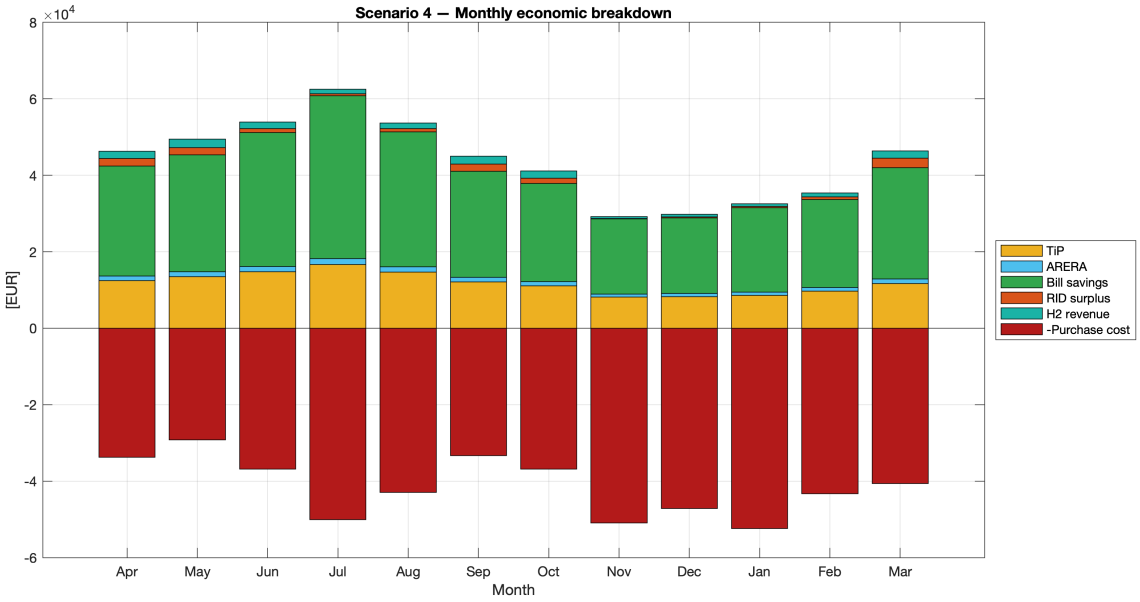


Figure 9.40: Scenario 4, monthly breakdown of revenue components (Tariffa Premio, ARERA compensation, bill savings, RID surplus, hydrogen revenue) against the residual grid purchase cost.

The monthly hydrogen production and revenue profile (Figure 9.41) mirrors the electrolyzer's seasonal operating pattern, ranging from 2874,5 kg/year overall down to under 100 kg in the lowest winter months, with a corresponding revenue swing between roughly EUR 540 and EUR 2290 per month.

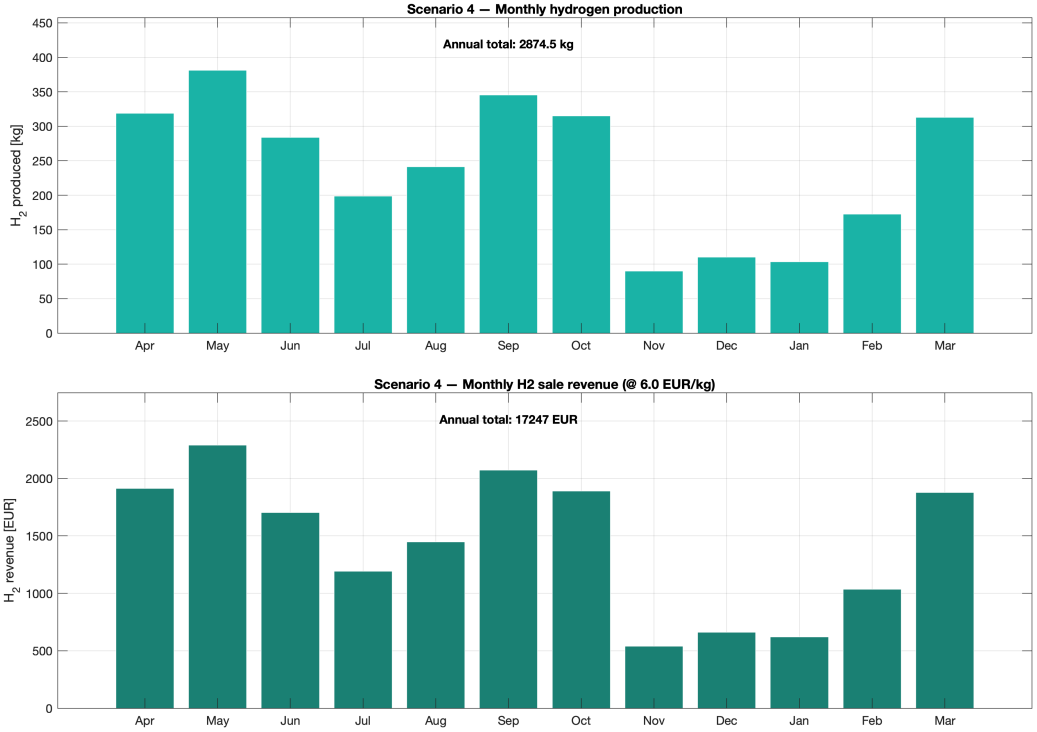


Figure 9.41: Scenario 4, monthly hydrogen production (top) and corresponding sale revenue (bottom, at the assumed price of 6,0 EUR/kg).

Environmental Impact Using the ISPRA 2025 grid emission factor for reference year 2023 (0,216 $kgCO_2/kWh$), the electricity component of avoided emissions ranges between 278,1 tCO_2/year (lower bound, on shared energy) and 343,7 tCO_2/year (upper bound, on total PV production), both unchanged from Scenario 3. Using the CertifHy grey-hydrogen comparator (10,92 $kgCO_2/kgH_2$), the hydrogen produced avoids a further 31,4 tCO_2/year relative to fossil-based hydrogen, bringing the total avoided emissions to 309,5 tCO_2/year.

9.5 Comparative financial analysis of the scenarios

Once the energy flows have been characterized and the annual revenues associated with each plant configuration determined, the energy assessment must be complemented by a strictly economic and financial analysis, aimed at verifying its sustainability over time and its convenience with respect to the invested capital. For this purpose, the Discounted Cash Flow (DCF) methodology is adopted, a tool that makes it possible to compare scenarios characterized by different initial outlays and different economic return profiles, by bringing future cash flows back to an equivalent present value and thereby accounting for the time value of money. The time horizon chosen for the comparison is 20 years, consistent with the duration of the incentive period recognized for Renewable Energy Communities; over this time span, the aim is to identify, among the four configurations examined, the one offering the best trade off between investment efficiency and overall profitability.

9.5.1 Methodology and analysis parameters

For each scenario, a cash flow model was built, based on the following parameters and assumptions.

- **Capital expenditure (CAPEX)**: represents the total turnkey cost for the realization of the plant. It was calculated starting from a reference price list, reported in tabular form for each scenario.

- **Operating and maintenance expenditure (OPEX)**: represents the annual costs required to guarantee the efficiency and correct operation of the system, including maintenance, insurance and administrative management. It was estimated as a fixed percentage, equal to 1,5%, of the total CAPEX of each scenario.

- **Annual revenues (R_t)**: unlike the gross total revenue calculated in the previous sections, for the purposes of this specific bankability analysis the cash inflow considered is the revenue deriving from the sale of energy fed into the grid through the Dedicated Withdrawal scheme (Ritiro Dedicato, RID), supplemented by a share equal to 25% of the incentives generated by the REC, namely the Premium Tariff (TiP) and the ARERA compensation. It is in fact assumed that the remaining 75% of the incentives on shared energy does not contribute to the amortisation of the investment, since it is intended for redistribution among the members of the community. For simplicity, RID revenues are assumed to remain constant throughout the analysis.

- **Analysis duration (N)**: fixed at 20 years, in line with the incentive period provided for by the CACER Decree.

- **Discount rate (i)**: fixed at 4%, representing the opportunity cost of capital used to discount future cash flows to their present value.

- **Annual depreciation rate (Dep. Rate)**: for tax purposes, the CAPEX of each scenario was depreciated on a straight line basis over a period (Dep. time) of 15 years, according to the relation

$$\text{Dep. Rate} = \frac{\text{CAPEX}}{\text{Dep. time}} \tag{9.2}$$

  The resulting quota is subtracted from the taxable base only for years $n \leq 15$; for $n > 15$ taxes are computed directly on the difference $(R_t - \text{OPEX}_n)$. It should be noted that the depreciation rate, although it reduces the tax due, does not represent an actual cash outflow, since it is a non cash cost, given that the CAPEX has already been fully discounted at year $n = 0$.

- **Tax rate (t)**: fixed at 24%, corresponding to the IRES rate currently in force for capital companies in Italy. Annual taxes are computed as

$$t \cdot (R_t - \text{OPEX}_n - \text{Dep. Rate}_n) \tag{9.3}$$

  whenever this term is positive; if it turns out to be negative, no taxes are applied.

Once the parameters have been defined, the methodology for computing the cumulated cash flow starts from the overall annual cost Cost_n, which takes a different form in the construction year compared with the operating years:

$$\text{Cost}_n = \begin{cases} \text{CAPEX} & n = 0 \\ \text{OPEX}_n & n = 1, \dots, N \end{cases} \tag{9.4}$$

where for $n = 0$ neither revenues ($R_0 = 0$) nor taxes are accounted for, since the entire first year is assumed to be dedicated to plant realisation, with no energy production yet taking place. The discounted cumulated cash flow, used to determine the Payback Time (PBT) and the Net Present Value (NPV), is therefore computed as the progressive sum of discounted cash flows from year 0 to year n:

$$\text{Cumulated cash flow}_n = \sum_{k=0}^{n} \frac{R_k - \text{Cost}_k - \text{taxes}_k}{(1+i)^k} \tag{9.5}$$

which, splitting the two branches explicitly, is equivalent to:

$$\text{Cumulated cash flow}_n = -\frac{\text{CAPEX}}{(1+i)^0} + \sum_{k=1}^{n} \frac{R_k - \text{OPEX}_k - \text{taxes}_k}{(1+i)^k} \tag{9.6}$$

The year in which this quantity first becomes positive identifies the Payback Time of the investment, while its value at year $n = N = 20$ coincides with the NPV of the scenario. It is worth stressing that the revenues considered here, being limited to RID and to a single share of the REC incentives, return the profitability perspective of the investor, which is distinct from, and generally more conservative than, the overall economic benefit generated by the energy community as a whole. This latter aspect is addressed separately in the final comparison, through the bill savings and distributed dividends indicators.

9.5.2 Scenario S1

Scenario S1 represents the baseline configuration, consisting solely of the 1 MWp ground mounted photovoltaic plant, without demand response strategies or storage systems. Table 9.4 summarizes the composition of CAPEX, annual OPEX and the revenues considered for the analysis.

Table 9.4: Composition of CAPEX, OPEX and revenues for scenario S1

Item	**Value [€]**	**Item**	**Value [€]**
PV panels	207792,00	Engineering and site management	4995,00
Fixed structure	34965,00	Project management	1998,00
DC cables	6993,00	Transport	4995,00
Electrical installation	9990,00	Commissioning	999,00
Mechanical installation	27972,00	Authorizations	69930,00
Inverter	56000,00	Legal costs	4995,00
Electrical panels	7700,00	Design costs	20000,00
AC cables	7700,00	Administrative costs	5000,00
LV/MV transformation	7700,00	Works supervision	25000,00
Civil works	19980,00		
Total CAPEX ($n = 0$)			**524704,00**
Annual OPEX (1,5% of CAPEX)			7870,56
RID			54153,00
Share of TiP + ARERA (25%)			29336,75
Total annual revenue			**83489,75**

Figure 9.42 shows the discounted cumulated cash flow over the 20 year horizon. The curve starts at −524704,00 €, corresponding to the initial CAPEX, and grows steadily thanks to an annual net cash flow that remains well above the operating cost throughout the whole period, since the revenue of 83489,75 € per year is more than ten times the OPEX. The curve crosses the zero axis between year 9 and year 10, giving a discounted Payback Time of 9,79 years, the shortest among the four scenarios. The NPV at year 20 reaches 349681,79 €, and the Internal Rate of Return is 10,80%, well above the 4% discount rate, confirming a solid margin of profitability. These results are consistent with the fact that S1 is the configuration with the lowest CAPEX and, at the same time, the one for which the largest share of energy is exported and remunerated through RID rather than redistributed within the community, which maximizes the portion of revenue actually available for the investor's amortization.

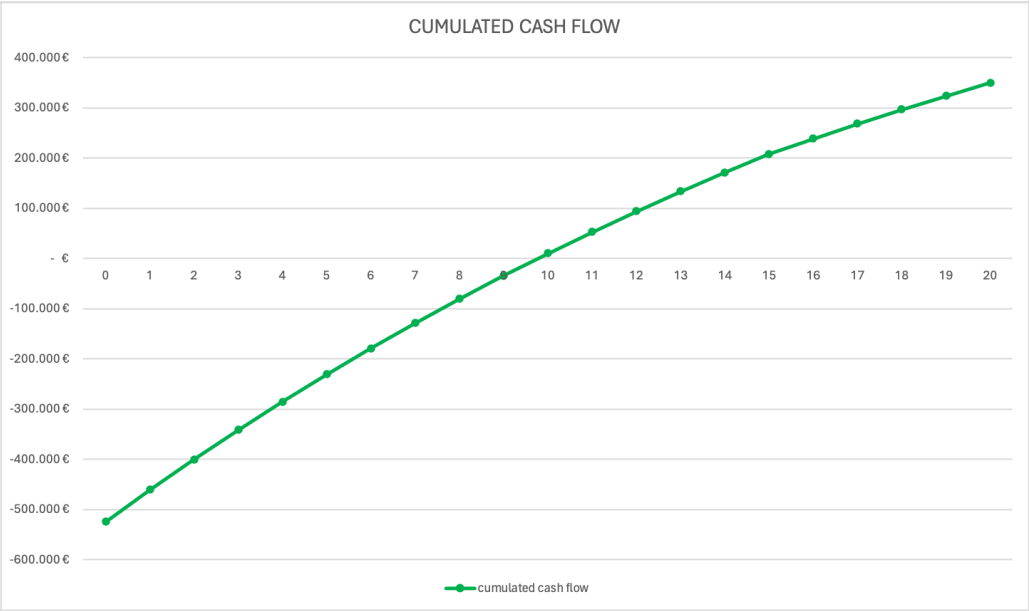


Figure 9.42: Discounted cumulated cash flow, scenario S1

9.5.3 Scenario S2

Scenario S2 adds a rule based demand response strategy on the residential load to the same photovoltaic plant considered in S1, without any additional capital investment, since load shifting only requires a management logic and not new hardware. The CAPEX and OPEX therefore remain identical to those of S1, as shown in Table 9.5, while the revenue structure changes, since a larger share of energy is now self consumed and shared within the community rather than exported.

As Figure 9.43 shows, the cumulated cash flow curve starts from the same initial value as S1, but its slope is visibly lower, a direct consequence of the reduced annual revenue, which drops from 83489,75 € to 68769,50 €. This decrease is not a loss of value in absolute terms, since the share of TiP and ARERA compensation actually increases, from 29336,75 € to 34108,50 €, reflecting the higher share of shared energy generated by the load shifting strategy; however, the RID component falls sharply, from 54153,00 € to 34661,00 €, and this component alone determines the revenue booked for the investor's amortization. The net effect is a longer Payback Time, equal to 12,35 years, an NPV of 197641,51 €, and an IRR of 8,04%. The comparison with S1 already highlights the central tension of this analysis, an increase in the volume of shared energy raises the value delivered to the community, but does not necessarily improve the return of the initial investment, since a decreasing share of that value is captured through RID.

Table 9.5: Composition of CAPEX, OPEX and revenues for scenario S2

Item	**Value [€]**	**Item**	**Value [€]**
PV panels	207792,00	Engineering and site management	4995,00
Fixed structure	34965,00	Project management	1998,00
DC cables	6993,00	Transport	4995,00
Electrical installation	9990,00	Commissioning	999,00
Mechanical installation	27972,00	Authorizations	69930,00
Inverter	56000,00	Legal costs	4995,00
Electrical panels	7700,00	Design costs	20000,00
AC cables	7700,00	Administrative costs	5000,00
LV/MV transformation	7700,00	Works supervision	25000,00
Civil works	19980,00		
Total CAPEX ($n = 0$)			**524704,00**
Annual OPEX (1,5% of CAPEX)			7870,56
RID			34661,00
Share of TiP + ARERA (25%)			34108,50
Total annual revenue			**68769,50**

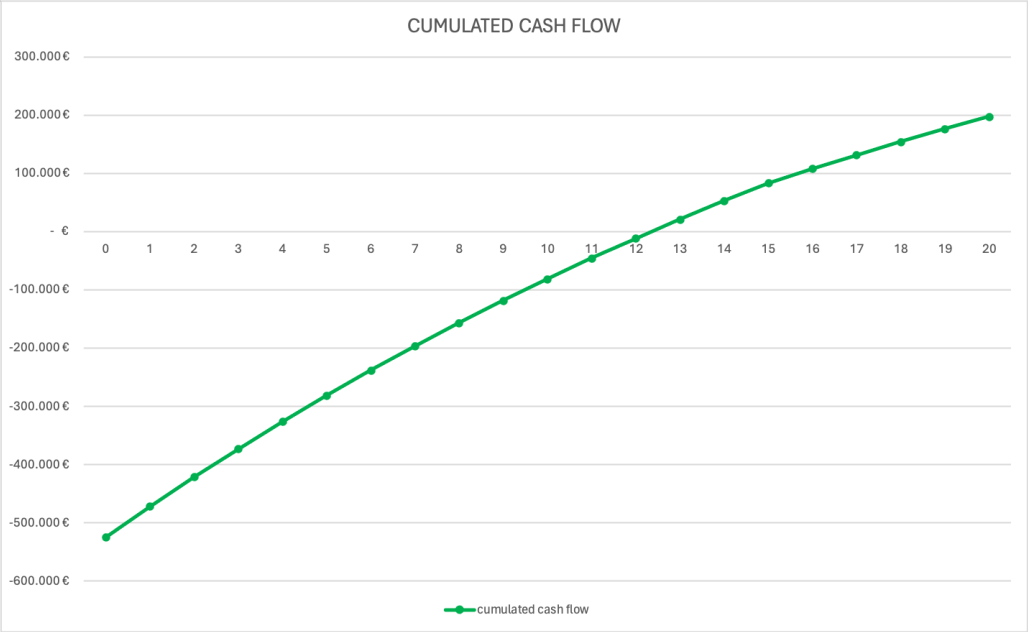


Figure 9.43: Discounted cumulated cash flow, scenario S2

9.5.4 Scenario S3

Scenario S3 introduces a battery energy storage system (BESS, model GSL-BESS-125K418, two modules, 835,98 kWh nominal capacity, 250 kW AC) in addition to the photovoltaic plant. The CAPEX increases by 110000,00 € compared with S1 and S2, reaching a total of 634704,00 €, and the annual OPEX increases proportionally, since it is computed as 1,5% of the new total CAPEX. Table 9.6 reports the full breakdown.

Table 9.6: Composition of CAPEX, OPEX and revenues for scenario S3

Item	**Value [€]**	**Item**	**Value [€]**
PV panels	207792,00	Transport	4995,00
Fixed structure	34965,00	Commissioning	999,00
DC cables	6993,00	Authorizations	69930,00
Electrical installation	9990,00	Legal costs	4995,00
Mechanical installation	27972,00	Design costs	20000,00
Inverter	56000,00	Administrative costs	5000,00
Electrical panels	7700,00	Works supervision	25000,00
AC cables	7700,00	BESS	110000,00
LV/MV transformation	7700,00		
Civil works	19980,00		
Engineering and site management	4995,00		
Project management	1998,00		
Total CAPEX ($n = 0$)			**634704,00**
Annual OPEX (1,5% of CAPEX)			9520,56
RID			27798,00
Share of TiP + ARERA (25%)			34868,50
Total annual revenue			**62666,50**

The cumulated cash flow, shown in Figure 9.44, starts from a deeper initial value than the previous two scenarios, −634704,00 €, and grows at an even shallower rate, since the annual revenue booked for amortization, 62666,50 €, is now the lowest recorded so far among the three scenarios examined up to this point. The RID component continues to fall, from 34661,00 € in S2 to 27798,00 € in S3, coherently with the fact that the battery, being AC coupled and located behind a single point of delivery, does not cross the community metering boundary

during charging, and therefore does not itself generate GSE recognized shared energy; it is the discharge phase, feeding stored energy to loads within the community, that increases the shared energy share and, with it, the TiP and ARERA component, which reaches 34868,50 €. The combined effect of a higher CAPEX and a lower amortizable revenue produces a discounted Payback Time of 18,55 years, an NPV of 27131,87 €, and an IRR of 4,50%, only half a percentage point above the discount rate itself. This is a first indication that, from the standpoint of the investor's return, the storage system alone yields a comparatively small numerical margin, this point is discussed further in the final comparison.

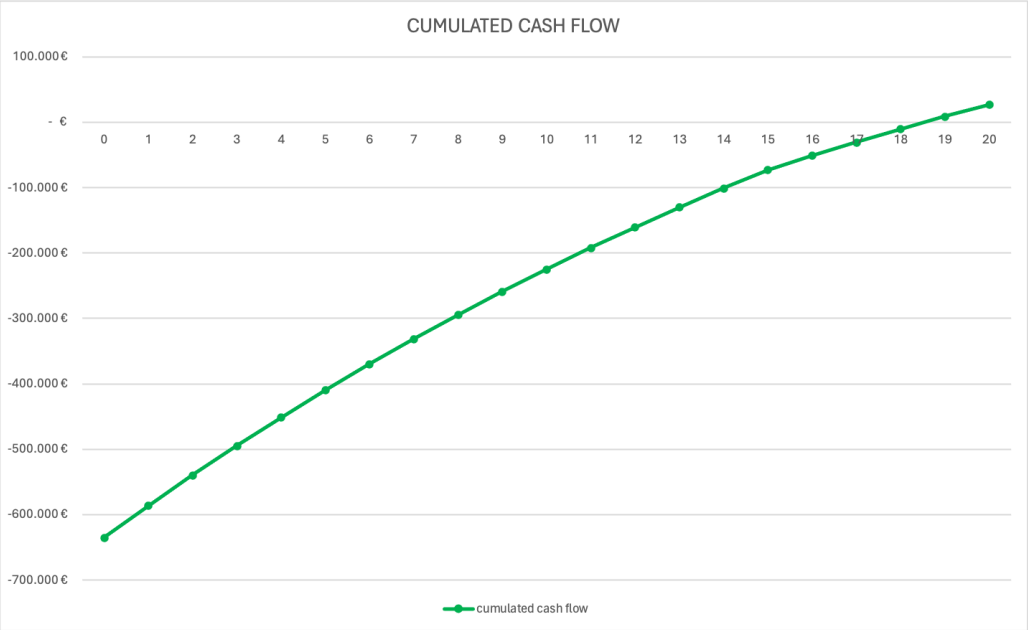


Figure 9.44: Discounted cumulated cash flow, scenario S3

9.5.5 Scenario S4

Scenario S4 represents the most complex configuration, combining the photovoltaic plant, the battery storage system already introduced in S3, and a PEM electrolyzer (model Rubri-PI-0020, 100 kW), connected as a separate point of delivery within the community and dedicated to green hydrogen production from surplus energy. The CAPEX increases further by 70000,00 € with respect to S3, reaching a total of 704704,00 €, as shown in Table 9.7.

Figure 9.45 shows the corresponding cumulated cash flow, which starts from the deepest initial value among all scenarios, −704704,00 €, coherent with the highest CAPEX. The RID component falls further, to only 13306,00 €, since most of the residual surplus that in S1 and S2 was exported to the grid is now absorbed by the electrolyzer, which by design operates only on surplus energy not otherwise self consumed or shared. This is compensated by two effects, the TiP and ARERA share grows again, to 38834,25 €, and a new revenue stream appears, the sale of hydrogen, valued at 6,0 €/kg for the approximately 2874,5 kg of H_2 produced annually, contributing 17247,00 € per year. The combination of these effects brings the total annual revenue back up to 69387,25 €, slightly higher than in S3. As a result, the discounted Payback Time is 18,63 years, marginally longer than in S3, while the NPV reaches 28155,64 €, essentially in line with, and marginally higher than, the 27131,87 € of S3, and the IRR is 4,46%, again just above the discount rate. The hydrogen revenue is therefore sufficient to offset the additional 70000,00 € of CAPEX and to keep the investment indicators of S4 comparable to those of S3, without however producing a substantial improvement in the pure financial return.

Table 9.7: Composition of CAPEX, OPEX and revenues for scenario S4

Item	**Value [€]**	**Item**	**Value [€]**
PV panels	207792,00	Transport	4995,00
Fixed structure	34965,00	Commissioning	999,00
DC cables	6993,00	Authorizations	69930,00
Electrical installation	9990,00	Legal costs	4995,00
Mechanical installation	27972,00	Design costs	20000,00
Inverter	56000,00	Administrative costs	5000,00
Electrical panels	7700,00	Works supervision	25000,00
AC cables	7700,00	BESS	110000,00
LV/MV transformation	7700,00	Electrolyzer	70000,00
Civil works	19980,00		
Engineering and site management	4995,00		
Project management	1998,00		
Total CAPEX ($n = 0$)			**704704,00**
Annual OPEX (1,5% of CAPEX)			10570,56
RID			13306,00
Share of TiP + ARERA (25%)			38834,25
H_2 sales			17247,00
Total annual revenue			**69387,25**

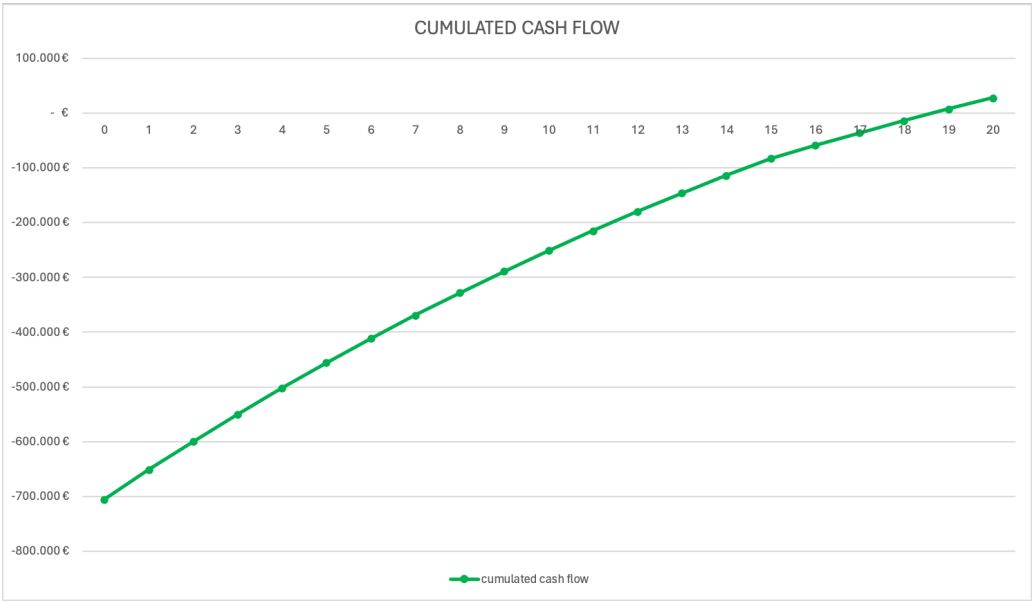


Figure 9.45: Discounted cumulated cash flow, scenario S4

9.5.6 Final comparison between scenarios

Table 9.8 summarizes the key financial indicators, PBT, NPV and IRR, together with the community level indicators, bill savings, dividends distributed within the REC, and avoided CO_2 emissions, for all four scenarios.

Table 9.8: Comparative summary of the four scenarios

Indicator	**S1**	**S2**	**S3**	**S4**
PBT [years]	9,79	12,35	18,55	18,63
NPV [€]	349681,79	197641,51	27131,87	28155,64
IRR [%]	10,80	8,04	4,50	4,46
Bill savings [€/year]	281531,00	330238,00	339365,00	339365,00
REC dividends [€/year]	88010,25	102325,50	104605,50	116565,75
Avoided CO_2 in REC [kg/year]	234248	272614	278094	278094
Avoided CO_2 from H_2 [kg/year]	–	–	–	31389

The comparison brings out a clear and consistent pattern across the four configurations. Moving from S1 to S4, every additional technological layer, demand response, storage, electrolysis, increases the value delivered to the community, bill savings rise from 281153,00 € to 339365,00 € per year, dividends distributed within the REC rise from 88010,25 € to 116565,75 €, and avoided emissions rise from 234248 kg/year to 278094 kg/year, plus a further 31389 kg/year avoided through the substitution of grey hydrogen with the green hydrogen produced in S4. At the same time, every additional layer worsens the purely financial indicators computed from the investor's perspective, the Payback Time nearly doubles between S1 and S3, the NPV drops from 349681,79 € to 27131,87 €, and the IRR falls from 10,80% to 4,50%. This

divergence is not a modelling inconsistency, but a direct and expected consequence of the accounting boundary adopted for the DCF analysis, which credits the investor with RID revenue and only 25% of the TiP and ARERA incentives, while the remaining 75% and the bill savings themselves accrue to the community members rather than to the plant owner. The financial appraisal presented in this chapter therefore measures the profitability of the capital actually invested by the plant developer, and should be read together with, rather than as a substitute for, the community wide benefit captured by the bill savings, dividend and emission indicators, since the two accounting bases are not directly comparable and mixing them would overstate the investor's return.

A second observation worth highlighting concerns the transition from S3 to S4. The two scenarios show almost identical bill savings, 339365,00 € in both cases, which confirms the internal consistency of the model, the electrolyser, dispatched only on residual surplus energy and metered as a separate point of delivery, does not alter the energy actually allocated to the community's residential and public members, and therefore leaves their bill savings unchanged. The additional 70000,00 € invested in the electrolyser is almost entirely offset, from a purely financial standpoint, by the hydrogen sales revenue, so that NPV and IRR remain essentially at the same level as S3, the NPV difference is only about 3,8% and the IRR difference less than half a percentage point. The real added value of S4, in other words, is not visible in the investor's cash flow, but in the additional decarbonisation delivered through green hydrogen, an aspect that a purely financial reading of the results would fail to capture.

Finally, it should be noted that the IRR values of S3 and S4, respectively 4,50% and 4,46%, are only marginally above the 4% discount rate assumed for the analysis. This indicates that the positive NPV obtained for these two scenarios is numerically thin, and therefore sensitive to the underlying assumptions, a moderate downward revision of the hydrogen price, of the electricity purchase price used to compute bill savings, or of the incentive framework, could in principle bring the NPV of S3 or S4 close to zero or negative over the 20 year horizon. This sensitivity is not explored quantitatively in the present chapter, but it represents a relevant caveat when interpreting the comparison, and a natural candidate for a dedicated sensitivity analysis.

Taken together, the results indicate that S1 is the preferable configuration if the sole objective is to maximise the return on the capital invested by the plant developer, while S4 is the configuration that maximises the value delivered to the community and the environmental benefit, at the cost of a financial return for the investor that is barely above the assumed cost of capital. The choice among the four scenarios therefore depends on which objective, investor profitability or community and environmental value, is assigned greater weight in the governance of the energy community.

Chapter 10

Conclusions

This thesis analyzed four progressively more complex configurations of a Renewable Energy Community located in Minervino di Lecce, with the aim of quantifying, in a coherent and verifiable way, the contribution that each additional technology, demand response, electrochemical storage, electrolysis, brings relative to the baseline photovoltaic configuration. The four scenarios share the same 1 MWp plant and the same aggregate community consumption profile, which made it possible to isolate the marginal effect of each individual technology without the differences being confounded by variations in plant size or served demand.

On the energy side, the results show a coherent and, in some respects, predictable progression. Scenario S1 returns a Self-Consumption Index of 68,2% and a Self-Sufficiency Index of 32,0%, values that are already relatively high for a plant sized at less than one third of the community's annual demand: this is explained by the structure of the load, dominated for 84% by the residential component, which guarantees a concurrent demand wide enough to absorb most of the PV output even in the shoulder seasons. The demand response mechanism of S2 raises the IAC to 79,3% by acting exclusively on the temporal redistribution of the load, without increasing the available production; the storage system of S3 brings the IAC to 81,8% and, more importantly, the IAS to 38,0%, demonstrating, unlike DR, a genuine capacity to shift energy between surplus and shortage periods rather than merely optimizing its daily allocation. The electrolyzer of S4, finally, pushes the IAC to 91,0% by absorbing the share of surplus that would otherwise have been sold to the grid through Ritiro Dedicato, but with no effect on the IAS, since it behaves as an additional load internal to the community rather than as a source covering electricity demand. This distinction, seemingly subtle, is in fact one of the clearest results of the work: self-consumption and self-sufficiency are not the same quantity, and the technologies examined improve them through physically distinct mechanisms.

The economic comparison carried out through a 20-year DCF analysis returns a more articulated picture, and one that is in some respects counterintuitive if read in isolation from the rest of the chapter. From the standpoint of investor return, S1 is by far the preferable configuration: a Payback Time of 9,79 years, an NPV of EUR 349681,79 and an IRR of 10,80%. Every additional technology systematically worsens these indicators, the Payback Time nearly doubles between S1 and S3, the NPV collapses to EUR 27131,87 and the IRR falls to 4,50%, a margin barely above the 4% discount rate assumed for the analysis. This trend is not a modelling artefact, but the direct and intended consequence of the accounting boundary adopted for the DCF, the investor is credited with the entire RID revenue and only 25% of the Premium Tariff and ARERA compensation incentives, while the remaining 75% and the bill savings themselves accrue to the community members. Read from this perspective, the growth in bill savings (from EUR 281531/year in S1 to EUR 339365/year in S3 and S4) and in the dividends distributed within the REC (from EUR 88010,25 to EUR 116565,75/year) tells the opposite story to the NPV, the total value generated by the system increases at every scenario, but it progressively shifts from the investor toward the collective of members. This is the central tension that the

results chapter brings out, and it is arguably the most relevant message of the entire work from the standpoint of REC governance, neither reading, the investor's or the community's, is sufficient on its own to guide an investment decision, and the choice of the optimal configuration ultimately depends on which of the two stakeholders, private capital or collective benefit, the community intends to prioritize.

The case of S3 deserves a separate remark, since the PSO-based sizing optimization showed that the optimum from the standpoint of the individual investor (one module, VAN of EUR 175335) is structurally misaligned with the two-module configuration adopted as the reference throughout the thesis, and even more so with the three-module sizing identified by the multi-objective analysis as the knee point of the Pareto frontier, a configuration which, while increasing the gross benefit to the community by approximately EUR 19880/year, drives the private VAN into negative territory. The reason is the same highlighted above on a larger scale, the investor bears 100% of the incremental capital cost of storage but captures only 25% of the incentive proceeds, so private profitability decreases monotonically with battery size across the entire explored search range. For this reason, consistently, the two-module configuration was retained as the reference for the cross-scenario comparison, while the PSO analysis remains a useful diagnostic tool for quantifying how far the socially optimal storage size diverges from the privately optimal one under the current incentive framework.

The transition from S3 to S4 offers a finding of a different, and in some sense more encouraging, nature. Bill savings remain identical between the two scenarios (EUR 339365/year), confirming that the electrolyzer, operating only on the residual surplus after battery charging and metered as a separate point of delivery, leaves the energy actually available to the community's residential and public members entirely unchanged. The revenue from hydrogen sales (EUR 17247/year, at the assumed price of 6,0 EUR/kg) almost entirely offsets the EUR 70000 CAPEX increase associated with the electrolyzer, keeping NPV and IRR essentially in line with those of S3 (NPV difference below 4%). The real added value of S4 therefore does not show up in the investor's cash flow, which remains nearly unchanged, but in the environmental contribution, to the 278,1 tCO_2/year avoided through electricity generation like in S3, a further 31,4 tCO_2/year is added by displacing grey hydrogen with the green hydrogen produced on site, bringing the total to 309,5 tCO_2/year, a benefit that a purely financial reading would fail to capture.

A limitation should finally be noted that qualifies, without undermining, the soundness of the economic results for S3 and S4, the IRR values obtained, 4,50% and 4,46% respectively, exceed the assumed discount rate (4%) by a margin narrow enough that the sign of the NPV itself is sensitive to even modest revisions of the underlying assumptions, a downward revision of the hydrogen price, of the avoided retail electricity price, or of the incentive framework could in principle bring the NPV of these two scenarios close to zero or negative over the 20-year horizon considered. A quantitative sensitivity analysis on these parameters was not carried out in this work and represents its natural continuation, together with a refinement of the analysis at the level of the individual community member, needed to quantify, rather than only qualitatively state as done here, the impact of the Premium Tariff redistribution constraint set by the CACER Decree above the 55% shared-energy threshold, a threshold that is exceeded by a wide margin in all four scenarios (from 68,2% in S1 to 90,2% in S4).

In summary, the work confirms that no single configuration among the four examined is unambiguously "best", but rather two alternative, and partly opposing, optimization trajectories, S1 maximizes the return on invested capital, S4 maximizes the value transferred to the community and the environmental benefit, at the cost of an investor return barely sufficient to justify the risk exposure. The choice between these two extremes, or among the intermediate configurations represented by S2 and S3, is ultimately a governance decision for the energy community, rather than a question that can be settled on technical and economic grounds alone.

Bibliography

[1] European Commission - Directorate-General for Energy. *Clean energy for all Europeans package completed: good for consumers, good for growth and jobs, and good for the planet.* European Commission. May 22, 2019. URL: https://commission.europa.eu/news-and-media/news/clean-energy-all-europeans-package-completed-good-consumers-good-growth-and-jobs-and-good-planet-2019-05-22_en (visited on 04/22/2026).

[2] Parlamento europeo e Consiglio dell'Unione europea. *Direttiva (UE) 2018/2001 del Parlamento europeo e del Consiglio dell'11 dicembre 2018 sulla promozione dell'uso dell'energia da fonti rinnovabili (rifusione).* GU L 328 del 21.12.2018, pp. 82–209. Dec. 11, 2018. URL: https://eur-lex.europa.eu/IT/legal-content/summary/renewable-energy.html (visited on 04/22/2026).

[3] Parlamento europeo e Consiglio dell'Unione europea. *Direttiva (UE) 2019/944 del Parlamento europeo e del Consiglio del 5 giugno 2019 relativa a norme comuni per il mercato interno dell'energia elettrica e che modifica la direttiva 2012/27/UE (rifusione).* GU L 158, 14.6.2019, pp. 125–199. June 5, 2019. URL: https://eur-lex.europa.eu/legal-content/IT/TXT/PDF/?uri=CELEX:32019L0944 (visited on 04/22/2026).

[4] Parlamento europeo e Consiglio dell'Unione europea. *Direttiva (UE) 2023/2413 del Parlamento europeo e del Consiglio del 18 ottobre 2023 che modifica la direttiva (UE) 2018/2001, il regolamento (UE) 2018/1999 e la direttiva n. 98/70/CE per quanto riguarda la promozione dell'energia da fonti rinnovabili e che abroga la direttiva (UE) 2015/652 del Consiglio.* GU L 2023/2413, 31.10.2023. Oct. 18, 2023. URL: https://eur-lex.europa.eu/legal-content/IT/TXT/PDF/?uri=OJ:L_202302413 (visited on 04/22/2026).

[5] Repubblica Italiana. *Decreto legislativo 8 novembre 2021, n. 199. Attuazione della direttiva (UE) 2018/2001 del Parlamento europeo e del Consiglio, dell'11 dicembre 2018, sulla promozione dell'uso dell'energia da fonti rinnovabili.* Gazzetta Ufficiale della Repubblica Italiana, n. 285 del 30 novembre 2021, Suppl. Ordinario n. 42. Nov. 8, 2021. URL: https://www.gse.it/normativa_site/GSE%20Documenti%20normativa/ITALIA_DLGS_n199__08_11_2021.pdf (visited on 04/22/2026).

[6] Gestore dei Servizi Energetici (GSE). *CER, le novità introdotte dal decreto MASE e approfondimenti sulle regole operative.* Slide webinar formativo. Documento formativo su configurazioni CACER e comunità energetiche rinnovabili. 2024. URL: https://www.gse.it/media_site/media-gallery_site/Documents/FORMAZIONE%20WEBINAR%20CACER.pdf (visited on 04/22/2026).

[7] Repubblica Italiana. *Decreto legislativo 9 gennaio 2026, n. 5. Attuazione della direttiva (UE) 2023/2413 del Parlamento europeo e del Consiglio, del 18 ottobre 2023, che modifica la direttiva (UE) 2018/2001, il regolamento (UE) 2018/1999 e la direttiva n. 98/70/CE per quanto riguarda la promozione dell'energia da fonti rinnovabili e che abroga la direttiva (UE) 2015/652 del Consiglio.* Gazzetta Ufficiale della Repubblica Italiana, Serie Generale n. 15 del 20 gennaio 2026. Jan. 9, 2026. URL: https://www.gazzettaufficiale.it/eli/id/2026/01/20/26G00018/sg (visited on 04/22/2026).

[8] La Redazione. *Recepimento RED III: D.Lgs. in vigore, ecco i nuovi target italiani sulle rinnovabili*. Rinnovabili.it. Jan. 21, 2026. URL: https://www.rinnovabili.it/energia/infrastrutture/recepimento-red-iii-novita-fer-dlgs-deadline/ (visited on 04/22/2026).

[9] ABB SACE. *Quaderni di applicazione tecnica N.10 – Impianti fotovoltaici*. Quaderno tecnico di applicazione. ABB S.p.A., 2013. URL: https://library.e.abb.com/public/9b8b2685a780f657c125780e00407e1b/1SDC007109G0902.pdf (visited on 04/22/2026).

[10] ENEA - Solaritaly. *Global Horizontal Irradiation (GHI) Map of Italy (2006–2022)*. Mappe della radiazione solare in Italia, database Solaritaly ENEA. 2023. URL: https://www.solaritaly.enea.it/Radiazione/ (visited on 04/22/2026).

[11] Michele De Bastiani et al. "All Set for Efficient and Reliable Perovskite/Silicon Tandem Photovoltaic Modules?" In: *Solar RRL* 6 (2021). DOI: 10.1002/solr.202100493.

[12] Gestore dei Servizi Energetici (GSE). *Rapporto Statistico 2024 – Solare Fotovoltaico*. Rapporto statistico. Dati sullo sviluppo del fotovoltaico in Italia aggiornati al 2024. GSE S.p.A., 2025. URL: https://www.gse.it/documenti_site/Documenti%20GSE/Rapporti%20statistici/Solare%20Fotovoltaico%20-%20Rapporto%20Statistico%202024.pdf (visited on 04/22/2026).

[13] Mohammad Faisal et al. "Review of Energy Storage System Technologies in Microgrid Applications: Issues and Challenges". In: *IEEE Access* 6 (2018). DOI: 10.1109/ACCESS.2018.2841407.

[14] Marco Stecca et al. "A Comprehensive Review of the Integration of Battery Energy Storage Systems Into Distribution Networks". In: *IEEE Open Journal of the Industrial Electronics Society* (2020). DOI: 10.1109/OJIES.2020.2981832.

[15] University course material. *Energy Storage*. Academic year 2024/2025. 2025.

[16] Patrick Timothy Moseley and Jürgen Garche. *Electrochemical Energy Storage for Renewable Sources and Grid Balancing*. Elsevier, 2014.

[17] Terna. *Studio sulle tecnologie di riferimento per lo stoccaggio di energia elettrica. Allegato B al DCO ARERA 168/2025/R/EEL*. Gennaio 2025. 2025. URL: https://www.arera.it/fileadmin/allegati/docs/25/168-2025-R-eel-ALLEGATO_B.pdf.

[18] Aritra Ghosh. "Solar-Powered Green Hydrogen from Electrolyzer (PV-H2): A Review". In: *Solar RRL* 9 (2025). DOI: 10.1002/solr.202500150.

[19] Furat Dawood, G. M. Shafiullah, and Martin Anda. "Stand-Alone Microgrid with 100% Renewable Energy: A Case Study with Hybrid Solar PV-Battery-Hydrogen". In: *Sustainability* (2020). DOI: 10.3390/su12052045.

[20] Massimo Santarelli. *Water Splitting: Notes on Electrolysis and Other VRE-Based Processes*. Course material, Energy Department, Politecnico di Torino, STEPS Group. 2024.

[21] Massimo Santarelli. *H2 Storage*. Course material, Energy Department (DENERG), Politecnico di Torino, Academic year 2025/2026. 2026.

[22] Ricerca sul Sistema Energetico (RSE). *Le comunità energetiche in Italia. Orange Book*. 2022. URL: https://www.rse-web.it/wp-content/uploads/2022/02/OrangeBook-22-Le-Comunita-Energetiche-in-Italia-DEF.pdf.

[23] Governo della Repubblica Italiana. *Decreto legge 30 dicembre 2019, n. 162, coordinato con la legge di conversione 28 febbraio 2020, n. 8. Disposizioni urgenti in materia di proroga di termini legislativi, di organizzazione delle pubbliche amministrazioni, nonche' di innovazione tecnologica*. 2019. URL: https://www.gazzettaufficiale.it/eli/id/2020/02/29/20A01353/sg.

[24] Autorità di Regolazione per Energia Reti ed Ambiente (ARERA). *Delibera 4 agosto 2020 318/2020/R/eel. Regolazione delle partite economiche relative all'energia elettrica condivisa da un gruppo di autoconsumatori di energia rinnovabile che agiscono collettivamente in edifici e condomini oppure condivisa in una comunità di energia rinnovabile*. 2020. URL: https://www.arera.it/fileadmin/allegati/docs/20/318-20.pdf.

[25] Ministero dello Sviluppo Economico. *Decreto Ministeriale 16 settembre 2020. Individuazione della tariffa incentivante per la remunerazione degli impianti a fonti rinnovabili inseriti nelle configurazioni sperimentali di autoconsumo collettivo e comunità energetiche rinnovabili*. 2020. URL: https://www.gazzettaufficiale.it/eli/id/2020/11/16/20A06191/sg.

[26] Autorità di Regolazione per Energia Reti ed Ambiente (ARERA). *Delibera 27 dicembre 2022 727/2022/R/eel. Definizione, ai sensi del decreto legislativo 199/21 e del decreto legislativo 210/21, della regolazione dell'autoconsumo diffuso. Approvazione del Testo Integrato Autoconsumo Diffuso*. 2022. URL: https://www.arera.it/fileadmin/allegati/docs/22/727-22.pdf.

[27] Gestore dei Servizi Energetici (GSE). *Gruppi di autoconsumatori e comunità di energia rinnovabile*. 2025. URL: https://www.gse.it/servizi-per-te/autoconsumo/gruppi-di-autoconsumatori-e-comunita-di-energia-rinnovabile.

[28] Gestore dei Servizi Energetici (GSE). *DECRETO CACER e TIAD – Regole operative per l'accesso al servizio per l'autoconsumo diffuso e al contributo PNRR*. Versione del 16 luglio 2025. Regole per l'attuazione del Decreto CACER e del TIAD per la valorizzazione e l'incentivazione dell'energia elettrica condivisa. 2025. URL: https://www.gse.it.

[29] Ministero dell'Ambiente e della Sicurezza Energetica (MASE). *Decreto Ministeriale 7 dicembre 2023, n. 414. Configurazioni di Autoconsumo per la Condivisione dell'Energia Rinnovabile (CACER)*. 2023. URL: https://www.gazzettaufficiale.it/eli/id/2024/01/24/24A00377/sg.

[30] Gestore dei Servizi Energetici (GSE). *Ritiro Dedicato (RID). Servizio per la commercializzazione dell'energia elettrica prodotta e immessa in rete*. La remunerazione è basata sui Prezzi Zonali Orari. 2025. URL: https://www.gse.it/servizi-per-te/fotovoltaico/ritiro-dedicato.

[31] Ministero dell'Ambiente e della Sicurezza Energetica (MASE). *I passi per creare una CER*. 2025. URL: https://culturaeconsapevolezza.mase.gov.it/news/i-passi-per-creare-una-cer.

[32] Gestore dei Servizi Energetici (GSE). *Mappa interattiva delle cabine primarie*. Mappa interattiva delle aree convenzionali sottese alle cabine primarie e delle configurazioni di autoconsumo diffuso presenti sul territorio nazionale. 2025. URL: https://www.gse.it/servizi-per-te/autoconsumo/mappa-interattiva-delle-cabine-primarie.

[33] Mario Lamagna et al. "Hourly energy profile determination technique from monthly energy bills". In: *Building Simulation* 13 (2020), pp. 1235–1248.

[34] Gestore dei Servizi Energetici (GSE). *Modalità di profilazione dei dati di misura e relative modalità di utilizzo ai sensi dell'articolo 9 dell'Allegato A alla Delibera 318/2020/R/eel*. 2022. URL: https://www.gse.it/documenti_site/Documenti%20GSE/Servizi%20per%20te/AUTOCONSUMO/Modalita_profilazione_dati_misura.pdf.

[35] JA Solar. *JAM72D40-LB - Modulo fotovoltaico bifacciale N-Type TOPCon da 575–600 W*. Scheda tecnica. 2025. URL: https://www.solarenergypoint.it/immagini/pdf/download/fotovoltaico/moduli-fotovoltaici/ja-solar/jam72d40-lb/ja-solar-jam72d40-xxx-lb-modulo-fotovoltaico-bifacciale-575-600w-scheda-tecnica.pdf.

[36] Sigenergy. *Sigen Hybrid M1-HYB - Inverter fotovoltaico commerciale ibrido trifase*. Scheda tecnica. 2025. URL: https://www.solarenergypoint.it/immagini/pdf/download/fotovoltaico/inverter/sigenergy/sigen-hybrid/sigenergy-sigen-hybrid-xxxm1-hyb-inverter-fotovoltaico-commerciale-ibrido-trifase-scheda-tecnica.pdf.

[37] Prysmian. *PRYSOLAR H1Z2Z2-K 1,0/1,0 kV AC (1,5/1,5 kV DC) - Cavo fotovoltaico*. Scheda tecnica. 2023. URL: https://www.prysmianclub.it/wp-content/uploads/2023/04/Scheda-tecnica-Prysolar_v.2.pdf.

[38] ABB. *Tabelle ABB per il dimensionamento degli impianti elettrici*. Manuale tecnico consultato online. 2025. URL: http://massimombonini.studiombm.it/pdf_impianti_elettrici/Tabelle_ABB.pdf.

[39] Baldassari Cavi. *FG16OR16 0,6/1 kV - Cavo multipolare per energia*. Scheda tecnica. 2019. URL: https://www.baldassaricavi.it/wp-content/uploads/2019/12/10-FG16OR16-10.pdf.

[40] Baldassari Cavi. *FG16R16 0,6/1 kV - Cavo unipolare per energia*. Scheda tecnica. 2019. URL: https://www.baldassaricavi.it/wp-content/uploads/2019/10/9-FG16R16.pdf.

[41] GSL Energy. *GSL-BESS-418K - 125 kW / 418 kWh Liquid-Cooled Battery Energy Storage System*. Technical datasheet. 2025. URL: https://www.gsl-energy.com/125kw-418kwh-liquid-cooled-bess-commercial-solar-battery-storage-system-manufacturer.html.

[42] Hefei Sinopower Technologies. *Rubri-P1-0020 - 20 Nm3/h 100 kW PEM Hydrogen Electrolyzer System*. Technical datasheet. 2025. URL: https://www.hfsinopower.com/20nm3h-100kw-pem-hydrogen-electrolyzer-system-hydrogen-gas-equipment.

[43] Francesco Mancini et al. "How the Italian Residential Sector Could Contribute to Load Flexibility in Demand Response Activities: A Methodology for Residential Clustering and Developing a Flexibility Strategy". In: *Energies* 13 (2020). DOI: 10.3390/en13133411.

[44] Sarah O'Connell and Stefano Riverso. *Flexibility Analysis for Smart Grid Demand Response*. Research report. 2017. DOI: 10.48550/arXiv.1704.01308.

[45] Patricia Ercoli, Alice Mugnini, and Alessia Arteconi. "Demand Response for Renewable Energy Communities: Exploring Coordination of Prosumer-Generated PV and Flexible Aggregated Demand in the Italian Framework". In: *Applied Energy* (2025). DOI: 10.1016/j.apenergy.2025.126549.

[46] J. Kennedy and R. Eberhart. "Particle Swarm Optimization". In: *Proceedings of ICNN'95 - International Conference on Neural Networks*. Vol. 4. 1995, pp. 1942–1948. DOI: 10.1109/ICNN.1995.488968.

[47] Kalyanmoy Deb. *Multi-Objective Optimization Using Evolutionary Algorithms*. Chichester: John Wiley & Sons, 2001. ISBN: 047187339X.